

**Aus dem Max-Planck-Institut für
Hirnforschung in Frankfurt am Main**

Stimulus and task-dependent gamma activity in monkey V1

Dissertation
zur Erlangung des Doktorgrades der
Naturwissenschaften

vorgelegt beim Fachbereich Biowissenschaften
der Johann Wolfgang Goethe - Universität
in Frankfurt am Main

von

Bruss Rebouças Coelho Lima

aus Brasília, Brasilien

Frankfurt am Main 2010

(D 30)

Vom Fachbereich Biowissenschaften der Johann Wolfgang Goethe-Universität als Dissertation
angenommen

Dekanin: Prof. Dr. Anna Starzinski-Powitz

1. Gutachter: Prof. Dr. Wolf Singer

2. Gutachter: Prof. Dr. Manfred Kössl

3. Gutachter: Prof. Dr. Peter König

Datum der Disputation: 22. März 2011

Table of contents

List of figures and tables	ix
Glossary of terms and abbreviations	xi
Summary	xiii
Chapter 1 - General introduction	1
1.1 - Functional organization of the visual system	2
1.1.1 - Serial and Parallel processing	4
1.1.2 - Modular and Topographic organization of the visual system	7
1.2 - Cooperative mechanisms of neural activity	8
1.2.1 - Synchronous processes in the visual system	9
1.2.2 - Oscillatory processes in the visual system	10
1.2.3 - Instrumental role of oscillatory activity in neuronal processing	15
1.2.4 - Attentional modulation of oscillatory activity	17
1.3 - Figure-ground segregation and feature binding	19
1.3.1 - The binding problem	20
1.3.2 - The binding-by-synchronization (BBS) hypothesis	20
1.4 - Outline and goals	23
1.5 - References	24
Chapter 2 - Directional responses of visual wulst neurones to grating and plaid patterns in the awake owl	33
2.1 - Abstract	34
2.2 - Introduction	34
2.3 - Material and Methods	35
2.3.1 - Animal training	35
2.3.2 - Surgical procedures	35
2.3.3 - Recordings	35
2.3.4 - Stimulation protocol	36
2.3.5 - Data analysis	36
2.3.6 - General statistics	38
2.4 - Results	38
2.4.1 - General observations	38
2.4.2 - Direction-selective response properties	38
2.4.3 - Neuronal responses to plaids	40
2.4.4 - Effect of plaid angles on partial correlation coefficients	41
2.4.5 - Response inhibition to plaid patterns	43
2.4.6 - Temporal dynamics of component direction selectivity	44
2.5 - Discussion	45

2.5.1 - Receptive field properties in the visual wulst	47
2.5.2 - Incidence, strength and precision of directional selectivity	48
2.5.3 - Motion integration	49
2.5.4 - Concluding remarks	50
2.6 - Acknowledgements	50
2.7 - Abbreviations	50
2.8 - References	50
Chapter 3 - Synchronization dynamics in response to plaid stimuli in monkey V1	53
3.1 - Abstract	54
3.2 - Introduction	54
3.3 - Material and methods	55
3.3.1 - Training and visual paradigm	56
3.3.2 - Preparation and recording procedures	56
3.3.3 - Data collection and spike sorting.....	56
3.3.4 - Data analysis	56
3.4 - Results	57
3.4.1 - Disruption of ongoing gamma responses	57
3.4.2. Shifts in gamma oscillation frequency	60
3.4.3 - Gamma signatures	62
3.4.4 - Segmentation of surfaces	62
3.4.5 - Selective attention.....	63
3.5 - Discussion.....	65
3.5.1 - Gamma responses	65
3.5.2 - Breaking the waves	66
3.5.3 - Scene segmentation	68
3.6 - Notes	69
3.7 - References	69
3.8 - Supplementary Material	72
Chapter 4 - Gamma responses correlate with temporal expectation in monkey primary visual cortex	77
4.1 -Abstract	78
4.2 - Introduction	78
4.3 - Experimental Procedures.....	80
4.3.1 - Training and visual paradigm	80
4.3.2 - Preparation and recording procedures	82
4.3.3 - Data collection and spike sorting.....	82
4.3.4 - Data analysis	83
4.4 - Results	86
4.4.1 - Building expectation in stimulus sequences	87
4.4.2 - Building expectation in trial blocks	89
4.4.3 - Cueing effects.....	91
4.4.4 - Neuronal coherence	94

4.4.5 - Impact on orientation selectivity	94
4.4.6 - Reward effects	97
4.5 - Discussion.....	98
4.6 - Acknowledgements.....	102
4.7 - References	102
4.8 - Supplementary Material.....	108
4.8.1 - Control for microsaccades	108
4.8.2 - Expectation effect without visual stimulation	111
4.8.3 - Learning reward value.....	112
4.9 - Supplementary References	113
Chapter 5 - Gamma-phase shifting in awake monkey visual cortex	115
5.1- Abstract	116
5.2 - Introduction	116
5.3 - Material and methods	116
5.4 - Results	118
5.5 - Discussion.....	121
5.6 - References	122
Chapter 6 - General discussion	125
6.1 - The different perspectives of observed brain function	126
6.2 - Motion integration: a comparative study in the owl	129
6.3 - The variability of gamma processes in monkey V1	130
6.4 - Orientating attention in time.....	133
6.5 - Binding-by-synchronization (BBS) in V1 of the behaving monkey.....	135
6.6 - The brain as an analogue operator	137
6.7 - Concluding Remarks	138
6.8 - References	139
Appendix	145
Detailed summary	165
Zusammenfassung	171
Acknowledgements	179

List of figures and tables

2.1 - Representative examples of receptive field properties in the visual wulst of the awake burrowing owl.	39
2.2 - Directional tuning properties of neurons sampled in the visual wulst.	40
2.3 - Directional tuning of component direction-selective neurons to drifting sine wave gratings and 90° plaids.	42
2.4 - Directional tuning of unclassified neurons to drifting sine wave gratings and 90° plaids.	43
2.5 - Scatter plot of partial correlations for the component prediction (Rc) and pattern prediction (Rp) of direction-selective neurons sampled within the owl visual wulst.	44
2.6 - Relationship between component motion selectivity and direction selectivity for the population of directionally selective neurons.	44
2.7 - Influence of plaid angle on the partial correlations for component prediction (R) and pattern prediction (R) of direction-selective neurons.	45
2.8 - Distribution of plaid inhibition ratios for direction-selective neurons.	45
2.9 - Scatter plots of partial correlations for the component prediction (Rc) and pattern prediction (Rp) during the first 200 ms after stimulus onset.	46
2.10 - Population summary of the temporal evolution of component direction-selective (CDS) neuron responses.	47
T3.1 - Recording sites with significant gamma oscillations for the MUA.	57
3.1 - Examples of disruption in the oscillatory patterning of spiking responses to plaid stimuli.	58
3.2 - Spectral analysis for the LFP and MUA for responses to single and superimposed components of the plaid stimuli.	59
3.3 - Coherence analysis for grating and plaid stimuli.	60
3.4 - Parametric study on the disruption of the ongoing spike gamma oscillations.	61
3.5 - Gamma frequency shifts of LFP oscillations.	61
3.6 - Relation between RF eccentricity and oscillation frequency of the LFP.	62
3.7 - Spectral signatures for the three monkeys studied.	63
T3.2 - Peak gamma oscillation frequencies for the grating and plaid stimuli across monkeys and hemispheres.	63
3.8 - Relations between synchrony and stimulus coherence for recordings obtained from the same electrode.	64
3.9 - Relations between synchrony and stimulus coherence for recordings obtained from different electrodes.	65
3.10 - Effects of selective attention to one of the surfaces of the plaids on gamma activity.	66
S3.1 - Control for effects due to component 2 onset transient.	73
S3.2 - Firing rate responses, LFP and MUA spectra, and LFP-MUA coherence for the full range of movement directions tested.	73
S3.3 - Decay of the LFP-LFP, MUA-MUA and LFP-MUA gamma coherence with the distance between the sites of a recording pair.	74
S3.4 - Control for effects of spatial frequency and speed on LFP gamma activity.	74
S3.5 - Control for oscillation cycle skipping.	75
4.1 - Spectral analysis for the sequence-protocol.	88
4.2 - Spectral analysis for the block-protocol.	90

4.3 - Time-frequency analysis of the LFP acquired during a cue-protocol.	92
4.4 - Spectral analysis for the cue protocol.	93
4.5 - Coherence analysis of the gamma activity during temporal expectation.	95
4.6 - Changes in selectivity with temporal expectation.	96
4.7 - Effect of reward value expectation.	97
S4.1 - Microsaccadic pattern and gamma power.	109
S4.2 - The impact of stimulus spatial jitter on gamma activity.	110
S4.3 - Effects of temporal expectation on neuronal activity with no visual stimulation.	111
S4.4 - Learning the association between reward value and a cue along an experimental session.	112
5.1 - Spike-LFP phase-locking spectra.	118
5.2 - Match between stimulus orientation preference determines spike phase in the gamma cycle.	119
5.3 - Population results for orientation-dependent phase shift.	119
5.4 - Temporal evolution of spike density and spike phase during the trial.	120
5.5 - The relationship between spike density and spike phase.	120
5.6 - Relationship between strength of rhythmic input and gamma-phase shifting.	121

T, table; S, supplementary figure.

Glossary of terms and abbreviations

APB	2-amino-4-phosphonobutyrate
BBS	binding by synchronization
cd	candela
CDS	component direction selective
ci	confidence interval
CTC	communication through coherence
DI	direction index
EEG	electroencephalogram
EPSP	excitatory postsynaptic potential
ERP	event-related potential
FFT	fast Fourier transform
fMRI	functional magnetic resonance imaging
FP	fixation point
GABA	gamma-aminobutyric acid
HA	hyperpallium apicale
IPSP	inhibitory postsynaptic potential
LFP	local field potential
LGN	lateral geniculate nucleus
LTD	long-term depression
LTP	long-term potentiation
LM	pretectal nucleus lentiformis mesencephali
MEG	magnetoencephalogram
MRF	mesencephalic reticular formation
ms	milliseconds
MT	middle temporal area
MUA	multi-unit activity
nBOR	nucleus of the basal optic root
OI	orientation index
PDS	pattern direction selective
PSTH	post-stimulus time histogram
R_c	partial correlation coefficient for the component prediction
R_p	partial correlation coefficient for the pattern prediction
RF	receptive field
RT	reaction time
s	seconds
SD	standard deviation
SEM	standard error of the mean
STDP	spike timing-dependent plasticity
SUA	single-unit activity
V1	striate cortex or primary visual cortex

Summary

The single unit doctrine proposes that each one of our percepts and sensations is represented by the activity of specialized high-level cells in the brain. A common criticism applied to this proposal is the one referred to as the “combinatorial problem”. We are constantly confronted with unlimited combinations of elements and features, and yet we face no problem in recognizing patterns and objects present in visual scenes. Are there enough neurons in the brain to singly code for each one of our percepts? Or is it the case that perceptions are represented by the distributed activity of different neuronal ensembles? We lack a general theory capable of explaining how distributed information can be efficiently integrated into single percepts. The working hypothesis here is that distributed neuronal ensembles signal relations present in the stimulus by selectively synchronizing their spiking responses. Synchronization is generally associated with oscillatory activity in the brain. Gamma oscillations in particular have been linked to various integrative processes in the visual system. Studies in anesthetized animals have shown a conspicuous increase in power for the gamma frequency band (30 to 60 Hz) in response to visual stimuli. Recently, these observations have been extended to behavioral studies which addressed the role of gamma activity in cognitive processes demanding selective attention.

The initial motivation for carrying out this work was to test if the binding-by-synchronization (BBS) hypothesis serves as a neuronal mechanism for perceptual grouping in the visual system. To this aim we used single and superimposed grating stimuli. Superimposed gratings (plaids) are bi-stable stimuli capable of eliciting different percepts depending on their physical characteristics. In this way, plaids can be perceived either as a single moving surface (pattern plaids), or as two segregated surfaces drifting in different directions (component plaids). While testing the BBS hypothesis, we performed various experiments which addressed the role of both stimulus and cortical architecture on the properties of gamma oscillations in the primary visual cortex (V1) of monkeys. Additionally, we investigated whether gamma activity could also be modulated by allocating attention in time. Finally, we report on gamma-phase shifts in area V1, and how they depend on the level of neuronal activation.

Spiking activity and the local field potential (LFP) were recorded from area V1 of four behaving rhesus monkeys (*Macaca mulatta*). Recordings were performed with multiple electrodes in the central (~3°) and parafoveal (~10°) representations of the visual field. Monkeys were trained to fixate a small red point (fixation point, FP) on a computer screen. A typical trial started when the monkey fixated and pressed a lever. Throughout the trial, fixation had to remain within 1° of the FP. The monkeys were required to immediately release the lever upon a color change of the FP (from red to green) or a luminance change in the stimulus. Correctly performed trials were rewarded with fruit juice.

Based on the binding-by-synchronization hypothesis, we made predictions on how neurons in area V1 should synchronize their activity depending on stimulus configuration. None of our predictions held, regardless of whether the monkey passively viewed the stimulus or actively attended to one of its surfaces. To better understand these negative results, we performed several experiments in order to investigate which main factors determine the properties of gamma activity in the primary visual cortex. First of all, we observed that gamma interactions in V1 are relatively local. Therefore, gamma activity was predominantly dependent on the local properties of the stimulus, and not on its global properties as we had initially hypothesized. Additionally, we describe several parameters capable of modulating gamma oscillation frequency. The pattern of cortical activation (single versus superimposed gratings) was one of them. The second factor was the eccentricity of the recording site. Oscillation frequency was inversely related to eccentricity in a way that peak frequency systematically decreased for sites representing more peripheral portions of the visual field. A third factor was selective attention. Oscillation frequency depended on which surface of the plaid stimulus

the monkey attended to. Finally, inter-individual variability also played a role. For equal stimulation conditions, we observed that each of the monkeys had a specific peak oscillation frequency in the gamma band. Despite the inter-individual differences, the spectral profile within the same individual was incredibly consistent, as revealed by measurements across hemispheres and different recording sessions.

In accordance with several recently published studies, we found that attention can strongly modulate gamma activity. We here describe that directing attention in time impacts both gamma power and coherence in monkey V1. Gamma activity was systematically enhanced during conditions of higher temporal expectation. Concomitant to gamma increases, we observed an associated alpha power suppression. Additionally, modulation of oscillatory activity was shown to be widespread in V1. Finally, similar to the hippocampal theta phase precession, we report gamma-phase shifts in V1. The timing of the spike relative to the gamma oscillation cycle shifted as a function of the neuronal activation strength. Neurons that were strongly activated spiked earlier in the gamma cycle. The phase of the spike in the gamma cycle can thereby provide an instantaneous analog representation of neuronal excitation.

Chapter 1

General introduction

1.1 - FUNCTIONAL ORGANIZATION OF THE VISUAL SYSTEM

When asked by his students how neurons represent objects, neuroscientist Jerome Lettvin came up in 1969 with a humorous and fictitious story that has gradually become a serious theme in neuroscience circles (Gross, 2002). The main personage of his tale was his second cousin, Dr. Akakhi Akakhievitch, a neurosurgeon living in the distant Ural Mountains. Dr. Akakhievitch was convinced that single neurons were capable of representing ideas. Ever more obsessed, he decided to search for those neurons representing the most primitive of all objects: one's mother. He was able to find some 18,000 neurons in the human brain that responded exclusively to a mother, which ever way she was presented. Not only was Dr. Akakhievitch very pleased with his breakthrough, he also found immediate practical application for his discovery when a patient named Portney entered his office. Portney was psychologically tormented by problems involving his own mother, and Dr. Akakhievitch was ready to help. After being led to the operating table and having each one of his 18,000 mother neurons ablated, all his problems were finally solved: he lost the concept of his mother. After solving the enigma of the mother cells, Dr. Akakhievitch then turned to his next great challenge: the grandmother cells.

Lettvin's interest on mother and grandmother cells probably originated from his own work in the frog (Lettvin *et al.*, 1959). While recording in the frog's retina he was able to describe cells coding for various complex stimuli. One special type of ganglion cell, described as a "bug detector", responded uniquely when a small dark object entered its receptive field and moved about intermittently thereafter. Additional evidence coming from monkey recordings began to definitively convince the neuroscience community of the existence of cells capable of uniquely responding to specific complex objects (Gross *et al.*, 1969; 1972). While recording from the inferotemporal cortex of the anesthetized monkey, Gross and collaborators observed that the receptive fields were large and generally included the fovea and both visual hemifields. But most interestingly, single cells responded to complex features, such as a monkey's hand, presented anywhere within its receptive field. Several other works published thereafter not only confirmed these findings but extended them in describing cells responding specifically to other complex objects such as faces (Perrett *et al.*, 1982; Desimone *et al.*, 1984).

By the time the "grandmother cells" were discovered in the monkey temporal cortex, the hierarchical description of the visual system, as put forward by David Hubel and Torsten Wiesel (Hubel and Wiesel, 1962, 1968), was already widely accepted. Based on the recording of single, well isolated units in the early visual cortex, they proposed that the projection of LGN neurons having aligned receptive fields could entirely explain the origin of orientation selective cells in the primary visual cortex. These would initially consist in the simple cells, with their well determined ON

and OFF sub-regions. The convergence of several simple cells would give rise to the complex cells capable of generalizing the coding of a specific orientation throughout its receptive field. Complex cells would give rise to the hypercomplex cells following this same line of thought (Hubel and Wiesel, 1968). In this framework, the “grandmother cells” constituted a natural unfolding of how the visual system, and ultimately the brain, would build a representation of complex stimuli in the visual world.

In 1972, Horace Barlow proposed the “neuron doctrine” which linked sensation directly to the activity of single units in the brain. In part, Barlow’s proposal offered a significant paradigm shift. The activity of individual cells was considered too unreliable to be examined singly. Therefore, many turned to more macroscopic manifestations of neuronal activity, such as the electroencephalogram (EEG), in order to understand behavior. Barlow, on the other hand, was able to capture and synthesize a thinking that would dominate neurophysiology for many years to come: that single neurons are the prime movers leading to our perceptions and sensations (Hubel, 1982a). Not every cortical neuron’s activity had necessarily a simple perceptual correlate, but active high-level neurons directly and simply caused the elements of our perception. The mechanism by which this was achieved consisted in the frequency of neural impulses. Barlow argued that the rate of firing coded the certainty that the cause of a percept was present in the external world.

A pertinent criticism generally applied to the single unit doctrine is the one commonly referred to as “combinatorial problem” or “combinatorial explosion” (Singer and Gray, 1995). We are constantly confronted with unlimited combinations of elements and features, and yet we face no problem in recognizing patterns and objects presented in our visual scene. Additionally, we can easily cope with patterns not previously exposed to us, and we can effortlessly recognize objects encountered in unusual orientations and sizes, under different illumination conditions, or partially occluded by other objects (Logothetis and Sheinberg, 1996). Even though it may seem difficult to imagine that each one of our percepts is represented by a single high-level neuron, it has been suggested that there is a reasonable match between the number of possible percepts and the number of high-level neurons in the brain (Ghose and Maunsell, 1999). Contrary to what is usually assumed, however, Barlow did not believe in the existence of “grandmother cells” (Barlow, 1972). He acknowledged that there would not be enough “grandmother cells” or, as he called them, “pontifical cells” to account for the enormous variety of our perceptions. He believed that the activity of a single neuron would not be able to convey the richness of our sensations, which consist on the combination of our various percepts. Barlow, therefore, proposed the term “cardinal cells” instead of “pontifical cells” to explain how the brain represented the world. The interaction of various “cardinal” cells, which are lower in the hierarchy and more numerous than “popes”, would be responsible for the emergence of our perceptions and sensations.

The general mechanism used by the brain to build high level representations of the world is still largely unknown. We have, on the other hand, accumulated some knowledge regarding the functional organization of the visual system, which provides clues and constraints on how this representation might take place. I will start by discussing some aspects of neuronal pathways so as to illustrate two basic points of early visual processing. First, that different features of a stimulus are processed by parallel pathways. Second, that the early visual system is organized in a modular and topographic fashion such that a single object activates spatially distributed neurons with appropriate specificity. These two basic characteristics will be further used to justify that additional mechanisms are necessary in order to coordinate the neural activity processed in such a highly distributed manner.

1.1.1 - SERIAL AND PARALLEL PROCESSING

That serial processing takes place in the brain is quite apparent and widely accepted. What may be less obvious are the numerous operations executed in parallel, making the visual system a highly distributed system. Parallel processing starts already in the retina, the obligatory entry point of all external visual information to the brain. The retina is not the equivalent of a single sensitive film from which neural images are formed. It is better compared to millions of tiny and overlapping neural films, each one of them breaking-up the optical image formed by the eye and transmitting a separate filtered version for further visual processing (Shapley and Perry, 1986). Hartline (1938) was the first to establish that single ganglion cells respond to restricted portions of space. By dissecting and recording from individual optic nerve fibers in the frog, he observed discharges only when specific areas of the retina were illuminated. This region he defined as the “receptive field” of the neuron, being the first to use this denomination for a sensory system. Hartline, however, used a single dot of light to stimulate the retina and could not, therefore, advance further into the detailed structure of ganglion cell receptive fields. Using two independently controlled light beams, Kuffler (1953) was able to describe the centre-surround structure of ganglion cell receptive fields in the cat retina. He reported that the receptive fields had a central region which had a discharge pattern opposite of that found in the surround. The “ON” center ganglion cells required luminance increments for the center, and decrements for the surround, in order to discharge. The reverse was true for the “OFF” center cells. Interestingly, retinal ganglions cells responded very poorly to homogenous illumination over their receptive fields. This property introduced an important concept in visual processing: relative contrast is far more important for information encoding than absolute luminance. But why have two complementary systems of “ON” and “OFF” center retinal ganglion cells? Schiller *et al.* (1986) provided insight to this question by selectively blocking the “ON” center pathway with intra-vitreous injections of APB (2-amino-4-phosphonobutyrate) in monkey retina. Detection of light increment but not light decrement was severely impaired, suggesting that both

“ON” and “OFF” systems are necessary to yield equal sensitivity for both incremental and decremental light stimuli.

In addition to the “ON” and “OFF” center systems, the retina is also the origin of the magnocellular and parvocellular visual pathways (reviewed in Merigan and Maunsell, 1993). Both pathways are considered to work in parallel performing complementary functions. The most striking difference between them is the sensitivity of the parvocellular pathway to color, absent for the magnocellular system. Parvocellular neurons also show a more tonic response to persistent light stimulation when compared to magnocellular neurons. The magnocellular pathway, however, is much more sensitive to contrast than the parvocellular system. For other dimensions such as temporal and spatial frequency sensitivity, both systems cover a wide range of values despite significant differences in their mean response.

The segregation between the magno- and parvocellular pathways is preserved in the projections from the retina to the lateral geniculate nucleus of the thalamus, as evidenced by physiological (Schiller and Malpeli, 1978) and anatomical (Conley and Fitzpatrick, 1989; Perry *et al.*, 1984) studies. Projections of both pathways from the LGN to the primary visual cortex are also believed to remain segregated. Hubel and Wiesel (1972) verified that projections of the magnocellular pathway terminated preferentially in layer 4C α , while projections of the parvocellular pathway terminated preferentially in layer 4C β of the primary visual cortex. The intrinsic connectivity of V1 and its pattern of projections to downstream visual areas suggested that the segregation between the magno- and parvocellular system could pervade throughout the visual system. Early studies, for example, reported that layer 4B received inputs from layer 4C α but not from layer 4C β (Lund, 1988), implying that neuronal processing in layer 4B was dominated by the magnocellular system. This was particularly relevant because layer 4B provides major projections to MT, an area of crucial importance to visual motion processing. Based on the evidence that distinct channels of information arising in the retina remain segregated to the highest levels of the cortex, Livingston and Hubel (1988) proposed that the visual system comprised two largely independent subsystems. One, mainly derived from the parvocellular pathway, would mediate visual behavior related to color and form. The other, dependent on the magnocellular pathway, would be responsible for the perception of movement and depth. A vast amount of anatomical and physiological evidence, however, suggested intense interactions between the magno- and parvocellular systems already in V1, and that their segregation was far from complete (Merigan and Maunsell, 1993). Sawatari and Callaway (1996), for example, reported that 4B layer neurons do in fact receive projections from layer 4C β , and that the parvocellular system does indeed project to areas responsible for motion processing.

Another influential model which emphasized parallel processing in the visual system came from the work of Ungerleider and Mishkin (1982) and Mishkin *et al.* (1983). These authors also proposed the existence of two pathways for visual processing. However, different from the proposal of Livingstone and Hubel (1988), their model did not rely on the segregation of the magno- and parvocellular pathways. Mishkin and collaborators argued that the primary visual cortex and not the retina was the major source of two pathways. One of the pathways, the ventral stream, interconnected the primary visual cortex with the inferior temporal areas and enabled the identification of objects. The other pathway, the dorsal stream, interconnected the primary visual cortex with parietal areas and allowed for the localization of objects. Experimental evidence for this model relied heavily on lesion studies performed in primates. Pohl (1973) demonstrated a dissociation of visual effects after inferior temporal and posterior parietal lesions in monkeys. Temporal but not parietal lesions produced severe impairment on object discrimination tasks, suggesting that the inferior temporal cortex participates mainly in acts of noticing and remembering the quality of objects. Parietal but not temporal lesions, on the other hand, produced deficits in localization tasks, suggesting that the posterior parietal cortex is concerned with spatial relations among objects and not their intrinsic qualities.

We usually experience our perceptions as single and unique events. Therefore, parallel processes being executed in our brains need to be eventually bound together into coherent percepts and actions. We still lack, however, a general mechanism for perceptual binding that is supported by solid experimental evidence. Mishkin and collaborators argued that the ventral and dorsal streams have both connections to the temporal and frontal lobe, and that each of these target areas constitute a potential site of convergence for object and space information. Single cells responding to the location of a specific object in space have been indeed described in the entorhinal cortex (Suzuki *et al.*, 1997) and hippocampal formation (Rolls *et al.*, 2005). This solution for perceptual binding, however, only exacerbates the problem of “combinatorial explosion” already discussed for the “grandmother cell” proposal. Additionally, a growing number of reports show appreciable anatomical cross-talk between the ventral and dorsal streams (Felleman and Van Essen, 1991; DeYoe and Van Essen, 1998), suggesting that binding may alternatively take place in a distributed manner rather than at highly convergent sites. Alternative mechanisms for perceptual binding, based on the precise timing of spiking responses, have been proposed and will be discussed below (Section 1.3.2). The advantage of such mechanisms is that they are flexible and can operate at various levels along the visual pathway. But they too face challenges posed by the architecture of the visual system. Consider, for example, the difference in conduction velocity for discharges traveling along fibers of the magno- and parvocellular pathways. The stouter magnocellular pathway cells conduct impulses more rapidly (Gouras, 1969). Therefore, retinal signals carrying

information about color appear to be propagating some milliseconds slower than signals coding for other properties of the same object.

1.1.2 - MODULAR AND TOPOGRAPHIC ORGANIZATION OF THE VISUAL SYSTEM

Mountcastle (1957) observed that nearby neurons recorded in the cat somatosensory cortex showed very similar response properties: they had almost identical receptive fields and responded to the same class of peripheral receptors. By reporting that neurons with similar response characteristics were organized in thin cylinders spanning all cortical layers, Mountcastle was the first to describe the “cortical column” and to consider it as an independent unit of function. A comprehensible functional role for the cortical column, however, was only attributed a few years later by the work of Hubel and Wiesel in the visual system. Recording in the anesthetized cat, Hubel and Wiesel (1959) discovered that neurons in the primary visual cortex were selective to features that retinal and geniculate neurons were not, namely the orientation and sometimes the direction of motion of the visual stimulus. Moreover, they demonstrated that orientation selectivity was a main feature determining the organization of the cortical column in area V1 (Hubel and Wiesel, 1962, 1963). In line with their hierarchical model of visual processing, they went on to suggest that the columnar organization of V1 enabled the successive transformations of receptive field structure (Hubel and Wiesel, 1968). The first step consisted in transforming cells with concentric center-surround receptive fields, as observed in the LGN-recipient layer 4C, into neurons with selectivity for orientation. Subsequent steps comprised the transformation of orientation-selective units into neurons with successively higher levels of complexity (complex and hypercomplex cells). Gradually, columns emerged as a fundamental unit of cortical architecture leading eventually to the concept of a hypercolumn (Hubel and Wiesel, 1974). Essentially, a defined portion of the visual field would be represented in the primary visual cortex by cells coding for the full range of orientation selectivity. A hypercolumn would, therefore, encompass the complete set of orientation columns representing a defined portion of visual space corresponding approximately to the size of the receptive fields. Thousands of hypercolumns, arranged side by side on the two dimensional plane, would give rise to the modular organization of the primary visual cortex. Apart from the intense set of connections within a single column (Lund, 1988), modulatory interactions between columns are accomplished by long-range horizontal projections connecting columns with similar orientation preferences (Gilbert and Wiesel, 1979, 1983).

Another important aspect of V1 organization is that maps representing feature domains, such as orientation selectivity, must coexist with a topographic map of the visual world. Hubel (1982b) wrote that in the beginning of his scientific career he was always surprised with the constant thickness of the striate cortex. Due to the fact that there is a much larger number of ganglion cells in the fovea as compared to other regions of the retina, he expected the cortex representing the

fovea in the striate cortex to be correspondingly thicker. Systematic mapping experiments, however, revealed that the visual field is represented in the area and not in the thickness of V1 cortex (Daniel and Whitteridge, 1961). In addition to retinal position and stimulus orientation, ocular dominance columns are also represented in V1 cortical surface. The accommodation of several dimensions into a two-dimensional plane gives rise to the anisotropic representation of V1 (Gattass *et al.*, 2005). Approximately half of V1 surface is devoted to the representation of the central 5 degrees of the visual field (Gattass *et al.*, 1987), implying that a huge proportion of cortical tissue is dedicated to the processing of stimuli presented at our center of gaze. As it will be discussed below (Section 1.2.4), attentional mechanisms further allocate resources in space and time in order to enhance the processing of behaviorally relevant stimuli.

As outlined above, local features of an object will activate spatially distributed neurons. Filtering mechanisms, which start in the retina and LGN and continue in the cortex, decompose the visual image into borders defined by contrast, orientation and color among others. The corresponding neurons coding for these features are usually located in separate columns or even in different visual areas. Objects are usually not alone in the visual scene, but appear superimposed on a background or mingled with other objects. We perceive objects, however, as single coherent entities. How does the visual system manage to segregate elements apart and group together features belonging to the same object? This topic will be further addressed in Section 1.3 and in Chapters 2 and 3.

1.2 - COOPERATIVE MECHANISMS OF NEURAL ACTIVITY

How fast and how precise can visual information processing be? Evidence from event-related potential studies indicates that neural categorization of complex visual scenes can be very fast, taking place within less than 150 ms after stimulus presentation (Thorpe *et al.*, 1996). This result apparently challenges the mechanisms of visual processing based on long integration time windows for firing rates, with the simple argument that it would be too slow. The weak projections from the thalamus to the cortex are believed to rely on synchronization in order to increase their efficacy (Bruno and Sakmann, 2006). This indicates that visual processing can also be very precise. Another set of evidence suggesting that precise timing is relevant for neuronal processing comes from studies on learning and plasticity. Markram *et al.* (1997) and Bi and Poo (1998) described a few years ago the spike time-dependent plasticity (STDP). These authors essentially showed that precise time relations (on the order of milliseconds) between pre- and postsynaptic activation are determinant for synaptic plasticity. Thus, spikes contributing to the discharge of the postsynaptic

cell would lead to long-term potentiation (LTP) at the synapse, while spikes that arrive after the discharge would lead to long-term depression (LTD) at the synapse. It has been argued that visual processing follows the same basic rules as those used for plasticity and learning (Singer, 1993). This is because synaptic strength, which is refined in an experience-dependent manner, is a major determinant of how neurons participate in an ensemble.

The working hypothesis here is that the brain uses the time domain as an additional dimension in order to integrate and process visual information (Singer, 1999). The prediction is that this mechanism would be approximately one order of magnitude faster than those relying on long integration time windows for firing rate (Harris, 2005). Speed, precision and flexibility would be attained by dynamic and cooperative mechanisms of neuronal activity. The term “cooperative dynamics” is meant to indicate that groups of neurons are able of coordinating their activity in a very precise time frame (on the order of milliseconds). For this to be possible, the nervous system must not only support precise time relations in its neuronal activity (encoding), but must also be able to read out these relations and use them in a meaningful way for further processing (decoding). Additionally, the brain would need an internally self-generated time base to serve as reference for neuronal processing, independent of external stimulus timing. The conceptual framework and candidate mechanisms capable of implementing such a coding strategy in the brain will be presented in this section.

1.2.1 - SYNCHRONOUS PROCESSES IN THE VISUAL SYSTEM

Pioneering work done by Wolf Singer, Charles Gray and collaborators provided the experimental ground for how the time domain could be used for neuronal coding (Gray and Singer, 1989; Gray *et al.*, 1989). A major innovation in their experimental approach was the simultaneous recording of spiking activity and local field potential (LFP). The LFP was taken as a measure of synchronized postsynaptic activity originating from the population of neurons recorded around the electrode tip. A prominent feature in their results was that the LFP exhibited oscillations with a frequency at around 40 Hz (gamma frequency band), showing that an ensemble of neurons was capable of engaging into coordinated activity of high temporal precision. Spiking activity recorded from the same electrode did not necessarily exhibit gamma oscillations. However, neuronal discharges tended to occur at specific phases of the LFP, showing that synchronized membrane fluctuations determined spike timing. Additionally, oscillations were dependent on, but were not phase locked to the stimulus, suggesting that the time base for rhythmic oscillations was internally determined. These results gave rise to the binding-by-synchronization hypothesis, which will be discussed in Section 1.3.2. Work in humans also supports the notion that long range phase synchronization in the gamma band may be capable of bringing together a widely distributed set of neurons into a coherent ensemble (Rodriguez *et al.*, 1999). Moreover, desynchronization of neural ensembles

would be equally important when disengaging from one cognitive state and entering another. But before discussing the role of synchronization in perceptual binding, the neuronal mechanisms of oscillatory activity will be addressed, since they are intimately associated with synchronous activity in the brain.

1.2.2 - OSCILLATORY PROCESSES IN THE VISUAL SYSTEM

Oscillatory processes in the central nervous system can be observed at the macro-, meso-, and microscopic scales (see Buzsáki, 2006). The electro- and the magnetoencephalograms are non-invasive methods widely used to probe oscillatory activity of a large number of neurons at the macroscopic level. The meso- and microscopic scales of oscillatory activity can be observed with intracortical microelectrode recordings. Using this technique, a compound signal composed of spiking activity and local field potential (LFP) can be acquired. Low-pass filtering can later isolate the LFP from the spikes. Depending on the electrode properties, the LFP can express the average behavior of either tens, hundreds or thousands of neurons (Logothetis, 2003a, 2003b). Since the LFP reflects an average population activity, it is specially sensitive to coordinated fluctuations in membrane potential. Synchronous extracellular currents, resulting from excitatory and inhibitory postsynaptic potentials (EPSPs and IPSPs, respectively), are believed to be the main components contributing to the generation of the LFP (Mitzdorf, 1987). The contribution of spiking activity to the LFP is believed to be negligible during normal brain activity. The reasons for this are twofold. Even though EPSPs and IPSPs have much lower amplitude as compared to spikes, they have a much longer duration (up to tens of milliseconds). This gives the postsynaptic potentials a higher chance of overlapping and summing with one another than is the case for spikes. Second, only a small number of neurons reach spike threshold at any given moment, while postsynaptic events are much more frequent. Therefore, features observed in the LFP are mainly the result of coordinated subthreshold postsynaptic processes. These features may not necessarily be oscillatory. But oscillatory processes observed in the LFP give a powerful insight into the synchronous activity going on in the brain. Despite the little contribution of spikes to the LFP, oscillatory activity can be clearly observed in the pattern of neuronal discharges. Gray and Singer (1989) reported that spike oscillations in cat area 17 usually occur in bursts. Every burst contained between 2 and 5 spikes, accounting to an intra-burst firing rate of around 800 spikes per second. The oscillatory structure of the firing pattern was given by the regular reoccurrence of bursting activity in intervals of approximately 15 to 20 ms. Additionally, they showed that the oscillations in the spiking activity and in the LFP were strongly correlated: the burst events occurred preferentially during the depolarizing phases of the LFP.

How is oscillatory activity generated in the brain? Are the basic mechanisms localized within individual neurons or is it dependent on the interaction among neurons? In other words, is it a

cellular or a network property? Although we do not have a final answer to this question, it is likely that oscillatory activity is an emergent property involving various scales. Gray and McCormick (1996) described single cells in cat area 17 capable of generating 20-70 Hz repetitive burst firing during visual stimulation, similar to the behavior of oscillatory cells described by Gray and Singer (1989). By recording intracellularly, they showed that suprathreshold depolarizing current injections was enough to trigger oscillatory behavior. Additionally, they observed no evidence of subthreshold oscillations in these cells prior to the current injection, showing that the oscillatory behavior could not be explained by the pattern of inputs to the neuron. Moreover, these neurons (named chattering cells by the authors) were found to have axon collaterals that extended horizontally and ramified within layers 1, 2, 3, and 5, suggesting that they are in a key anatomical position to recruit a large population of cells into synchronously firing assemblies.

Recent experimental evidence, however, has increasingly pointed to another class of neurons as the major player in the rhythmic pacing of neuronal activity. Classically, inhibitory neurons have been known to shape response properties (Sillito, 1975), and to improve the signal-to-noise ratio of neuronal activity through gain control mechanisms (reviewed in Buzsáki *et al.*, 2007). Recordings from slices of rat hippocampus and neocortex, however, have revealed yet another potential role for inhibitory neurons in the brain (reviewed in Bartos *et al.*, 2007). Wittington *et al.* (1995) reported robust 40 Hz gamma oscillations emerging from networks of inhibitory neurons. Interneurons generated rhythmic activity regardless of whether their excitatory drive was rhythmic. The gamma oscillations were triggered by the activation of metabotropic glutamate receptors, but they were actually generated by recurrent inhibitory connections dependent on GABA_A receptors. Important properties, such as the oscillation frequency, were determined by the kinetics of the inhibitory postsynaptic potential. Inhibitory networks would, therefore, be largely responsible for the dissemination of higher frequency activity in the cortex by imposing rhythmic inhibition onto the pyramidal cells (Hasenstaub *et al.*, 2005). Experiments employing optogenetic methods provided the first direct evidence that fast-spiking inhibitory neurons causally and selectively generated gamma oscillations (Cardin *et al.*, 2009). Activation of pyramidal neurons, on the other hand, modulated only lower frequency oscillations.

Neuronal oscillations *in vivo* have been associated with several brain functions such as motor control (Murthy and Fetz, 1996) and perception (reviewed in Uhlhaas *et al.*, 2009, see appendix). Alternatively, psychiatric diseases have been connected with dysfunctions in oscillatory patterns (reviewed in Uhlhaas and Singer, 2010). Robust high frequency oscillations can already be observed in the retina (Neuenschwander and Singer, 1996). Since the mammalian retina receives no feedback projections from higher brain structures, it is particularly interesting to observe how coordinated rhythmic activity emerges on the first stage of visual processing. Castelo-Branco *et al.*

(1998) demonstrated that retinal oscillations are reliably transmitted to the LGN and, under certain conditions, to the cortex, in a phenomenon the authors termed feedforward synchronization. Neuronal oscillations show a wide range of frequencies, ranging from approximately 0.05 Hz to 500 Hz (reviewed in Buzsáki and Draguhn, 2004). Different frequency bands have been associated with different brain states. The specific oscillatory pattern is usually complex, with different frequency bands either coexisting or competing with each other. Berger (1929), who performed pioneering studies in human EEG, first described the 10 Hz oscillation while recording electric potentials from the scalp of his 15 year old son Klaus. This rhythmic activity, initially named Berger waves and currently known as alpha waves, was typically observed in subjects under rest (sitting quietly with eyes closed). Engagement into “active” behavior caused dramatic changes in the brain waves. Simply opening the eyes or solving math problems with the eyes shut shifted the oscillation frequency to the (higher) beta range. Curiously, the frequency shift was accompanied by a decrease in oscillation amplitude. Influenced by the work of Hans Berger, idle behavioral states have been classically associated with “synchronized” brain activity due to the high amplitude of the alpha oscillations. Attentive behavior, on the other hand, has been linked to “desynchronized” brain states due to the low amplitude of the oscillations. Desynchronized states, despite the low amplitude, are characterized by higher frequency oscillations. An effective way to “desynchronize” the EEG is to activate the mesencephalic reticular formation (MRF). Using this procedure to simulate arousal states in the anesthetized cat, Munk *et al.* (1996) reported that low frequency oscillations were suppressed and gamma band oscillations induced. In a subsequent work, Herculano-Houzel *et al.* (1999) demonstrated that aroused states, classically termed as “desynchronized” states, were associated with precise synchronization of activity at higher frequencies (beta and gamma frequency bands). The term “desynchronized” state seemed, therefore, inappropriate to describe what was happening for higher frequencies during arousal. Accordingly, the authors suggested the use of the term “activated state”, instead of “desynchronized state”, for the aroused or attentive brain.

The study of the evoked potential has been central to the field of electroencephalography. This trend can in part be explained by the clinical applications of the evoked potential (Nuwer, 1998). Visual evoked and event-related potentials are obtained by stimulus-locked averaging of the EEG signal. Therefore, signal components common to all trials are preserved, while all other signals unrelated to the stimulus-onset event are averaged out. This procedure substantially increases the signal-to-noise ratio of the measurements. However, if one is interested in internal states of the brain and its self-generated dynamics, stimulus-locked averaging has one major disadvantage: it eliminates ongoing neuronal activity. Due to the fact that induced gamma oscillations have a different phase in each single measurement, they are typically cancelled out when extracting the evoked potential. The investigation of induced activity requires the analysis of single-trial events.

Due to signal detectability, however, this constitutes a major technical challenge. The advent of the voltage sensitive dyes enabled valuable insight into the ongoing dynamics of orientation maps, providing a framework of how internal context can influence incoming visual information (Kenet *et al.*, 2003). Intracortical LFP recordings also exhibit a high signal-to-noise ratio, allowing oscillatory activity to be evaluated in single trials. Fries *et al.* (2001a) observed that ongoing gamma oscillations during spontaneous brain activity could predict the single-trial response latency of visual neurons to external stimulation.

A detailed investigation of how gamma activity is related to visual processing has been extensively performed by Singer and collaborators during the last 20 years. In the first of a series of publications, Gray and Singer (1989) described the 40 Hz oscillations in cat visual area 17. These gamma oscillations, which actually ranged from 30-60 Hz, were highly dependent on stimulus properties, could be observed both in the spikes and the LFP, and were not phase-locked to stimulus onset. Additionally, LFP gamma power exhibited a similar orientation tuning as the one observed for the firing rate responses, suggesting that the generation of gamma oscillations was restricted to a small volume of cortical tissue equivalent to a single column. Peak oscillation frequency, however, did not vary significantly as a function of either orientation or direction of stimulus movement. Two subsequent publications further explored the auto- and the cross-correlation of neuronal discharges. Gray *et al.* (1990) reported that complex cells in area 17 were more prone to oscillate than simple cells, and that layers 2, 3 and 5 showed a higher incidence of oscillatory neurons than layers 4 and 6. Moreover, oscillatory activity was enhanced with binocular stimulation and occurred preferentially in response to moving as compared to stationary stimuli. The velocity of the stimulus, however, could strongly modulate oscillation frequency: the faster the stimulus, the higher the frequency. Engel *et al.* (1990) investigated if oscillatory activity was correlated between different sites recorded in cat area 17. Sites with overlapping receptive fields showed significant synchronization even if their orientation preferences were different. For sites with non-overlapping receptive fields, however, correlations decreased with increasing differences in the orientation preference or with increasing distance in the cortex. It is important to note that cells exhibiting correlations did not necessarily fire simultaneously. Usually one site fired systematically before the other, maintaining a constant phase-relationship during their oscillatory responses.

Another set of work investigated the synchronization of activity between cortical areas. Eckhorn *et al.* (1988) demonstrated correlated neuronal activity between areas 17 and 18 in the cat, while Engel *et al.* (1991c) reported synchronization of oscillatory activity between areas 17 and PMLS. Synchrony within the same area was generally stronger than interactions between areas. The demonstration of synchronization between the two hemisphere, however, provided great insight into the nature of correlated activity in the cortex. It was generally assumed that temporal

correlation with zero phase-lag reflected common input and could not be accounted for by reciprocal connections with finite conduction delays. Recording simultaneously from both areas 17, Engel *et al.* (1991a) showed that synchronization between hemispheres was of comparable strength as the one found within area 17. Additionally, interhemispheric synchronization could occur with zero phase-lag, despite the finite transcallosal conduction delays in the range of 4-6 ms. This finding supports the hypothesis that synchronization is achieved by cortico-cortical connections rather than by common input from the thalamus (synchronization was abolished with the transection of the corpus callosum).

Recent work performed in the awake animal has further elucidated the role of gamma oscillations in visual perception. Gray and Di Prisco (1997) showed that the gamma activity obtained in the awake cat has the same properties as the one described for the anesthetized preparation. It occurred, however, with greater probability and larger amplitude when the animal was alert. Therefore, as reported by Munk *et al.* (1996) and Herculano-Houzel *et al.* (1999), the state of arousal significantly modulates the strength of oscillatory firing (Section 1.2.4 will address how oscillatory firing is modulated by attention). Results obtained in the strabismic cat during conditions of binocular rivalry (Fries *et al.*, 1997) indicate that gamma activity is also part of the competitive mechanisms selecting which eye which will convey information to further processing stages. In addition to how behavioral states modulate gamma processes, what is the impact of stimulus structure on high frequency oscillations? Physiological responses of visual neurons have been traditionally studied by using artificial stimuli. In the case of the primary visual cortex, this usually includes oriented bars or gratings moving in the preferred direction, speed, spatial frequency and contrast of the recorded neurons. Kayser *et al.* (2003) used natural movies to study the response of neurons in area 17 of the awake cat. The activity patterns elicited by drifting gratings were quantitatively and qualitatively different from the ones elicited by natural movies. While gratings induced single band 40 Hz oscillations, natural movies induced oscillations distributed throughout the spectrum.

Work done in the awake monkey has extended the findings on gamma oscillations initially described in the cat. Friedman-Hill *et al.* (2000) reported that gamma activity in monkey V1 is also highly dependent on the stimulus. Stimuli at the preferred orientation were nearly seven times more likely to induce oscillatory firing than those presented at the orthogonal orientation. Neurons rarely exhibited gamma-band activity in the absence of stimulation and, as in the cat, stimulus velocity was the only parameter that systematically influenced oscillation frequency. The pattern of synchronization between sites was also similar to the cat data (Maldonado *et al.*, 2000). The magnitude and probability of synchronous firing was found to be inversely related to the spatial separation between cells. Additionally, the presence of gamma oscillations in the firing patterns

was a strong predictor of synchronous firing between sites. The intimate relationship between oscillation and correlation suggests that neuronal rhythmicity is an important mechanism contributing to synchronization.

Does oscillatory activity have a causal relationship to behavior? The answer to this question has always been limited by the techniques capable of selectively disrupting oscillations without affecting firing rates. Recently developed optogenetic methods may prove valuable in this respect. Additional work, specially in the behaving animal, will be needed to reveal the physiological mechanisms of how oscillations can assist neuronal processing.

1.2.3 - INSTRUMENTAL ROLE OF OSCILLATORY ACTIVITY IN NEURONAL PROCESSING

Before addressing the functional role of oscillations, one is faced with the numerous frequency bands coexisting in the brain (Buzsáki and Draguhn, 2004). How do the various oscillatory frequencies interact with one another? Lakatos *et al.* (2005) suggested that the different frequency bands are hierarchically organized, in a way that the phase of delta oscillations modulates theta amplitude, and the phase of theta oscillations modulates gamma amplitude. In a subsequent study, Lakatos *et al.* (2007) proposed a novel mechanism for multisensory integration based on oscillations. The authors observed that somatosensory stimuli were able to reset the phase of low-frequency neuronal oscillations taking place in the auditory cortex. In this way, incoming auditory inputs could arrive during an ideal, high excitability phase of the oscillatory cycle. Due to the hierarchical organization of the various frequency bands, the phase-reset event impacts the whole range of the frequency spectrum. von Stein and Sarnthein (2000), on the other hand, proposed a complementary role for the different frequency bands. Long range integration of signals in the brain requires lower frequency oscillations, such as alpha and theta, while local integration is performed in the gamma frequency band. As mentioned before, investigations on the causal role of oscillations in neuronal processing are limited by the techniques available to selectively disrupt oscillations without affecting the rate of discharges. Therefore, most of the work done so far has been restricted to correlative evidence associating changes in behavior to changes in oscillatory activity. One of the few exceptions is the report of Robbe *et al.* (2006). Using cannabinoids, the primary psychoactive constituent of marijuana, the authors were able to selectively disrupt theta and gamma oscillations in the rat hippocampus without significantly affecting firing rates. They found that the reduction of theta activity intimately correlated with memory impairment in a hippocampus-dependent task.

The oscillatory cycle can be divided in two phases: the depolarizing and the hyperpolarizing phase. EPSPs arriving during the depolarizing phase are much more likely to elicit spikes in the postsynaptic neuron as compared to EPSPs arriving during the hyperpolarizing phase. Therefore,

the main impact of oscillations on the membrane potential would be to coordinate the neuronal excitability of sub-populations of neurons. Higher frequencies would cause faster fluctuations of the membrane potential as compared to lower frequency oscillations. Neurons integrate incoming post-synaptic potentials in order to discharge. How long is the integration window, and how sensitive are neurons to coincident incoming EPSPs (Singer, 1999; Harris, 2005)? Does the firing probability of the cell change depending on the underlying oscillation frequency? Azouz and Gray (2000, 2003) used intracellular recordings *in vivo* to show that spiking threshold is not fixed but highly dynamic. The authors observed an inverse relation between membrane potential slope and spiking threshold. Firing probability was enhanced during rapid depolarizations of membrane potential as compared to periods where depolarization was slow. This suggests that fast variations in membrane potential, as it is usually the case during gamma oscillations, facilitate spike output. Following the principle that neuronal oscillations can serve as a fundamental mechanism for coordinating activity in the brain, Fries (2005) proposed the communication through coherence (CTC) hypothesis. Through this mechanism, different neuronal groups could selectively communicate by means of coherent oscillatory activity. Due to the rhythmic changes in excitability, the different phases of the oscillatory cycle would open windows for communication, making reciprocal input optimally timed and thereby maximally effective. The first experimental evidence supporting the CTC hypothesis was obtained in humans (Schoffelen *et al.*, 2005). The authors observed that the coherence of gamma oscillatory activity between neurons in the motor cortex and the spinal cord increased with the readiness of the subjects to respond. Corroborating evidence in the cat and monkey visual systems was subsequently reported by Womeldorf *et al.* (2007).

Oscillatory activity measured in the LFP reflects coordinated processes taking place in a sub-population of neurons. Within this temporal framework, the timing of neuronal discharges relative to the oscillatory cycle could be used to code for additional information. An elegant experimental finding, the hippocampal phase precession, was the first to support this hypothesis. O'Keefe and Recce (1993) observed that the discharge timing of pyramidal cells relative to the theta oscillation cycle occurred successively earlier as the rat moved across the place field, probably because pyramidal neurons received successively stronger excitatory drive and could discharge before depolarization reached its maximum. The authors argued that the unidirectional precession of spike timing during spatial behavior could be used to improve the accuracy with which place cells code for space. Harris *et al.* (2002) extended the findings of O'Keefe and Recce (1993) in a very fundamental way. They investigated the relation between spike timing and the ongoing theta rhythm when the rat engaged in non-spatial tasks, such as wheel running (with stationary head position) and REM sleep. What they observed was that phase precession is the manifestation of a more fundamental principle governing the timing of pyramidal cell discharge. In tasks where the

animal did not engage in spatial behavior phase precession was still clearly present. Spike phase correlated with instantaneous discharge rate and still preceded unidirectionally in the theta cycle, suggesting that excitatory drive to the pyramidal cells is the major factor causing phase precession. Fries *et al.* (2007) proposed an equivalent phenomenon to the hippocampal theta phase-precession for the neocortex, but using gamma oscillations instead. The advantages of this mechanism would be two-fold. Phase precession is a powerful encoding strategy because the excitatory input to the pyramidal cell is converted into a temporal code (higher amplitude excitatory drive generates spikes earlier in the gamma cycle). This mechanism would be fast since readout could be done within a single oscillation cycle and would not need to rely on rate integration. The second advantage is an increase in the signal-to-noise ratio. Pyramidal cells provide the main input to inhibitory neurons. Therefore, the first pyramidal cells to discharge would trigger an inhibitory drive preventing other pyramidal cells from firing. Through this competitive mechanism only the strongest excitatory drive would elicit spikes and thereby be selected for further processing. Chapter 5 will provide experimental evidence for this mechanism in monkey V1.

1.2.4 - ATTENTIONAL MODULATION OF OSCILLATORY ACTIVITY

Even simple visual scenes provide our retina with an overwhelming amount of information. The capacity of our visual system to process this information, however, is rather limited (Desimone and Duncan, 1995). By selectively allocating resources in space, in time or to certain features, attention can significantly enhance neuronal processing for behaviorally relevant objects, events or attributes of the visual scene. In this way, the study of attention has provided considerable insight into the endogenous processes going on in the brain (reviewed in Reynolds and Chelazzi, 2004; Fries, 2009).

As mentioned in Section 1.1.2, the early visual system is topographically organized. This architecture is particularly suitable for implementing models of spatial attention, since neurons representing neighboring positions in the visual field are also located nearby in the brain. Not surprisingly, the “focus” of our attention is believed to be represented by a neuronal “spotlight” that enhances activity in the corresponding topographic region of the early visual cortex (Crick, 1984). Attentional modulation in the visual pathway can take place as early as in the thalamus. McAlonan *et al.* (2006) provided experimental evidence supporting the notion that a “spotlight” of spatial attention can be implemented by thalamic reticular neurons, thereby gating the information that reaches the cortex. The attentional modulation of neuronal activity increases both along the hierarchy of visual processing (Mehta *et al.*, 2000; Maunsell and Cook, 2002) and with task difficulty (Spitzer *et al.*, 1988; Boudreau *et al.*, 2006). Pioneering work by Moran and Desimone (1985) showed that attending to different objects within the receptive field modulated the response of single cells in monkey area V4. It also introduced the idea that attention is an emergent property

based on the hypothesis that objects compete for neuronal representation (Desimone and Duncan, 1995). Competition, however, would be biased towards information and objects relevant for behavior. Subsequent work in areas MT and MST also demonstrated attentional modulation for single neurons in the dorsal visual stream (Treue and Maunsell, 1996). Attentional systems are also capable of selecting specific features of the visual scene, such as color or direction of motion, independent of their spatial location (Maunsell and Treue, 2006). Finally, attention has been reported to modulate not only the magnitude, but also the selectivity of neuronal responses (Spitzer *et al.*, 1988; Motter, 1993; Martinez-trujillo and Treue, 2004).

Attention is one of the most investigated fields in visual neuroscience. Despite this fact, we still lack a unified mechanism for how attentional modulation is implemented in the brain. A particularly interesting proposal is that attention and the encoding of contrast share a close relationship (Martinez-Trujillo and Treue, 2002; Reynolds and Desimone, 2003). Paying attention to an object would, therefore, be equivalent to increasing its apparent contrast. In this way, attention would not need a separate neuronal substrate, but would make use of already existing ones. As it is normally the case with emergent properties, however, this proposal alone seems insufficient to account for the whole problem. Attention requires the coordinated activity of numerous brain areas, ultimately bringing together perception and behavioral output. How can large scale coordination take place efficiently in a short time scale? Ascending projections from the mesencephalic reticular formation (MRF) modulate cortical activity in a widespread manner, and are thought to regulate both consciousness and arousal (Moruzzi and Magoun, 1949). A particularly prominent feature in MRF stimulation experiments is a profound change in the pattern of brain oscillatory activity (Munk *et al.*, 1996; Herculano-Houzel *et al.*, 1999). Activated states in the cat visual cortex were characterized by high frequency gamma oscillations, which were synchronized across different recording sites. These findings suggests that gamma activity may serve as a coordinating mechanism not only during states of arousal, but also during states of attention. An influential work published by Fries *et al.* (2001b) provided direct evidence that spatial attention modulates gamma power and gamma-band synchronization in monkey area V4. Subsequent work confirmed these main findings under different behavioral tasks and recording procedures (Bichot *et al.*, 2005; Taylor *et al.*, 2005). Recent investigations have put special emphasis on how attention modulates synchronization between different cortical areas (Roelfsema *et al.*, 1997; Buschman and Miller, 2007; Saalmann *et al.*, 2007; Doesburg *et al.*, 2008; Gregoriou *et al.*, 2009). Future studies in this direction will be important to reveal whether synchronous neuronal oscillations can serve as a unified mechanism capable of coordinating large-scale activity in the brain.

1.3 - FIGURE-GROUND SEGREGATION AND FEATURE BINDING

Intuitively, visual processing is usually conceived as a chain of serial operations, starting in the retina and ending up in temporal, parietal and frontal regions. The higher order areas would eventually control motor output and behavior. It is also widely recognized, however, that feedback projections are abundant in the visual pathway (Gattass *et al.*, 2005), even though their functional role has remained mysterious (Bullier, 2001). The metaphor involving forests, trees, sometimes even leaves, and which comes first or last in our perception illustrates an ongoing debate in visual neuroscience. The interplay between feedforward, feedback and local connections and their role on global and local perception is, therefore, central to this discussion (Hochstein and Ahissar, 2002).

Gestalt psychology, with its principle “the whole is different from the sum of its parts”, revolutionized the way we think about perception (reviewed in Rock and Palmer, 1990). Its founders were the first to elaborate on how perception can segregate objects from each other and from the background. To this end, Gestalt psychologists created a set of laws which predicted how perception would group separate elements into single objects. These laws state that elements tend to be grouped together if they are similar or close to one another, if they form a closed contour, or if they move in the same direction. Gestalt principles implicitly assumed, therefore, that grouping could occur early and automatically in the visual system. Interestingly, the functional organization of the early visual system suggests that this can indeed be the case. Oriented line segments, which are collinear and proximal to one another, can be readily perceived as contours of a single object (see section “Building expectations: New vistas for gamma oscillations” in the Appendix). Accordingly, receptive field activity in area V1 is specially sensitive to collinear flanks in its immediate surround (Gilbert *et al.*, 1996). This property can be largely explained by the pattern of horizontal projections, which connect columns with similar orientation preferences (Schmidt *et al.*, 1997). Therefore, important Gestalt rules can be traced back to the functional anatomy of the early visual cortex. Another interesting example, using direction of movement as criteria, deals with the segregation of objects from their background. Ölüveczky *et al.* (2003) described a subset of ganglion cells that responded to motion in the receptive field center, but only if the wider surround moved in a different direction. Starting already in the retina, the visual system is able to use contextual information for figure-ground segregation. The notion that simple grouping mechanisms can derive from the built-in architecture of the visual system suggests that feature binding is a highly distributed phenomenon in the brain. As such, grouping would be an emergent property, being executed in a highly parallel way. As it will be addressed below, Singer and collaborators have proposed the binding-by-synchronization (BBS) hypothesis as a mechanism of how the brain

makes use of the Gestalt rules to further extract global properties of the stimulus. Before that, a short introduction to the binding problem will be given.

1.3.1 - THE BINDING PROBLEM

Does the binding problem actually exist? Wolfe and Cave (1999), citing various studies in human psychophysics, affirm that it does. One of the clearest evidences for this assertion comes from experiments in which binding fails. In a classical study performed by Treisman and Gelade (1980), the authors reported that human subjects can rapidly detect the individual features present in a visual scene. To bind the appropriate features into unitary percepts, however, focal attention was required. This was specially the case if the task being performed was demanding. In the absence of attention, the authors argued that the detected features remained unbound or “free floating” in perception. In a follow-up work, Treisman and Schmidt (1982) presented sets of objects for very short intervals. Subjects were required to direct attention to a pair of objects within a larger sample and to report their identity. Due to task overload, subjects were not able to direct attention to all objects in the sample. When asked about the properties of the unattended objects, illusory conjunctions occurred. Subjects, for example, erroneously attributed the color of object A to object B, and vice-versa for their orientation. The detected features did not have the opportunity to be appropriately bound together and, therefore, remained “free floating” in perception.

For the present project, the main argument suggesting that binding mechanisms are necessary in perception is based on the functional anatomy of the visual system. As discussed in Sections 1.1.1 and 1.1.2, different features and parts of the stimulus are represented at spatially segregated portions of the brain. It is assumed that this parallel processing needs to be eventually bound into a coherent percept. Additionally, it is assumed that simple forms of binding occur automatically in the early visual cortex, regardless of attention. One of the primary aims of this work was to investigate if feature binding can be subserved by synchronized activity in area V1 (Chapter 3).

1.3.2 - THE BINDING-BY-SYNCHRONIZATION (BBS) HYPOTHESIS

As put forward at the beginning of the introduction, the conventional view is that binding operations in the brain are carried out by fixed anatomical connections that converge into high level, conjunction-specific neurons. These neurons are generally referred to as “grandmother cells”. Limitations to this proposal, such as the “combinatorial problem”, were subsequently addressed. An alternative concept is that binding is an emergent property taking place throughout the visual system. The architecture of the visual pathways supports this hypothesis. Visual processing is performed by parallel pathways, which extract different features of the stimuli (Sections 1.1.1 and 1.1.2). Consequently, representations of the same object are scattered in different parts of the

neuronal tissue. The assumption pursued here is that these separate representations need to be further bound together.

Theoretical work done by von der Malsburg (1981) proposed that the strength of individual synapses could be modulated at a very fast time scale (in the order of milliseconds). The main idea was to have a flexible mechanism capable of creating a unique assembly of synchronously active neurons for every new percept. Crick (1984) speculated that focal attention, as described by Treisman and Gelade (1980), would be the agent responsible for transiently and dynamically modifying synaptic strength. We still lack the methodological tools capable of accessing large scale dynamic changes in synaptic strength as proposed by von der Malsburg. Work by Gray *et al.* (1989), however, provided solid experimental evidence that synchronously oscillating assemblies do exist in the brain and that they can subserve feature binding in the early visual cortex. The authors used bars in different configurations to stimulate pairs of receptive visual in area 17 of the cat. In the first configuration, a single long bar activated both receptive fields. This condition was compared to when the receptive fields were stimulated by separate bars. Synchronous oscillations between the pair of recording sites were significantly stronger when a single object stimulated both receptive fields. The authors argued that synchronization of responses reflected the global properties of the stimulus and could, therefore, serve as the neuronal substrate for feature binding. In subsequently published reviews (Singer and Gray, 1995; Singer, 1999), the authors further emphasized the advantages of synchronized activity. Apart from all the benefits regarding coding flexibility, one of the major advantage of synchronous discharges is that they optimally summate in target cell populations.

Following studies reported that synchronous oscillations between different visual areas were also sensitive to global stimulus features (Engel *et al.*, 1991c). Engel *et al.* (1991b) used the “conflicting bars” stimuli to verify if the BBS hypothesis also applied for overlapping receptive fields in cat area 17. The conflicting stimuli consisted either of a single moving bar or of a pair of superimposed bars moving in different directions. Since the recorded receptive fields usually had different orientation preferences, the single bar was shown in the intermediate orientation that best activated the cells. For the two-bar condition, each bar moved in a direction that optimally activated one of the respective receptive fields. Synchronization was systematically higher for the single bar condition, in line with the results of Gray *et al.* (1989) for non-overlapping receptive fields. Kreiter and Singer, 1996, while recording from area MT in the fixating monkey, were able to reproduce the results of Engel *et al.* (1991b) in the awake preparation. By using plaid stimuli, Castelo-Branco *et al.* (2000) made a significant contribution to the understanding of how synchronous activity may support surface segmentation in the early visual cortex. Plaids are composed of two superimposed grating stimuli (Adelson and Movshon, 1982). Gratings presented alone are capable of strongly activating

neurons in early visual areas. Therefore, when recording from pairs of sites, each of the two grating components of the plaid can be set to optimally activate one of the sites. Plaid stimuli can be perceived as two surfaces sliding over each other (component motion), or as a single surface moving in a direction that is intermediate to the movement of both gratings (pattern motion). Castelo-Branco and collaborators biased perception towards single or two surfaces by manipulating the luminance of the intersection where both gratings superimposed. The authors, therefore, devised an ingenious paradigm to test the BBS hypothesis during conditions of surface segmentation. The predictions were two. Neurons having similar orientation preferences should synchronize their activity when responding to a single grating because in this case they are also responding to the same surface. Additionally, this pattern of synchronous activity should not be disturbed when a second grating is superimposed. The second prediction refers to when the recording sites have different orientation preferences. In this case, when each site responds selectively to one of the grating components of the plaids, their synchronization should depend on the global properties of the stimulus. For the condition of component motion (two surfaces), no consistent pattern of synchronization should be observed between the sites due to the fact that they respond to different objects. The opposite is true for the pattern motion condition. Because they are responding to the same object, the prediction is that they synchronize their activity in the millisecond time scale. The authors were able to successfully demonstrate with recordings in areas 18 and PMLS of the anesthetized cat that the BBS hypothesis held true. Using the same basic paradigm, Thiele and Stoner (2003) tried to replicate the results of Castelo-Branco *et al.* (2000) in the awake fixating monkey. For one of their monkeys, Thiele and Stoner also performed behavioral tests where the monkey had to distinguish component from pattern motion. In this way, they confirmed not only that the monkey's perception was influenced by the transparency manipulations of the plaid stimulus, but also that their perceptual judgments matched those of humans. This constituted a major advantage in their study since they could claim that their physiological results were backed-up by behavioral data. In clear contradiction to the work of Castelo-Branco *et al.* (2000), Thiele and Stoner found higher synchronization for component motion as compared to the pattern motion condition, disproving the BBS hypothesis. Also recording in the awake fixating monkey, Palanca and DeAngelis (2005) further questioned the BBS hypothesis. The authors used either one or two polygons to stimulate receptive fields in area MT. Interestingly, the stimulation within the classical receptive field was kept constant. Configuration of the stimulus outside the receptive field is what defined if neurons were being stimulated by the same or different objects. Synchronization was indeed higher for conditions where receptive field pairs were stimulated by the same object. The authors argued, however, that the modulation was small relative to the variability of synchronization across sites. Moreover, higher correlation values were observed for overlapping and collinear sites, which are also known to be preferentially connected by horizontal projections.

Palanca and DeAngelis concluded that in these cases synchronous activity is an epiphenomenon of cortical wiring. For the case where receptive fields are non-overlapping and non-collinear, synchronization it is not a reliable predictor of feature grouping. Lamme and Spekreijse (1998) also argued that correlated activity was a byproduct of cortical architecture.

As one can see, the BBS is a powerful but controversial hypothesis awaiting further experimental testing. The critics of this proposal argue that the performance of individual neurons can equal behavioral performance (Ghose and Maunsell, 1999; Shadlen and Movshon, 1999). Indeed, there are studies showing that perception can be controlled by microstimulating local groups of neurons (Salzman *et al.*, 1990) or even single cells (Houweling and Brecht, 2008). On the other hand, as described several times above, neuronal activity in the brain can be precise within the millisecond time scale. This precision is correlated across regions, suggesting that activity in the brain is spatiotemporally coordinated. Experimental evidence reveals that specialized circuits actively generate different types of fast rhythmic activity, arguing in favor that coordinated activity can causally impact behavior, and is not simply an epiphenomenon of neural activity (Middleton *et al.*, 2008). For these reasons, the field will remain controversial for years to come.

1.4 - OUTLINE AND GOALS

Chapters 3 and 4 constitute the main projects of my work. The central goal of Chapter 3 was to test the BBS hypothesis in area V1 of the awake behaving monkey. Plaid stimuli were used in a paradigm similar to the one described by Castelo-Branco *et al.* (2000). In addition to auto- and cross-correlation analysis, coherence measures were applied in order to quantify synchronization between different recording sites. Since we were able to record from many sites in four monkeys, this study also offered an opportunity to characterize the dependency of gamma activity on the physical properties of the stimulus. In particular, we could observe how the peak frequency of the gamma oscillations varied across different individuals and eccentricities. In contraction to our initial hypothesis, synchronization in monkey V1 revealed not to be correlated with the global properties of the stimulus. On the contrary, gamma oscillations were shown to be dependent on cortical architecture and on the physical characteristics of the stimulus. This also held true for tasks where the monkey selectively attended to one of the plaid surfaces. Gamma and alpha oscillations, on the other hand, were strongly modulated by temporal expectation. Chapter 4 characterized this effect for different types of behavioral protocols where the monkey was required to direct attention in time. Recordings from different regions of V1 revealed that oscillatory activity was equally modulated throughout various eccentricities, suggesting a widespread effect in the cortex.

Temporal expectation was also tested in a paradigm where the monkey responded to Gestalt figures embedded in two dimensional arrays of Gabor patches (see section “Building expectations: New vistas for gamma oscillations” in the Appendix). Chapter 2 was a project done in collaboration with the group of Jerome Baron at the Federal University of Minas Gerais (Brazil). This work used sinusoidal plaid stimuli to study motion integration in the visual wulst of the awake owl. The visual wulst receives direct projections from the thalamus and is, therefore, considered analogous to the early visual area in mammals. Both Chapters 2 and 3 used plaid stimuli to study integrative mechanisms in the brain. While Chapter 3 focused on oscillatory activity, Chapter 2 addressed firing rates and how neurons in the visual wulst could either extract or integrate the motion direction of individual grating components. Finally, results presented in Chapter 5 were obtained in collaboration with the group of Pascal Fries in the Donders Institute for Brain, Cognition and Behaviour. It explored an aspect of oscillatory activity that has gained increasing interest, namely the precise phase of the ongoing gamma rhythm in which individual neurons discharge. Parallels are made with the theta phase precession described in the hippocampus (O’Keefe and Recce, 1993), and how this mechanism can serve visual processing.

1.5 - REFERENCES

- Adelson EH, Movshon JA. 1982. Phenomenal coherence of moving visual patterns. *Nature*. **300**: 523-525.
- Azouz R, Gray CM. 2000. Dynamic spike threshold reveals a mechanism for synaptic coincidence detection in cortical neurons in vivo. *Proc. Natl. Acad. Sci. U.S.A.* **97**: 8110-8115.
- Azouz R, Gray CM. 2003. Adaptive coincidence detection and dynamic gain control in visual cortical neurons in vivo. *Neuron*. **37**: 513-523.
- Barlow HB. 1972. Single units and sensation: A neuron doctrine for perceptual psychology? *Perception*. **1**: 371-394.
- Bartos M, Vida I, Jonas P. 2007. Synaptic mechanisms of synchronized gamma oscillations in inhibitory interneuron networks. *Nat. Rev. Neurosci.* **8**: 45-56.
- Berger H. 1929. Über das Elektrenkephalogramm des Menschen. *Arch. Psychiatr. Nervenkr.* **87**: 527-570.
- Bi GQ, Poo MM. 1998. Synaptic modifications in cultured hippocampal neurons: dependence on spike timing, synaptic strength, and postsynaptic cell type. *J. Neurosci.* **18**: 10464-10472.
- Bichot NP, Rossi AF, Desimone R. 2005. Parallel and serial neural mechanisms for visual search in macaque area V4. *Science*. **308**: 529-534.
- Boudreau CE, Williford TH, Maunsell JH. 2006. Effects of task difficulty and target likelihood in area V4 of macaque monkeys. *J. Neurophysiol.* **96**: 2377-2387.

- Bruno RM, Sakmann B. 2006. Cortex is driven by weak but synchronously active thalamocortical synapses. *Nature*. **312**: 1622-1627.
- Bullier J. 2001. Integrated model of visual processing. *Brain Res. Rev.* **36**: 96-107.
- Buschman TJ, Miller EK. 2007. Top-down versus bottom-up control of attention in the prefrontal and posterior parietal cortices. *Science*. **315**: 1860-1862.
- Buzsáki G. 2006. Rhythms of the brain. Oxford University Press.
- Buzsáki G, Draguhn A. 2004. Neuronal oscillations in cortical networks. *Science*. **304**: 1926-1929.
- Buzsáki G, Kaila K, Raichle M. 2007. Inhibition and brain work. *Neuron*. **56**: 771-783.
- Cardin JA, Carlén M, Meletis K, Knoblich U, Zhang F, Deisseroth K, Tsai LH, Moore CI. 2009. Driving fast-spiking cells induces gamma rhythm and controls sensory responses. *Nature*. **459**: 663-667.
- Castelo-Branco M, Goebel R, Neuenschwander S, Singer W. 2000. Neural synchrony correlates with surface segregation rules. *Nature*. **405**: 685-689.
- Castelo-Branco M, Neuenschwander S, Singer W. 1998. Synchronization of visual responses between the cortex, lateral geniculate nucleus, and retina in the anesthetized cat. *J. Neurosci.* **18**: 6395-6410.
- Conley M, Fitzpatrick D. 1989. Morphology of retinogeniculate axons in the macaque. *Vis. Neurosci.* **2**: 287-296.
- Crick F. 1984. Function of the thalamic reticular complex: the searchlight hypothesis. *Proc. Natl. Acad. Sci. U.S.A.* **81**: 4586-4590.
- Daniel PM, Whitteridge D. 1961. The representation of the visual field on the cerebral cortex in monkeys. *J. Physiol. (London)* **159**: 203-221.
- Desimone R, Albright TD, Gross CG, Bruce C. 1984. Stimulus-selective properties of inferior temporal neurons in the macaque. *J. Neurosci.* **4**: 2051-2062.
- Desimone R, Duncan J. 1995. Neural mechanisms of selective visual attention. *Annu. Rev. Neurosci.* **18**: 193-222.
- DeYoe EA, Van Essen DC. 1988. Concurrent processing streams in monkey visual cortex. *Trends Neurosci.* **11**: 219-226.
- Doesburg SM, Roggeveen AB, Kitajo K, Ward LM. 2008. Large-scale gamma-band phase synchronization and selective attention. *Cereb. Cortex.* **18**: 386-396.
- Eckhorn R, Bauer R, Jordan W, Brosch M, Kruse W, Munk M, Reitboeck HJ. 1988. Coherent oscillations: a mechanism of feature linking in the visual cortex? Multiple electrode and correlation analyses in the cat. *Biol. Cybern.* **60**: 121-130.
- Engel AK, König P, Gray CM, Singer W. 1990. Stimulus-Dependent Neuronal Oscillations in Cat Visual Cortex: Inter-Columnar Interaction as Determined by Cross-Correlation Analysis. *Eur. J. Neurosci.* **2**: 588-606.

- Engel AK, König P, Kreiter AK, Singer W. 1991a. Interhemispheric synchronization of oscillatory neuronal responses in cat visual cortex. *Science*. **252**: 1177-1179.
- Engel AK, König P, Singer W. 1991b. Direct physiological evidence for scene segmentation by temporal coding. *Proc. Natl. Acad. Sci. U.S.A.* **88**: 9136-9140.
- Engel AK, Kreiter AK, König P, Singer W. 1991c. Synchronization of oscillatory neuronal responses between striate and extrastriate visual cortical areas of the cat. *Proc. Natl. Acad. Sci. U.S.A.* **88**: 6048-6052.
- Felleman DJ, Van Essen DC. 1991. Distributed hierarchical processing in the primate cerebral cortex. *Cereb. Cortex*. **1**: 1-47.
- Friedman-Hill S, Maldonado PE, Gray CM. 2000. Dynamics of striate cortical activity in the alert macaque: I. Incidence and stimulus-dependence of gamma-band neuronal oscillations. *Cereb. Cortex*. **10**: 1105-1116.
- Fries P. 2005. A mechanism for cognitive dynamics: neuronal communication through neuronal coherence. *Trends. Cogn. Sci.* **9**: 474-480.
- Fries P. 2009. Neuronal gamma-band synchronization as a fundamental process in cortical computation. *Annu. Rev. Neurosci.* **32**: 209-224.
- Fries P, Neuenschwander S, Engel AK, Goebel R, Singer W. 2001a. Rapid feature selective neuronal synchronization through correlated latency shifting. *Nat. Neurosci.* **4**: 194-200.
- Fries P, Nikolic D, Singer W. 2007. The gamma cycle. *Trends Neurosci.* **30**: 309-316.
- Fries P, Reynolds JH, Rorie AE, Desimone R. 2001b. Modulation of oscillatory neuronal synchronization by selective visual attention. *Science*. **291**: 1560-1563.
- Fries P, Roelfsema PR, Engel AK, König P, Singer W. 1997. Synchronization of oscillatory responses in visual cortex correlates with perception in interocular rivalry. *Proc. Natl. Acad. Sci. U.S.A.* **94**: 12699-12704.
- Gattass R, Sousa APB, Rosa MGP. 1987. Visual topography of V1 in the *Cebus* monkey. *J. Comp. Neurol.* **259**: 529-548.
- Gattass R, Nascimento-Silva S, Soares JGM, Lima B, Jansen AK, Diogo ACM, Farias MF, Marcondes M, Botelho EP, Mariani OS, Azzi J, Fiorani M. 2005. Cortical visual areas in monkeys: location, topography, connections, columns, plasticity and cortical dynamics. *Philos. Trans. R. Soc. London Ser. B.* **360**: 709-731.
- Ghose GM, Maunsell J. 1999. Specialized representations in visual cortex: a role for binding? *Neuron*. **24**: 79-85, 111-125.
- Gilbert CD, Das A, Ito M, Kapadia M, Westheimer G. 1996. Spatial integration and cortical dynamics. *Proc. Natl. Acad. Sci. U.S.A.* **93**: 615-622.
- Gilbert CD, Wiesel TN. 1979. Morphology and intracortical projections of functionally characterised neurones in the cat visual cortex. *Nature*. **280**: 120-125.
- Gilbert CD, Wiesel TN. 1983. Clustered intrinsic connections in cat visual cortex. *J. Neurosci.* **3**: 1116-1133.
- Gouras P. 1969. Antidromic responses of orthodromically identified ganglion cells in monkey retina. *J. Physiol. (London)* **204**: 407-419.

- Gray CM, Di Prisco GV. 1997. Stimulus-dependent neuronal oscillations and local synchronization in striate cortex of the alert cat. *J. Neurosci.* **17**: 3239-3253.
- Gray CM, Engel AK, König P, Singer W. 1990. Stimulus-Dependent Neuronal Oscillations in Cat Visual Cortex: Receptive Field Properties and Feature Dependence. *Eur. J. Neurosci.* **2**: 607-619.
- Gray CM, König P, Engel AK, Singer W. 1989. Oscillatory responses in cat visual cortex exhibit inter-columnar synchronization which reflects global stimulus properties. *Nature.* **338**: 334-337.
- Gray CM, Singer W. 1989. Stimulus-specific neuronal oscillations in orientation columns of cat visual cortex. *Proc. Natl. Acad. Sci. U.S.A.* **86**: 1698-1702.
- Gray CM, McCormick DA. 1996. Chattering cells: superficial pyramidal neurons contributing to the generation of synchronous oscillations in the visual cortex. *Science.* **274**: 109-113.
- Gregoriou GG, Gotts SJ, Zhou H, Desimone R. 2009. High-frequency, long-range coupling between prefrontal and visual cortex during attention. *Science.* **324**: 1207-1210.
- Gross CG. 2002. Genealogy of the "Grandmother Cell". *Neuroscientist.* **8**: 512-518.
- Gross CG, Bender DB, Rocha-Miranda CE. 1969. Visual receptive fields of neurons in inferotemporal cortex of the monkey. *Science.* **166**: 1303-1306.
- Gross CG, Rocha-Miranda CE, Bender DB. 1972. Visual properties of neurons in inferotemporal cortex of the Macaque. *J. Neurophysiol.* **35**: 96-111.
- Harris KD. 2005. Neural signatures of cell assembly organization. *Nat. Rev. Neurosci.* **6**: 399-407.
- Harris KD, Henze DA, Hirase H, Leinekugel X, Dragoi G, Czurkó A, Buzsáki G. 2002. Spike train dynamics predicts theta-related phase precession in hippocampal pyramidal cells. *Nature.* **417**: 738-741.
- Hartline HK. 1938. The response of single optic nerve fibers of the vertebrate eye to illumination of the retina. *Amer. J. Physiol.* **121**: 400-415.
- Hasenstaub A, Shu Y, Haider B, Kraushaar U, Duque A, McCormick DA. 2005. Inhibitory postsynaptic potentials carry synchronized frequency information in active cortical networks. *Neuron.* **47**: 423-435.
- Herculano-Houzel S, Munk MH, Neuenschwander S, Singer W. 1999. Precisely synchronized oscillatory firing patterns require electroencephalographic activation. *J. Neurosci.* **19**: 3992-4010.
- Hochstein S, Ahissar M. 2002. View from the top: hierarchies and reverse hierarchies in the visual system. *Neuron.* **36**: 791-804.
- Houweling AR, Brecht M. 2008. Behavioural report of single neuron stimulation in somatosensory cortex. *Nature.* **451**: 65-68.
- Hubel DH. 1982a. Cortical neurobiology: a slanted historical perspective. *Ann. Rev. Neurosci.* **5**: 363-370.
- Hubel DH. 1982b. Exploration of the primary visual cortex, 1955-1978. *Nature.* **299**: 515-524.
- Hubel DH, Wiesel TN. 1959. Receptive fields of single neurones in the cat's striate cortex. *J. Physiol. (London)* **148**: 574-591.

- Hubel DH, Wiesel TN. 1962. Receptive fields, binocular interaction and functional architecture in the cat's visual cortex. *J. Physiol. (London)* **160**: 106-154.
- Hubel DH, Wiesel TN. 1963. Shape and arrangement of columns in cat's striate cortex. *J. Physiol. (London)* **165**: 559-568.
- Hubel DH, Wiesel TN. 1968. Receptive fields and functional architecture of monkey striate cortex. *J. Physiol. (London)* **195**: 215-243.
- Hubel DH, Wiesel TN. 1972. Laminar and columnar distribution of geniculo-cortical fibers in the macaque monkey. *J. Comp. Neurol.* **146**: 421-450.
- Hubel DH, Wiesel TN. 1974. Uniformity of monkey striate cortex: a parallel relationship between field size, scatter, and magnification factor. *J. Comp. Neurol.* **158**: 295-305.
- Kayser C, Salazar RF, Konig P. 2003. Responses to natural scenes in cat V1. *J. Neurophysiol.* **90**: 1910-1920.
- Kenet T, Bibitchkov D, Tsodyks M, Grinvald A, Arieli A. 2003. Spontaneously emerging cortical representations of visual attributes. *Nature.* **425**: 954-956.
- Kreiter AK, Singer W. 1996. Stimulus-dependent synchronization of neuronal responses in the visual cortex of the awake macaque monkey. *J. Neurosci.* **16**: 2381-2396.
- Kuffler SW. 1953. Discharge patterns and functional organization of mammalian retina. *J. Neurophysiol.* **16**: 37-68.
- Lakatos P, Chen CM, O'Connell MN, Mills A, Schroeder CE. 2007. Neuronal oscillations and multisensory interaction in primary auditory cortex. *Neuron.* **53**: 279-292.
- Lakatos P, Shah AS, Knuth KH, Ulbert I, Karmos G, Schroeder CE. 2005. An oscillatory hierarchy controlling neuronal excitability and stimulus processing in the auditory cortex. *J. Neurophysiol.* **94**: 1904-1911.
- Lamme VA, Spekreijse H. 1998. Neuronal synchrony does not represent texture segregation. *Nature.* **396**: 362-366.
- Lettvin JY, Maturana HR, McCulloch WS, Pitts WH. 1959. What the frog's eye tells the frog's brain. *Proc. Inst. Radio. Engin.* **47**: 1940-1951.
- Livingstone M, Hubel D. 1988. Segregation of form, color, movement and depth: anatomy, physiology and perception. *Science.* **240**: 740-749.
- Logothetis NK. 2003a. The underpinnings of the BOLD functional magnetic resonance imaging signal. *J. Neurosci.* **23**: 3963-3971.
- Logothetis NK. 2003b. MR imaging in the non-human primate: studies of function and of dynamic connectivity. *Curr. Opin. Neurobiol.* **13**: 630-642.
- Logothetis NK, Sheinberg DL. 1996. Visual object recognition. *Ann. Rev. Neurosci.* **19**: 577-621.
- Lund JS. 1988. Anatomical organization of macaque monkey striate visual cortex. *Ann. Rev. Neurosci.* **11**: 253-288.

- Maldonado PE, Friedman-Hill S, Gray CM. 2000. Dynamics of striate cortical activity in the alert macaque: II. Fast time scale synchronization. *Cereb. Cortex*. **10**: 1117-1131.
- Markram H, Lübke J, Frotscher M, Sakmann B. 1997. Regulation of synaptic efficacy by coincidence of postsynaptic APs and EPSPs. *Science*. **275**: 213-215.
- Martínez-Trujillo JC, Treue S. 2002. Attentional modulation strength in cortical area MT depends on stimulus contrast. *Neuron*. **35**: 365-370.
- Martínez-Trujillo JC, Treue S. 2004. Feature-based attention increases the selectivity of population responses in primate visual cortex. *Curr. Biol*. **14**: 744-751.
- Maunsell JH, Cook EP. 2002. The role of attention in visual processing. *Philos. Trans. R. Soc. London Ser. B*. **357**: 1063-1072.
- Maunsell JH, Treue S. 2006. Feature-based attention in visual cortex. *Trends Neurosci*. **29**: 317-322.
- McAlonan K, Cavanaugh J, Wurtz R. 2006. Attentional modulation of thalamic reticular neurons. *J. Neurosci*. **26**: 4444-4450.
- Mehta AD, Ulbert I, Schroeder CE. 2000. Intermodal selective attention in monkeys. I: distribution and timing of effects across visual areas. *Cereb. Cortex*. **10**: 343-358.
- Merigan WH, Maunsell JHR. 1993. How parallel are the primate visual pathways? *Annu. Rev. Neurosci*. **16**: 369-402.
- Middleton S, Jalics J, Kispersky T, LeBeau FE, Roopun AK, Kopell NJ, Whittington MA, Cunningham MO. 2008. NMDA receptor-dependent switching between different gamma rhythm-generating microcircuits in entorhinal cortex. *Proc. Natl. Acad. Sci. U.S.A.* **105**: 18572-18577.
- Mishkin M, Ungerleider LG, Macko KA. 1983. Object vision and spatial vision: two cortical pathways. *Trends Neurosci*. **6**: 414-417.
- Mitzdorf U. 1987. Properties of the evoked potential generators: current source-density analysis of visually evoked potentials in the cat cortex. *Int. J. Neurosci*. **33**: 33-59.
- Moran J, Desimone R. 1985. Selective attention gates visual processing in the extrastriate cortex. *Science*. **229**: 782-784.
- Moruzzi G, Magoun HW. 1949. Brain stem reticular formation and activation of the EEG. *Electroencephalogr. Clin. Neurophysiol*. **1**: 455-473.
- Motter BC. 1993. Focal attention produces spatially selective processing in visual cortical areas V1, V2, and V4 in the presence of competing stimuli. *J. Neurophysiol*. **70**: 909-919.
- Mountcastle VB. 1957. Modality and topographic properties of single neurons of cat's somatic sensory cortex. *J. Neurophysiol*. **20**: 408-434.
- Munk MH, Roelfsema PR, König P, Engel AK, Singer W. 1996. Role of reticular activation in the modulation of intracortical synchronization. *Science*. **272**: 271-274.

- Murthy VN, Fetz EE. 1996. Oscillatory activity in sensorimotor cortex of awake monkeys: synchronization of local field potentials and relation to behavior. *J. Neurophysiol.* **76**: 3949-3967.
- Neuenschwander S, Singer W. 1996. Long-range synchronization of oscillatory light responses in the cat retina and lateral geniculate nucleus. *Nature.* **379**: 728-732.
- Nuwer MR. 1998. Fundamentals of evoked potentials and common clinical applications today. *Electroencephalogr. Clin. Neurophysiol.* **106**: 142-148.
- O'Keefe J, Recce ML. 1993. Phase relationship between hippocampal place units and the EEG theta rhythm. *Hippocampus.* **3**: 317-330.
- Ölveczky BP, Baccus SA, Meister M. 2003. Segregation of object and background motion in the retina. *Nature.* **423**: 401-408.
- Palanca BJ, DeAngelis GC. 2005. Does neuronal synchrony underlie visual feature grouping? *Neuron.* **46**: 333-346.
- Perrett DI, Rolls ET, Caan W. 1982. Visual neurones responsive to faces in the monkey temporal cortex. *Exp. Brain Res.* **47**: 329-342.
- Perry VH, Oehler R, Cowey A. 1984. Retinal ganglion cells that project to the dorsal lateral geniculate nucleus in the macaque monkey. *Neuroscience.* **12**: 1101-1123.
- Pohl W. 1973. Dissociation of spatial discrimination deficits following frontal and parietal lesions in monkeys. *J. Comp. Physiol. Psychol.* **82**: 227-239.
- Reynolds JH, Desimone R. 2003. Interacting roles of attention and visual salience in V4. *Neuron.* **37**: 853-863.
- Reynolds JH, Chelazzi L. 2004. Attentional modulation of visual processing. *Annu. Rev. Neurosci.* **27**: 611-647.
- Robbe D, Montgomery SM, Thome A, Rueda-Orozco PE, McNaughton BL, Buzsaki G. 2006. Cannabinoids reveal importance of spike timing coordination in hippocampal function. *Nature Neurosci.* **9**: 1526-1533.
- Rock I, Palmer S. 1990. The legacy of Gestalt psychology. *Sci. Am.* 48-61.
- Rodriguez E, George N, Lachaux JP, Martinerie J, Renault B, Varela FJ. 1999. Perception's shadow: long-distance synchronization of human brain activity. *Nature.* **397**: 430-433.
- Roelfsema PR, Engel AK, König P, Singer W, 1997. Visuomotor integration is associated with zero time-lag synchronization among cortical areas. *Nature.* **385**: 157-161.
- Rolls ET, Xiang J, Franco L. 2005. Object, space, and object-space representations in the primate hippocampus. *J. Neurophysiol.* **94**: 833-844.
- Saalmann YB, Pigarev IN, Vidyasagar TR. 2007. Neural mechanisms of visual attention: how top-down feedback highlights relevant locations. *Science.* **316**: 1612-1615.
- Salzman CD, Britten KH, Newsome WT. 1990. Cortical microstimulation influences perceptual judgements of motion direction. *Nature.* **346**: 174-177.

- Sawatari A, Callaway EM. 1996. Convergence of magno- and parvocellular pathways in layer 4B of macaque primary visual cortex. *Nature*. **380**: 442-446.
- Schmidt KE, Kim DS, Singer W, Bonhoeffer T, Löwel S. 1997. Functional specificity of long-range intrinsic and interhemispheric connections in the visual cortex of strabismic cats. *J. Neurosci*. **17**: 5480-5492.
- Shadlen MN, Movshon JA. 1999. Synchrony unbound: a critical evaluation of the temporal binding hypothesis. *Neuron*. **24**: 67-77, 111-125.
- Schiller PH, Malpeli JG. 1978. Functional specificity of lateral geniculate nucleus laminae of the Rhesus monkey. *J. Neurophysiol*. **41**: 788-797.
- Schiller PH, Sandell JH, Maunsell JH. 1986. Functions of the ON and OFF channels of the visual system. *Nature*. **322**: 824-825.
- Schoffelen JM, Oostenveld R, Fries P. 2005. Neuronal coherence as a mechanism of effective corticospinal interaction. *Science*. **308**: 111-113.
- Shapley R, Perry VH. 1986. Cat and monkey retinal ganglion cells and their visual functional roles. *Trends Neurosci*. **9**: 229-235.
- Sillito AM. 1975. The contribution of inhibitory mechanisms to the receptive field properties of neurones in the striate cortex of the cat. *J. Physiol. (London)* **250**: 305-329.
- Singer W. 1993. Synchronization of cortical activity and its putative role in information processing and learning. *Annu. Rev. Physiol*. **55**: 349-374.
- Singer W. 1999. Neuronal synchrony: a versatile code for the definition of relations? *Neuron*. **24**: 49-65, 111-125.
- Singer W, Gray CM. 1995. Visual feature integration and the temporal correlation hypothesis. *Ann. Rev. Neurosci*. **18**: 555-586.
- Spitzer H, Desimone R, Moran J. 1988. Increased attention enhances both behavioral and neuronal performance. *Science*. **240**: 338-340.
- Suzuki WA, Miller EK, Desimone R. 1997. Object and place memory in the macaque entorhinal cortex. *J. Neurophysiol*. **78**: 1062-1081.
- Taylor K, Mandon S, Freiwald WA, Kreiter AK. 2005. Coherent oscillatory activity in monkey area v4 predicts successful allocation of attention. *Cereb. Cortex*. **15**: 1424-1437.
- Thiele A, Stoner G. 2003. Neuronal synchrony does not correlate with motion coherence in cortical area MT. *Nature*. **421**: 366-370.
- Thorpe S, Fize D, Marlot C. 1996. Speed of processing in the human visual system. *Nature*. **381**: 520-522.
- Treisman AM, Gelade G. 1980. A feature-integration theory of attention. *Cogn. Psychol*. **12**: 97-136.
- Treisman A, Schmidt H. 1982. Illusory conjunctions in the perception of objects. *Cogn. Psychol*. **14**: 107-141.

- Treue S, Maunsell JH. 1996. Attentional modulation of visual motion processing in cortical areas MT and MST. *Nature*. **382**: 539-541.
- Uhlhaas PJ, Pipa G, Lima B, Melloni L, Neuenschwander S, Nikolić D, Singer W. 2009. Neural synchrony in cortical networks: history, concept and current status. *Front. Integr. Neurosci.* **3**: 1-19.
- Uhlhaas PJ, Singer W. 2010. Abnormal neural oscillations and synchrony in schizophrenia. *Nat. Rev. Neurosci.* **11**: 100-113.
- Ungerleider LG, Mishkin M. 1982. Two cortical visual systems. In *The Analysis of Visual Behavior*, ed. DJ Ingle, RJW Mansfield, MS Goodale, pp. 549-586. Cambridge, Mass: MIT Press.
- Whittington MA, Traub RD, Jefferys JG. 1995. Synchronized oscillations in interneuron networks driven by metabotropic glutamate receptor activation. *Nature*. **373**: 612-615.
- Wolfe JM, Cave KR. 1999. The psychophysical evidence for a binding problem in human vision. *Neuron*. **24**: 11-17, 111-125.
- Womelsdorf T, Schoffelen JM, Oostenveld R, Singer W, Desimone R, Engel AK, Fries P. 2007. Modulation of neuronal interactions through neuronal synchronization. *Science*. **316**: 1609-1612.
- von der Malsburg C. 1981. The Correlation Theory of Brain Function. Internal Report 81-2 (Department of Neurobiology, Max-Planck-Institute for Biophysical Chemistry, Goettingen, F.R.G.).
- von Stein A, Sarnthein J. 2000. Different frequencies for different scales of cortical integration: from local gamma to long range alpha/theta synchronization. *Int. J. Psychophysiol.* **38**: 301-313.

Chapter 2

Directional responses of visual wulst neurones to grating and plaid patterns in the awake owl

Reprint of Baron J, Pinto L, Dias MO, Lima B and Neuenschwander S. (2007). *Eur J Neurosci.* **26**: 1950-1968.

This work was done in collaboration with the Federal University of Minas Gerais, Brazil, as part of the German-Brazilian Exchange Program Probral-CAPES-DAAD (D/03/23569).

My participation in this work consisted in implementing the recording techniques and performing the initial experiments in the awake owl in Brazil.

Directional responses of visual wulst neurones to grating and plaid patterns in the awake owl

Jerome Baron,¹ Lucas Pinto,¹ Marcelo Oliveira Dias,¹ Bruss Lima² and Sergio Neuenschwander²

¹Department of Physiology and Biophysics, Institute of Biological Sciences, Federal University of Minas Gerais, Av. Antonio Carlos 6627, Belo Horizonte, MG 31270-901, Brazil

²Max-Planck Institute for Brain Research, Frankfurt am Main, Germany

Keywords: burrowing owl, evolution, motion integration, visual forebrain

Abstract

The avian retinorecipient pathway reaches the telencephalon in an area known as visual wulst. A close functional analogy between this area and the early visual cortex of mammals has been established in owls. The goal of the present study was to assess quantitatively the directional selectivity and motion integration capability of visual wulst neurones, aspects that have not been previously investigated. We recorded extracellularly from a total of 101 cells in awake burrowing owls. From this sample, 88% of the units exhibited modulated directional responses to sinusoidal gratings, with a mean direction index of 0.74 ± 0.03 and tuning bandwidth of $28 \pm 1.16^\circ$. A direction index higher than 0.5 was observed in 66% of the cells, thereby qualifying them as direction selective. Motion integration was tested with moving plaids, made by adding two sinusoidal gratings of different orientations. We found that 80% of direction-selective cells responded optimally to the motion direction of the component gratings, whereas none responded to the global motion of plaids, whose direction was intermediate to that of the gratings. The remaining 20% were unclassifiable. The strength of component motion selectivity rapidly increased over a 200 ms period following stimulus onset, maintaining a relatively sustained profile thereafter. Overall, our data suggest that, as in the mammalian primary visual cortex, the visual wulst neurones of owls signal the local orientated features of a moving object. How and where these potentially ambiguous signals are integrated in the owl brain might be important for understanding the mechanisms underlying global motion perception.

Introduction

Many neurones in the primary visual cortex (V1) of carnivores and primates exhibit some degree of directional selectivity (Hubel & Wiesel, 1962, 1968). Although these neurones are presumed to be important for mediating motion perception, their individual contribution to this process is potentially ambiguous. Indeed, receptive fields in V1 are small, meaning that most contours constituting an object will extend outside the suprathreshold response area of a cell. Ambiguities may thus arise as a cell's preferred direction, orthogonal to a contour's orientation (Henry *et al.*, 1974; Schiller *et al.*, 1976), might not be the same as the direction of the whole object. These ambiguities, commonly referred to as the aperture problem, somehow need to be overcome in order to recover an object's correct trajectory (Wallach, 1935; Fennema & Thompson, 1979; Marr & Ullman, 1981). Cortical models have traditionally favoured a hierarchically organized two-stage process whereby several local motion signals available in V1 are disambiguated by binding operations taking place in higher motion-specific areas (Movshon *et al.*, 1985). However, how such binding operations are exactly accomplished and whether they are actually at all necessary remain unclear (van Wezel & van der Smagt, 2003; Singer, 2004; Majaj *et al.*, 2007).

With the aim of providing comparative insights into this issue, we have here assessed whether neurones in the visual wulst of the owl are

capable of signalling global motion. The visual wulst is the telencephalic recipient of the avian retinorecipient pathway (Shimizu & Bowers, 1999). In owls, this structure is particularly developed (Stingelin, 1958; Iwaniuk & Hurd, 2005; Iwaniuk & Wylie, 2006) and, like V1, it contains neurones that have small retinotopically organized receptive fields, a high degree of binocular integration, selectivity for orientation and motion direction, and binocular disparity tuning (Pettigrew & Konishi, 1976; Pettigrew, 1979; Wagner & Frost, 1993, 1994; Nieder & Wagner, 2000, 2001a,b). Such response properties would suggest that the aperture problem is present at the level of the visual wulst but this remains speculative because the available information about directional selectivity is limited and of qualitative nature. Moreover, some physiological features of the wulst are known to resemble more closely those found in extrastriate areas (Pettigrew, 1979; Wagner & Frost, 1994; Nieder & Wagner, 1999; Liu & Pettigrew, 2003), leaving open the possibility that motion integration occurs at an early level in the owl.

Our approach relied on a now classical paradigm, introduced by Movshon *et al.* (1985) for studying motion integration. This paradigm uses plaid patterns, consisting of two superposed, non-parallel gratings, in order to classify cells on the basis of whether they respond preferentially to the motion of each component grating or to the motion of the plaid as a whole. In our study, we found that most visual wulst neurones respond selectively to the individual component gratings and thus do not signal the global motion of the plaids. Parts of these results have been reported in abstract form (Pinto *et al.*, 2006, 2007).

Correspondence: Dr Jerome Baron, as above.
E-mail: jbaron@icb.ufmg.br

Received 20 May 2007, revised 17 July 2007, accepted 24 July 2007

Materials and methods

Animal training

Experiments were performed on five adult burrowing owls (*Athene cunicularia*), weighing between about 160 and 190 g. Burrowing owls are small, long-legged owls, residents of open dry grasslands and desert habitats, and are very common in south-eastern Brazil. They are highly visual animals and have a marked fovea (Bravo & Pettigrew, 1981). Unlike most owls, they are active during the day (Coulombe, 1971) and lack the prominent facial disks that facilitate nocturnal owls in locating prey by sound (Norberg, 1977; Konishi, 1993). The animals that took part in the present experiments were housed in spacious outdoor aviaries together with the rest of the owl colony that we maintain in our laboratory under licence from the Brazilian Institute for the Environment and Natural Renewable Resources (IBAMA, licence no. 02015.004197/03).

Extracellular recordings from awake, passively fixating burrowing owls were obtained by following a method recently developed by our group. At this point, it is important to highlight that, in owls, passive fixation can be achieved by head fixation only, owing to the fact that eye movements are extremely limited in these birds (Steinbach *et al.*, 1974; Pettigrew & Konishi, 1976; Knudsen, 1982) reaching, in the burrowing owl, a maximum amplitude of 0.5° (Cooper & Pettigrew, 1979). Our approach was therefore to train owls to tolerate body restraint and rigid head fixation for periods long enough to accommodate cell recordings. Training initially began by taming the owls, handling them daily during a period of approximately 4 weeks. Using standard falconry techniques, the animals were carried around as much as possible to get them used to all sights and sounds of the laboratory. In particular, the birds were left to explore the recording booth. Following this initial taming period, the owls underwent surgery for the implantation of a recording chamber, as detailed below. After a minimum of 4 days of recovery, the owls were then trained to get used to head fixation. Positive reinforcement in the form of small pieces of meat was used and handling was executed with as much calm as possible in order to avoid conditioning of aversive responses. Owls were accustomed to wearing a leather jacket and being secured onto a perch by wrapping Velcro® straps around their claws. After about 1 week, head restraint was introduced and quickly combined with electrophysiological recordings. Installation into the head-fixation apparatus was fast and relatively stress-free for the animals. Once secured, and provided that no brusque movements were made around them, the owls typically remained in a state of quiet wakefulness for progressively longer periods. Thereafter, they often began to fidget or show signs of tiredness and, as soon as this was detected, the session was interrupted. Periods of head fixation were limited to about 3–4 h and their effect on animal welfare was closely monitored during and between recording sessions.

All procedures used in the present work were approved by the Ethics Committee for Animal Experimentation (CETEA, licence no. 2004/01) of the Federal University of Minas Gerais and were conducted in accordance with the European Communities Council Directive of 24 November 1986 (86/609/EEC).

Surgical procedures

A lightweight recording chamber was surgically mounted over the cranial area above the visual wulst. In addition to providing access to the brain, this chamber was used to fix the head of the animal during the recordings. It consisted of a single cylindrical metal piece (1.5 mm thick and 8 mm high) with a 10 mm internal diameter and weighing 1 g. For surgery, anaesthesia was induced and maintained with

Zoletil® 50 (1 : 1 mixture of tiletamine and zolazepam, Virbac, Carros, France) administered in the pectoral muscle at a dose of 20 mg/kg (half doses for maintenance). After loss of reflexes, the animal was wrapped into a leather jacket and its head was fixed into a stereotaxic frame (model 1430, David Kopf Instruments, Tujunga, CA, USA). To expose the surface of the skull, the skin was incised 25–30 mm along the midline and retracted laterally. The position of the craniotomy was marked out on the skull according to stereotaxic coordinates preliminarily worked out in our laboratory to target the visual wulst in the middle of its anterior/posterior dimension and proximate to its lateral margin, adjacent to the valleculla. This region corresponds to the foveal and parafoveal representations in the visuotopic map described in the wulst by Pettigrew (1979). The recording chamber was centred over this stereotaxic reference point and cemented to the skull in an upright position such that electrode penetrations could be roughly made perpendicular to the wulst. Care was taken to ensure that the dental cement (Vitro Fil®, DFL, Rio de Janeiro, RJ, Brazil) could also make its way into the spongy bone cavities exposed at various sites around the cylinder. This provided strong adherence of the cement to the cranium. After suturing the midline incision around the cylinder, a circular craniotomy (about 3 mm in diameter) was then made. Surgery took approximately 1 h and antiseptic conditions were maintained throughout. A broad-spectrum antibiotic (50 mg/kg of Terramicine®, Pfizer Laboratories, São Paulo, SP, Brazil) as well as an analgesic/anti-inflammatory (2 mg/kg of Ketofen® 1%, Merial, São Paulo, SP, Brazil) were administered post-operatively by intramuscular injections.

Recordings

Spiking activity was recorded from individual neurones or small groups of neurones using quartz-insulated platinum/tungsten electrodes (Thomas Recording, Giessen, Germany) with an impedance of 0.3–0.8 M Ω at 1 kHz. Signals were amplified ($\times 1000$) and band-pass filtered between 300 Hz and 7 kHz (HST/16025 headset, 32-channel pre-amplifier box, Plexon, Dallas, TX, USA) before being digitized at 32 kHz by a high-speed, 16-bit resolution A/D card with onboard trigger and timer capabilities (PCI-6259, National Instruments, Austin, TX, USA). The A/D board was also programmed to provide a second amplification stage of $\times 10$. Signal display, acquisition and storage were controlled through custom software written in LABVIEW (National Instruments) hosted in a 2 GHz AMD Athlon PC.

For independent positioning of the electrodes, we have developed, at the Max-Planck Institute, a recording device that consists essentially of three precision hydraulic microdrives mounted onto an X/Y stage (MO95, Narishige Scientific Instrument Laboratory, Tokyo, Japan). Each electrode was back-loaded into a guide tube and connected to a single microdrive. The device was secured to the recording chamber via a coupling ring adapter screwed on top of the chamber by means of a thread made inside it. The same thread was also used for fastening a protective cap when no recordings were made. The recording device was held in place by a metallic arm and this ensemble provided sufficient rigidity to fixate the head of the animal. With such an arrangement, negligible relative movements occurred between the electrodes and the head of the animal and good recording stability was therefore obtained. The relative positions of penetrations were defined by pre-set coordinates from the X/Y stage. These coordinates were varied across recording sessions in order to sample as many sites as possible. The electrodes were lowered inside their protecting guide tubes until contact with the dura was signalled by a characteristic noise in the recorded signal. The search for neurones was based on the

quality of unit signals, not responsiveness. Cells isolated along the same track were spaced at 200 μm intervals or greater. In some penetrations, the first 1000 μm were ignored so that sampling biases across the different layers of the wulst could be minimized.

Only spikes exceeding a pre-set threshold were detected, and saved, together with their time of occurrence. This detection threshold was set as a multiple of the SD of the whole voltage trace. We typically used thresholds between 2 and 3 SDs. Single unit activity was determined on the basis of the constant amplitude and shape of the extracted waveforms, using several online sorting tools available in our software.

Unit isolation was further refined offline by using spike-sorting software developed at the Max-Planck Institute for Brain Research by Nan-Hui Chen. This program uses a semiautomatic clustering procedure based on a dynamic template-matching algorithm. The estimation of the number of units present, as well as the assignment of each spike to a unit, was based on a conventional distance metric (residual sum of squares) between a spike and a template. Based on this distance, a similarity index threshold was calculated to decide how many units were present and if a spike should be assigned to a particular template or to noise. Threshold setting was dynamically computed by an artificial neural network based on the Adaptive Resonance Theory (Carpenter & Grossberg, 1987). Sorting was initiated by leaving the template-matching algorithm to find as many clusters as possible automatically. We then switched to a manual mode in which the experimenter could decide which clusters to merge, if any. Numerous graphical and analytical tools, such as the refractory period seen in the auto-correlogram, were available to guide this decision. A change in waveform amplitude over time was also computed and displayed for each cluster to identify and reject any single units with significant instability during a recording session. Correct spike assignment was validated if distinct clusters could be seen in two- and three-dimensional plots of spike principal-component-analysis scores, and if the overall separation of these clusters could be confirmed by objective measurements provided by the J3 and Pseudo-F statistics [more details on how these values are calculated can be found in Spath (1980) and Wheeler (1999)].

Overall, a yield of one unit per recording electrode was the most frequent outcome of the aforementioned analysis. Only occasionally could two, and rarely up to three, units per electrode be confidently isolated. Not only the numbers of offline-isolated units per electrode but also the response profile of such units were globally coherent with prior online estimation. These considerations, combined with the fairly stringent criteria adopted for offline sorting, made us confident that only well-isolated units were considered for the analysis described below.

Stimulation protocol

Visual stimuli were displayed on a 19-inch RGB video monitor (Samsung SyncMaster 955DF) at a resolution of 1024×768 pixels and a video frame rate of 100 Hz. The video monitor was placed 57 cm from the owl's eye and, at this distance, the usable part of the screen subtended $27 \times 36^\circ$ of visual angle. Using custom software written in LABVIEW (National Instruments), stimuli were prepared as sequences of bitmap images, which were then presented with timing accuracy as movies by the ACTIVESTIM software (<http://www.activestim.com>).

Once a cell was isolated, its receptive field was plotted on the screen as a minimum response field (Barlow *et al.*, 1967) by listening to neuronal discharges and presenting mouse-controlled objects such as

spots, bars, checkboards and so forth. Ocular dominance and optimal orientation/direction of motion were also determined in a similar way. If any doubts were cast upon the reliability of this qualitative evaluation, all of the above response properties were reassessed quantitatively. This was done mainly by analysing a two-dimensional spatial map of neuronal responsiveness derived from a stimulation protocol in which a single bar (10° in length and 0.5° in width) was swept across the screen in 16 different orientations (Azzi, 2004). Following this preliminary assessment, all receptive field measurements were then made: (i) through the eye that more effectively activated the cell (the non-dominant eye was covered) and (ii) with the centre of the receptive field roughly at the centre of the monitor screen. We usually assessed the preferences of the neurone for spatial and temporal frequency, either qualitatively or quantitatively. Such evaluation was performed by analysing the cell responses to a full-contrast drifting sine-wave grating, optimized for direction, and presented in varying spatial and temporal frequencies inside the receptive field. We did not attempt to control for eye movements because, as previously mentioned, such movements are very limited in owls.

Our primary goal in this study was to compare the selectivity of visual wulst neurones to the direction of motion of grating and plaid patterns, and for this we used a stimulation protocol fairly similar to those used by previous related studies in mammals (see for example Gizzi *et al.*, 1990; Movshon & Newsome, 1996; Guo *et al.*, 2004). All visual stimuli were made to appear within a circular aperture of 10° diameter that was aligned with the centre of the receptive field. Conventional sine-wave gratings were used. Their spatial and temporal frequencies were optimized according to preliminarily established values and their Michelson contrast was set to 0.45. Plaids were obtained by adding two such gratings separated by 90 or 135° in orientation (plaid mean luminance 35.1 cd/m^2). Both grating and plaid stimuli were presented over 360° in 16 steps of 22.5° . As the same 16 directions were used for all tests on all neurones, a total of 32 different stimulus conditions were shown. Each stimulus appeared for 10 trials on a pseudorandom schedule to counter repetition effects. In a trial, a stimulus was presented for 2 s, immediately preceded and followed by 500 ms periods of blank, during which a homogeneous grey field with the same mean luminance as that of the stimulus was shown. An interstimulus interval of 2 s was introduced to minimize potential interactions between the sequential stimuli. With 10 repeated presentations for each condition, the stimulus protocol required about 25 min to complete.

When referring to the motion direction of grating and plaid patterns, we used the following conventions: a grating with vertically orientated stripes moving rightwards was considered to have a direction of motion of 0° , whereas a grating with horizontally orientated stripes moving upwards was considered to have a direction of 90° . The drift direction of a plaid was referenced by the same polar coordinate system as that adopted for gratings and was defined as the direction of global motion perceived by a human observer. For the type of plaids used in this study, this corresponds to a direction of motion that lies equidistant between the directions of the two component gratings.

Data analysis

Data were initially screened with peristimulus time histograms and raster plots. The measure of neuronal response used for comparing the effects of different stimulus conditions was the mean spike rate computed within a specific time window. For the main part of the analysis, a window of 1800 ms, starting 200 ms after stimulus onset, was chosen to calculate the mean evoked response. By excluding the

first 200 ms of stimulus presentation, we sought to minimize the eventual contribution of onset components not directly related to the motion direction of the drifting pattern. In the final part of the Results, we perform an additional analysis on this initial 200 ms period in order to assess the direction of motion selectivity in the earliest phase of responses. Spontaneous activity was calculated as the mean spike rate across all stimulus conditions measured 500 ms before stimulus onset, which corresponded to the initial blank periods with no stimuli present on the monitor screen.

The attribution of directional selectivity to a particular cell was based on a combination of statistical and threshold-based criteria, which were applied on cell responses to drifting sinusoidal gratings, plotted on a linear scale or in a polar coordinate system as a function of motion direction (direction tuning curves). First, we made sure that each neurone considered for further analysis had significantly stronger evoked responses than its mean spontaneous activity when it was stimulated with gratings of optimal direction of motion. This was done by comparing, for this particular condition, the firing frequency in a 500 ms window immediately before and after stimulus onset using the one-tailed Wilcoxon matched-pairs signed-rank test ($P < 0.05$). Following well-established conventions, the motion direction for which the response was significantly greater than both the spontaneous activity and all other data points in the tuning curve was formally defined as the preferred direction. The direction 180° away from the preferred direction was defined as the antipreferred direction. Next, we performed an ANOVA using direction of motion as the main factor and a criterion of $P < 0.05$ to determine whether there was a statistically significant relationship between firing rate and motion direction. Depending on the normality of the sampled mean responses (Lilliefors test, $P < 0.05$, see the *General statistics* section below), this statistical analysis was carried out using either ANOVA or its non-parametric analogue, namely the Kruskal–Wallis test. Cells that yielded non-significant terms in ANOVA were considered as omnidirectional and excluded from our data set. For the remainder, a direction index (DI) was calculated as:

$$DI = 1 - [(R_{\text{anti}} - R_{\text{spont}})/(R_{\text{pref}} - R_{\text{spont}})]$$

where R_{pref} and R_{anti} , respectively, represent the responses to motion in the preferred and antipreferred directions relative to the spontaneous activity (R_{spont}). DI values increase from 0, for cells equally responsive to both directions, to 1, for cells that respond exclusively to one direction of motion, and can be greater than 1 if the cell responds below spontaneous activity levels for motion in the antipreferred direction. Cells with a $DI \geq 0.5$ were considered as direction selective and only these were further analysed with respect to their selectivity for the direction of motion of plaid patterns. Cells with a $DI < 0.5$ were referred to as non-direction selective.

The width of direction tuning was calculated by first fitting parametric curves to neuronal responses as a function of the direction of grating motion and then by taking the half-width at half-maximum of the fitted curves. All fits were based on the probability density function of the von Mises distribution, which is the circular statistics analogue of the normal distribution. As proposed by Swindale *et al.* (2003), we used the sum of two von Mises functions for cells that exhibited a visible peak in the antipreferred direction. In this case, the fitting parametric curve was:

$$M(\phi) = m + A_1 e^{[k_1(\cos(\phi - \phi_1) - 1)]} + A_2 e^{[k_2(\cos(\phi - \phi_2) - 1)]}$$

In the above expression, ϕ is the grating direction of motion for which the response is being estimated and m , A_1 , A_2 , ϕ_1 , ϕ_2 , k_1 and k_2 are free parameters. m corresponds to the baseline level. The

parameters A_1 and A_2 represent the maximum heights of the individual peaks, ϕ_1 and ϕ_2 are the centre directions (in radians) of each peak, and k_1 and k_2 , known as concentration factors, are inversely related to the widths of each peak. For cells with no visible peaks in the antipreferred direction, A_2 was constrained to equal 0, which removed the second von Mises function from the above equation. All of the parameters were adjusted by an iterative least-square fitting method, using the trust region for non-linear minimization algorithm (Branch *et al.*, 1999) available in the Matlab Curve Fitting Toolbox (Math-Works, Natick, MA, USA). As initial values, we used the following: $A_1 =$ the maximum value of the data, $A_2 = 0.7 A_1$, $k_1 = k_2 = 2.0$ (corresponding to a bandwidth of 50°) and $\phi_2 = \phi_1 + 180^\circ$. Fits that accounted for less than 80% of the variance, as determined by the R^2 statistics, were rejected.

To assess whether the directional selectivity of visual wulst neurones was better described as component (CDS) or pattern (PDS) direction selective, we used a revised version (Rodman & Albright, 1989; Movshon & Newsome, 1996) of the partial correlation analysis introduced by Movshon *et al.* (1985). Essentially, this analysis involved comparing the response of each neurone to the plaid pattern with the predictions of idealized models of pattern and component direction selectivity. Both modelled predictions were generated from the response of the neurone to the drifting grating. The predicted response for the pattern model was identical to the grating tuning curve. The predicted response for the component model was generated by taking the sum of two grating tuning curves, each shifted by $\pm 45^\circ$ for 90° plaid angles or $\pm 67.5^\circ$ for 135° plaid angles. For this latter prediction, spontaneous activity was subtracted from the response to the grating and added back after the prediction had been computed. To control for potential non-independence of the two model predictions, the degree of similarity between the actual plaid tuning curve and the predicted tuning curves for pattern and component direction selectivity was quantified by two partial correlation coefficients:

$$R_p = (r_p - r_c r_{pc}) / \sqrt{[(1 - r_c^2)(1 - r_{pc}^2)]}$$

$$R_c = (r_c - r_p r_{pc}) / \sqrt{[(1 - r_p^2)(1 - r_{pc}^2)]}$$

where R_p is the partial correlation coefficient for the pattern prediction, R_c is the partial correlation coefficient for the component prediction, r_c is the Pearson's linear correlation coefficient between the response to plaids and the model prediction for an idealized component neurone, r_p is the linear correlation coefficient between the response to plaids and the modelled pattern neurone response, and r_{pc} is the linear correlation coefficient between the two modelled predictions.

The statistical significance of R_p and R_c was determined by a parametric statistical value, t , calculated first by converting both partial correlation coefficients (R_x , with $x = p$ and c) into Z-scores (Z_x) using Fisher's r -to- Z transformation (Papoulis, 1990):

$$Z_x = 0.5 \times \ln[(1 + R_x)/(1 - R_x)]$$

and then by computing the difference between the Z-scores as follows:

$$t = (Z_p - Z_c) / \sqrt{(2/DoF)}$$

In this equation, DoF refers to the degrees of freedom and is equal to the number of conditions used to measure directional tuning curves minus three (in our study $DoF = 13$, as 16 directions were used for measuring tuning curves). As in previous related studies, a conditional

probability of $P = 0.1$ was chosen as the significance threshold for R_p and R_c . The reason for choosing this non-conservative criterion is that the present statistical procedure is not a true test for significance but is expected to adequately reduce the data (Movshon *et al.*, 1985; Gizzi *et al.*, 1990; Scannell *et al.*, 1996). Accordingly, for a cell to be classified as a PDS cell, R_p had to be significantly greater than either R_c or zero. Similarly, R_c had to exceed R_p or zero above chance level, for a cell to be classified as CDS. If a cell met neither of these criteria, it was considered unclassified.

To get an idea of the relative strength between component-like selectivity and pattern-like selectivity expressed by each neurone in response to plaid patterns, we computed a component index defined as $R_c^2 - R_p^2$ (Stoner & Albright, 1992; Pack *et al.*, 2001; Guo *et al.*, 2004). R_c^2 and R_p^2 are effectively the variance accounted for by the component and pattern predictions, respectively.

General statistics

In addition to the partial correlation analysis, several standard statistical tests were also computed. Before datasets were compared, we used the Lilliefors modification of the Kolmogorov-Smirnov test to check whether the datasets in question were significantly different from normal distributions of unspecified mean and variance. If normality was established, we applied a t -test to compare the means of two populations or an ANOVA test if comparisons were made between more than two populations. If normality was not established, the Wilcoxon rank-sum or Kruskal-Wallis tests were used, as non-parametric equivalents of the t - and ANOVA tests, respectively. To calculate the significance of differences in categorical properties, we applied a χ^2 test. Relationship between groups was assessed with the non-parametric Spearman's rank correlation test. The significant level used for all of the tests was $P < 0.05$. Unless otherwise specified, population measurements were presented as the arithmetic mean \pm SEM.

Results

General observations

A total of 107 visually responsive neurones were studied in 53 vertical electrode penetrations through the visual wulst of five owls. Typically, the restrained owls remained quiet for reasonably long periods of time, which facilitated the obtention of stable recordings. Only six isolated units were lost in the course of stimulation protocols. Offline spike-sorting analysis showed that these cells had merged into unsortable clusters. This left us with 101 neurones for the analyses detailed in the sections to follow. Another fact attesting to the stability of our recordings is that many single units could be held and characterized for as much as 3 h. As our recordings were limited to a few hours, we could only obtain a small yield of neurones per track (approximately two), even though we occasionally isolated as many as five units in a single penetration.

The response properties of the cells that we encountered were consistent with those previously described in other owl species (Pettigrew & Konishi, 1976; Pettigrew, 1979). Visual receptive fields were usually well defined and small; they never exceeded 5° in their largest dimension. Almost all cells in our sample were responsive to stimulation of either eye (Fig. 1A). Only three cells were found to be exclusively driven by one eye (Fig. 1B). At this point, it is important to reiterate that the grating and plaid stimuli that we subsequently used to characterize the directional responses of neurones were only presented to the dominant eye. Cells in our sample also typically

showed tuned profiles for the spatial and temporal frequency of optimally moving full-contrast gratings. In some cases, we determined quantitatively the preferred value for these two dimensions and found them to be consistent with our qualitative estimates (Fig. 1C and D). Pettigrew (1979) reported the presence of several cell classes in the owl visual wulst, most of them having their correspondent in the mammalian V1. The response profiles that we encountered were consistent with many of these classes. Most notably, this also includes a cell type known as 'black bar specialists', unique for their preference to orientated dark bars moving against a light background.

To estimate the depth of our recordings within the visual wulst, we relied on readings from our microdrives, using as reference the electrode entrances into and exits from the neural tissue. Clearly, such estimates should be used with caution, as they are prone to inaccuracies due, for example, to tissue dimpling. However, the fact that readings made at the entrances usually coincided with those at the exits argues that the latter phenomenon was probably not a significant source of error. The distribution of our depth estimates ranged from 10 to 2360 μm . Most cells ($\sim 80\%$) were recorded within the first 1200 μm , a depth that corresponds approximately to the lower border of the most superficial and thickest layer of the visual wulst ($\sim 40\%$ of the thickness of this structure), namely the hyperpallium apicale (HA), which is the main output layer (Karten *et al.*, 1973). The visual wulst extends further down for another 1600 μm (making up a total of approximately 2800 μm), where there are three additional layers (Karten *et al.*, 1973; Pettigrew, 1979; Reiner *et al.*, 2004): the interstitial nucleus of HA, hyperpallium intercalatum and hyperpallium densocellulare. According to our microdrive readings, only a few cells ($\sim 20\%$) were sampled from within the interstitial nucleus of HA (granular layer) and none from the hyperpallium intercalatum or hyperpallium densocellulare.

Direction-selective response properties

To test whether visual wulst neurones are capable of signalling global motion, we restricted the analyses to neurones that exhibited at least some degree of directional selectivity. An objective assessment of this property was based on the evaluation of neuronal responses to the sinusoidal gratings used in the plaid protocols. Such gratings had optimal, or close to optimal, spatial and temporal frequencies, and their Michelson contrast was 0.45. Three out of the 101 well-isolated units were excluded because their mean firing rates across all stimulus directions did not significantly exceed baseline levels. Although these neurones had well-defined visual receptive fields, their activity was in fact suppressed in the presence of moving gratings. Another group of nine neurones was also excluded from our sample because they were judged to be omnidirectional after ANOVA performed across the 16 different directions of stimulus drift (see Materials and methods). Of the remaining 89 neurones, 67 (around 75%) were classified as directional selective, as their DI values were equal to or greater than the cut-off value of 0.5 (see Materials and methods). The remaining 22 cells were classified as non-direction selective.

The pattern of directional responses during presentation of gratings is shown for two representative neurones in Fig. 2A and C. It can be observed in this figure that both neurones responded selectively to particular directions of motion, exhibiting sustained discharge rates throughout stimulus presentation after occasional initial transient components. These transient components were not considered for the main part of our analysis (the first 200 ms after stimulus onset was

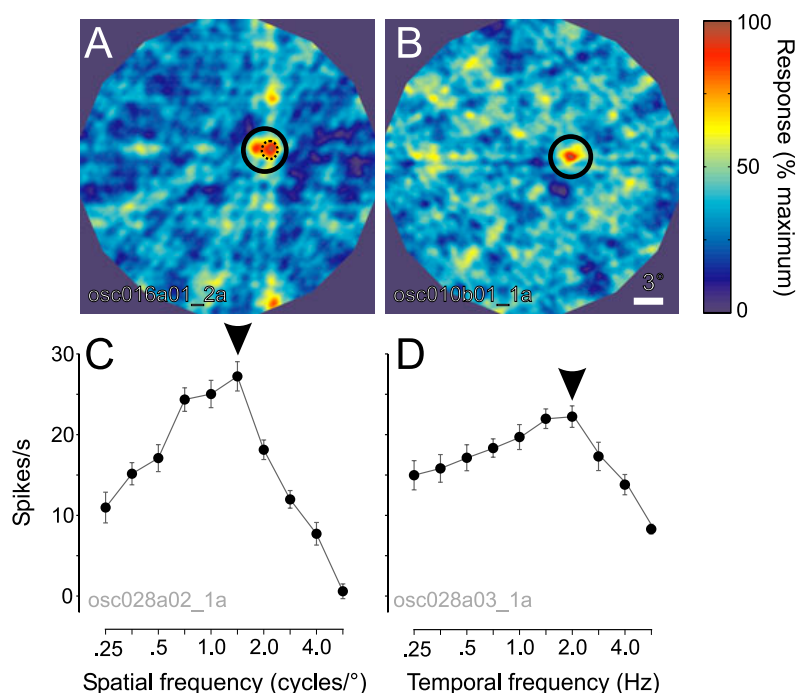


FIG. 1. Representative examples of receptive field properties in the visual wulst of the awake burrowing owl. Top panels show results of a quantitative receptive field-mapping procedure applied to (A) a binocular cell (the type of cell most frequently encountered in our experiments) and (B) a monocular cell, driven by the contralateral eye (a type of cell rarely found). The mapping procedure consisted of constructing two-dimensional maps of neuronal responses to a binocularly presented single bar (10° in length and 0.5° in width) swept across the screen in 16 different orientations with 10 repetitions of each. The maps were normalized to the maximum amplitude of the responses. The centre of the receptive field was defined as the point in the two-dimensional map of maximal responsiveness indicated by the solid-line circle. In the case of the binocular unit shown in A, two distinct but partially overlapping patches of more intense activity can be seen, indicating the presence of two receptive fields, one for each eye. Stimuli subsequently used in the main experimental protocols were always monocularly presented in the centre of the receptive field of the dominant eye, i.e. the eye for which greater responses were obtained (dotted-line circle). (C) Spatial-frequency tuning curve of a cell, measured with a full-contrast grating drifting in the preferred direction at a rate of 1 Hz. (D) Temporal tuning curve of the same cell shown in C, measured with the same grating at a fixed spatial frequency of 2 cycles/ $^\circ$. In both tuning curves, data points represent the mean spike rate (spikes/s) for 10 repetitions of 2 s stimulus presentations minus spontaneous activity. Error bars indicate \pm SEM. The arrows indicate the optimal frequency values.

excluded), as they could have been induced by stimulus features unrelated to motion.

Directional tuning curves of the neurones whose responses are represented in Fig. 2A and C are plotted on a linear scale in Fig. 2B and D, respectively. We also show the fits that we applied to the tuning curves in order to estimate the directional tuning half-widths at half-maximum response. As apparent in both examples, and true for the rest of our sample, the fits provided a good description of the data. Only six out of 89 neurones had to be discarded for not having passed our goodness-of-fit criterion (R^2 , see Materials and methods). For the remaining 83 neurones, R^2 was on average $0.91 (\pm 0.09$ SD; range 0.81–0.99). In other words, 91% of the data could be explained by the fits. The latter were based on the sum of two von Mises functions, whose parameters for peak positions, heights and widths were free. Such parameters could be adjusted to obtain adequate descriptions of the unimodal tuning profiles of strongly directional cells (DI value around 1, Fig. 2B), as well as the bimodal profiles of directional cells less strongly selective due to subsidiary peaks in the antipreferred direction (Fig. 2D). As a consequence of this, the higher peak of the fits, from which our estimates of bandwidths were derived, was always found around the preferred direction.

Population data of DIs and tuning bandwidths are presented as histograms in Fig. 2E and F, respectively. The strength of directional

selectivity ranged from non-directional (DI = 0.10) to strongly unidirectional, with suppression in relation to spontaneous activity in the antipreferred direction (DI = 1.35). For the large subpopulation of direction-selective cells, DI values were concentrated around a mean of 0.9, indicating a tendency towards unidirectionality without inhibition in the antipreferred direction, which was seen only in 20% of cells. The variability of tuning bandwidth values, which was apparent in the tuning curves shown in Fig. 2B and D, was reflected in the broad distribution shown in Fig. 2F (range 14.2 – 61.0°). The mean for the whole sample was 28.0° and roughly 45% of the cells had bandwidth values ranging between 20 and 30° . Values for directionally selective cells were not significantly different from those of non-direction-selective cells ($27.8 \pm 1.25^\circ$ vs. $29.0 \pm 3.0^\circ$, respectively; Wilcoxon rank sum test, $P = 0.89$).

Among the population of directionally selective neurones, no preferred direction was represented significantly more often than would be expected of a homogeneous distribution ($\chi^2 = 22.1$; DoF = 15; $P = 0.105$). However, we did observe a certain bias for downward motions. Preferred directions of 270° were indeed seen twice as often as any of the other 15 angular values. Interestingly, a similar bias is apparent in the middle temporal (MT) area of the primate (Albright, 1984, 1989) and has been found to be significant in a study by Diogo *et al.* (2003).

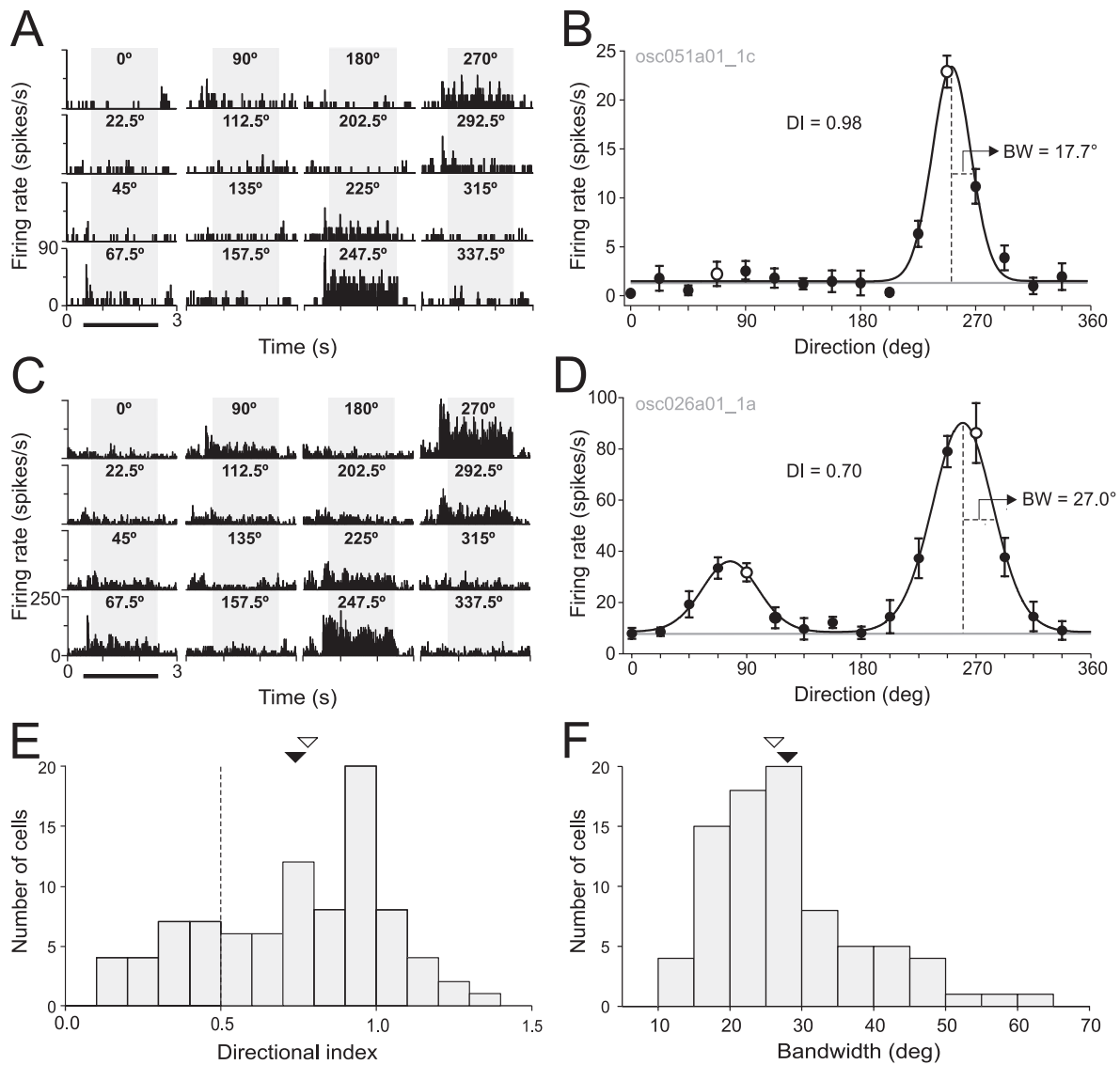


FIG. 2. Directional tuning properties of 89 neurons sampled in the visual wulst. (A–D) Responses of two representative direction-selective neurones to 45% contrast sinusoidal gratings drifting at optimal spatial and temporal frequencies. Left panels: Responses are shown as average peristimulus time histograms (PSTHs) for 16 different stimulus directions (as indicated on top of each histogram) with 10 repeated measures at each using a randomized order of stimulus presentation (bin size = 10 ms). Spontaneous activity was collected before the onset of the stimulus (first 500 ms of the PSTHs). Gratings were presented from 500 to 2500 ms, as indicated by the bars beneath the first column of PSTHs. The grey-shaded rectangles delineate the 1800 ms period considered for the analyses, after the exclusion of the 200 ms period following stimulus onset. Right panels: Direction tuning curves in which mean firing rate (spikes/s), computed over the whole stimulation period minus the initial 200 ms, is plotted as a function of stimulus direction. The open circles indicate mean response amplitude in the preferred and antipreferred direction. Solid lines represent the fitted models used to determine the half width at half height of the model peak response, which was our measure of the cell's directional tuning bandwidth (BW). Bars indicate the confidence interval of the mean at the 95% level. The models were based on the sum of two von Mises functions, as described in Materials and methods. (E) Distribution of direction indices (DIs). The DI has positive values that increase from 0 to 1 as mean response in the preferred direction increase relative to that in the antipreferred direction, with values above 1 if the response is inhibited (below spontaneous activity level). The dashed line indicates the boundary between orientation-selective (DI < 0.5) and direction-selective (DI ≥ 0.5) neurones. (F) Distribution of direction bandwidths. Mean and median values are represented for both DI and bandwidth distributions by the filled and empty triangles, respectively.

Neuronal responses to plaids

The 67 direction-selective units were tested with respect to their ability to signal the global motion of plaid patterns. The key aspect

of the test was the dissociation of component and pattern motions in the plaid stimulus, as the apparent motion of the whole plaid was intermediate to the actual motion of its component gratings. If a neurone is selectively responsive to global pattern

motion, its tuning curves for the grating and plaid stimuli should be essentially the same. However, if a neurone is selectively responsive to component motion, its tuning curve for the plaid stimulus should be bilobed, peaking when either of the component gratings matches the preferred direction of motion of the neurone.

A representative sample of three CDS cells is shown in Fig. 3. In this and in the next figure, responses are plotted in a polar representation where the distance of a point from the origin represents the firing rate in spikes per second and the angle indicates the direction of motion of the stimuli. In response to gratings drifting in 16 different directions through its receptive field, the first neurone (Fig. 3A) had a marked preference for the upward direction and the strength ($DI = 0.91$) and narrowness of the bandwidth ($BW = 27.0^\circ$) of its directional tuning were typical of many direction-selective neurones in our data set (see Fig. 2A and B). In response to plaids (Fig. 3B), this neurone showed two peaks of activity at motion directions symmetrically opposite to one another by an angle of 45° with respect to the upward direction. This is what would be expected from a neurone that responds independently to each of the component gratings of 90° plaids. To verify this observation objectively, we used the direction tuning measured for gratings to predict the model responses of an ideal CDS cell (represented by the dotted black lines in Fig. 3B, D and F) and of an ideal PDS cell (not shown) to plaids, and compared those models with the experimentally measured plaid tuning curves. The predicted direction tuning for a CDS model neurone is the sum of the direction tunings for the two gratings presented alone, whereas the prediction for a PDS model cell is identical to the measured direction tuning for gratings (see *Data analysis* section in Materials and methods). It can be observed that the plaid tuning curve of the unit in Fig. 3B closely matches the CDS prediction. This was confirmed numerically by computing the partial correlation coefficients between the plaid responses and the two model predictions. With a high component partial correlation ($R_c = 0.95$) and low pattern partial correlation ($R_p = -0.15$) this unit was unambiguously classified as CDS. A similar classification was obtained for cells that exhibited a variety of directional properties, such as, for example, a lower DI (Fig. 3C and D) or a broader tuning bandwidth (Fig. 3E and F).

Although most of the direction-selective neurones that we sampled within the visual wulst showed a CDS profile to drifting plaids, several of them did not concur with either component or pattern prediction. Figure 4 exemplifies three different reasons why this occurred. The unit in Fig. 4A and B illustrates the case of several neurones broadly tuned for gratings that were unclassifiable because their responses to plaids, although clearly directional, were somehow intermediate between the component and pattern predictions. The example in Fig. 4C and D illustrates another type of unclassified cell that had an attenuated response to plaids, without any clear unidirectional or bidirectional response profile. The behaviour of the cell in Fig. 4E and F was rather atypical. This unit was highly directional ($DI = 1.06$) and broadly tuned (bandwidth, $BW = 49.16$) for the gratings. In response to plaids, it showed two clear peaks at angles corresponding to each of the components of the plaids. However, it failed to be classified as CDS because its plaid tuning curve was rotated anticlockwise by an angle of around 45° with respect to the component prediction. This angular shift seemed to be genuine as it was found again when we repeated the experiment with 135° plaids (see below and Fig. 7). Notably, when we artificially compensated for this angular deviation by rotating the actual plaid tuning curve by a 45° clockwise angle, the cell became CDS with $R_c = 0.60$ and $R_p = -0.23$.

Figure 5 shows a scatter plot in which the values of the pattern and component correlation coefficients of all direction-selective visual wulst neurones are plotted against one another, as first used by Movshon *et al.* (1985). The plot is divided into three statistically distinct regions that were used to categorize neurones as CDS, PDS or unclassifiable (regions labelled as COMPONENT, PATTERN or UNCLASSIFIED, respectively). The predominance of CDS cells in our population data is evident. Out of 67 cells, 54 (~80%) were indeed classified as such. They responded best to a moving plaid pattern when the axis of motion of one of the component gratings coincided with their preferred axis of motion and their tuning curves were best described by the component prediction. The remaining 13 cells (~20%) were unclassifiable and no PDS neurones were encountered. Globally, the proportions of CDS and unclassifiable cells found in this study are fairly similar to those reported in the striate cortex of cats and primates (Movshon *et al.*, 1985; Gizzi *et al.*, 1990; Guo *et al.*, 2004). However, in the awake owl, we did not find the small population of PDS cells (9%) that Guo *et al.* (2004) encountered in V1 of monkeys performing a fixation task.

In order to assess the degree to which a cell expressed component-type selectivity more strongly than pattern-type selectivity, we computed a component index by subtracting the variance accounted for by the component prediction from that accounted for by the pattern prediction ($R_c^2 - R_p^2$). Positive values signify close conformity with the component prediction, whereas negative values support the pattern prediction. The distribution of these values is shown in Fig. 6A. As expected, the difference between the mean component indices of CDS cells (0.62 ± 0.02) and those of unclassifiable cells (0.10 ± 0.05) was highly significant (Wilcoxon rank sum test, $z = -5.3$, $P < 0.001$). The large majority (85%) of CDS cells had a component index greater than 0.5, indicating that most neurones classified as CDS by our statistical procedure retained a low degree of pattern motion selectivity. Moreover, it is interesting to note that the degree of component selectivity of a neurone within the visual wulst could not be predicted from its directional selective properties measured with drifting gratings only. As is apparent in Fig. 6B, there was no significant relationship between component motion selectivity and the strength of a neurone's direction selectivity (Spearman rank correlation, $\rho = -0.04$, $P = 0.61$). There was also no significant systematic shift to component motion selectivity with increasing direction tuning width (Spearman rank correlation, $\rho = -0.16$, $P = 0.88$, Fig. 6C).

Effect of plaid angles on partial correlation coefficients

The reliability of partial correlation coefficient measurements depends, to some extent, on choosing an appropriate plaid angle. For example, it is obvious that the bilobed profile in the plaid tuning curve of a typical CDS cell would not show up for plaid angles that are much smaller than the direction tuning width of the cell. In general, it is also true that the smaller the angle between the two component gratings of the plaid, the more similar the component and pattern predictions will tend to be, and consequently the less likely are the chances of finding a definitive difference between the two predictions. Ultimately, this situation will increase the likelihood of categorizing cells as unclassified and, at this point, it is important to stress that cells categorized as such are not somehow 'intermediate' between CDS and PDS cells. Rather, they should be considered as cells for which the particular test conditions and statistics used were not sufficiently sensitive to classify them. In the present study, we chose a plaid angle of 90° , a value that has often been used to probe the pattern motion selectivity of cells in the mammalian striate cortex (Movshon *et al.*, 1985; Gizzi *et al.*,

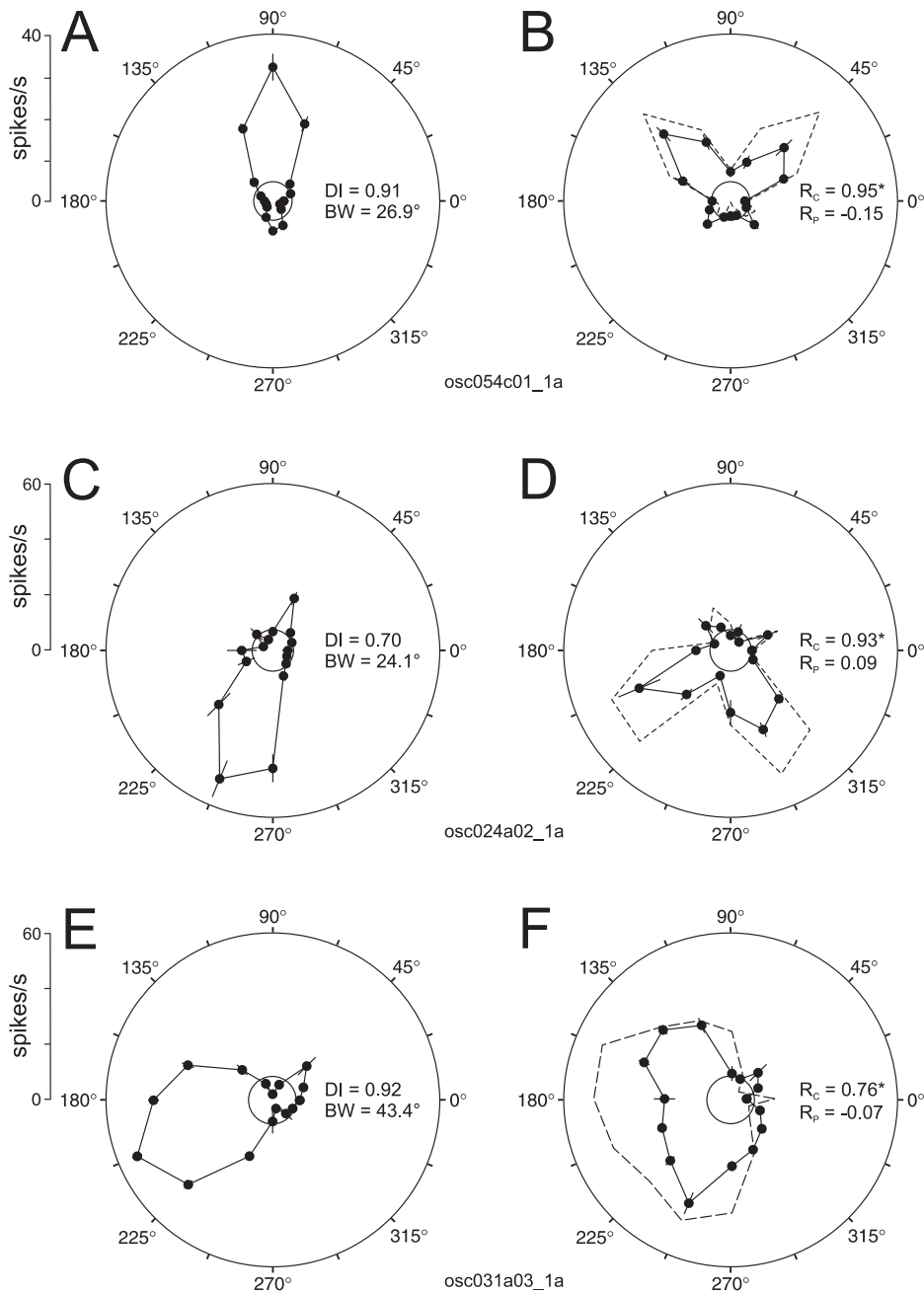


FIG. 3. Directional tuning of three component direction-selective neurones to drifting sine wave gratings (A, C and E) and 90° plaids (B, D and F). The angle on each polar plot shows the stimulus direction of motion, whereas the radial dimension represents response amplitude (spikes/s). The black circle centred on the origin indicates the mean level of spontaneous activity. The solid lines and data points depict the actual response of the neurone, and error bars represent $1 \pm \text{SEM}$. The dashed lines in B and D indicate the component prediction, which represents the direction tuning for plaids if the neurone responded only to the motions of the two component gratings. This component prediction is generated by adding two direction tuning curves obtained for gratings, with one rotated 45° clockwise and the other rotated 45° anticlockwise. DI, direction index; BW, directional tuning bandwidth defined as in Fig. 2. R_c and R_p are the partial correlations for the component and pattern predictions, respectively. The asterisk indicates statistical significance ($P \leq 0.1$).

1990; Tinsley *et al.*, 2003; Guo *et al.*, 2004). Given the distribution of direction tuning bandwidths and the relatively small proportion of unclassifiable cells described earlier, we believe that this choice was suitable for capturing the motion sensitivity of visual wulst neurones

in response to plaid patterns. Even so, we assessed the likelihood of this inference by repeating our partial correlation measurements with 135° plaids for a subset of neurones. It is clear from the graph in Fig. 7 that a substantial 45° increase in plaid angle did not fundamentally

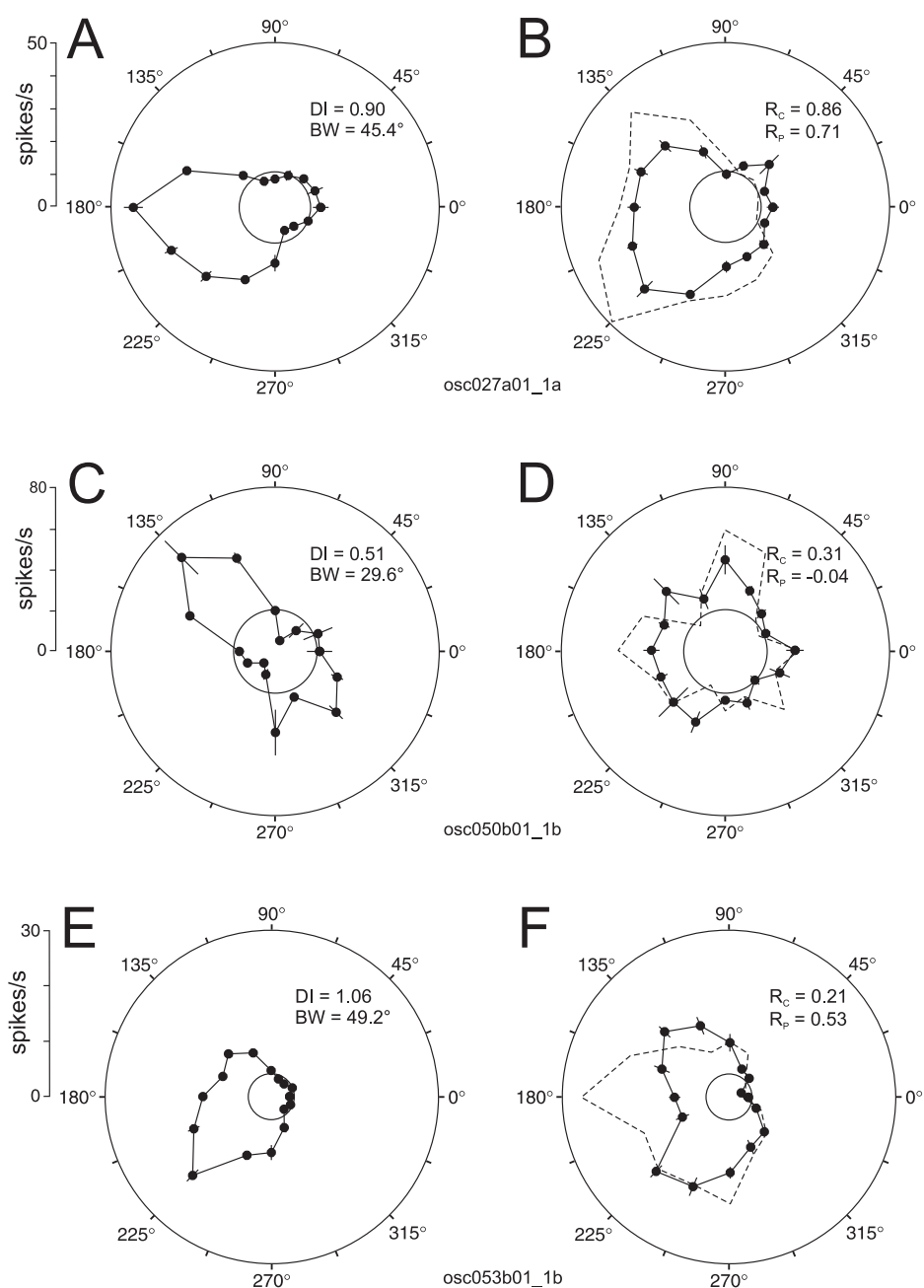


FIG. 4. Directional tuning of three unclassified neurones to drifting sine wave gratings (A, C and E) and 90° plaids (B, D and F). Conventions as in Fig. 3. Note that none of the partial correlation values are marked with an asterisk because for unclassified neurones such values do not reach statistical significance.

change the classification of the 17 retested neurones. Only one of them changed category, migrating from the UNCLASSIFIED to the COMPONENT zone. Across the whole cell sample presented in Fig. 7, changes in correlation coefficient values could be observed following a plaid angle increase. However, as determined by the Wilcoxon signed-rank test, R_c values calculated for 90° plaids were not significantly different from those calculated for 135° plaids ($z = -1.21$, $P = 0.23$). This was also true with respect to R_p

($z = -1.30$, $P = 0.20$) and component index ($z = 1.10$, $P = 0.27$) values.

Response inhibition to plaid patterns

The partial correlation method that we used to classify neurones into CDS and PDS effectively compares the shape between the tuning

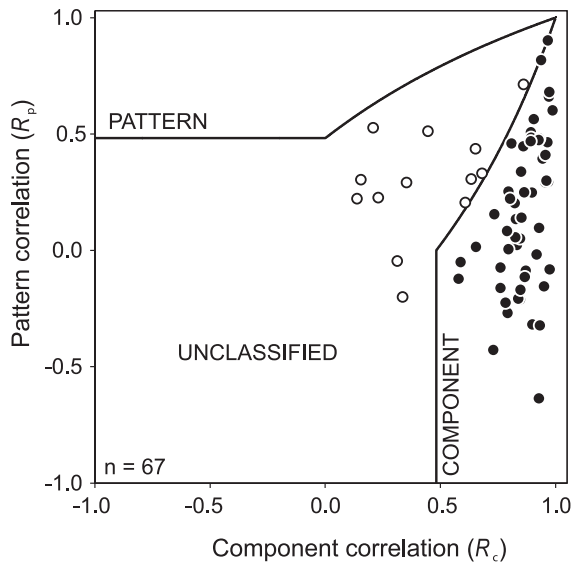


FIG. 5. Scatter plot of partial correlations for the component prediction (R_c) and pattern prediction (R_p) of 67 direction-selective neurones sampled within the owl visual wulst. The graph shows partial correlations in response to 90° plaids. The bullet-shaped line divides the plot into three zones of interest. Points falling in the region marked COMPONENT indicate cells whose R_c significantly exceeds either zero or the value of R_p . Such cells are classified as component direction selective (CDS). Similarly, data points belonging to the region marked PATTERN contain those cells for which R_p significantly exceeds either zero or the value of R_c . Such cells are classified as pattern direction selective (PDS). The intermediate region referred to as UNCLASSIFIED contains cells for which neither correlation coefficient differed from zero or the two coefficients did not differ significantly from each other. Cells classified as CDS are indicated as black filled circles, whereas those unclassified by the partial correlation method are indicated as open circles. Note that no cell satisfies the requirements for PDS classification. The statistical procedure used to define the three regions of interest in the scatterplot is based on a critical value of t for 10% level of significance (for more details see *Data analysis* section in Materials and methods).

curves measured for plaids and the predicted tuning curves for component and pattern direction selectivity. However, this comparison does not take into account absolute differences in response strength. This is an important point, considering the fact that response levels to plaids were often lower than those predicted from the gratings (see, for examples, Fig. 3B and D). In order to quantify the relative magnitude of these inhibitory effects in our dataset, we calculated a plaid inhibition ratio, which compares the actual peak response to plaids with the predicted peak response. As apparent in Fig. 8, the values of this ratio were normally distributed and tightly clustered around a mean of 0.72 ± 0.08 . Only seven cells (10%) showed a plaid peak response higher than the maximal response of the model prediction (plaid inhibition ratio > 1). No statistical differences were found between the distributions of CDS and unclassifiable cells. Strikingly similar mean ratios have been reported in other plaid studies carried out within the mammalian V1 (Movshon *et al.*, 1985; Gizzi *et al.*, 1990; Guo *et al.*, 2004). In those studies, the suppression effect of plaids is interpreted as a manifestation of a form of inhibition known to exist in the striate cortex, namely cross-orientation inhibition (Blakemore & Tobin, 1972; Morrone *et al.*, 1982; Bonds, 1989; DeAngelis *et al.*, 1992). Accordingly, the response to one of the plaid component gratings would be inhibited by the presence of the other component.

Temporal dynamics of component direction selectivity

All of the observations made so far were based on analyses in which neuronal discharges occurring within the first 200 ms of stimulation were excluded. By doing so, we sought to minimize the potential contamination of activity not directly related to the motion direction of the stimuli. However, as exemplified in Fig. 2A and C, the presence of transient peaks of activity shortly after stimulus onset was mostly noticeable for stimuli moving at or near preferred and/or antipreferred directions, suggesting that these early responses are, at least to some extent, directionally selective. We therefore decided to examine the component/pattern motion selectivity of our sample during this initial 200 ms period, comparing it with that determined for the latter (more sustained) part of the response.

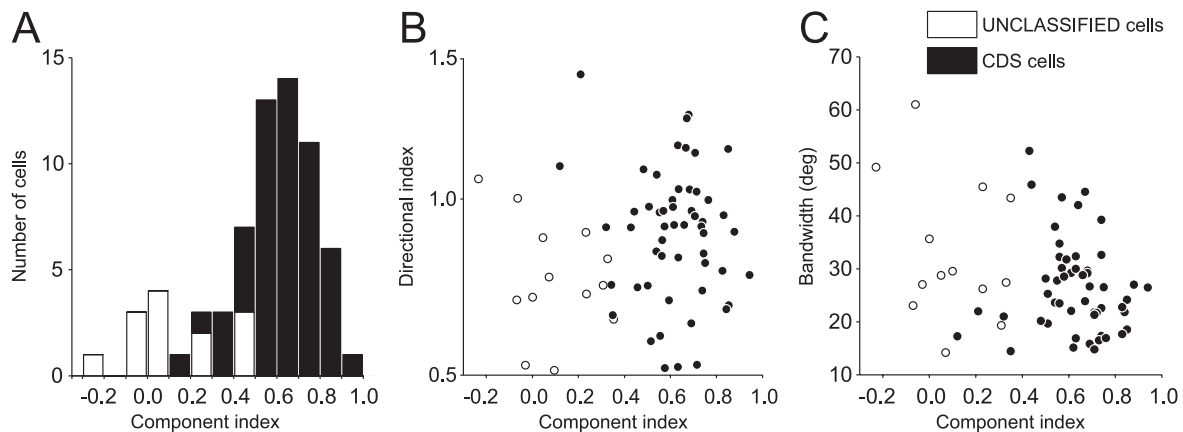


FIG. 6. Relationship between component motion selectivity and direction selectivity for the population of directionally selective neurones. (A) Distribution of component index values calculated for each of the 67 direction-selective visual wulst neurones in response to 90° plaid patterns. The component index is equal to $R_c^2 - R_p^2$ and reflects the strength of component selectivity relative to pattern selectivity. (B) Scatter plot of component vs. direction indices. (C) Scatter plot of component indices vs. directional tuning bandwidth values for the same population of neurones. Black filled symbols refer to component direction-selective (CDS) neurones and open symbols indicate unclassified neurones. R_c , partial correlation coefficient for the component prediction; R_p , partial correlation coefficient for the pattern prediction.

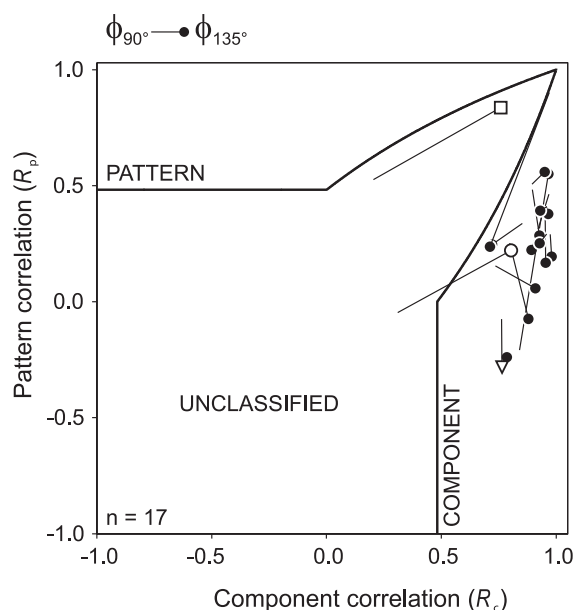


FIG. 7. Influence of plaid angle on the partial correlations for component prediction (R_c) and pattern prediction (R_p) of 17 direction-selective neurones. For each cell, a line connects the partial correlations in response to 90° plaids (no symbols) to those obtained with 135° plaids (symbols). The direction of the lines therefore illustrates the shift in the partial correlations due to the change of plaid angle. All black circles refer to cells that have not been presented in previous figures. Other units: open triangles, osc031a03_1a; open squares, osc053b01_1b; and open circles, osc050b01_1b. The tuning curve of these units has been presented for 90° plaids in Figs 3 and 4.

Figure 9 presents the distribution of partial correlation coefficients in four cumulative windows starting from 0 to 50 ms after stimulus onset and expanding by 50 ms in each successive analysis window. The temporal evolution of these coefficients is shown for five representative cells (Fig. 9A) and for the whole population of direction-selective neurones (Fig. 9B). The colour assignment of the data points in these plots refers to the cell classification established in Fig. 5, thereby providing a means of comparing this previous classification with that obtained for the first 200 ms of stimulation. Two features stand out from this figure. The first concerns the population of unclassified cells, which maintain themselves steady in the UNCLASSIFIED region from as early as the first 50 ms window except for one cell, which expresses significant, albeit less stable, PDS tuning. The second concerns the population of CDS neurones, which migrates gradually from the UNCLASSIFIED to the COMPONENT region of the plot as the window is enlarged to 200 ms. In the first 50 ms, only one out of 54 cells (2%) is classified as CDS. This proportion grows steadily to 11/54 (20%), 24/54 (44%) and 36/54 (67%) over the second, third and fourth plots, respectively, indicating a significant early development of CDS-like tuning. However, by 200 ms of stimulus presentation, one-third of CDS neurones have not significantly gained their characteristic response tuning, as determined when averaging the later part of the response. One possible explanation for this is that stimulus features other than motion may be interfering with responses right after stimulus onset. Nevertheless, care is needed in interpreting this result as such, because responses are being averaged across two windows with very different time spans. Averaging spike counts over shorter intervals may result in noisier

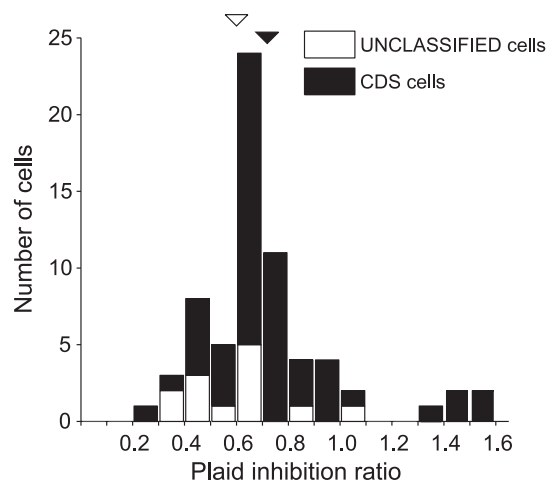


FIG. 8. Distribution of plaid inhibition ratios for direction-selective neurones ($n = 67$). A ratio was calculated for each cell by dividing the actual peak response to plaids by the peak response predicted from the model of component direction selectivity (with spontaneous activity subtracted). A ratio < 1 indicates plaid inhibition and a ratio > 1 indicates facilitation. Note that the majority of cells show some sign of inhibition. Black filled bars refer to component direction-selective (CDS) neurones and open bars indicate unclassified neurones. Mean values for each cell category are represented by the triangles that are colour coded to conform to the convention used for the bars.

tuning curves, favouring unclassifiable outcomes of directional selectivity.

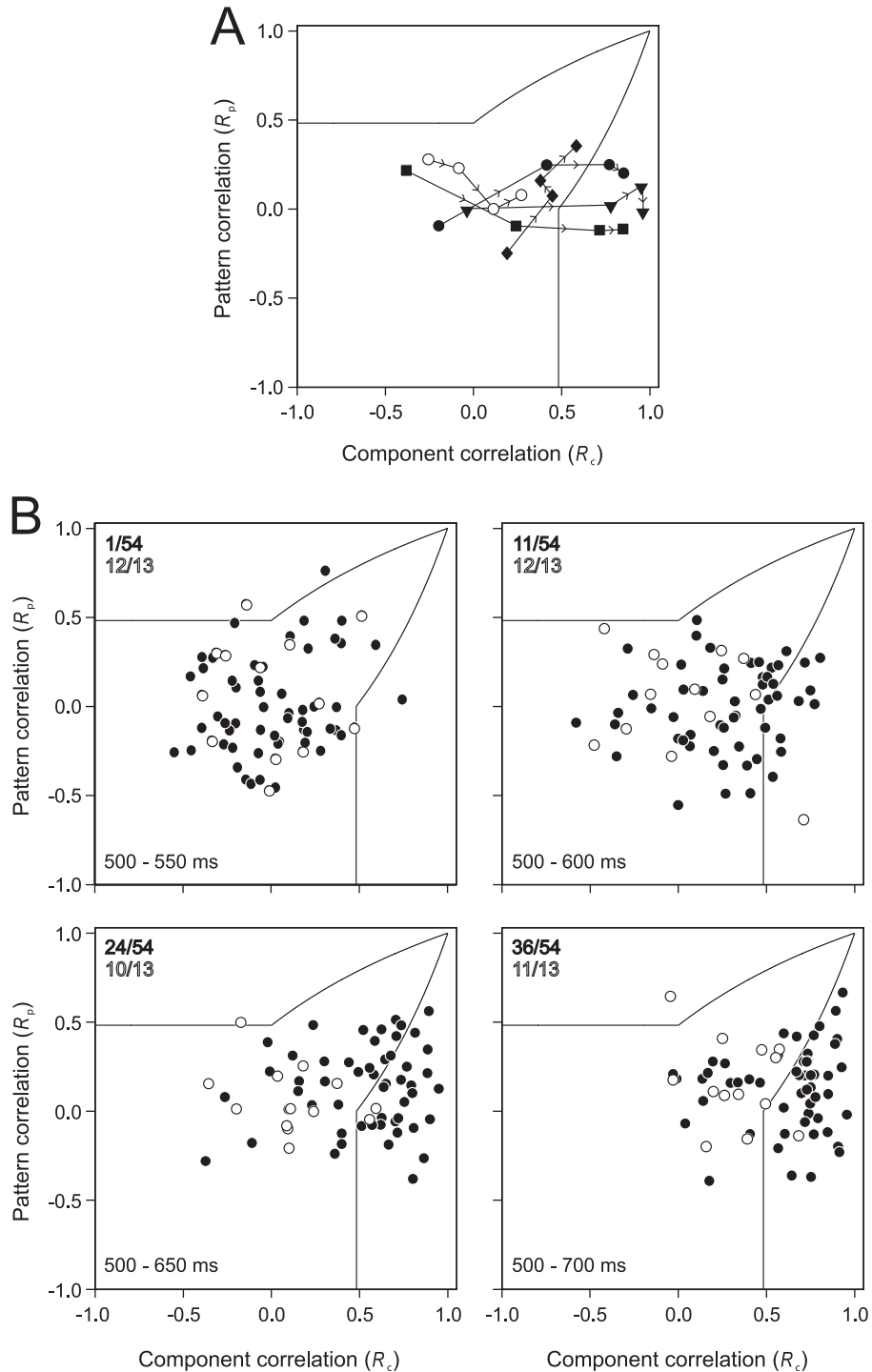
The above results and considerations enticed us to examine, using a different approach, the way in which component selectivity varied during the time course of the entire stimulus presentation. For this, we calculated the average component index for each of a series of 100 ms windows sliding over the whole period of stimulus presentation in 50 ms increments. Results from this analysis are presented in Fig. 10A. Despite a fair amount of variability among cells, it is clear that the strength of component selectivity dynamically unfolds as an initial transient followed by a relatively steady component that remains well above the level observed at stimulus onset and offset. A sharp increase is already noticeable during the first 100 ms response window after stimulus onset (second data point of the curve) and peaks during the fourth window centred at 150 ms. This result suggests that the computation of component selectivity is a process that builds up during the first 150 ms of the neurones' response, confirming the results presented in Fig. 9. Furthermore, it shows that, although higher during the early phase of the response, the strength of component selectivity settles to a sustained level throughout the response to stimulus motion. As can be seen in Fig. 10B, the firing rate of the CDS neurone population in response to both gratings and plaids shows a fairly similar temporal profile, indicating that the strength of component selectivity is somehow linked to changes in neuronal responsiveness.

Discussion

The present experiments were performed with the aim of obtaining more information about the directional selectivity of neurones in the visual wulst of the owl. Responses to sinusoidal gratings were analysed to characterize direction-selective neurones in terms of their overall proportion, directional strength and tuning precision. Although

partially available for the wulst of pigeons (Miceli *et al.*, 1979) and chicks (Wilson, 1980b), such a quantitative description had not been explicitly reported for the owl. In our study, responses to gratings were also compared with those to plaids in order to evaluate whether wulst neurones are capable of spatially integrating local features for

signalling the global motion of a complex stimulus. Despite its fundamental importance for understanding motion perception, this question has never been addressed in the visual wulst. In the owl, this area is far more developed than in most other birds and has been shown to contain neurones that respond to illusory contours, which



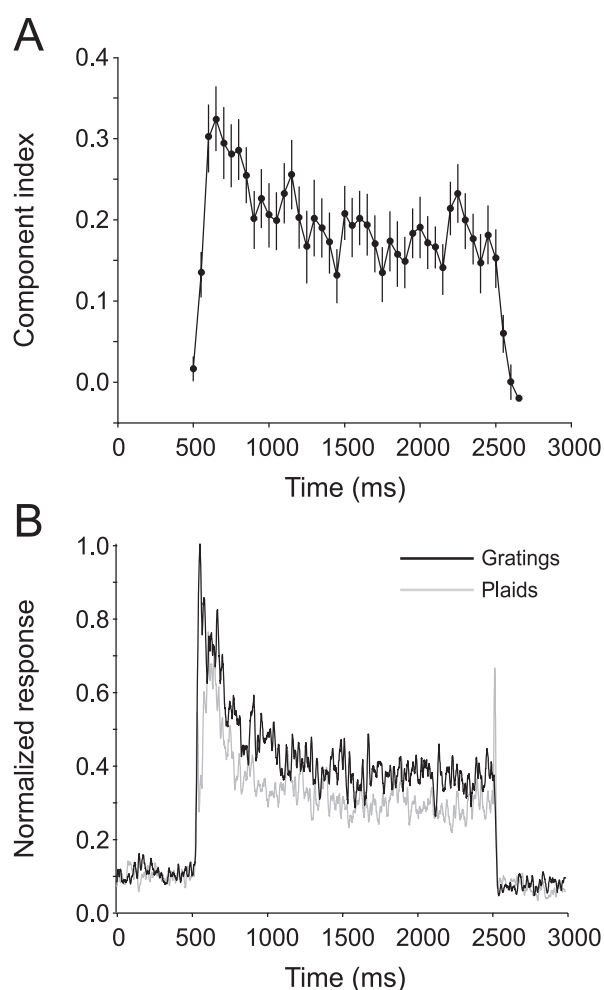


FIG. 10. Population summary of the temporal evolution of component direction-selective (CDS) neurone responses. (A) Temporal dynamics of component selectivity during the whole period of stimulus presentation (from 500 to 2500 ms). Data points indicate the mean component index (\pm SEM) for the population of 54 CDS neurones calculated in 100 ms windows moving in 50 ms steps over time (sliding windows). (B) Population response to gratings (black line) and plaids (grey line) as a function of time for the 54 CDS neurones. For each cell, an average spike density function was generated by convolving the trial-averaged, 1-ms binned, peak response to a particular stimulus type (gratings or plaids). The convolution kernel was a Gaussian with a 15 ms SD. Spike density functions were then normalized by the population peak response to gratings and averaged across neurones. Note the relative inhibition of neuronal responses to plaids.

FIG. 9. Scatter plots of partial correlations for the component prediction (R_c) and pattern prediction (R_p) during the first 200 ms after stimulus onset. All neurones were subjected to the same analysis as that shown in Fig. 5, except that here spike count was performed in four cumulative time windows, starting at 500 ms (stimulus onset) and extending by 50 ms in each successive analysis window. (A) Representative examples of five cells (each indicated by a different symbol), where each point represents R_p and R_c values for a specific time window. To indicate the temporal evolution of partial correlation coefficients, successive analysis windows are linked by arrow lines. (B) Temporal evolution of R_p and R_c values for the whole population of direction-selective cells. The ranges of time windows are indicated at the bottom left of each plot. The bottom right plot shows the distribution of partial correlation coefficients computed in a response window that covers the entire 200 ms stimulus period excluded while preparing Fig. 5. Conventions are as in Fig. 5. In both A and B, the black-filled symbols represent the cells previously classified (in Fig. 5) as component direction selective and the open circles represent those cells that were not classifiable. In B, for each of these two categories (same colour code), the proportion of cells reaching the same classification as in Fig. 5 is indicated in the upper left corner of each plot.

suggests that large-scale integration may take place within the wulst (Nieder & Wagner, 1999; but see Niu *et al.*, 2006). Here, we examined whether such global computation also takes place in the motion domain, as known to be the case in the mammalian visual cortex (Albright & Stoner, 1995).

Our findings can be summarized into two major points. First, the visual wulst of the owl contains a sizeable population of direction-selective neurones that respond robustly to one direction of an optimally orientated moving grating but little if at all to the opposite direction. On average, these neurones have relatively narrow directional tuning bandwidths, although a broad range of values can be observed. Second, when tested with plaids, direction-selective neurones do not show selectivity for the global motion of these stimuli. Instead, the majority yields bilobed tuning curves that can be well predicted by the linear sum of the responses to the two component gratings of the plaids measured separately. Thus, neurones usually show a CDS profile, responding to the motion direction orthogonal to the orientations of the contours that make up the plaid stimuli. The contribution of an orientation-sensitive mechanism in determining directional responses to plaids was further suggested by the fact that such responses were consistently lower than those to gratings alone and that this may be explained by the mutual inhibition of the two components in the orientation domain.

Altogether, our results indicate that directional selectivity is a distinctive characteristic of the visual wulst in the owl. They also indicate that the mechanisms responsible for directional responses are dependent on orientation-selective mechanisms sensitive to the motion of individual contours. Considering that wulst neurones usually have small receptive fields, the information that they are able to convey about object motion is therefore likely to be one-dimensional and local. In this respect, our study suggests that the motion aperture problem cannot be solved at the level of the wulst and leaves open the question as to how and where global motion is being recovered within the avian visual system. In order to ascertain the relevance of this issue, it would be necessary to demonstrate that owls are actually able to see the global motion pattern in plaids. However, there is no reason to believe otherwise, given the complex perceptual capabilities exhibited by these birds (see, for instance, Nieder & Wagner, 1999; van der Willigen *et al.*, 2003).

Receptive field properties in the visual wulst

Our findings confirm previous studies that report the presence of rather small receptive fields in the wulst. In the barn owl, Pettigrew (1979) found receptive fields as small as 1° in the region of central representation and even smaller receptive fields in the dorsolateral geniculate nucleus. The author also described a large over-representation of the central hemifield, with more than half of the total area of the wulst dedicated to the central 10° . Such visuotopic organization is typical of visual areas involved in fine-scale spatial analysis. *De facto*,

a number of electrophysiological studies in the pigeon (De Britto *et al.*, 1975; Jassik-Gerschenfeld *et al.*, 1976) and the chick (Wilson, 1980a; Pateromichelakis, 1981), as well as more recent lesion studies in the pigeon (Hahmann & Güntürkün, 1993; Budzynski & Bingman, 2004), support the notion that this capacity for high-resolution spatial analysis is a relatively well-conserved trait of the avian thalamofugal pathway.

Our results are also relevant to another hallmark property of the visual wulst, namely the orientational selectivity of its neurones (Pettigrew & Konishi, 1976; Pettigrew, 1979; Wilson, 1980b). In the barn owl, 90% of the 579 cells studied by Pettigrew (1979) were orientation selective. According to the author, within the superficial layer of the wulst (HA), many orientation-selective cells also show a directional bias in their response to moving stimuli. As HA is the main output layer of the wulst (Karten *et al.*, 1973), and is where most of our recordings were made, our results consequently deal with the final stages of processing in the wulst. Here, we not only provide a more detailed quantitative description of directional responses but also present direct evidence that direction-selective cells are primarily orientation-selective inasmuch as they are only sensitive to the individual contours of plaids. In other words, direction selectivity in the wulst is always secondary to orientation selectivity, which reinforces the idea that this area is more specifically involved with the detailed analysis of object spatial configurations. It also suggests that more complex forms of motion analysis must occur, at least in part, in other areas of the avian brain.

Another clue to the importance of orientation selectivity in the wulst is that it appears to be organized into regular, columnar patterns. Neurones recorded in penetrations normal to the wulst surface were found to have closely similar orientation preferences, whereas in tangential penetrations the preferred orientation changed progressively and in small steps (Pettigrew, 1979). Using intrinsic signal optical imaging, Liu & Pettigrew (2003) recently confirmed the presence of these iso-orientation domains in the barn owl and further showed that such domains were comparable to those found in area V2 of cat and monkey cortex. Our finding of the suppressive effect of plaids on cell responses may provide a new element of information regarding the functional organization of orientation selectivity within the wulst. Indeed, as stated above, this result hints at the existence of cross-orientation inhibition, which implies that, in the wulst, regions of differing orientation preferences are interconnected by lateral inhibitory projections. In the mammalian V1, this type of circuitry has been associated with the sharpening of orientation tuning relative to that provided by thalamic afferents (Ferster, 2004). A modelling study has also shown that it may favour the emergence of directional selectivity (Wörgötter *et al.*, 1991). The above considerations should therefore prompt future work to investigate more thoroughly orientation-specific inhibition and its functional role in the wulst.

An important feature that sets owls apart from most other birds is the frontal placement of their eyes, which allows them to have a large degree of binocular overlap (Martin, 1984; Wylie *et al.*, 1994) and stereoscopic depth vision (van der Willigen *et al.*, 1998, 2002). It is presumed that the wulst plays an important role in mediating stereopsis in the owl, as it contains a large majority of neurones that are binocular and tuned to horizontal and vertical disparities (Pettigrew & Konishi, 1976; Pettigrew, 1979; Wagner & Frost, 1993, 1994; Nieder & Wagner, 2000, 2001a,b). The fact that all of the direction-selective neurones that we sampled ($n = 67$) were also binocular is interesting, as it raises the possibility that motion and stereoscopic signals get integrated and perhaps interact at the single cell level in the wulst. A number of psychophysical and physiological studies indicate

that not only does such cue integration take place in the primate visual system but that it may also be of functional relevance (see, for example, Rogers & Collett, 1989; Bradley *et al.*, 1995; Bradshaw & Cumming, 1997). Theoretically, there are various advantages to processing motion and stereoscopic cues jointly (Richards, 1985). Foremost, both cues have the same prerequisite, which is to establish a correct match between retinal images. In the motion domain, this match needs to be established in time, across image sequences, whereas in the stereoscopic domain, the match needs to be made simultaneously between the eyes.

Incidence, strength and precision of directional selectivity

All of the functional properties previously reported for the visual wulst of the owl, and discussed above, have proved to be strikingly similar to those found in early visual cortical areas of carnivores and primates, in particular with respect to V1. However, when compared with most other birds or reptiles, this functional analogy between owls and mammals appears quite atypical, suggesting that it is probably due not to common ancestry but to independent evolution (Pettigrew, 1979; Shimizu & Bowers, 1999; Medina & Reiner, 2000). This hypothesis is also supported by developmental and anatomical evidence (Medina & Reiner, 2000). Thus, the owl visual system turns out to be an attractive experimental model to understand the fundamental question of how selective pressures have shaped the convergent or parallel evolution of modern amniotes' brains.

With this comparative perspective in mind, we deliberately followed methods commonly used in previous reports that have investigated the neural basis of motion perception in the visual cortex. To start with, we classified 66% of neurones in the owl visual wulst as directionally selective by adopting a DI threshold value of 0.5, thereby making the *a priori* assumption that the response strength of a direction-selective cell was at least two times greater in its preferred direction than in its antipreferred direction. Although to some extent arbitrary, this threshold value has been widely used to determine the directional selectivity of neurones in the visual cortex and is therefore adequate for comparative purposes.

In terms of the overall proportion of direction-selective cells, and keeping stimuli and classification criteria alike, our results closely match those found in V1 of cats, where most reported values range somewhere between 60 and 75% (Hamilton *et al.*, 1989; Gizzi *et al.*, 1990; Humphrey & Saul, 1998; Carandini & Ferster, 2000; Peterson *et al.*, 2004). Lower percentage values have been found in monkey V1 (20–50%) (De Valois *et al.*, 1982, 2000; Hawken *et al.*, 1988; Hamilton *et al.*, 1989; Snodderly & Gur, 1995; Movshon & Newsome, 1996; O'Keefe *et al.*, 1998; Tinsley *et al.*, 2003; Guo *et al.*, 2004; Gur *et al.*, 2005). However, this discrepancy diminishes if one considers that, in the latter, direction-selective cells are known to be mainly concentrated in layers 4b and 6, where such cells reach proportions of up to 70% (Schiller *et al.*, 1976; Hawken *et al.*, 1988; Snodderly & Gur, 1995; O'Keefe *et al.*, 1998; Gur *et al.*, 2005). As discussed earlier, the distribution of direction-selective cells is probably also layer-specific in the owl wulst and, accordingly, the latter would be more proximate to the striate cortex of the monkey than that of the cat. Anyway, it is clear that the representation of directional selectivity is less expressive in the wulst than in visual cortical areas highly specialized for motion processing, such as area MT in monkeys. In this area, for example, the average number of direction-selective cells is typically around 90% (Maunsell & van Essen, 1983; Albright, 1984; Felleman & Kaas, 1984; Rodman & Albright, 1987; Movshon & Newsome, 1996; Diogo *et al.*, 2003).

Our data on directional tuning bandwidths further support the notion of a close resemblance between the visual wulst and V1. Our population average for this band-pass characteristic was 28°. Similarly, in the V1 of both monkeys and cats, tuning bandwidths have been reported to range from 20° to 40° (Campbell *et al.*, 1968; Rose & Blakemore, 1974; Schiller *et al.*, 1976; De Valois *et al.*, 1982; Gizzi *et al.*, 1990; O'Keefe *et al.*, 1998; Carandini & Ferster, 2000; Gur *et al.*, 2005). Interestingly, the above-mentioned studies that used drifting sinusoidal gratings as stimuli had the closest results to our own. Again, figures in the wulst are quite different from those reported in area MT, where bandwidth estimates are on average twice as broad as those found in V1 and are more widely distributed (Maunsell & van Essen, 1983; Albright, 1984; Felleman & Kaas, 1984; Rodman & Albright, 1987; Lagae *et al.*, 1993; Britten & Newsome, 1998; Diogo *et al.*, 2003).

Motion integration

In response to plaid patterns, 80% of the direction-selective neurones in our sample were classified as CDS, none as PDS and 20% were unclassifiable. This distribution is, on the whole, strikingly similar to what has been described in the striate cortex of anaesthetized cats and monkeys (Movshon *et al.*, 1985; Gizzi *et al.*, 1990; Movshon & Newsome, 1996; Tinsley *et al.*, 2003; Guo *et al.*, 2004). The recent report by Guo *et al.* (2004) found that the incidence of pattern-selective cells was slightly higher in awake monkeys and speculated that this may be due to state-dependent feedback influences from extrastriate areas, MT in particular, on V1 cells. The lack of evidence for pattern selectivity in our study is solely based on experiments with animals that were awake and not actively engaged in a perceptual task related to the stimulus. Although this is also the case in Guo *et al.* (2004), it is still difficult to draw any conclusions about the non-existence of such feedback mechanisms in the owl. Moreover, although several visual areas project to the wulst (see Wild & Williams, 1999; Deng & Rogers, 2000), the paucity of available information concerning their functional properties does not permit, at the present stage, any conclusions about a hierarchical organization of the owl thalamofugal pathway at the level of the forebrain. In any case, the above considerations do not invalidate the two main points suggested by our results. First, like V1, the wulst seems to be the first stage of the thalamofugal pathway where directional selectivity is elaborated. Second, neurones in both of these areas signalize moving orientated contours instead of global motion.

In primates, converging evidence from anatomical, physiological and lesion studies suggests that increasingly complex motion computations take place along a parallel cortical pathway, which starts in V1 and heads towards the posterior parietal cortex (Andersen, 1997). In this pathway, area MT appears to play an important role in motion integration (Born & Bradley, 2005). To date, MT is in fact the only cortical area currently known in primates to have a considerable number of cells that responds to the global motion of plaids (roughly one-third) (Movshon *et al.*, 1985; Rodman & Albright, 1989; Movshon & Newsome, 1996; Pack *et al.*, 2001; Smith *et al.*, 2005). In cats, similar findings have been reported in regions of the lateral suprasylvian and ectosylvian cortices (Scannell *et al.*, 1996; Ouellette *et al.*, 2004). Although the exact mechanisms by which pattern motion selectivity emerges in those motion-specific areas still remain to be clarified (Majaj *et al.*, 2007), several lines of evidence indicate that they depend critically on inputs provided by CDS cells in V1 (Movshon *et al.*, 1985; Albright & Stoner, 1995). On the basis of such evidence, it has been proposed that V1 and MT might be the neural

substrates for the first and second stages of global motion computation, respectively. According to this model, initial motion measurements are locally made by orientation-sensitive neurones, giving rise to the aperture problem. Signals from such neurones are then combined at a second stage to obtain a unified estimate of object motion, thereby solving the aperture problem for planar-translational motion. This two-stage processing scheme is also supported by a wealth of psychophysical data (e.g. Adelson & Movshon, 1982; Movshon *et al.*, 1985) and computer models (e.g. Simoncelli & Heeger, 1998; Rust *et al.*, 2006).

Given the overall functional similarities that we and others have found between V1 and the visual wulst of the owl, it is reasonable to speculate that the computation of global motion in the owl brain may be carried out by a pathway that includes the wulst as an initial processing stage. To validate this hypothesis, future investigations will clearly be needed to identify a candidate site for the explicit integration of the CDS signals provided by the wulst. The latter is known to project to a plethora of visual areas located both in and outside the telencephalon, several of them, such as, for example, the perientopallium, optic tectum and pretectum, containing motion-sensitive neurones (Karten *et al.*, 1973; Shimizu & Bowers, 1999; Deng, 2006). At present, any of these areas is a potential candidate, especially with regard to telencephalic areas, for which functional data are scarce if not non-existent. In the cat, Merabet *et al.* (1998) provided evidence that suggests that motion integration relies on distributed circuit dynamics, involving not only cortico-cortical connections but also cortico-thalamic loops. Considering that this could be the case in the owl, future investigations should therefore pay attention to possible large-scale circuits connecting intra- and extratelencephalic visual areas.

To date, the only study before ours that examined directional responses to plaid patterns in an avian brain was performed in two component nuclei of the pretectum and accessory optic system of the pigeon, namely the pretectal nucleus lentiformis mesencephali (LM) and the nucleus of the basal optic root (nBOR), respectively (Crowder & Wylie, 2002). Highly conserved in vertebrates, these two structures are involved with the analysis of optic flow resulting from self-motion and with the generation of compensatory motor behaviours like the optokinetic response that facilitates retinal image stabilization (for reviews see Simpson, 1984; Grasse & Cynader, 1990). There, neurones have typically large receptive fields in the contralateral hemifield and exhibit direction selectivity to wide-field moving stimuli (Morgan & Frost, 1981; Gioanni *et al.*, 1984; Winterson & Brauth, 1985; Wylie & Frost, 1990; Wylie & Crowder, 2000). Interestingly, in response to plaids, a majority of LM and nBOR neurones were found to be PDS (~50%) and only a few were CDS. In pigeons, telencephalic projections onto such neurones are restricted to the wulst (Wylie *et al.*, 2005). It has also been shown that electrical stimulation of the latter evokes excitatory activity in about one-third of LM (Crowder *et al.*, 2004) and nBOR (Nogueira & Britto, 1991) neurones. However, the question as to whether wulst inputs are important for the elaboration of pattern selectivity observed in these two nuclei remains unclear. Indeed, conflicting results have been reported regarding the degree to which such inputs actually contribute to the directional selectivity of LM and nBOR neurones. A pair of studies based on wulst ablation argues in favour (Hamassaki *et al.*, 1988; Britto *et al.*, 1990), whereas a more recent study, in which the wulst was temporarily inactivated with lidocaine, provides evidence against (Crowder *et al.*, 2004). Moreover, the fact that Crowder & Wylie (2002) found only a few CDS cells in both LM and nBOR suggests that orientation-sensitive signals, like those coming from the wulst, do not predominantly influence the neuronal responses in those

nuclei. As hypothesized by the authors, global motion selectivity in the pretectum and accessory optic system of the pigeon may be due to orientation-insensitive mechanisms, which involve the integration of retinal inputs, the major source of afferents to these nuclei. It would be interesting to investigate whether such a hypothesis also holds for owls, in which the wulst may have a greater influence on this brainstem visuomotor network, as suggested by the fact that nBOR neurones in the owl, unlike those in pigeons, are predominantly binocular (Wylie *et al.*, 1994).

Concluding remarks

To conclude, it is clear that much remains to be done in order to understand the neural basis of motion integration in the owl brain. Apart from its intrinsic value, this understanding will certainly also help to clarify the extent to which the thalamofugal pathway of the owl is functionally analogous to that of carnivores and primates. Several studies have reported that neurones in the upper part of the wulst encode some aspects of intermediate level vision that are usually attributed to extrastriate areas in mammals (Pettigrew, 1979; Nieder & Wagner, 1999, 2000; Liu & Pettigrew, 2003). Because of these findings, it has remained unclear whether a strict functional analogy between the visual wulst and striate cortex can be posited. At least in the specific domain of motion, our results reinforce the idea that the visual wulst can in fact be regarded as a primary visual forebrain area, very much like V1.

Acknowledgements

This work is dedicated to Jack Pettigrew who initially encouraged us to study this wonderful bird, the burrowing owl. We thank Karine Radd and Guilherme Lamego for assistance with some of the recordings, Nan-Hui Chen for the spike-sorting program, Danko Nikolić for the stimulus presentation software, and Mario Fiorani for advice on the head-fixation method. We also wish to thank Wolf Singer for his continuous support, Michaela Klinkmann for manufacturing the recording electrodes, Jacques Baron for assistance, and Rob van der Willigen for helpful comments on the manuscript. This work was funded by grants from the Research Support Foundation of the State of Minas Gerais (FAPEMIG, CBB-1018/04), the German/Brazilian Exchange Program (PROBRAL-CAPES-DAAD, D/03/23569), the Program for Centers of Excellence PRONEX (CNPq-FAPERJ, E26/171210/2003), and the FINEP research grant Rede Instituto Brasileiro de Neurociência (IBN-Net 01.06.0842-00). L. P. received a scholarship from the Brazilian National Council for Scientific and Technological Development (CNPq).

Abbreviations

CDS, component direction selective; DI, direction index; HA, hyperpallium apicale; LM, pretectal nucleus lentiformis mesencephali; MT, middle temporal area; nBOR, nucleus of the basal optic root; PDS, pattern direction selective; R_c , partial correlation coefficient for the component prediction; R_p , partial correlation coefficient for the pattern prediction; V1, primary visual cortex.

References

Adelson, E.H. & Movshon, J.A. (1982) Phenomenal coherence of moving visual patterns. *Nature*, **300**, 523–525.
 Albright, T.D. (1984) Direction and orientation selectivity of neurons in visual area MT of the macaque. *J. Neurophysiol.*, **52**, 1106–1130.
 Albright, T.D. (1989) Centrifugal directional bias in the middle temporal visual area (MT) of the macaque. *Vis. Neurosci.*, **2**, 177–188.
 Albright, T.D. & Stoner, G.R. (1995) Visual motion perception. *Proc. Natl Acad. Sci. U.S.A.*, **92**, 2433–2440.
 Andersen, R.A. (1997) Neural mechanisms of visual motion perception in primates. *Neuron*, **18**, 865–872.

Azzi, J.C.B. (2004) O mapa do córtex visual primário é visuotópico e não retinotópico: visuotopia do ponto cego em V1 de primatas (cebus apella). PhD Thesis. Universidade Federal do Rio de Janeiro.
 Barlow, H.B., Blakemore, C. & Pettigrew, J.D. (1967) The neural mechanism of binocular depth discrimination. *J. Physiol.*, **193**, 327–342.
 Blakemore, C. & Tobin, E.A. (1972) Lateral inhibition between orientation detectors in the cat's visual cortex. *Exp. Brain Res.*, **15**, 439–440.
 Bonds, A.B. (1989) Role of inhibition in the specification of orientation selectivity of cells in the cat striate cortex. *Vis. Neurosci.*, **2**, 41–55.
 Born, R.T. & Bradley, D.C. (2005) Structure and function of visual area MT. *Annu. Rev. Neurosci.*, **28**, 157–189.
 Bradley, D.C., Qian, N. & Andersen, R.A. (1995) Integration of motion and stereopsis in middle temporal cortical area of macaques. *Nature*, **373**, 609–611.
 Bradshaw, M.F. & Cumming, B.G. (1997) The direction of retinal motion facilitates binocular stereopsis. *Proc. Biol. Sci.*, **264**, 1421–1427.
 Branch, M.A., Coleman, T.F. & Li, Y. (1999) A subspace, interior and conjugate gradient method for large-scale bound-constrained minimization problems. *SIAM J. Sci. Comput.*, **21**, 1–23.
 Bravo, H. & Pettigrew, J.D. (1981) The distribution of neurons projecting from the retina and visual cortex to the thalamus and tectum opticum of the barn owl, *Tyto alba*, and the burrowing owl, *Speotyto cunicularia*. *J. Comp. Neurol.*, **199**, 419–441.
 Britten, K.H. & Newsome, W.T. (1998) Tuning bandwidths for near-threshold stimuli in area MT. *J. Neurophysiol.*, **80**, 762–770.
 Britto, L.R., Gasparotto, O.C. & Hamassaki, D.E. (1990) Visual telencephalon modulates directional selectivity of accessory optic neurons in pigeons. *Vis. Neurosci.*, **4**, 3–10.
 Budzynski, C.A. & Bingman, V.P. (2004) Participation of the thalamofugal visual pathway in a coarse pattern discrimination task in an open arena. *Behav. Brain Res.*, **153**, 543–556.
 Campbell, F.W., Cleland, B.G., Cooper, G.F. & Enroth-Cugell, C. (1968) The angular selectivity of visual cortical cells to moving gratings. *J. Physiol.*, **198**, 237–250.
 Carandini, M. & Ferster, D. (2000) Membrane potential and firing rate in cat primary visual cortex. *J. Neurosci.*, **20**, 470–484.
 Carpenter, G.A. & Grossberg, S. (1987) Discovering order in chaos: stable self-organization of neural recognition codes. *Ann. N.Y. Acad. Sci.*, **504**, 33–51.
 Cooper, M.L. & Pettigrew, J.D. (1979) A neurophysiological determination of the vertical horopter in the cat and owl. *J. Comp. Neurol.*, **184**, 1–26.
 Coulombe, H.N. (1971) Behavior and population ecology of the burrowing owl, *Speotyto cunicularia*, in the Imperial Valley of California. *Condor*, **73**, 162–176.
 Crowder, N.A. & Wylie, D.R. (2002) Responses of optokinetic neurons in the pretectum and accessory optic system of the pigeon to large-field plaids. *J. Comp. Physiol. A Neuroethol. Sens. Neural Behav. Physiol.*, **188**, 109–119.
 Crowder, N.A., Dickson, C.T. & Wylie, D.R. (2004) Telencephalic input to the pretectum of pigeons: an electrophysiological and pharmacological inactivation study. *J. Neurophysiol.*, **91**, 274–285.
 DeAngelis, G.C., Robson, J.G., Ohzawa, I. & Freeman, R.D. (1992) Organization of suppression in receptive fields of neurons in cat visual cortex. *J. Neurophysiol.*, **68**, 144–163.
 De Britto, L.R., Brunelli, M., Francesconi, W. & Magni, F. (1975) Visual response pattern of thalamic neurons in the pigeon. *Brain Res.*, **97**, 337–343.
 Deng, C. (2006) Relative contributions of the two visual pathways to avian behavior. *Acta Zool. Sin.*, **52** (Suppl.), 379–383.
 Deng, C. & Rogers, L.J. (2000) Organization of intratelencephalic projections to the visual wulst of the chick. *Brain Res.*, **856**, 152–162.
 De Valois, R.L., Albrecht, D.G. & Thorell, L.G. (1982) Spatial frequency selectivity of cells in macaque visual cortex. *Vis. Res.*, **22**, 545–559.
 De Valois, R.L., Cottaris, N.P., Mahon, L.E., Elfar, S.D. & Wilson, J.A. (2000) Spatial and temporal receptive fields of geniculate and cortical cells and directional selectivity. *Vis. Res.*, **40**, 3685–3702.
 Diogo, A.C., Soares, J.G., Koulakov, A., Albright, T.D. & Gattass, R. (2003) Electrophysiological imaging of functional architecture in the cortical middle temporal visual area of *Cebus apella* monkey. *J. Neurosci.*, **23**, 3881–3898.
 Felleman, D.J. & Kaas, J.H. (1984) Receptive-field properties of neurons in middle temporal visual area (MT) of owl monkeys. *J. Neurophysiol.*, **52**, 488–513.
 Fennema, C. & Thompson, W.B. (1979) Velocity determination in scenes containing several moving images. *Comput. Graph. Image Proc.*, **9**, 301–315.

- Ferster, D. (2004) Assembly of receptive fields in primary visual cortex. In Chalupa, L.M. & Werner, J.S. (Eds), *The Visual Neurosciences*. A Bradford Book. MIT Press, Cambridge, MA, pp. 695–703.
- Gioanni, H., Rey, J., Villalobos, J. & Dalbera, A. (1984) Single unit activity in the nucleus of the basal optic root (nBOR) during optokinetic, vestibular and visuo-vestibular stimulations in the alert pigeon (*Columba livia*). *Exp. Brain Res.*, **57**, 49–60.
- Gizzi, M.S., Katz, E., Schumer, R.A. & Movshon, J.A. (1990) Selectivity for orientation and direction of motion of single neurons in cat striate and extrastriate visual cortex. *J. Neurophysiol.*, **63**, 1529–1543.
- Grasse, K.L. & Cynader, M.S. (1990) The accessory optic system in frontal-eyed animals. In Leventhal, A. (Ed.), *Vision and Visual Dysfunction*. McMillan, New York, pp. 111–139.
- Guo, K., Benson, P.J. & Blakemore, C. (2004) Pattern motion is present in V1 of awake but not anaesthetized monkeys. *Eur. J. Neurosci.*, **19**, 1055–1066.
- Gur, M., Kagan, I. & Snodderly, D.M. (2005) Orientation and direction selectivity of neurons in V1 of alert monkeys: functional relationships and laminar distributions. *Cereb. Cortex*, **15**, 1207–1221.
- Hahmann, U. & Güntürkün, O. (1993) The visual acuity for the lateral visual field of the pigeon (*Columba livia*). *Vis. Res.*, **33**, 1659–1664.
- Hamassaki, D.E., Gasparotto, O.C., Nogueira, M.I. & Britto, L.R. (1988) Telencephalic and pretectal modulation of the directional selectivity of accessory optic neurons in the pigeon. *Braz. J. Med. Biol. Res.*, **21**, 649–652.
- Hamilton, D.B., Albrecht, D.G. & Geisler, W.S. (1989) Visual cortical receptive fields in monkey and cat: spatial and temporal phase transfer function. *Vis. Res.*, **29**, 1285–1308.
- Hawken, M.J., Parker, A.J. & Lund, J.S. (1988) Laminar organization and contrast sensitivity of direction-selective cells in the striate cortex of the Old World monkey. *J. Neurosci.*, **8**, 3541–3548.
- Henry, G.H., Bishop, P.O. & Dreher, B. (1974) Orientation, axis and direction as stimulus parameters for striate cells. *Vis. Res.*, **14**, 767–777.
- Hubel, D.H. & Wiesel, T.N. (1962) Receptive fields, binocular interaction and functional architecture in the cat's visual cortex. *J. Physiol.*, **160**, 106–154.
- Hubel, D.H. & Wiesel, T.N. (1968) Receptive fields and functional architecture of monkey striate cortex. *J. Physiol.*, **195**, 215–243.
- Humphrey, A.L. & Saul, A.B. (1998) Strobe rearing reduces direction selectivity in area 17 by altering spatiotemporal receptive-field structure. *J. Neurophysiol.*, **80**, 2991–3004.
- Iwaniuk, A.N. & Hurd, P.L. (2005) The evolution of cerebrotypes in birds. *Brain Behav. Evol.*, **65**, 215–230.
- Iwaniuk, A.N. & Wylie, D.R. (2006) The evolution of stereopsis and the Wulst in caprimulgidiform birds: a comparative analysis. *J. Comp. Physiol. A Neuroethol. Sens. Neural Behav. Physiol.*, **192**, 1313–1326.
- Jassik-Gerschenfeld, D., Teulon, J. & Ropert, N. (1976) Visual receptive field types in the nucleus dorsolateralis anterior of the pigeon's thalamus. *Brain Res.*, **108**, 295–306.
- Karten, H.J., Hodos, W., Nauta, W.J. & Revzin, A.M. (1973) Neural connections of the 'visual wulst' of the avian telencephalon. Experimental studies in the pigeon (*Columba livia*) and owl (*Speotyto cunicularia*). *J. Comp. Neurol.*, **150**, 253–278.
- Knudsen, E.I. (1982) Auditory and visual maps of space in the optic tectum of the owl. *J. Neurosci.*, **2**, 1177–1194.
- Konishi, M. (1993) Listening with two ears. *Sci. Am.*, **268**, 66–73.
- Lagae, L., Raiguel, S. & Orban, G.A. (1993) Speed and direction selectivity of macaque middle temporal neurons. *J. Neurophysiol.*, **69**, 19–39.
- Liu, G.B. & Pettigrew, J.D. (2003) Orientation mosaic in barn owl's visual Wulst revealed by optical imaging: comparison with cat and monkey striate and extra-striate areas. *Brain Res.*, **961**, 153–158.
- Majaj, N.J., Carandini, M. & Movshon, J.A. (2007) Motion integration by neurons in macaque MT is local, not global. *J. Neurosci.*, **27**, 366–370.
- Marr, D. & Ullman, S. (1981) Directional selectivity and its use in early visual processing. *Proc. R. Soc. Lond. B Biol. Sci.*, **211**, 151–180.
- Martin, G.R. (1984) The visual fields of the tawny owl, *Strix aluco* L. *Vis. Res.*, **24**, 1739–1751.
- Maunsell, J.H. & van Essen, D.C. (1983) Functional properties of neurons in middle temporal visual area of the macaque monkey. I. Selectivity for stimulus direction, speed, and orientation. *J. Neurophysiol.*, **49**, 1127–1147.
- Medina, L. & Reiner, A. (2000) Do birds possess homologues of mammalian primary visual, somatosensory and motor cortices? *Trends Neurosci.*, **23**, 1–12.
- Merabet, L., Desautels, A., Minville, K. & Casanova, C. (1998) Motion integration in a thalamic visual nucleus. *Nature*, **396**, 265–268.
- Miceli, D., Gioanni, H., Reperant, J. & Peyrichou, J. (1979) The avian visual wulst. I. An anatomical study of afferent and efferent pathways. II. An electrophysiological study of the functional properties of single neurons. In Granada, A.M. & Maxwell, J.H. (Eds), *Neural Mechanisms of Behavior in the Pigeon*. Plenum Press, New York, pp. 223–254.
- Morgan, B. & Frost, B.J. (1981) Visual response characteristics of neurons in nucleus of basal optic root of pigeons. *Exp. Brain Res.*, **42**, 181–188.
- Morrone, M.C., Burr, D.C. & Maffei, L. (1982) Functional implications of cross-orientation inhibition of cortical visual cells. I. Neurophysiological evidence. *Proc. R. Soc. Lond. B Biol. Sci.*, **216**, 335–354.
- Movshon, J.A. & Newsome, W.T. (1996) Visual response properties of striate cortical neurons projecting to area MT in macaque monkeys. *J. Neurosci.*, **16**, 7733–7741.
- Movshon, J.A., Adelson, E.H., Gizzi, M.S. & Newsome, W.T. (1985) The analysis of moving visual patterns. In Chagas, C., Gattass, R. & Gross, C. (Eds), *Study Week on Pattern Recognition Mechanisms*. Pont. Acad. Scient. *Scrip. Varta*. Vatican Press, Vatican City, **Vol. 54**, pp. 117–151.
- Nieder, A. & Wagner, H. (1999) Perception and neuronal coding of subjective contours in the owl. *Nat. Neurosci.*, **2**, 660–663.
- Nieder, A. & Wagner, H. (2000) Horizontal-disparity tuning of neurons in the visual forebrain of the behaving barn owl. *J. Neurophysiol.*, **83**, 2967–2979.
- Nieder, A. & Wagner, H. (2001a) Encoding of both vertical and horizontal disparity in random-dot stereograms by Wulst neurons of awake barn owls. *Vis. Neurosci.*, **18**, 541–547.
- Nieder, A. & Wagner, H. (2001b) Hierarchical processing of horizontal disparity information in the visual forebrain of behaving owls. *J. Neurosci.*, **21**, 4514–4522.
- Niu, Y.Q., Xiao, Q., Liu, R.F., Wu, L.Q. & Wang, S.R. (2006) Response characteristics of the pigeon's pretectal neurons to illusory contours and motion. *J. Physiol.*, **577**, 805–813.
- Nogueira, M.I. & Britto, L.R. (1991) Extraretinal modulation of accessory optic units in the pigeon. *Braz. J. Med. Biol. Res.*, **24**, 623–631.
- Norberg, R.A. (1977) Occurrence and independent evolution of bilateral ear asymmetry in owls and implication in owl taxonomy. *Philos. Trans. R. Soc. Lond. Ser. B*, **280**, 375–408.
- O'Keefe, L.P., Levitt, J.B., Kiper, D.C., Shapley, R.M. & Movshon, J.A. (1998) Functional organization of owl monkey lateral geniculate nucleus and visual cortex. *J. Neurophysiol.*, **80**, 594–609.
- Ouellette, B.G., Minville, K., Faubert, J. & Casanova, C. (2004) Simple and complex visual motion response properties in the anterior medial bank of the lateral suprasylvian cortex. *Neuroscience*, **123**, 231–245.
- Pack, C.C., Berezovskii, V.K. & Born, R.T. (2001) Dynamic properties of neurons in cortical area MT in alert and anaesthetized macaque monkeys. *Nature*, **414**, 905–908.
- Papoulis, A. (1990) *Probability and Statistics*. Prentice Hall, Englewood Cliffs, NJ.
- Patermichelakias, S. (1981) Response properties of visual units in the anterior dorsolateral thalamus of the chick (*Gallus domesticus*). *Experientia*, **37**, 279–280.
- Peterson, M.R., Li, B. & Freeman, R.D. (2004) The derivation of direction selectivity in the striate cortex. *J. Neurosci.*, **24**, 3583–3591.
- Pettigrew, J.D. (1979) Binocular visual processing in the owl's telencephalon. *Proc. R. Soc. Lond.*, **204**, 435–454.
- Pettigrew, J.D. & Konishi, M. (1976) Neurons selective for orientation and binocular disparity in the visual Wulst of the barn owl (*Tyto alba*). *Science*, **193**, 675–678.
- Pinto, L., Dias, M.O., Lima, B., Neuenschwander, S. & Baron, J. (2006) Response of visual Wulst neurons to plaid patterns in the burrowing owl. In *XXI Reunião Anual Da Federação de Sociedades Brasileiras de Biologia Experimental-FeSBE 2006*, Águas de Lindóia, no. 05.125.
- Pinto, L., Dias, M.O., Lima, B., Neuenschwander, S. & Baron, J. (2007) Steady-state and dynamical aspects of component direction selectivity in the visual Wulst of awake owls. In *II International Neurosciences Symposium of the IINN*, Natal, No. 156.
- Reiner, A., Perkel, D.J., Bruce, L.L., Butler, A.B., Csillag, A., Kuenzel, W., Medina, L., Paxinos, G., Shimizu, T., Striedter, G., Wild, M., Ball, G.F., Durand, S., Gunturkun, O., Lee, D.W., Mello, C.V., Powers, A., White, S.A., Hough, G., Kubikova, L., Smulders, T.V., Wada, K., Dugas-Ford, J., Husband, S., Yamamoto, K., Yu, J., Siang, C. & Jarvis, E.D. (2004) Revised nomenclature for avian telencephalon and some related brainstem nuclei. *J. Comp. Neurol.*, **473**, 377–414.
- Richards, W. (1985) Structure from stereo and motion. *J. Opt. Soc. Am. [A]*, **2**, 343–349.
- Rodman, H.R. & Albright, T.D. (1987) Coding of visual stimulus velocity in area MT of the macaque. *Vis. Res.*, **27**, 2035–2048.
- Rodman, H.R. & Albright, T.D. (1989) Single-unit analysis of pattern-motion selective properties in the middle temporal visual area (MT). *Exp. Brain Res.*, **75**, 53–64.

- Rogers, B.J. & Collett, T.S. (1989) The appearance of surfaces specified by motion parallax and binocular disparity. *Q. J. Exp. Psychol. A*, **41**, 697–717.
- Rose, D. & Blakemore, C. (1974) An analysis of orientation selectivity in the cat's visual cortex. *Exp. Brain Res.*, **20**, 1–17.
- Rust, N.C., Mante, V., Simoncelli, E.P. & Movshon, J.A. (2006) How MT cells analyze the motion of visual patterns. *Nat. Neurosci.*, **9**, 1421–1431.
- Scannell, J.W., Sengpiel, F., Tovee, M.J., Benson, P.J., Blakemore, C. & Young, M.P. (1996) Visual motion processing in the anterior ectosylvian sulcus of the cat. *J. Neurophysiol.*, **76**, 895–907.
- Schiller, P.H., Finlay, B.L. & Volman, S.F. (1976) Quantitative studies of single-cell properties in monkey striate cortex. II. Orientation specificity and ocular dominance. *J. Neurophysiol.*, **39**, 1320–1333.
- Shimizu, T. & Bowers, A.N. (1999) Visual circuits of the avian telencephalon: evolutionary implications. *Behav. Brain Res.*, **98**, 183–191.
- Simoncelli, E.P. & Heeger, D.J. (1998) A model of neuronal responses in visual area MT. *Vis. Res.*, **38**, 743–761.
- Simpson, J.I. (1984) The accessory optic system. *Annu. Rev. Neurosci.*, **7**, 13–41.
- Singer, W. (2004) Synchrony, oscillations and relational codes. In Chalupa, L.M. & Werner, J.S. (Eds), *The Visual Neurosciences*. A Bradford Book. MIT Press, Cambridge, MA, pp. 1665–1681.
- Smith, M.A., Majaj, N.J. & Movshon, J.A. (2005) Dynamics of motion signaling by neurons in macaque area MT. *Nat. Neurosci.*, **8**, 220–228.
- Snodderly, D.M. & Gur, M. (1995) Organization of striate cortex of alert, trained monkeys (*Macaca fascicularis*): ongoing activity, stimulus selectivity, and widths of receptive field activating regions. *J. Neurophysiol.*, **74**, 2100–2125.
- Spath, H. (1980) *Cluster Analysis Algorithms for Reduction and Classification of Objects*. Ellis Horwood, West Sussex, UK.
- Steinbach, M.J., Angus, R.G. & Money, K.E. (1974) Torsional eye movements of the owl. *Vis. Res.*, **14**, 745–746.
- Stingelin, W. (1958) Vergleichend-morphologische Untersuchungen am Vorderhirn der Vögel auf cytologischer und cytoarchitektonischer Grundlage. Helbing & Lichtenhahn, Basel, Switzerland.
- Stoner, G.R. & Albright, T.D. (1992) Neural correlates of perceptual motion coherence. *Nature*, **358**, 412–414.
- Swindale, N.V., Grinvald, A. & Shmuel, A. (2003) The spatial pattern of response magnitude and selectivity for orientation and direction in cat visual cortex. *Cereb. Cortex*, **13**, 225–238.
- Tinsley, C.J., Webb, B.S., Barraclough, N.E., Vincent, C.J., Parker, A. & Derrington, A.M. (2003) The nature of V1 neural responses to 2D moving patterns depends on receptive-field structure in the marmoset monkey. *J. Neurophysiol.*, **90**, 930–937.
- Wagner, H. & Frost, B. (1993) Disparity-sensitive cells in the owl have a characteristic disparity. *Nature*, **364**, 796–798.
- Wagner, H. & Frost, B. (1994) Binocular responses of neurons in the barn owl's visual wulst. *J. Comp. Physiol. A*, **174**, 661–670.
- Wallach, H. (1935) Über visuell wahrgenommene Bewegungsrichtung. *Psychol. Forsch.*, **20**, 325–380.
- van Wezel, R.J. & van der Smagt, M.J. (2003) Motion processing: how low can you go? *Curr. Biol.*, **13**, R840–R842.
- Wheeler, B.C. (1999) Automatic discrimination of single units. In Nicolelis, M.A.L. (Ed.), *Methods of Neural Ensemble Recording*. Methods in Life Sciences. CRC Press, Boca Raton, FL, pp. 61–78.
- Wild, J.M. & Williams, M.N. (1999) Rostral wulst of passerine birds. II. Intratelencephalic projections to nuclei associated with the auditory and song systems. *J. Comp. Neurol.*, **413**, 520–534.
- van der Willigen, R.F., Frost, B.J. & Wagner, H. (1998) Stereoscopic depth perception in the owl. *Neuroreport*, **9**, 1233–1237.
- van der Willigen, R.F., Frost, B.J. & Wagner, H. (2002) Depth generalization from stereo to motion parallax in the owl. *J. Comp. Physiol. A Neuroethol. Sens. Neural Behav. Physiol.*, **187**, 997–1007.
- van der Willigen, R.F., Frost, B.J. & Wagner, H. (2003) How owls structure visual information. *Anim. Cogn.*, **6**, 39–55.
- Wilson, P. (1980a) The organization of the visual hyperstriatum in the domestic chick. II. Receptive field properties of single units. *Brain Res.*, **188**, 333–345.
- Wilson, P. (1980b) The organization of the visual hyperstriatum in the domestic chick. I. Topology and topography of the visual projection. *Brain Res.*, **188**, 319–332.
- Winterson, B.J. & Brauth, S.E. (1985) Direction-selective single units in the nucleus lentiformis mesencephali of the pigeon (*Columba livia*). *Exp. Brain Res.*, **60**, 215–226.
- Wörgötter, F., Niebur, E. & Koch, C. (1991) Isotropic connections generate functional asymmetrical behavior in visual cortical cells. *J. Neurophysiol.*, **66**, 444–459.
- Wylie, D.R. & Crowder, N.A. (2000) Spatiotemporal properties of fast and slow neurons in the pretectal nucleus lentiformis mesencephali in pigeons. *J. Neurophysiol.*, **84**, 2529–2540.
- Wylie, D.R. & Frost, B.J. (1990) The visual response properties of neurons in the nucleus of the basal optic root of the pigeon: a quantitative analysis. *Exp. Brain Res.*, **82**, 327–336.
- Wylie, D.R., Shaver, S.W. & Frost, B.J. (1994) The visual response properties of neurons in the nucleus of the basal optic root of the northern saw-whet owl (*Aegolius acadicus*). *Brain Behav. Evol.*, **43**, 15–25.
- Wylie, D.R., Ogilvie, C.J., Crowder, N.A., Barkley, R.R. & Winship, I.R. (2005) Telencephalic projections to the nucleus of the basal optic root and pretectal nucleus lentiformis mesencephali in pigeons. *Vis. Neurosci.*, **22**, 237–247.

Chapter 3

Synchronization dynamics in response to plaid stimuli in monkey V1

Reprint of Lima B, Singer W, Chen N-H and Neuenschwander S. *Cereb Cortex*. (2010). 20: 1556-1573.

I took part in all aspects of this work.

Synchronization Dynamics in Response to Plaid Stimuli in Monkey V1

Bruss Lima, Wolf Singer, Nan-Hui Chen and Sergio Neuenschwander

Max-Planck Institute for Brain Research, 60528 Frankfurt am Main, Germany

Gamma synchronization has generally been associated with grouping processes in the visual system. Here, we examine in monkey V1 whether gamma oscillations play a functional role in segmenting surfaces of plaid stimuli. Local field potentials (LFPs) and spiking activity were recorded simultaneously from multiple sites in the opercular and calcarine regions while the monkeys were presented with sequences of single and superimposed components of plaid stimuli. In accord with the previous studies, responses to the single components (gratings) exhibited strong and sustained gamma-band oscillations (30–65 Hz). The superposition of the second component, however, led to profound changes in the temporal structure of the responses, characterized by a drastic reduction of gamma oscillations in the spiking activity and systematic shifts to higher frequencies in the LFP (~10% increase). Comparisons between cerebral hemispheres and across monkeys revealed robust subject-specific spectral signatures. A possible interpretation of our results may be that single gratings induce strong cooperative interactions among populations of cells that share similar response properties, whereas plaids lead to competition. Overall, our results suggest that the functional architecture of the cortex is a major determinant of the neuronal synchronization dynamics in V1.

Keywords: attention, gamma, gratings, oscillation, visual cortex

Introduction

A major challenge in understanding perceptual organization is to explain how stable relationships are constructed dynamically in a multidimensional feature space. Given the distributed nature of cortical networks, an important goal is to identify the mechanisms by which selective neuronal interactions enable large-scale coordination of neuronal activity (Varela et al. 2001; Buzsáki and Draguhn 2004). Theoretical and experimental work suggests that temporal relationships in neuronal activity may serve as a linking mechanism for perceptual binding (reviewed in Gray 1999; Singer 1999; Engel et al. 2001). According to this concept, cell assemblies dynamically formed by synchronization of spiking activity constitute stable functional units, which allow for feature grouping processes, such as the pre-attentive segmentation of a visual scene (Gray et al. 1989; Engel et al. 1991; Kreiter and Singer 1996).

To validate this hypothesis, a general experimental goal has been to search for correlations between synchronously firing neuronal ensembles and perceptually coherent objects, such as moving bars, gratings, and dots (Gray et al. 1989; Engel et al. 1991; Eckhorn et al. 1993; Kreiter and Singer 1996; Palanca and DeAngelis 2005; Woelbern et al. 2002). In the majority of studies in which such correlations have been found,

synchronization is typically accompanied by rhythmic activity in the gamma frequency band (30–90 Hz). This has been observed for spiking activity of single cells (single-unit activity, SUA) and small neuronal clusters (multi-unit activity, MUA), as well as for mesoscale signals, such as the local field potential (LFP), the electroencephalogram (EEG), and the magnetoencephalogram (Tallon-Baudry and Bertrand 1999; Varela et al. 2001; Vidal et al. 2006; Sehatpour et al. 2008). Gamma oscillations in the LFP generally show precise phase-locking to local spiking activity (König et al. 1995a), suggesting that the temporal structure carried by oscillatory signals represents an important synchronizing mechanism (Womelsdorf et al. 2007; Fries et al. 2008). Moreover, it has been shown that selective attention is associated with synchronization of oscillatory responses specifically at the gamma band (Müller et al. 2000; Fries et al. 2001; Taylor et al. 2005; Womelsdorf et al. 2006; Womelsdorf et al. 2007; Fries et al. 2008), which may serve as a mechanism for selective communication within and across cortical areas (Fries 2005; Fries et al. 2007).

In a previous study in the visual cortex of anesthetized cats, we have used superimposed drifting gratings (plaids) to investigate the role of synchronization on surface segmentation (Castelo-Branco et al. 2000a). Plaid stimuli are ideal to study visual segmentation because perception can be biased in a predictive manner by the manipulation of the luminance of the intersections, from 2 surfaces sliding on top of each other (noncoherent motion) to a single surface moving in an intermediate direction (coherent motion) (Stoner and Albright 1996). Furthermore, periodic stimuli such as plaids allow for a sustained activation of the cells, which was not possible to obtain in the previous conflicting bar studies (Gray et al. 1989; Engel et al. 1991; Kreiter and Singer 1996). From the results of Castelo-Branco et al. (2000a), synchronization of responses appeared to be dependent not only on the characteristics of the stimulus but also on similarity of receptive field (RF) properties. If the recorded neurons shared the same direction preferences and had either overlapping or colinear RFs, correlated activity was present for both the coherent and the noncoherent motion of the stimulus, indicating that the neuronal responses were associated to the contours of only one of the components. On the other hand, cell pairs showing large dissimilarities (direction preferences larger than 20° and noncolinear RFs) exhibited response synchronization only for the coherent motion of the plaids. Overall, these findings support the notion that neuronal synchronization contributes to surface segmentation, in accordance with the binding-by-synchronization hypothesis.

A direct test for neuronal correlates of perception can, however, only be approached by a behavioral paradigm. To address this problem, Thiele and Stoner (2003) trained one

© 2009 The Authors

This is an Open Access article distributed under the terms of the Creative Commons Attribution Non-Commercial License (<http://creativecommons.org/licenses/by-nc/2.5/uk/>) which permits unrestricted non-commercial use, distribution, and reproduction in any medium, provided the original work is properly cited.

monkey to report the motion coherence of plaid stimuli. In disagreement with the study of Castelo-Branco et al. (2000a), correlation analysis of single- and multi-unit responses in the middle temporal area (MT) showed no consistent relations with motion coherence, at odds with the predictions of the binding-by-synchrony hypothesis (Singer 1999; Engel et al. 1991; Kreiter and Singer 1996). Several other studies in behaving monkeys also failed to find evidence that synchronous firing correlates with contour integration (Roelfsema et al. 2004; Palanca and DeAngelis 2005).

To reexamine this controversial issue, we recorded simultaneously the LFP and spiking activity from V1 in response to plaid stimuli of monkeys performing a behavioral task. In contrast to the classical approach introduced by Movshon et al. (1985), our stimulus paradigm consisted in presenting sequentially single and superimposed components within the same trial. Thus, we were able to follow the synchronization dynamics of responses to stimuli that were likely perceived as coherent (one moving grating) and noncoherent (2 independently moving gratings), respectively. To sample from distributed populations of neurons, recordings were made simultaneously at the central and peripheral representation of the visual field. Essentially, 2 reasons motivated our study. First, it is well established that neurons in monkey V1 exhibit robust, sustained, synchronous oscillations in response to drifting gratings (Friedman-Hill et al. 2000; Maldonado et al. 2000). Thus, plaid stimuli should be particularly suited to study context-dependent synchronization phenomena. Second, in our study in the cat, as in most previous studies in the monkey (Kreiter and Singer 1996; Friedman-Hill et al. 2000; Maldonado et al. 2000; Thiele and Stoner 2003), only spiking responses have been taken into account, despite the fact that oscillations in the LFP are known to be very informative about interactions within cortical networks (Gray and Singer 1989; Frien et al. 2000, 2001; Siegel and König 2003; Kayser et al. 2003; Gail et al. 2004; Taylor et al. 2005; Henrie and Shapley 2005; Niessing et al. 2005; Liu and Newsome 2006; Belitski et al. 2008; Berens et al. 2008).

In the present study, we compared the spectral characteristics of LFP and spiking responses with single and superimposed components of plaid stimuli. The responses to single components were often associated with stable and strong gamma oscillations, in accordance with previous studies (Frien and Eckhorn 2000; Friedman-Hill et al. 2000; Gail et al. 2004). The appearance of the second component (plaid stimuli), however, led to cessation of the ongoing oscillatory patterning of the responses, independent of changes in rates. The disruption of gamma synchronization in the spiking responses coincided with a systematic shift of oscillation frequencies in the LFP. These changes in synchronization dynamics were not correlated with perceptual coherence, even when the monkeys were required to selectively attend to one of the components. As discussed below, our findings make it unlikely that the binding of local features relevant for scene segmentation takes place in V1, which is probably accomplished in higher areas.

Materials and Methods

Training and Visual Paradigm

Four rhesus monkeys (*Macaca mulatta*) participated in this study. Experimental procedures were approved by the German local authorities (Regierungspraesidium, Hessen, Darmstadt) and were in full

compliance with the guidelines of the European Community for the care and use of laboratory animals (European Union directive 86/609/EEC).

Initially, the monkeys were trained on a fixation task. Each trial started with the appearance of a 0.15° square red fixation point (4×4 pixels; luminance, 10.0 cd/m^2), on which the monkeys were required to press a lever in the following 700 ms, and to maintain their gaze within a small virtual window ($\sim 1^\circ \times 1^\circ$) centered on the fixation point. In a random time point between 2500 and 4000 ms after fixation onset, the color of the fixation point changed from red to green. To obtain a reward, the monkey had to release the lever within a window of 200–500 ms after the color change of the fixation point. Trials were aborted when early or late lever releases occurred or whenever fixation was interrupted. For all aborted trials, a penalty pause of 2000 ms was added to the intertrial interval of 2000 ms, a period during which the animal was presented with a blank screen. Eye position was monitored continuously by a search coil system (DNI, Crist Instruments, USA; temporal resolution of 2 ms) or by an infrared eye tracker (Matsuda et al. 2000; temporal resolution of 33 ms). Typically, monkeys performed between 700 and 1500 correct trials in a 4-h session, thereby receiving their daily liquid requirement.

Stimuli were generated as sequences of bitmap images using an interface developed in LabVIEW by one of the authors (S.N.; LabVIEW, National Instruments, USA) and were presented as 1024×768 pixel resolution movies running at 100 or 120 frames per second using a standard graphical board (GeForce 6600-series, NVIDIA, Santa Clara, CA) controlled by ActiveStim (www.activestim.com). This software allowed high timing accuracy and stimulus onset jitters below 1 ms. The cathode ray tube monitor used for presentation (CM813ET, Hitachi, Japan) was gamma corrected to produce a linear relationship between output luminance and gray values and subtended a visual angle of $36^\circ \times 28^\circ$ (1024×768 pixels).

At the beginning of each recording session, RFs were mapped using an automatic procedure in which a bar was moved across the screen in 16 different directions ($n = 160$ trials). RF maps were obtained by computing an average matrix, in which the responses were added in 10 ms bins (corresponding to 0.2° in visual angle) for all directions (see examples in Fig. 7A). The test stimuli that were subsequently presented consisted of moving gratings and plaid stimuli. The gratings (or single components) had spatial frequency ranging from 1.25 to 2.0 cycles per degree and velocity ranging from 1.0 to $1.5^\circ/\text{s}$ (orthogonal to their orientation). These values were chosen because they elicited robust average responses in V1 (see example in Supplementary Fig. 4). The gratings were square-wave functions and had a duty cycle of 0.3. The plaids (or 2 superimposed components) were constructed by superimposing 2 gratings with an offset of 135° in their moving direction (45° orientation offset).

Plaid transparency was manipulated by varying the luminance of the individual components and their intersections (range, $1.0\text{--}32.0 \text{ cd/m}^2$ on a scale from 0.05 to 1.0; stimulus mean luminance, $\sim 14.0 \text{ cd/m}^2$). In this way, plaids could be perceived either as a single moving surface (pattern plaids) or 2 segregated surfaces drifting in different directions (depth-ordered and transparent plaids). For most of the experiments shown in this study, the depth-ordered configuration was used. Component 1, of higher luminance ($\sim 20.0 \text{ cd/m}^2$), was superimposed on component 2 ($\sim 8.0 \text{ cd/m}^2$). The visual stimulus extended from 4° to 16.0° of visual angle and was positioned at the average of the RF centers for all recorded neurons (see example in Fig. 6A for 2 RFs at the central and peripheral representation of the visual field).

Two behavioral paradigms were used in this study: 1) fixation point color change detection and 2) selective attention to one of the components of the plaids. For task (1) the monkeys were required to hold their gaze for 3200 ms on the fixation point and respond to a change in its color. The stimulus (irrelevant for the task) was always presented 800 ms after fixation onset and consisted of one of the following sequences: gratings-plaids, plaids-gratings, gratings-plaids-gratings, or plaids-gratings-plaids. Transition between stimuli occurred at 2000 ms for the sequences of 2 stimuli and at 1600 and 2400 ms for the sequences of 3 stimuli (points in time relative to fixation onset). A total of 16 motion directions (steps of 22.5°) were randomly presented within protocols of 320 trials. To assure artifact-free transitions within

a sequence, changes between gratings and plaids were implemented by a dynamical color table assignment method. Note that component 1 remained unchanged throughout the sequences presented, because it was always placed on the foreground.

In the selective attention task, one monkey was trained to attend to a luminance increase (~25%) of one of the components of a depth-ordered plaid. In this task, the fixation point remained unchanged and served only to hold the monkey's gaze. The grating to which attention had to be directed (cue grating) appeared first on the screen for a duration of 1000 ms. The second grating (distractor) was then displayed in front or behind the first. After 1000 ms, the luminance change occurred on either of the components with equal probability. The monkey was required to respond immediately to the luminance change of the cued grating. In case the luminance change occurred for the distractor grating, the monkey was required to wait another 1000 ms until the cued grating finally changed. Only the first plaid window (before any luminance increase occurred) was considered for further analysis. In this case the stimulus was physically the same, but attention could be directed to either of its surfaces.

Preparation and Recording Procedures

Each monkey was surgically implanted with a titanium bolt for stabilizing head position, a scleral search coil for measuring eye position, and a titanium recording chamber (internal diameter, 6 mm) that allowed microelectrode access to V1. The titanium pieces were fixed to the skull by means of orthopedic screws (Synthes, Germany) according to the methodology developed by N. K. Logothetis and collaborators at the Max-Planck Institute for Biological Cybernetics. All surgical procedures were conducted under aseptic conditions with isoflurane anesthesia (Baxter, Germany) and assisted by a pressure-controlled ventilation unit (1.8 l/min N₂O and 0.8 l/min O₂; Julian Station, Dräger Medical, Germany).

Recordings were made from the opercular region of V1 (RFs centers, 2.0°–3.0° eccentricity) and, occasionally, from the superior bank of the calcarine sulcus (10.0°–13.0° eccentricity). Electrodes were inserted independently into the cortex via guide tubes positioned above the dura (diameter, 300 μm; Ehrhardt Söhne, Germany) assembled in a customized recording device (designed by S.N.). This device comprised 5 precision hydraulic microdrives mounted onto an X-Y stage (MO-95, Narishige Scientific Instrument Laboratory, Japan), which was secured onto the recording chamber by means of a screw mount adapter, thereby providing great recording stability. Quartz-insulated tungsten-platinum electrodes (Thomas Recording, Germany; diameter, 80 μm) with impedances ranging from 0.3 to 1.0 MΩ were used to record simultaneously the extracellular activity from 4 to 5 sites in both superficial and deep layers of the cortex.

Data Collection and Spike Sorting

Spiking activity of small groups of neurons (MUA) and the LFP were obtained by amplifying (1000×) and band-pass filtering (MUA, 0.7–6.0 kHz; LFP, 0.7–170 Hz) the recorded signals with a customized 32 channels Plexon pre-amplifier connected to an HST16025 headset (Plexon Inc., USA). Additional 10× signal amplification was done by onboard amplifiers (E-series acquisition boards, National Instruments, USA). The signals were digitized and stored using a LabVIEW-based acquisition system developed in our laboratory (SPASS, written by S.N.). LFP was acquired with a resolution of 1.0 ms. Spikes were detected by amplitude thresholding, which was set interactively after online visualization of the spike waveforms (typically, 2–3 standard deviations above noise level). Spike events and corresponding waveforms were sampled at 32 kS/s (spike waveform length, 1.2 ms).

Off-line spike sorting was performed using a dynamic template matching method implemented in a custom software package (SpikeOne, developed by N.H.C.). Sorting was initiated by an automatic procedure that defined up to 12 different clusters. Various displays, such as tuning curves, autocorrelograms, and measurements of recording stability, were used to guide interactively which cluster to merge or delete. Only clusters well separated in 2D and 3D plots of spike principal component analysis scores were assigned to single-units (SUA) if a refractory period was confirmed in interspike interval distributions.

Data Analysis

Our analysis consisted essentially in obtaining measures of temporal patterning for local (SUA and MUA) and global (LFP) neuronal activity in V1. To maximize the insight into the data, both time domain and frequency domain approaches were used. For assessment of synchronous oscillations in MUA responses, auto- and cross-correlograms were computed on a trial-by-trial basis (resolution, 1.0 ms; time shifts, 80 ms) and then averaged over 15–20 repetitions for each stimulation condition. Shuffled cross-correlograms (shift predictors) were also routinely computed to control for correlations resulting from phase-locking to the stimulus onset. Because the shift predictors were always flat, they were not subtracted from the raw correlograms. A damped cosine function was fitted to the correlograms as described by König (1994) and used to extract 2 modulation amplitude ratios: one associated with the first satellite in the correlograms, which estimates the strength of oscillatory modulation, and the other one associated with the central peak, which estimates the strength of response synchronization. Peaks were measured from the offset of the fitted function, and the confidence limit for the statistical significance of their values was established as follows: Gabor fits had to account for ≥15% of the data variance and the *z*-scores of significant peaks had to be >2.

Spectral quantities were estimated for both spike and LFP signals using the multitaper method (Thomson 1982) implemented in Chronux 2.0 (Mitra and Bokil 2008), an open-source, MATLAB-based (Mathworks Inc., Natick, USA), data analysis toolbox available at <http://chronux.org>. Essentially, the multitaper method attempts to reduce the variance of spectral estimates by pre-multiplying the data with several orthogonal tapers known as Slepian functions. The frequency decomposition of multitapered data segments therefore provides a set of independent spectral estimates that, once averaged, provides an ensemble estimate that is more reliable for noisy data.

Mathematically, the multitapered power spectrum of a time series is defined for a given frequency as an average over all repetitions and tapers:

$$s_x(f) = \frac{1}{K} \sum_{k=1}^K |\tilde{x}_{n,k}(f)|^2,$$

where

$$\tilde{x}_{n,k}(f) = \frac{1}{N} \sum_{n=1}^N e^{-i2\pi f n} w_k(t) x_n(t),$$

is the discrete Fourier transform of the product of the measured time series sequence $\{x_n(t), n = 1, 2, \dots, N\}$ with the *k*-th Slepian taper, denoted $w_k(t)$. Numerically, $\tilde{x}_{n,k}(f)$ is computed as the Fast Fourier transform of the product. Data segments of 700 ms and 800 ms were padded with zeros to the length of 2048 before the Fourier transformation. Five Slepian tapers were used for both spike and LFP data. Hence, we obtained a spectral concentration of ±4.28 Hz and ±3.75 Hz for the data segments of 700 ms and 800 ms, respectively. For computation of the spectrograms, we used windows of 200 ms displaced at 50-ms steps. For this case, the spectral concentration was ±15 Hz.

The degree of synchronous oscillations between pairs of time series was also evaluated by computing a frequency domain measure known as coherence, defined as:

$$C_{yx}(f) = \frac{|S_{yx}(f)|}{\sqrt{S_x(f) S_y(f)}},$$

where $S_x(f)$ and $S_y(f)$ are the multitapered power spectrum estimates of the time series $x_n(t)$ and $y_n(t)$ averaged over *n* repetitions, respectively, and $S_{yx}(f)$ is the cross-power of these 2 time series. Coherence provides a normative measure of linear association between 2 processes on a scale from 0 to 1. In the absence of noise, a coherence value of 1 will be obtained at all frequencies if 2 processes are linearly related, that is, their amplitude covary and they maintain a constant phase relationship. If the 2 processes are independent, coherence will be equal to 0.

The 95% confidence bounds about spectral estimates were determined by the jackknife method across tapers and trials. A similar procedure was used to determine significant differences between 2 coherence measures (Arvesen jackknife test). Both tests were

implemented in the Chronux software package. Two analysis windows of 800 ms were positioned 200 ms after each stimulus onset for the sequences gratings-plaids-gratings and plaids-gratings. For the sequences gratings-plaids-gratings and plaids-gratings-plaids, windows of 700 ms were positioned 100 ms after the onset of the first 2 stimuli (the third stimulus in the sequence was discarded). The power spectrum measures were computed in z -score units relative to the spontaneous activity. Essentially, for each frequency bin and stimulus condition, the power spectrum of the baseline activity (epoch between fixation onset and stimulus onset) was subtracted from the power spectrum of the induced activity and divided by the standard deviation of the baseline activity (for the baseline activity, trials of all stimulus conditions were considered). A recording site was considered to have significant gamma oscillations if at least one bin in the frequency range between 30 and 90 Hz showed z -score value greater than 1.96 (95% threshold) for the preferred condition (stimulus condition where component 1 yielded the highest firing rate). To access significant differences in coherence measures, the same procedure was applied, but using the Arvesen jackknife test instead of the z -score. The preferred condition, consisting of the gratings (component 1) and plaids (component 1 + 2) stimuli, was considered for further analysis. The LFP spectrum is displayed in z -score units, whereas the MUA spectrum is displayed as power divided by firing rate for the same analysis window (Pesaran et al. 2002). Because both are normalized measures, responses from different recording sites could be directly pooled for population analysis. For visualization purposes in the single case plots, spectral quantities were smoothed with a cubic spline function (smoothing parameter $p = 0.1$).

Group data were compared by t -tests (paired and independent sample) and analysis of variance (ANOVA) (repeated and nonrepeated measures). Fisher's least significant difference test was used for multiple comparisons among means. Significant levels were set at 95% ($P < 0.05$).

Results

MUA and LFPs were acquired with multiple-electrode recordings from area V1 in 7 hemispheres of 4 macaque monkeys. For selected recording sites spike sorting of the MUA was performed in order to obtain SUA. All monkeys were trained to maintain fixation and to respond to a color change of the fixation point (correct trials, Monkey 1, 96%; Monkey 2, 80%; Monkey 3, 96%; Monkey 4, 90%). One monkey (Monkey 3) was trained in addition to attend to one of 2 superimposed moving gratings and to report a luminance change of that grating. Quantitative RF mapping and direction tuning curves were computed for all recorded sites.

A total of 471 recording sites across 109 sessions were obtained. Of these, 411 sites were located in the opercular region and 60 in the calcarine sulcus of V1, representing eccentricities in the visual field of approximately 3° and 10° , respectively. This gave rise to 737 cross-electrode recording pairs, 551 of which were pairs across operculum sites, 44 were pairs across calcarine sites, and 142 were pairs across operculum and calcarine sites. For the MUA, 89% of the sites showed significant responses to at least one of the 16 oriented moving gratings presented over their RFs ($P < 0.05$, 2-tailed z -score relative to the spontaneous activity). With the exception of 3 cases, all recordings exhibited an increase of firing rates in response to the stimulus.

Gamma Oscillatory Responses

Moving gratings with optimal orientation, spatial frequency, speed, and contrast are known to induce strong synchronous gamma oscillations visible in MUA, SUA, and the LFP (Gray and Singer 1989; Engel et al. 1990; Frien and Eckhorn 2000;

Friedman-Hill et al. 2000). In accord with these studies, we have observed significant gamma oscillations in the LFP for responses to the preferred orientation for 99% of all recording sites ($P < 0.05$, 2-tailed z -score relative to the spontaneous activity; see Material and Methods for significance criteria). The incidence of gamma oscillations in the MUA for the preferred orientation was substantially lower. Only 14% of all sites recorded exhibited significant oscillations ($P < 0.05$). The data for the 7 hemispheres studied are summarized in Table 1.

Figure 1A gives an example of strong gamma oscillations in MUA responses to optimal gratings (oscillation frequency of 65 Hz, average modulation amplitude of 1.49). Strong oscillations were also visible in single-cell responses, with frequencies precisely matching the one for the MUA (65 Hz, modulation amplitudes of 0.88 and 1.14). Cross-correlation analysis revealed that nearby cells engaged in rhythmic synchronous firing (Fig. 1B, modulation amplitude of 2.40), indicating strong local interactions. Analysis of an additional cell, recorded 3-mm away from the first electrode, showed similarly strong synchronous oscillations at the same frequency (65 Hz, modulation amplitude of 1.53). Notice that this latter pair of cells also had similar orientation preferences. These results confirm early findings in the cat and in the monkey that cells sharing similar properties often exhibit strong synchronous oscillatory firing in response to optimally oriented stimuli (Engel et al. 1990; Maldonado et al. 2000).

Overall, the temporal characteristics of the gamma responses to gratings that we observed in the behaving monkey closely resembled those described previously in areas 17 and 18 of the cat (Eckhorn et al. 1988; Gray et al. 1990; Engel et al. 1990) and area V1 of the monkey (Eckhorn et al. 1993; Frien and Eckhorn 2000; Friedman-Hill et al. 2000; Rols et al. 2001).

Disruption of Ongoing Gamma Responses

If segmentation of plaid surfaces is accomplished in V1, neurons sharing similar properties should synchronize their activity in response to the same surface in a condition of perceptual segmentation (Castelo-Branco et al. 2000a). To test this idea, we developed a paradigm in which the onset of the second component of a plaid was delayed relative to the onset of the first component. Plaid stimuli were displayed with equal luminance values for the intersection and the first component, which were set to be higher than the one for the second component (depth-ordered plaids, as in Thiele and Stoner 2003). For this configuration, we expected that synchronous responses to component 1 should be maintained as the cells

Table 1
Recording sites with significant gamma oscillations for the MUA

	Monkey 1 (nic)	Monkey 2 (lili)	Monkey 3 (jeb)	Monkey 4 (kai)
In response to gratings				
Left hemisphere	0	31%	8%	5%
Right hemisphere	1%	1/1 ^a	55%	—
In response to plaids				
Left hemisphere	0	2%	0	0
Right hemisphere	0	0	12%	—

^aSignificant MUA gamma oscillations for the gratings were observed for the only site recorded.

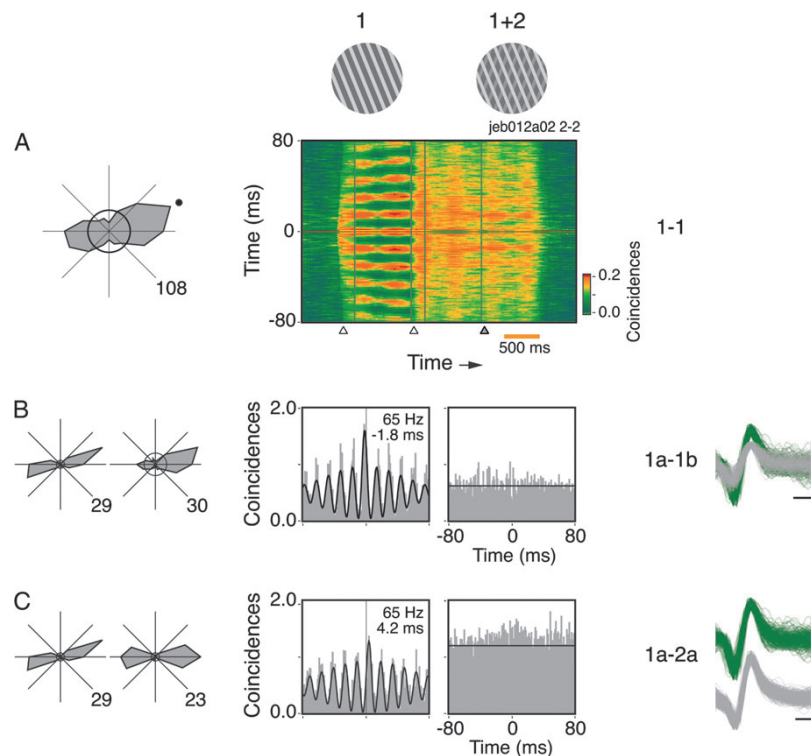


Figure 1. Examples of disruption in the oscillatory patterning of spiking responses to plaid stimuli (data obtained from Monkey 3). (A) The first component of the plaids (1), matching the preferred direction of the cells (black dot in the tuning curve, displayed to the left), induced strong gamma oscillations as seen from the sliding window autocorrelation analysis of the MUA. The onset of the second component of the plaid (1 + 2), presented behind the first, abolished almost completely the ongoing oscillatory patterning of the responses. The disruption effect was also visible in the cross-correlation analysis for single cells. Cross-correlograms obtained for a pair of cells with similar properties recorded from the same electrode (B), and for a pair of cells recorded from electrodes ~3-mm apart (C). Analysis windows are indicated by the boxes in (A). Spike waveforms of each isolated cell are displayed to the right. Maximum mean firing rate (spikes/s) is indicated at the right corner of each tuning curve. The circle in the center of the tuning curves represents the mean spontaneous rate. Stimulus timing events (onset of component 1, onset of component 2, and fixation point color change) are indicated by the arrow heads at the bottom of the sliding window panel. Oscillation frequency and phase shift indicated in the correlograms were obtained after fitting of a damped cosine function to the correlograms. Protocol identification labels are given at the top right-hand corner of the sliding window plot. The first 3 characters in the label identifies the monkey (nic corresponds to Monkey 1, lil corresponds to Monkey 2, and jeb corresponds to Monkey 3). The same convention is applied to all other Figures.

were still responding to this very surface. As shown in Figure 1, our results do not support this hypothesis. In this example, the neurons had overlapping RFs and shared similar orientation preferences (see tuning curves in Fig. 1). The strong gamma responses induced by component 1 alone (gratings, first window in the figure) ceased nearly completely after component 2 onset (plaids, second window). Notably, there were no signs of synchronization after the interruption of the oscillatory activity. Because disruption in gamma responses was observed also at the single-cell level, we could discard effects of recruitment of new cells contaminating the recorded MUA signal responding to the other component. Changes in firing rates are also unlikely to be an explanation. As demonstrated for the cell pair in Figure 1B, differences in the correlograms may be dramatic, despite negligible changes in rate.

As a control for effects related to the sudden onset of component 2, we have done experiments for which component 2 appeared gradually (Supplementary Fig. 1). This was important to rule out the effects of involuntary attentional capture by abrupt onsets as a possible explanation to our results. As shown in Supplementary Fig. 1, disruption in oscillatory patterning of the responses was clearly seen even when component 2 onset was void of transients.

In the LFP, the onset of component 2 led to a profound attenuation of oscillation strength in most of the cases. Moreover, these effects were systematically associated with shifts in oscillation frequency. As shown in the time-frequency analysis of Figure 2A, the strong and sustained oscillations induced by component 1 changed toward less sustained and weaker oscillations at a higher frequency. Note that the prominent 62-Hz peak for component 1 is shifted to 69 Hz after component 2 onset. The reduction in power of the LFP was ~54%, as measured for the entire gamma band (62% peak amplitude reduction). In this study, the spectral power of the LFP was estimated as a function of standard deviation units (*z*-score) of the spontaneous activity.

Figure 2B shows, for the same recording site, the disruption effect for the power of MUA responses. In this case, different from the example of Figure 1A, the disruption was not complete in the MUA. Nevertheless, the remaining oscillation does not appear to be a continuation of the oscillatory process initially triggered by the single component. There is a clear shift in oscillation frequency, of the same amount as the one observed for the LFP. The attenuation in gamma power was striking with a drop to about 33% (65% peak amplitude reduction). Cases in which the MUA gamma oscillations

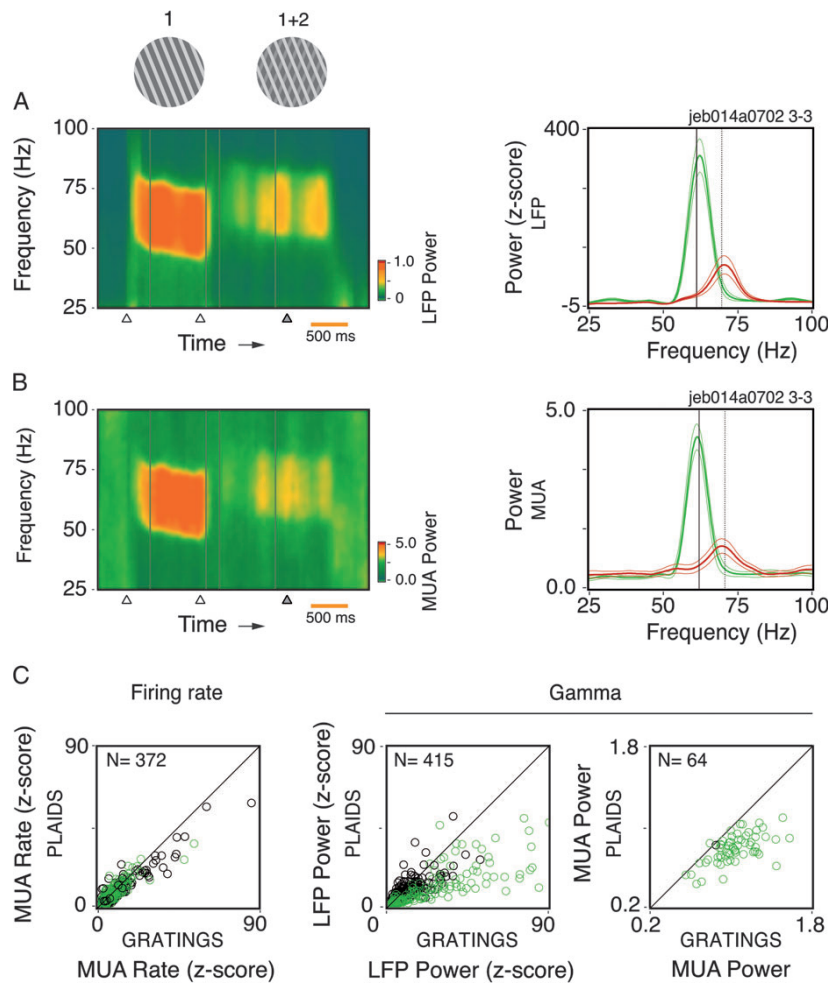


Figure 2. Spectral analysis for the LFP and MUA for responses to single (1) and superimposed components (1 + 2) of the plaid stimuli. (A) Time–frequency analysis and power spectrum computed for the LFP (e.g., from Monkey 3). The thick green and red traces represent single component (gratings) and 2 superimposed component stimuli (depth-ordered plaids), respectively, averaged over 24 trials. The thinner traces enclose the 95% confidence interval of the mean. Notice that the onset of component 2 led to reduction of gamma power and a shift toward higher oscillation frequency. (B) Spectral analysis for MUA, same recording as in (A). (C) Population data for rates, LFP gamma power, and MUA gamma power in response to single and superimposed grating components (depth-ordered plaids). Black circles represent recording sites from Monkey 1, whereas green circles represent recording sites from Monkeys 2, 3, and 4. Only those sites showing a significant increase in activity for component 1 relative to the baseline are plotted. Component 2 onset significantly reduced LFP gamma power (average of 54% decrease, paired *t*-test, $df = 179$, $P < 10^{-6}$) for Monkeys 2, 3, and 4. Monkey 1 showed only a weak effect (10% decrease, paired *t*-test, $df = 234$, $P = 0.017$). A significant reduction in MUA gamma power was also observed for all monkeys (24%, paired *t*-test, $df = 63$, $P < 10^{-6}$). On average, there was no significant change in the firing rates (paired *t*-test, $df = 163$, $P = 0.76$), with the exception of Monkey 1 (12% reduction, paired *t*-test, $df = 207$, $P < 10^{-3}$). Data shown correspond to the condition eliciting the strongest spiking response to component 1.

persisted after component 2 onset represented only a small fraction of our total sample (15% of the recording sites). Analysis at the population level confirmed the results above, despite a clear variability across monkeys (Fig. 2C). Notice that there are no strong signs of cross-orientation suppression when component 2 is added. The reason for this probably lies in the fact that in our study most of the stimuli had much higher luminance values for component 1 than for component 2. Taken together, the results obtained for the spiking responses and for the LFP indicate that in our paradigm component 2 induces a new network dynamics, disrupting the ongoing synchronization process. This happens even for cell pairs responding selectively to the same surface (Fig. 1B,C), in contradiction with our initial hypothesis. Additional analysis for

all conditions tested is documented in Supplementary Results and Supplementary Fig. 2.

To further evaluate the impact of the second component on synchronization, coherence values were computed for the LFP–LFP and the MUA–MUA (across electrodes) and the LFP–MUA (from the same electrode and across electrodes) (Fig. 3). In the example shown in Figure 3A, consistent with the spectral analysis above, we observed a clear shift in frequency for all coherence measures (from 64 to 72 Hz), with particularly striking attenuation for the MUA–MUA and the LFP–MUA (65% and 52% decrease, respectively). For the LFP–LFP coherence, the attenuation effect was weak. Actually, in responses to the plaids, there was a clear dissociation in the oscillatory patterning between the LFP and MUA. As shown in

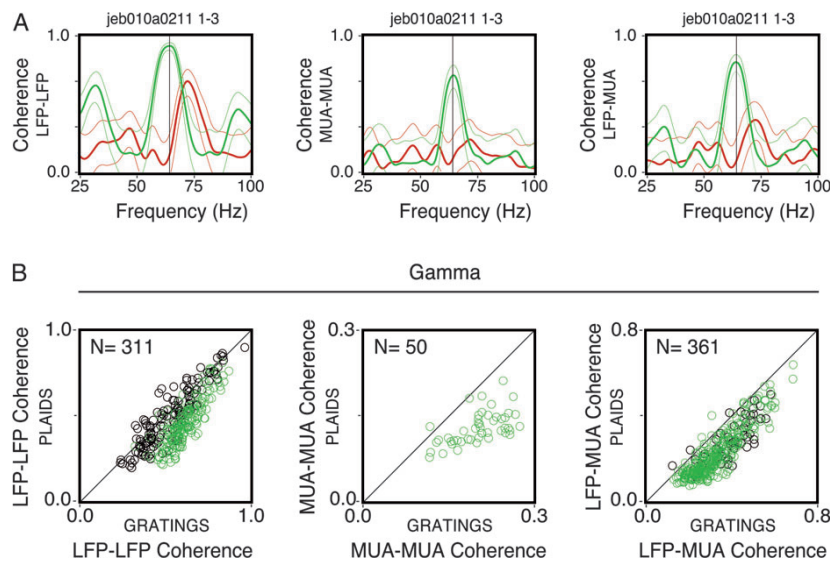


Figure 3. Coherence analysis. (A) Example of LFP-LFP, MUA-MUA, and LFP-MUA coherence measures for the grating (green) and plaid (red) stimuli derived from the same pair of recording sites (Monkey 3). Thin lines correspond to the 95% confidence interval (estimated by the jackknife procedure). (B) Population data for each of the corresponding coherence measures presented in (A). Black circles represent data points from Monkey 1, whereas green circles represent sites from Monkeys 2, 3, and 4. The number of site pairs for each analysis is given on the top left-hand side. Data shown correspond to the condition eliciting the highest joint firing rate response to component 1, as measured by the geometric mean for each pair of sites. Only those sites showing a significant increase in coherence for component 1 relative to the baseline are plotted. Plaids were depth-ordered.

Figure 3A, the phase-locking for the LFP-LFP was largely absent for the MUA-MUA and for the LFP-MUA. Notice that this dissociation effect was present for the plaids, but not for the gratings. Population data are shown in the scatter plots of Figure 3B. Only the recording pairs showing a significant increase in coherence for the preferred condition of the gratings are shown (310 out of 643 pairs for the LFP, 50 out of 643 pairs for the MUA, and 361 out of 1704 pairs for the LFP-MUA). For all monkeys, the coherence estimates exhibited a significant reduction (17% for the LFP, paired t -test, degrees of freedom [df] = 310, $P < 10^{-6}$; 35% for the MUA, paired t -test, df = 49, $P < 10^{-6}$; 29% for the LFP-MUA, paired t -test, df = 360, $P < 10^{-6}$). For the LFP-MUA, the reduction was more accentuated for recording pairs obtained from different electrodes as compared with pairs obtained from the same electrode (36% and 22%, respectively). Notice that this effect was less evident for the LFP coherence of Monkey 1 (5% reduction, paired t -test, df = 130, $P < 10^{-6}$). Furthermore, no recording pair for this monkey showed a significant increase in the MUA coherence. This is not unexpected because Monkey 1 rarely showed any rhythmic spiking responses and hence low coherence even for single gratings. It is important to emphasize that coherence was strongly dependent on cortical distances. As shown in Supplementary Results and Supplementary Fig. 3, coherence values were extremely attenuated for recording pairs across the operculum and the calcarine sulcus.

To study parametrically the impact of component 2 on the gamma responses, we varied in 2 cases its luminance and angle offset relative to component 1 (Fig. 4, example from Monkey 2). As shown by autocorrelation analysis, increasing in a few steps the luminance of component 2 led to a complete disruption of the ongoing gamma activity in the MUA (relative luminance from 0.15 to 0.20, Fig. 4A). Changing systematically the relative direction of component 2 led to similar results. For

direction offsets between the components greater than 20° , there was a complete disruption of gamma, as shown in the cross-correlograms of Figure 4B. This effect is particularly intriguing in view of the data currently available for the cortical-cortical connectivity. It has been shown that excitatory connections are biased for iso-orientation domains, within $\pm 20^\circ$ (Kisvárdy et al. 1997; Malach et al. 1993). Interestingly, we have observed that gamma synchronization was not disrupted when the direction of component 2 was offset by 180° (opposing directions). In this particular condition, the orientation of the 2 components was the same, and the activated neurons shared similar orientation preferences (see Supplementary Fig. 2). Similar results were also obtained by Lamme and Spekreijse (1998) for opposing moving textured surfaces. These findings suggest that the disruption of gamma oscillations is caused by the coactivation of columns with differing orientation preferences rather than by the properties of the stimulus per se.

Shifts in Gamma Oscillation Frequency

As shown above, component 2 led in most of the cases to a reduction of the gamma responses in the LFP. Moreover, we observed systematic shifts in gamma frequency for all monkeys studied. This effect was independent of the attenuation in oscillation strength. In Figure 5, we show LFP data for the same stimulus paradigm described in the previous figure but obtained from a different monkey (Monkey 1). Small increments in component 2 luminance resulted in systematic shifts in the gamma oscillation peak (Fig. 5A). For a low luminance value the shift in frequency was negligible. For the next luminance steps, however, shifts in frequency were considerable, eventually reaching asymptote at 70 Hz. The same effect on frequency was also present when the relative direction of

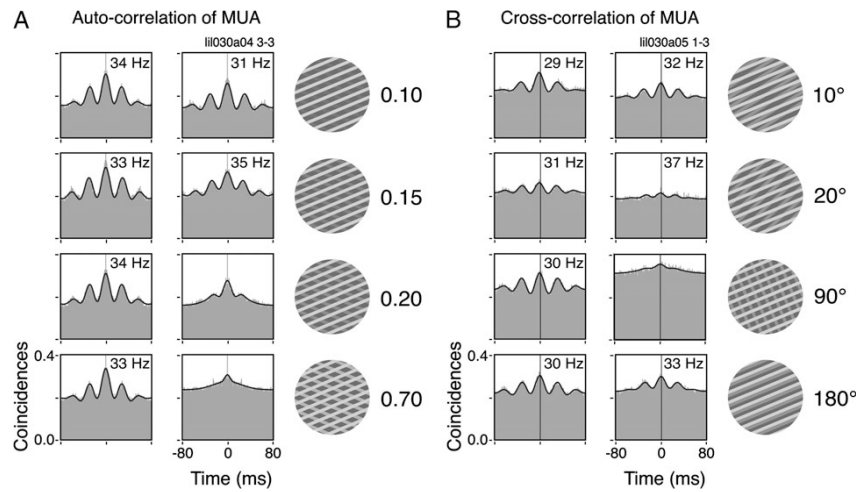


Figure 4. Parametric study on the disruption of the ongoing spike gamma oscillations. Correlograms for the single and superimposed components (depth-ordered plaids) are shown to the left and to the right of each panel, respectively. (A) Successive luminance increases of component 2 led to increasing attenuation of the spiking gamma oscillations. (B) Component 2 is presented in different directions of motion relative to component 1. The more orthogonal both components are, the higher the attenuation of spiking gamma oscillations. Note that very small increments of luminance (A) or relative direction difference (B) are sufficient to virtually abolish the oscillatory patterning of the responses.

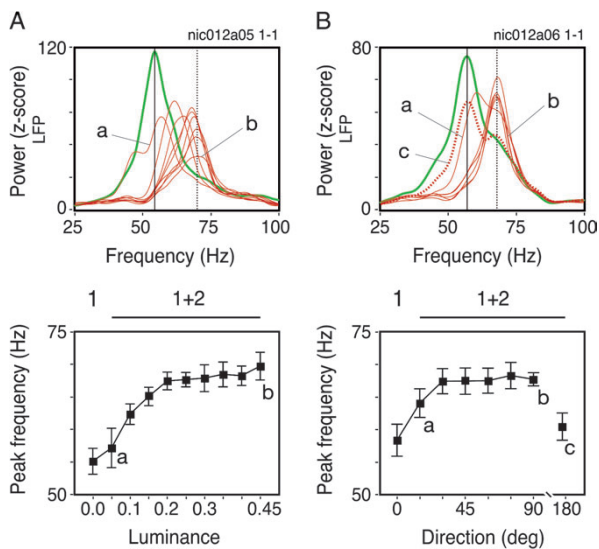


Figure 5. Gamma frequency shifts of LFP oscillations for the same experimental paradigm described in Figure 4. Green and red curves represent single and superimposed grating components, respectively. (A) Luminance increments of component 2 induced successive increases in the LFP gamma frequency, as represented by the thin red traces. (B) Relative angle deviations leading to more perpendicular crossings of both grating components similarly led to successively higher frequencies. The dotted red curve represents superimposed gratings with the same orientation but moving in opposite directions. For this case no frequency shift was observed. The panels below the power spectra plots depict the gamma frequency as a function of component 2 luminance (left) or component 2 angle offset relative to component 1 (right). Error bars enclose the 95% confidence interval of the mean. Data points in (A) and (B) consist on the average of 24 and 30 trials, respectively.

component 2 was varied (Fig. 5B). For this paradigm, oscillation frequency rapidly increased from 58 to 68 Hz. Notice that in this case the frequency shift progression was highly nonlinear. For direction offsets greater than 20°, the frequency shift was

near its asymptotic value. When the 2 components were presented in opposing directions, however, oscillation frequency was similar to the one observed for the gratings. These observations are consistent with the MUA data (Fig. 4B).

Control experiments were made for the confounding effects of stimulus spatial frequency and velocity (Supplementary Material, Fig. 4). It has been shown for the visual cortex in humans that gamma oscillation frequency depends on the spatial frequency of grating stimuli (Hadjipapas et al. 2007). To exclude the possibility that our frequency shift effects could be explained simply by an increase in spatial frequency upon the appearance of component 2, we computed tuning curves for gamma power of the LFP as function of stimulus spatial frequency (see in Supplementary Fig. 4A a representative example from a total of 5 sites studied). Our results show that the spatial frequency had a profound effect on both the gamma strength and on the firing rates (one-way ANOVA, $F(5, 232) = 32.3$; $P < 10^{-6}$ and $F(5, 232) = 86.5$, $P < 10^{-6}$, respectively). A control experiment using sinusoidal gratings showed similar results (data not shown). Despite the impact of spatial frequency on gamma power we observed, however, only a minor effect on oscillation frequency, in disagreement with the work of Hadjipapas et al. (2007). Even though we could measure a significant effect on the oscillation frequency (one-way ANOVA, $F(5, 232) = 3.3$; $P = 0.0061$), this could explain only 5% of its variance ($\omega^2 = 0.047$). In any case, the frequency shifts we observed for the plaids were clearly above the effects resulting from changes in spatial frequency.

A remaining concern was stimulus velocity. It is known that the speed of grating stimuli has an effect on the gamma oscillation frequency (Gray et al. 1990; Friedman-Hill et al. 2000; see also our Supplementary Fig. 4B). Thus, our frequency shift effects might have been due to changes in speed, because the intersections of plaid stimuli may have higher velocities than the individual components (Adelson and Movshon 1982). We have 2 reasons to exclude this possibility. First, we did see shifts in oscillation frequency even for plaids with intersections moving at the same speed as the individual components (*t*-test,

df = 153, $P < 10^{-5}$; see in Supplementary Fig. 4B a representative example from a total of 4 sites studied). For this, we constructed plaids of orthogonal surfaces, in which only component 1 moved. Second, in the experiments where the direction offset between the components was systematically varied (Figs 4B and 5B), stimulus velocity appeared not to be correlated with oscillation frequency. As documented in Figure 5B, plaid stimuli with small offsets, and thus higher resultant velocities (Movshon et al. 1985), led to smaller shifts in frequency. This trend is opposite to that derived from speed tuning curves (Supplementary Fig. 4B).

Gamma Signatures

The stimulus per se was not the only determinant of the gamma oscillation frequency. When we compared data simultaneously acquired from the regions of the central and the peripheral representation of the visual field (operculum, $\sim 3^\circ$; calcarine sulcus, $\sim 10^\circ$ eccentricity), we found that the oscillation frequency was systematically lower for the periphery. Note that the stimulus was the same for both recording sites. Examples are shown in Figure 6A separately for responses to

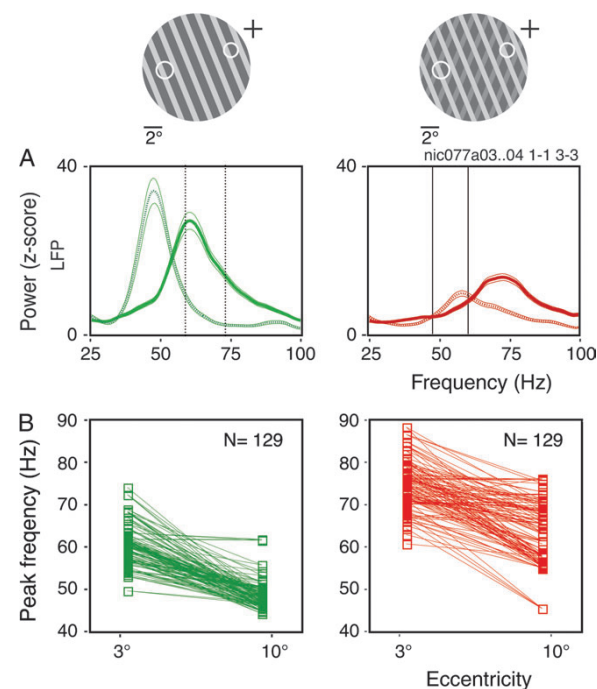


Figure 6. Relation between RF eccentricity and oscillation frequency of the LFP. (A) Simultaneously recorded neurons with RFs at central and peripheral regions of the visual field (RFs are indicated by circles and the fixation point by a cross) were stimulated by the same grating (left panel) or plaid (right panel) stimulus (Monkey 1). Central sites refer to $\sim 3^\circ$ eccentricity and are represented by the continuous curves on both panels. Peripheral sites refer to $\sim 10^\circ$ eccentricity and is represented by the dotted curves. Higher eccentricities induced lower frequencies, whereas the plaids continued to induce higher frequencies than the gratings for a given eccentricity. Thin traces enclose the 95% confidence interval of the mean. Vertical lines depict the peak frequency: Continuous lines for the gratings and dotted lines for the plaids. (B) Population data for all electrode pairs ($n = 129$) simultaneously recorded at central and peripheral sites. Straight lines link data points simultaneously acquired, confirming the overall trend described for the single case shown in (A). Each curve (A) or data point (B) is the average across the 16 directions of movement.

gratings and plaids. Because oscillation frequency was independent of stimulus orientation, data from all conditions were pooled. For responses to gratings, oscillation frequency was 60 Hz for the operculum and 47 Hz for the calcarine sulcus. This amounts to a difference of 13 Hz (21% lower). For responses to the plaids, frequencies were 73 Hz and 58 Hz, for the operculum and calcarine sulcus, respectively (20% lower). This would represent for a 20-ms oscillation cycle (50 Hz) a difference of about 5 ms (90° of the gamma cycle). In the analysis of population data (129 pairs of recording sites, Fig. 6B), the differences were highly significant (paired t -test, df = 128, $P < 10^{-6}$). Notice that these differences in frequency exist independently of variations due to the stimulus (plaids generally induce higher frequencies than gratings). For a given stimulus, the magnitude of change was about the same for the different eccentricities.

In this study, we obtained data from V1 of the 2 hemispheres in 3 out of the 4 monkeys studied. Comparisons across monkeys revealed surprisingly high variability in the frequency distribution of the LFP (Fig. 7). In responses to gratings at the preferred direction (comparable stimulus size, spatial frequency, and speed), the peak frequency at the gamma band varied approximately 2-fold across the monkeys, from 30 to 65 Hz. A similar variance was also seen for responses to plaids, from 32 to 76 Hz. Importantly, comparisons across the 2 hemispheres of the same monkey revealed a surprising similarity in the frequency distributions. For Monkey 1, although there were large differences in peak width, frequencies were matched across hemispheres (quantitative measures are given in Table 2). Observe that in this monkey there was no attenuation in the average power of gamma oscillations for the plaids. In addition, peaks in the alpha range were consistently visible across the 2 hemispheres. For Monkey 2, we observed the lowest gamma-band frequencies for both the gratings and the plaids. For Monkey 3, the peaks were narrow and consistent across the 2 hemispheres. Notice the strong reduction of power for responses to the plaids (Monkeys 2 and 3). Overall, these results indicate that different individuals differ with respect to the frequency range of gamma processes, which could be viewed as a spectral signature related to the functional architecture of the cortex.

Segmentation of Surfaces

An important goal of our study was to examine whether gamma synchronization contributes to the segmentation of surfaces in V1. The bulk of our experiments was designed to test specifically whether ensembles responding to the same surface remained stable after being challenged by a second surface in a condition associated with perceptual segmentation. Therefore, we have used depth-ordered plaids in most of the experiments. Here we provide additional data for transparent and pattern plaids. Different stimulus configurations were obtained by varying the luminance of the intersections. The plaid stimuli were constructed in a way that at least one of its components matched the tuning properties of the cells. In Figure 8 (Monkey 3), we show a case of spectral analysis obtained for cells recorded from the same electrode. Because in this case the cells were responding to the same component, one expected to see a persistence of oscillatory patterning to all plaid configurations, as it was predicted by Castelo-Branco et al. (2000a). In disagreement with this hypothesis, power and

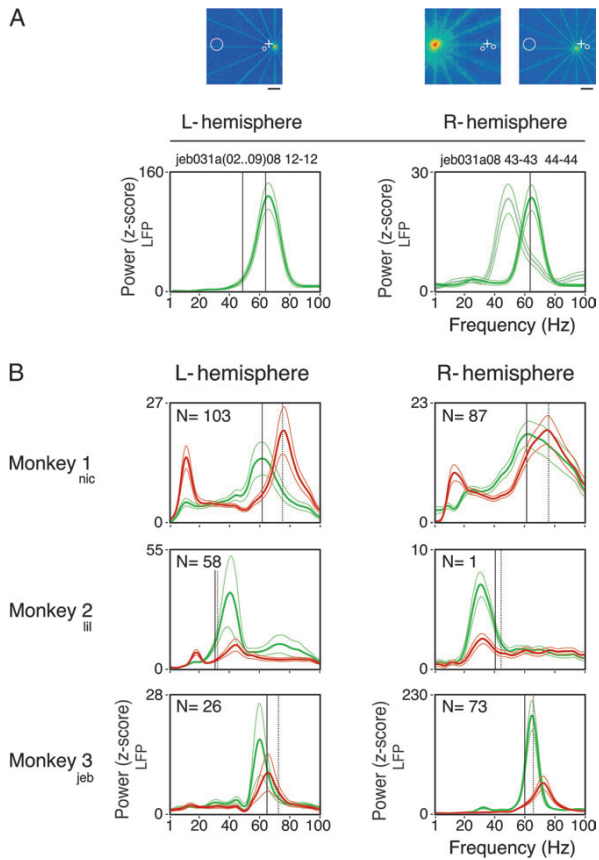


Figure 7. Spectral signatures. (A) Comparison of LFP power across the 2 hemispheres (e.g., from Monkey 3). The RF maps for the 3 simultaneously recorded sites in area V1 are plotted above (scale bar, 4°). Warmer colors, representing higher firing rates, reflect the center and extent of each RF. The fixation point position is indicated by a white cross in each map. The 2 central sites (electrodes 1 and 2 for the left and right hemispheres, respectively) were recorded at $\sim 2^\circ$ eccentricity. Electrode 3 was recorded from the calcarine sulcus of the right hemisphere ($\sim 25^\circ$ eccentricity). Observe that both central sites have similar oscillation frequencies (~ 64 Hz), which are considerably higher than the one observed at the peripheral site (~ 49 Hz). (B) Comparisons across monkeys. Even though the stimuli employed in all cases were physically similar, each subject had a characteristic spectral profile. In particular, each subject had a dominant gamma frequency for the grating (green curves), stable across recording sessions and hemispheres. Independent of the frequency induced by component 1, the appearance of component 2 increased the peak gamma frequency (red curves). L and R stand for left and right hemispheres, respectively. Each curve is the average of N recordings sites as stated on the top-left corner of each plot. Only those sites recorded in the operculum were included in this analysis, with the exception of Monkey 2 (right hemisphere) where the only site recorded was obtained in the calcarine sulcus. Observe that the gamma peaks were rather narrow, showing that increases in gamma activity could not be attributed to shifts of a $1/f$ spectral distribution. The thinner traces enclose the 95% confidence interval of the mean. Vertical guidelines were positioned to help localize the induced gamma frequency for the corresponding stimulus in the opposite hemisphere: continuous lines for the grating and dotted lines for the plaids. Plaids were depth-ordered.

coherence analysis showed a complete disruption for the transparent and pattern configurations. For the depth-ordered plaid, there was a clear reduction in the LFP power and the LFP-MUA coherence, as described previously. Overall, these results suggest that the heterogeneous activation of the cortex may have profound consequences to the generation of gamma oscillations, independent of the stimulus coherence per se.

Table 2

Peak gamma oscillation frequencies for the grating and plaid stimuli across monkeys and hemispheres and the P value associated with the peak difference between both stimuli

	Gratings (C1)	Plaids (C1 + C2)	P (paired t -test)
(A) Left hemisphere			
Monkey 1	62.1 Hz	76.1 Hz	$<10^{-6}$
Monkey 2	40.5 Hz	44.4 Hz	0.0026
Monkey 3	60.1 Hz	65.6 Hz	0.013
Monkey 4	46.1 Hz	55.9 Hz	0.032
(B) Right hemisphere			
Monkey 1	62.2 Hz	75.1 Hz	$<10^{-6}$
Monkey 2	30.7 Hz	32.2 Hz	n/a ^a
Monkey 3	65.1 Hz	72.5 Hz	$<10^{-6}$

^aOnly one site recorded.

Figure 9 shows an example of recordings with overlapping and nonoverlapping RFs obtained from different electrodes at the operculum and the calcarine sulcus. In this case, each component of the plaids matched the properties of a pair of cells. With this configuration we expected to see synchronization of oscillatory responses to the individual components only for the coherent stimulus, that is, the pattern plaids (Castelo-Branco et al. 2000a). Coherence estimates gave different results for the LFP and MUA data. Figure 9A displays the LFP power computed for the 3 sites. Notice that there was a selective increase in power for single gratings that matched the orientation preferences of the cells (as measured by the area corresponding to the gamma band, from 30 to 90 Hz). In response to the 2 superimposed components, gamma was strongly attenuated, consistent with our previous observations. In the case of the pattern plaids, however, this attenuation was less pronounced for the LFP power and LFP-LFP coherence. Shifts in oscillation frequency, nevertheless, were present in all cases, indicating the emergence of a new network dynamics. In Figures 9B,C, coherence analysis is shown for short (1-2 cell pair, overlapping RFs) and long distances (1-3 cell pair, nonoverlapping RFs), respectively. For responses to the pattern plaids (coherent stimulus), the LFP-LFP coherence exhibited robust peaks at 70 Hz that did not decay with distance (peaks for the 1-2 and the 1-3 pairs were equally high). For responses to the noncoherent stimuli (depth-ordered and transparent plaids), on the other hand, the coherence was significantly lower as compared with the coherent stimulus (jackknife procedure of Arvesen, $P < 0.05$ for 65-75 Hz). These results could be interpreted as strong evidence for the synchronization hypothesis, because coherence measures are indicators of precise phase-locking of oscillatory responses (Womelsdorf et al. 2007). In accord with this notion, for cases where the LFP-LFP coherence was high, one would expect to see similarly high values for the MUA-LFP (spike-field) coherence. This was not the case in our data. As shown in Figures 9B,C, the MUA-LFP coherence was equally flat for all plaid configurations, irrespective of the perceptual coherence of the stimulus. The MUA-MUA coherence (data not shown) was also flat for all conditions.

Selective Attention

A common criticism of the use of a fixation task for studying perceptual mechanisms is that there is no attentional engagement with the stimulus. To address this issue we have designed a series of experiments in which one monkey (Monkey 3) was trained to selectively respond to changes in one of the

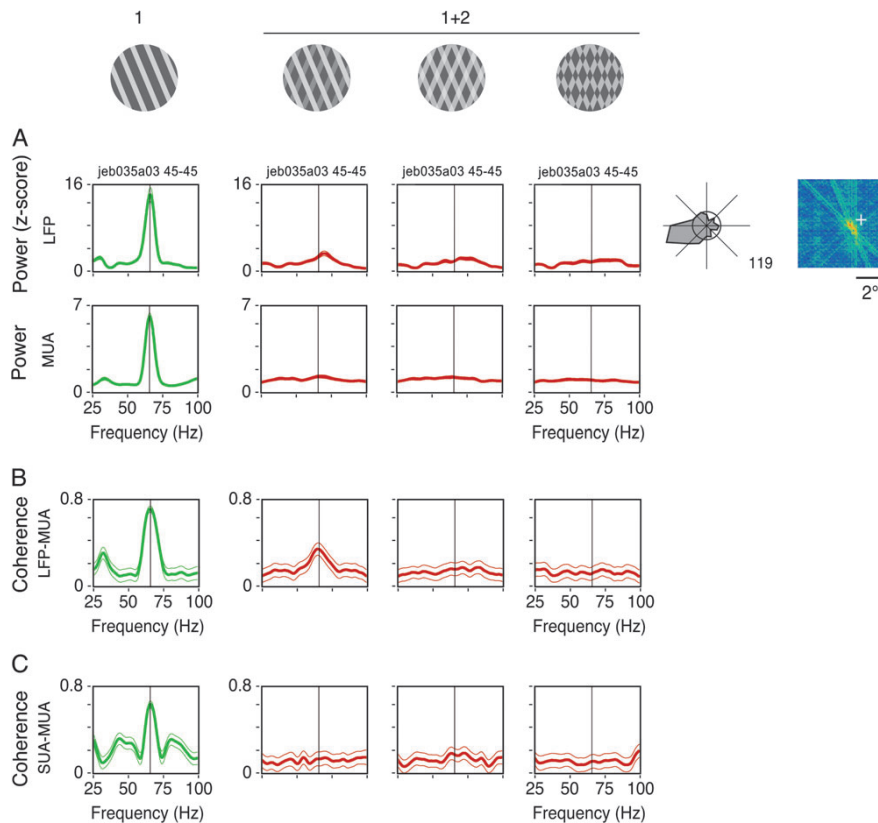


Figure 8. Relations between synchrony and stimulus coherence for recordings obtained from the same electrode. Plaid stimuli (1 + 2) were displayed in the following configurations: depth-ordered, transparent, and pattern plaids (columns from left to right). Depth-ordered and transparent plaids had physical properties compatible with perception of noncoherent motion, whereas the pattern plaid was compatible with perception of coherent motion. (A) Spectral power of the LFP (z-score) and MUA computed for each stimulus configurations (Monkey 3). (B) LFP-MUA coherence. (C) As in (B), but for SUA-MUA obtained from the same electrode. From a total of 9 cases studied in 2 monkeys, all showed similar results.

components of depth-ordered plaids. In this task, attention was actively maintained on one of the surfaces, while ignoring changes in the other one. The first component to appear was the one to which attention had to be directed to (cued surface). The second component worked as distractor, appearing in front of or behind the first component (details on task timing are given in the Materials and Methods). The component on the foreground (component 1) had always higher luminance as compared with the component on the background (component 2). This was a demanding task, requiring lengthy training. On average, Monkey 3 reached a performance level of 92% correct responses. Spectral and coherence analysis were made for recordings obtained from the opercular region (Fig. 10). Only cells showing clear orientation selectivity were analyzed (31 out of 50 recording sites). As before, the direction of component 1 was chosen to match the preferences of the cells. Analysis windows were placed at 2 epochs: 1) during the responses to the cued surface (first component, gratings) and 2) during the responses after appearance of the distractor surface (component plaids). Observe that for the plaids window, attention had been directed either to the component in the front or to the component in the background. In Figure 10A (same recording site as in Fig. 1), an example is shown for attention being

directed to the component in the front (component 1). Sliding window analysis of the MUA showed that the onset of the second component led to a nearly complete disruption of the ongoing oscillation. These results are essentially the same as for the passive fixation task (Fig. 1A). Spike-triggered averages of the LFP computed for the same data (Supplementary Fig. 5) indicate that the disruption of the oscillatory patterning could not be explained simply by spikes skipping oscillation cycles. Thus, attention was not sufficient to preserve the oscillatory dynamics induced by the gratings, even though perceptually this surface remained unchanged throughout the trial.

A closer analysis of the LFP, however, revealed that our attentional paradigm had a clear effect on the oscillation frequency, indicating that the monkey actually did attend selectively to one of the surfaces. As shown in the power spectra of Figure 10B, for average and single trials, the oscillation frequency peaks for the responses to the plaids were clearly different depending on which surface the monkey was attending to. When attention was directed to the foreground (component 1), peak frequencies were ~70 Hz, whereas when it was directed to the background, peaks shifted to ~75 Hz (t -test, $df = 48$, $P < 10^{-5}$). It is important to emphasize that, for the second analysis window, the stimulus was exactly the same in both conditions. Interestingly, when these

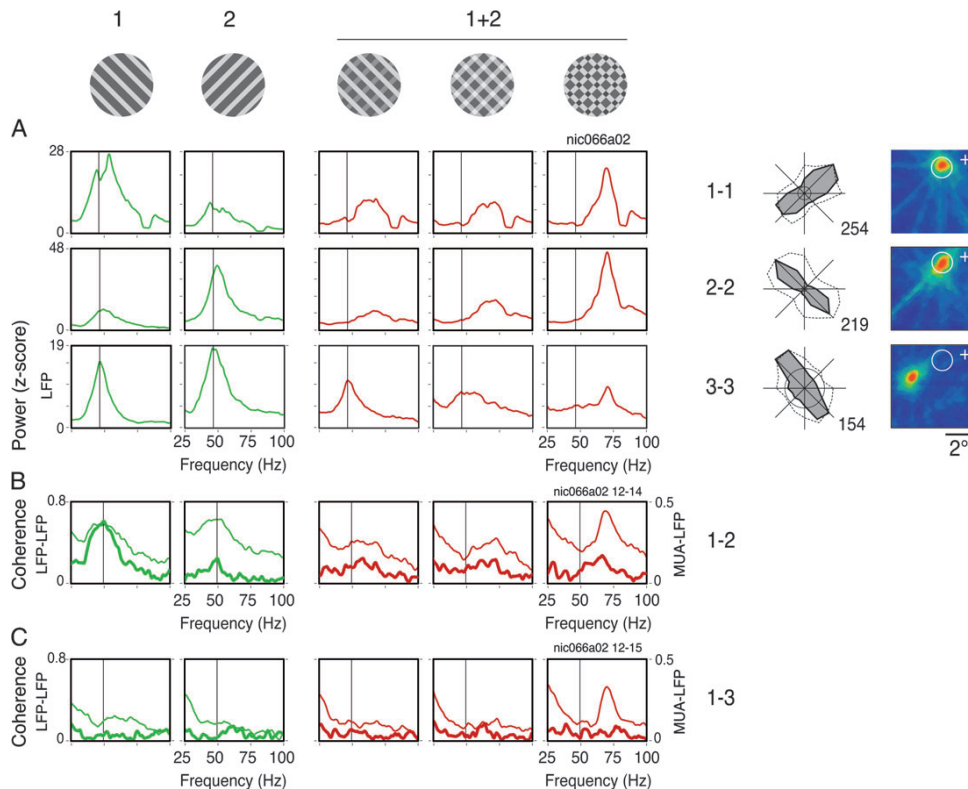


Figure 9. Relations between synchrony and stimulus coherence for recordings obtained from different electrodes (e.g., from Monkey 1). Data shown were obtained for 3 sites recorded simultaneously in area V1 (RF maps are shown to the right, conventions as in Fig. 7). Neurons recorded in the operculum (electrodes 1 and 2, $\sim 3^\circ$ eccentricity) had overlapping RFs, whereas the RFs of neurons recorded in the calcarine (electrode 3, $\sim 10^\circ$ eccentricity) were nonoverlapping with those recorded from the operculum. Tuning curves for direction of movement are presented to the left of the RF maps (conventions as in Fig. 1), both for gamma of the LFP (dotted line) and for the spiking responses (solid line). The stimulus used for each condition is shown at the top of each respective column. Direction of motion of components 1 and 2 of the plaids were chosen in accord with the tuning properties of the neurons (component 1 matching the properties of electrode 1 and component 2 matching the properties of electrodes 2 and 3). Plaid stimuli (1 + 2) were displayed in the following configurations: depth-ordered, transparent, and pattern plaid (columns from left to right). Depth-ordered and transparent plaids had physical properties compatible with perception of noncoherent motion, whereas the pattern plaid was compatible with perception of coherent motion. (A) Spectral power of the LFP (z-score) computed for each condition and recording site. (B) LFP-MUA coherence (thick curves) and LFP-LFP coherence (thin curves) computed for the pair of overlapping RF sites (1–2). (C) As in (B), but for one pair of nonoverlapping RF sites (1–3). From a total of 5 cases studied in 2 monkeys, all showed similar results.

frequencies are compared with the frequency observed for the passive fixation task (72 Hz), we end up with a progression similar to our luminance curve experiment (Fig. 5A). As discussed below, this can be understood in view of some current models of attention (Carrasco et al. 2004; Reynolds and Chelazzi 2004). It is possible that selective attention works as a contrast gain mechanism, with impact on surface saliency comparable to our luminance manipulations.

In Figure 10C we show results for the comparison between the passive fixation and attentional tasks. There were no significant differences, neither for firing rates (paired t -test, $df = 30$, $P = 0.22$) nor for MUA-LFP coherence (paired t -test, $df = 30$, $P = 0.59$). Comparisons for attention to the foreground and to the background surfaces are shown in Figure 10D. Note that attentional effects exist only for the oscillation frequency (paired t -test, $df = 30$, $P < 10^{-6}$).

Discussion

To determine whether synchronous firing in V1 correlates with perceptual segmentation of surfaces, we developed a new paradigm based on plaid stimuli, which enabled us to follow the

synchronization dynamics over time. For intersection luminance values compatible with surface segmentation (e.g., nontransparent, depth-ordered plaids), we expected the synchronization patterns induced by single gratings to persist with component plaids. On the contrary, our spectral and coherence analysis of both the LFP and spiking responses revealed profound changes in the ongoing interaction patterns of the neurons. Moreover, the observed changes in synchronization dynamics were not correlated with perceptual coherence of the plaids. As discussed below, these findings are at odds with the notion that different assemblies oscillate in response to different surfaces.

Gamma Responses

In our study, synchronization was generally associated with gamma oscillations. In the cat, it has been shown that cortical states characterized by high levels of EEG activation are associated with high amplitude, sustained gamma oscillations (Herculano-Houzel et al. 1999; Siegel and König 2003), suggesting that synchronization of spiking responses may be facilitated by oscillatory activity. Accordingly, Samonds and Bonds (2005) have shown that for synchronization to be sustained throughout

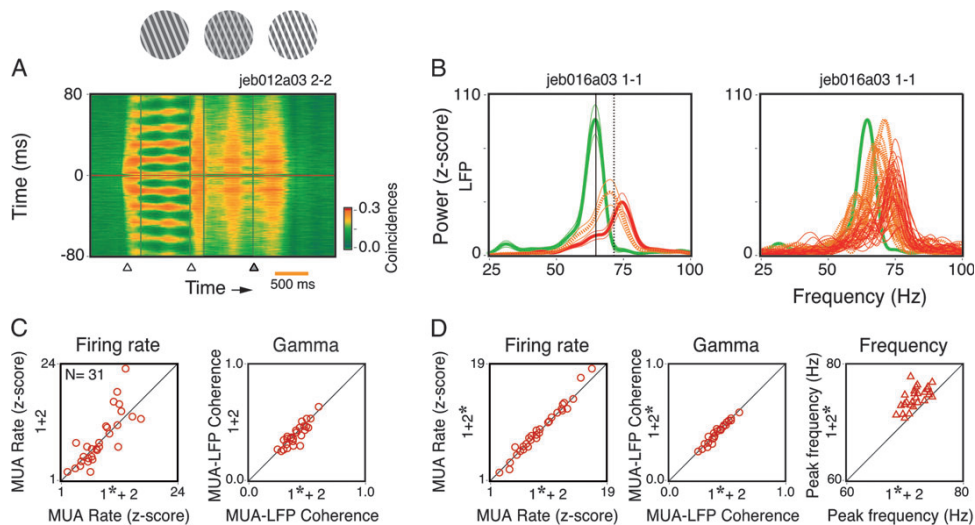


Figure 10. Effects of selective attention to one of the surfaces of the plaids. Monkey 3 was trained to direct attention to the first grating (cue) appearing on the screen. After 1000 ms of cue onset, the second component appeared in front of or behind the first component. The monkey was required to respond with a lever release only when the cued grating changed luminance, ignoring changes on the noncued surface. (A) Sliding window autocorrelation of the MUA for the same recording site studied in Figure 1A. After the addition of component 2, but with attention directed to component 1, oscillatory activity was still disrupted, similar as to when no attention was paid to the stimulus (Fig. 1). (B) LFP spectra for the gratings (green curves) and for the plaids. For the latter case, orange traces represent attention directed to the surface in the foreground, whereas the red traces indicate attention directed to the surface in the background. Continuous and dotted vertical lines indicate the frequency induced by the grating and plaid stimuli, respectively, when attention was directed to the fixation point. Single-trial traces are shown to the right. (C) No significant differences in firing rate or spike-field coherence were found depending on whether the monkey was paying attention to the fixation point, to component 1 or to component 2, as shown in (C) and (D). The * symbol in $1^* + 2$ or $1 + 2^*$ indicates to which component attention was directed to. No symbol ($1 + 2$) indicates that attention was directed to the fixation point. However, the oscillation frequency for the population of sites systematically shifted depending on to which surface the monkey directed its attention to. Thin traces in (B), left panel enclose the 95% confidence interval of the mean.

the stimulation period (over seconds), it has to be maintained by oscillatory patterning. In our study, we have rarely seen synchronization without accompanying oscillation, and when it occurred, it was very weak. Maldonado et al. (2000) have found that, for nearly three-quarters of short distance pairs and two-thirds of long distance pairs, synchronization was accompanied by gamma oscillations. Similarly, König et al. (1995b) have shown in the cat that synchronization of responses between sites more than 2-mm apart or between the 2 hemispheres was nearly always associated with oscillatory patterning.

In the present study we have systematically recorded from V1 of the 2 hemispheres in 4 monkeys (3 are shown in Fig. 7). This enabled us to compare oscillation frequencies between individuals across a much larger sample than in previous studies. Comparisons across monkeys revealed surprisingly high interindividual variability in gamma frequency (up to 2-fold). Interhemispheric comparisons, on the other hand, revealed a rather small intraindividual variability. Why such a large variability exists across individuals remains unresolved. Possible explanations are genetic variations in connectivity (Kaschube et al. 2002) and channel kinetics. We have also observed differences in oscillation frequency between sites at the central and the peripheral representation of the visual field in V1. As shown in Figure 6 for pairs of recording sites in the operculum and the calcarine sulcus, oscillation frequency was clearly higher for sites at lower eccentricities. These differences could be attributed to the way stimulus velocity interacts with the cortical magnification factor. It is known that the speed of the visual stimulus has an effect on the oscillation frequency of the cortex: the faster the stimulus, the faster the oscillation (Gray et al. 1990; Friedman-Hill et al. 2000; see also our Supplementary Fig. 4B). Because at lower eccentricities the

displacement of the stimulus relative to the cortical map is larger, one would expect a faster oscillation. Interestingly, we have observed that for static stimuli, such as Gabor patches set to match the orientation preferences of the cells (Neuenschwander et al. 2008), the oscillation frequency was the same for responses from the operculum and the calcarine sulcus. Differences in oscillation frequency may constrain synchronization for long distances. This may explain our finding of weaker synchronization across sites at central and peripheral representation regions, even for responses to a single coherently moving grating (Supplementary Fig. 3).

It remains an open question how local gamma oscillations in V1 are. Similar to our results (Supplementary Fig. 2), early studies in the cat and in the monkey (Gray and Singer 1989; Frien et al. 2000) have found that the tuning of gamma oscillations in the LFP closely matches the orientation and direction preferences of the local cluster of cells (MUA). It has been argued that the gamma components of the LFP are bound to the scale of a column (Liu and Newsome 2006; Katzner et al. 2009; but see Berens et al. 2008). In our study, we have observed that interactions in V1 are mostly local. As shown in Supplementary Fig. 3, coherence measures for the LFP and MUA decreased steeply as function of cortical distance. Recently, Gieselmann and Thiele (2008) have shown that oscillation strength increases monotonically with stimulus size. Thus, it is possible that gamma patterning requires a critical mass of activity, comprising interactions among several columns.

Breaking the Waves

The main finding of this study was that the coactivation of neuronal populations with different orientation preferences, as

it occurs for plaid stimuli, led to the disruption of ongoing gamma synchronization. Nonadditive plaid images, as those used in our study, contain Fourier power concentrated at multiple orientation components (Stoner and Albright 1996; see Figure 7A of Schmidt et al. 2006). For depth-ordered plaids image, spectral power predominates at one of the components, whereas in pattern plaids power is more evenly distributed, encompassing also components in the intermediate direction. Plaid stimuli, therefore, are capable of activating populations with different orientation preferences, their relative contribution depending on parameters such as angle between the 2 components and luminance values of the individual components and their intersections (Schmidt et al. 2006). In our results, disruption occurred both for pattern and component plaids (Fig. 8), even when the second component had very low contrast (Fig. 4). Thus, a relatively weak activation of other orientation columns was enough to drive the neuronal network into a new dynamical state characterized by near cessation of oscillations in the spiking responses and shifts toward higher oscillation frequencies in the LFP (Fig. 5). These observations were robust and consistent across all monkeys studied.

It is known that the spatial and temporal characteristics of the stimulus can have profound effects on the temporal patterning of the neuronal responses. In a study in the awake cat, Kayser et al. (2003) have shown that the spectral profiles of responses to natural movies are quantitatively and qualitatively different from those to gratings. Whereas gratings induced responses with spectral power largely concentrated at 40 Hz, natural movies led to a uniform increase in power over the whole gamma band and beyond (frequencies above 100 Hz). We have obtained similar results from our recordings in V1 (S.N. and B.L., unpublished observations). Thus, it is likely that complex stimuli, such as plaids and natural scenes, induce fundamentally different patterns of interactions in the cortex, as compared with moving bars or gratings.

Why are gratings so effective in inducing gamma oscillations in the visual cortex? Grating stimuli allow for a steady-state, selective activation of large populations. The very notion of local spatiotemporal filters has been derived from studies using gratings, leading to the Fourier-based approach to vision (Campbell and Robson 1968). Gratings, not surprisingly, have been central for the characterization of orientation domains based on optical imaging techniques (Bonhoeffer and Grinvald 1991). They have also been largely used in investigations on cortical dynamics (e.g., in the monkey, Maldonado et al. 2000; Fries et al. 2001; Gail et al. 2000, 2004; Henrie and Shapley 2005; Womelsdorf et al. 2007). Recently, in a study combining imaging of intrinsic signals and recordings of the LFP, Niessing et al. (2005) found a link between the blood oxygen level-dependent signal and gamma oscillations for responses to full-field gratings. A possible reason for this link is that grating stimuli are capable of activating selectively columns sharing the same properties, which are known to be preferentially connected (Stettler et al. 2002; Schmidt et al. 1997; Weliky et al. 1995; Malach et al. 1993; Gilbert and Wiesel 1989). Cross-correlation analysis has shown that interactions across cells with the same orientation preference are strong, following the layout of the intrinsic horizontal connections (Ts'o et al. 1986; Schwarz and Bolz 1991). Moreover, long-distance gamma synchronization occurs primarily between cells with similar orientation preferences (Engel et al. 1990). In accordance with

these previous studies, Smith and Kohn (2008), by means of a high-density sampling of the cortex, have demonstrated that synchronization depends strongly on orientation similarity. Nauhaus et al. (2009) have found that spiking activity triggers traveling waves in the LFP, which propagate long distances in V1 depending on stimulus contrast. Similar to the patterning of horizontal connections, these traveling waves were biased along sites with similar orientation preferences. Thus, it is conceivable that the limit cycle dynamics (narrow-band gamma oscillations) commonly seen in responses to gratings results from cooperative interactions of subpopulations that are preferentially connected.

This does not explain, however, why minimal activation of columns with dissimilar orientation preferences had such a profound impact on the ongoing oscillatory patterns, as shown in Figure 4A. This is even more intriguing if one considers that the disruption effect was maximal for the orthogonal orientation offset between the components (Fig. 4B). Any explanation for these findings should account for the generation mechanisms of gamma activity, which, as discussed before, seems to be local. It is known from intracellular recordings that local inhibitory networks are key players in the generation of the gamma rhythmicity in the hippocampus and in the cortex (Hasenstaub et al. 2005; Tamás et al. 1998; Whittington et al. 1995; for review see Bartos et al. 2007). Connections across orientation columns are known to be excitatory and inhibitory (Dalva et al. 1997). The concurrent excitatory (or inhibitory) drive from cross-orientation columns apparently interferes with the local generation of the gamma oscillations.

Recently, Zhou et al. (2008) have investigated the impact of stimulus continuity on the modulation of synchronized activity. In responses to gratings onto which noise was superimposed, coherence in the gamma band was impaired, suggesting that spatial continuity is required for the generation of gamma oscillations. Our study offers an alternative interpretation to these results. We observed that the disruption of gamma activity occurred even when the foreground component was left intact and undisturbed. From this perspective, it is possible that the reduction in coherence reported by Zhou et al. (2008) arises because of the activation of cells with dissimilar properties responding to the new orientation components added by the noise.

An important and somehow surprising finding in our study was that the oscillatory patterning of the LFP in response to plaids was dissociated from the spiking activity (Fig. 3A). Gieselmann and Thiele (2008) have also reported a dissociation between neuronal firing and LFP activity in area V1. In their study, LFP gamma power was maximal for large grating stimuli covering the surround regions of the RFs, whereas spiking activity showed a clear suppression. It was suggested that the increase in inhibition in the responses to the larger stimuli could be responsible for both the suppression in rates and enhancement of gamma oscillations. We observed, however, no systematic differences in firing rate between the grating and plaid stimuli, despite profound differences in the gamma oscillatory patterning. Thus, it is unlikely that a simple model based on a modulation of inhibition in the cortical network could account for the properties of gamma synchronization we have observed in V1. Another possibility is that the LFP reflects not only activity generated within V1 but also the synaptic activity of reentrant inputs from higher visual areas.

Scene Segmentation

In early investigations, a common strategy for studying perceptual grouping was to use superimposed objects at different configurations (e.g., 1 single bar vs. 2 crossing bars; Engel et al. 1991; Kreiter and Singer 1996). Castelo-Branco et al. (2000a) generalized these results for the segmentation of surfaces with a paradigm based on plaid stimuli. As in the bar experiments, coherent stimuli (pattern plaids) were associated with synchronization, whereas noncoherent stimuli (component plaids) were not. These results, however, have been recently challenged by a number of studies in the awake behaving monkey, which showed contradictory or negative evidence for the segmentation by synchronization hypothesis (Thiele and Stoner 2003; Roelfsema et al. 2004; Palanca and DeAngelis 2005; Dong et al. 2008).

Contrary to the study of Castelo-Branco et al. (2000a), we found little evidence that synchronization in V1 reflects the global properties of plaid stimuli. For depth-ordered plaids, synchronization should have persisted because component 1 was left unchanged during the whole trial, and the cells continued to respond vigorously to that very surface. Moreover, we expected to see clear differences in synchronization dynamics associated with the perceptual coherence of the stimulus. As shown in Figures 8 and 9, synchronization between the LFP-MUA was equally absent for all plaid configurations. An important difference between our study and the one of Castelo-Branco et al. (2000a) is that, in the anesthetized cat, MUA synchronization occurred without signs of oscillatory patterning of the responses (the LFP was not studied). In a later report, however, Castelo-Branco et al. (2000b) analyzed the oscillatory properties of responses to plaid stimuli and found, as in the present study, that gamma patterning of the responses was prominent for gratings matching the preferences of the cells and nearly absent for the plaids (see also Figure 2B of Castelo-Branco et al. 2000a). This happened regardless of the stimulus configuration (coherent or noncoherent plaids), indicating that the oscillations were unlikely to be related to perceptual coherence. In a study using circular gratings, Samonds et al. (2006) also found synchronous firing without oscillations. As in the report of Castelo-Branco et al. (2000b), synchrony (but not the oscillatory patterning per se) reflected stimulus coherence. Thus, in the cat, coactivation of columns with different orientation preferences appears to reduce oscillations but does not necessarily abolish synchrony among nearby columns.

Thiele and Stoner (2003) have designed a behavioral paradigm to test for the role of synchronization on surface segmentation. In their experiments, monkeys were trained to report stimulus coherence, thus enabling a more direct link between neuronal synchronization and perception. Surprisingly, noncoherent plaid stimuli induced more synchronization than did coherent plaids. In their study, however, no LFPs were analyzed, and therefore, it is unknown whether there were changes in oscillatory patterns at the population level. Recently, Palanca and DeAngelis (2005) have used coherence analysis of the MUA and LFP to test for binding of oriented contours in area MT. Essentially, comparisons were made for bar segments presented over the RFs that could belong to the same or to distinct polygon objects. In this paradigm, binding depended on contextual relationships outside the classical RF. Their results showed that synchrony was tightly correlated with RF properties and not to feature grouping per se.

As in our study, coherence was much stronger for the LFP than for the MUA and was heavily dependent on the RF overlap and similarity of direction preferences. Thus, it is likely that the functional architecture of the cortex is more determinant of the neuronal synchronization dynamics than previously thought.

In most of our experiments, the monkeys performed a fixation task for which the stimulus was actually ignored. As a control for attentional effects, we trained one monkey to direct attention to one of the surfaces of the plaids, while ignoring the other surface. Similar to the results obtained for the passive fixation task, oscillatory responses to the plaids were also disrupted in the attentional task (Fig. 10A). These dramatic changes could not be explained by spikes skipping oscillation cycles (see control in Supplementary Fig. 5). Notably, directing attention to one of the surfaces led to a shift in the oscillation frequency of the LFP, which was similar to that obtained by enhancing the contrast of the second grating (Figs 5A and 10B, respectively). Selective attention to a stimulus is known to increase its effective contrast or saliency (Carrasco et al. 2004) and may increase the contrast gain of cell responses (Reynolds et al. 2000; Martínez-Trujillo and Treue 2002). Thus, in our study, attending to the foreground surface of the plaids (which had higher luminance) would enhance its effective contrast relative to the background surface (lower luminance). Alternatively, attending to the background surface would decrease the effective contrast between the 2 components, resulting in more interference. Other models, however, such as the response gain or the additive models (Thiele et al. forthcoming), may also account for these effects in V1. These results show that internal states, such as attention, are capable of modulating gamma oscillation frequency. The mechanisms responsible for these dynamical changes are still unknown. In slice preparations, it has been shown that gamma oscillation frequency depends on GABA_A channel conductance and on the decay time constant of inhibitory postsynaptic potentials (Traub et al. 1996; Whittington et al. 1995). It has been shown recently that attention-dependent modulation is stronger for putative inhibitory interneurons (Mitchell et al. 2007). These findings are consistent with the proposal that inhibitory networks, which are central for the generation of gamma oscillations, play an important role in attentional processes (see review in Fries 2009).

The puzzling question remains why we do not see a correlation between synchronization and stimulus coherence, as described for the cat visual cortex (Castelo-Branco et al. 2000a). One reason could be the greater specialization of monkey visual areas as compared with those of the cat. Due to massive expansion of the foveal representation, monkey V1 may be concerned only with the analysis of very local relations, leaving context assessment required for scene segmentation to higher areas. In the cat, on the other hand, global operations could already occur in early areas. This may explain why the only evidence we found for perceptual binding was revealed by the LFP-LFP coherence (Fig. 9B,C). It is possible that reentrant inputs from higher visual areas represent an important component of LFPs recorded in V1, explaining our apparent dissociation between LFP oscillations and the spiking activity. Interestingly, intracerebral EEG recordings in humans have shown strong modulation of gamma in response to complex stimuli such as faces for the parietal and temporal regions but not for the primary visual cortex (Lachaux et al. 2005). These findings suggest that gamma

synchronization related to grouping of complex features occurs primarily in higher visual areas, independent of V1 oscillatory patterning.

In conclusion, our results do not support the notion that gamma synchronization in V1 is a correlate of perceptual binding, as it has been suggested in early studies in A17 and A18 of the cat (Engel et al. 1991; Castelo-Branco et al. 2000a) and area MT of the monkey (Kreiter and Singer 1996). On the contrary, our findings indicate that synchronous gamma oscillations in monkey V1 are relatively local, showing only weak phase-locking over long distances (operculum vs. calcarine). In this respect, synchronization of oscillatory responses cannot solve the aperture problem within V1, which probably requires processing in higher areas, with larger RFs and compressed visual field representations, despite the negative evidence found in recent studies in MT (Thiele and Stoner 2003; Palanca and DeAngelis 2005) and V2 (Dong et al. 2008).

Funding

This work has been supported by the Max-Planck Society. B.L. was supported during his doctoral studies by the Graduiertenkolleg, J. W. Goethe University—Frankfurt, the Max-Planck Society, and the Frankfurt Institute for Advanced Studies.

Supplementary Material

Supplementary material can be found at: <http://www.cercor.oxfordjournals.org/>

Notes

We thank Michaela Klinkmann and Johanna Klon-Lipok for technical assistance and Dr Christiane Kiefert and Clemens Sommers for animal care. We thank Mario Fiorani for the implementation of the RF mapping algorithm, Pascal Fries for introducing us to the multitaper spectral analysis, and to Partha Mitra and collaborators for the Chronux analysis software. Thanks also to Miguel Castelo-Branco, Jerome Baron, Matthias Munk, and Kerstin Schmidt for insightful discussions and support.

Conflict of Interest: None declared.

Address correspondence to Dr Sergio Neuenschwander, Max-Planck Institute for Brain Research, Deutschordenstrasse 46, 60528 Frankfurt am Main, Germany. Email: neuenschwand@mpih-frankfurt.mpg.de.

References

Adelson EH, Movshon JA. 1982. Phenomenal coherence of moving visual patterns. *Nature*. 300:523–525.

Bartos M, Vida I, Jonas P. 2007. Synaptic mechanisms of synchronized gamma oscillations in inhibitory interneuron networks. *Nat Rev Neurosci*. 8:45–56.

Belitski A, Gretton A, Magri C, Murayama Y, Montemurro M, Logothetis N, Panzeri S. 2008. Low-frequency local field potentials and spikes in primary visual cortex convey independent visual information. *J Neurosci*. 28:5696–5709.

Berens P, Keliris GA, Ecker AS, Logothetis NK, Tolias AS. 2008. Comparing the feature selectivity of the gamma-band of the local field potential and the underlying spiking activity in primate visual cortex. *Front Syst Neurosci*. 2:1–11.

Bonhoeffer T, Grinvald A. 1991. Iso-orientation domains in cat visual cortex are arranged in pinwheel-like patterns. *Nature*. 353:429–431.

Buzsáki G, Draguhn A. 2004. Neuronal oscillations in cortical networks. *Science*. 304:1926–1929.

Campbell FW, Robson JG. 1968. Application of Fourier analysis to the visibility of gratings. *J Physiol (Lond)*. 197:551–566.

Carrasco M, Ling S, Read S. 2004. Attention alters appearance. *Nat Neurosci*. 7:308–313.

Castelo-Branco M, Goebel R, Neuenschwander S, Singer W. 2000a. Neural synchrony correlates with surface segregation rules. *Nature*. 405:685–689.

Castelo-Branco M, Neuenschwander S, Goebel R, Singer W. 2000b. Oscillatory firing of neurons in cat visual cortex in response to plaid stimuli. Program No. 251.3 in Abstract Viewer/Itinerary Planner. Society for Neuroscience, New Orleans (LA).

Dalva MB, Weliky M, Katz LC. 1997. Relationships between local synaptic connections and orientation domains in primary visual cortex. *Neuron*. 19:871–880.

Dong Y, Mihalas S, Qiu F, von der Heydt R, Niebur E. 2008. Synchrony and the binding problem in macaque visual cortex. *J Vision*. 8:1–16.

Eckhorn R, Bauer R, Jordan W, Brosch M, Kruse W, Munk M, Reitboeck HJ. 1988. Coherent oscillations: a mechanism of feature linking in the visual cortex? Multiple electrode and correlation analyses in the cat. *Biol Cybern*. 60:121–130.

Eckhorn R, Frien A, Bauer R, Woelbern T, Kehr H. 1993. High frequency (60–90 Hz) oscillations in primary visual cortex of awake monkey. *Neuroreport*. 4:243–246.

Engel AK, Fries P, Singer W. 2001. Dynamic predictions: oscillations and synchrony in top-down processing. *Nat Rev Neurosci*. 2:704–716.

Engel AK, König P, Gray CM, Singer W. 1990. Stimulus-dependent neuronal oscillations in cat visual cortex: inter-columnar interaction as determined by cross-correlation analysis. *Eur J Neurosci*. 2:588–606.

Engel AK, König P, Singer W. 1991. Direct physiological evidence for scene segmentation by temporal coding. *Proc Natl Acad Sci USA*. 88:9136–9140.

Friedman-Hill S, Maldonado PE, Gray CM. 2000. Dynamics of striate cortical activity in the alert macaque: I. Incidence and stimulus-dependence of gamma-band neuronal oscillations. *Cereb Cortex*. 10:1105–1116.

Frien A, Eckhorn R. 2000. Functional coupling shows stronger stimulus dependency for fast oscillations than for low-frequency components in striate cortex of awake monkey. *Eur J Neurosci*. 12:1466–1478.

Frien A, Eckhorn R, Bauer R, Woelbern T, Gabriel A. 2000. Fast oscillations display sharper orientation tuning than slower components of the same recordings in striate cortex of the awake monkey. *Eur J Neurosci*. 12:1453–1465.

Fries P. 2005. A mechanism for cognitive dynamics: neuronal communication through neuronal coherence. *Trends Cogn Sci*. 9:474–480.

Fries P. 2009. Neuronal gamma-band synchronization as a fundamental process in cortical computation. *Ann Rev Neurosci*. 32:209–224.

Fries P, Nikolić D, Singer W. 2007. The gamma cycle. *Trends Neurosci*. 30:309–316.

Fries P, Reynolds JH, Rorie AE, Desimone R. 2001. Modulation of oscillatory neuronal synchronization by selective visual attention. *Science*. 291:1560–1563.

Fries P, Womelsdorf T, Oostenveld R, Desimone R. 2008. The effects of visual stimulation and selective visual attention on rhythmic neuronal synchronization in macaque area V4. *J Neurosci*. 28:4823–4835.

Gail A, Brinksmeyer HJ, Eckhorn R. 2000. Contour decouples gamma activity across texture representation in monkey striate cortex. *Cereb Cortex*. 10:840–850.

Gail A, Brinksmeyer HJ, Eckhorn R. 2004. Perception-related modulations of local field potential power and coherence in primary visual cortex of awake monkey during binocular rivalry. *Cereb Cortex*. 14:300–313.

Gieselmann MA, Thiele A. 2008. Comparison of spatial integration and surround suppression characteristics in spiking activity and the local field potential in macaque V1. *Eur J Neurosci*. 28:447–459.

Gilbert CD, Wiesel TN. 1989. Columnar specificity of intrinsic horizontal and corticocortical connections in cat visual cortex. *J Neurosci*. 9:2432–2442.

Gray CM. 1999. The temporal correlation hypothesis of visual feature integration: still alive and well. *Neuron*. 24:31–47, 111–125.

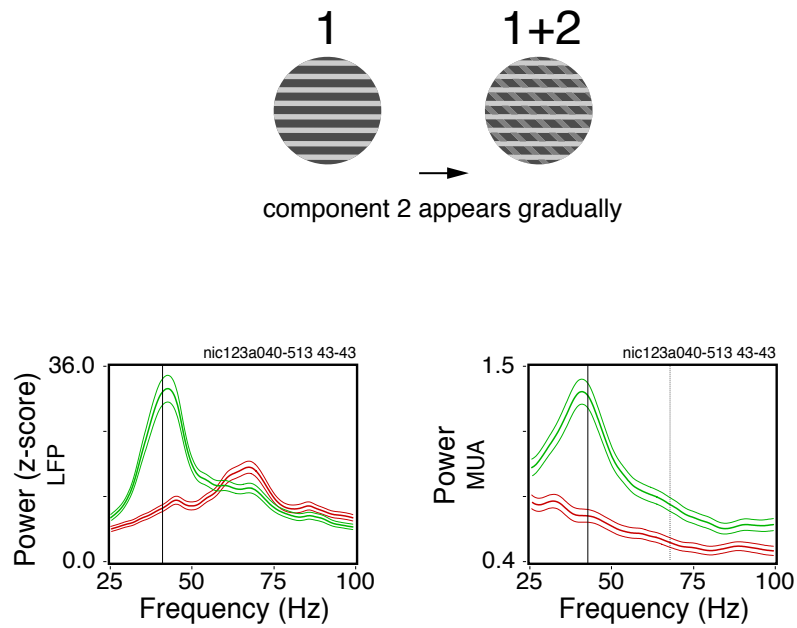
- Gray CM, Engel AK, König P, Singer W. 1990. Stimulus-dependent neuronal oscillations in cat visual cortex: receptive field properties and feature dependence. *Eur J Neurosci*. 2:607-619.
- Gray CM, König P, Engel AK, Singer W. 1989. Oscillatory responses in cat visual cortex exhibit inter-columnar synchronization which reflects global stimulus properties. *Nature*. 338:334-337.
- Gray CM, Singer W. 1989. Stimulus-specific neuronal oscillations in orientation columns of cat visual cortex. *Proc Natl Acad Sci USA*. 86:1698-1702.
- Hadjipapas A, Adjamian P, Swettenham JB, Holliday IE, Barnes GR. 2007. Stimuli of varying spatial scale induce gamma activity with distinct temporal characteristics in human visual cortex. *Neuroimage*. 35:518-530.
- Hasenstaub A, Shu Y, Haider B, Kraushaar U, Duque A, McCormick DA. 2005. Inhibitory postsynaptic potentials carry synchronized frequency information in active cortical networks. *Neuron*. 47:423-435.
- Henrie JA, Shapley R. 2005. LFP power spectra in V1 cortex: the graded effect of stimulus contrast. *J Neurophysiol*. 94:479-490.
- Herculano-Houzel S, Munk MH, Neuenschwander S, Singer W. 1999. Precisely synchronized oscillatory firing patterns require electroencephalographic activation. *J Neurosci*. 19:3992-4010.
- Kaschube M, Wolf F, Geisel T, Löwel S. 2002. Genetic influence on quantitative features of neocortical architecture. *J Neurosci*. 22:7206-7217.
- Katzner S, Nauhaus I, Benucci A, Bonin V, Ringach DL, Carandini M. 2009. Local origin of field potentials in visual cortex. *Neuron*. 61:35-41.
- Kayser C, Salazar RF, König P. 2003. Responses to natural scenes in cat V1. *J Neurophysiol*. 90:1910-1920.
- Kisvárdy ZF, Tóth E, Rausch M, Eysel UT. 1997. Orientation-specific relationship between populations of excitatory and inhibitory lateral connections in the visual cortex of the cat. *Cereb Cortex*. 7:605-618.
- König P. 1994. A method for the quantification of synchrony and oscillatory properties of neuronal activity. *J Neurosci Methods*. 54:31-37.
- König P, Engel AK, Roelfsema PR, Singer W. 1995a. How precise is neuronal synchronization? *Neural Comput*. 7:469-485.
- König P, Engel AK, Singer W. 1995b. Relation between oscillatory activity and long-range synchronization in cat visual cortex. *Proc Natl Acad Sci USA*. 92:290-294.
- Kreiter AK, Singer W. 1996. Stimulus-dependent synchronization of neuronal responses in the visual cortex of the awake macaque monkey. *J Neurosci*. 16:2381-2396.
- Lachaux J-PP, George N, Tallon-Baudry C, Martinerie J, Hugueville L, Minotti L, Kahane P, Renault B. 2005. The many faces of the gamma band response to complex visual stimuli. *Neuroimage*. 25:491-501.
- Lamme VA, Spekreijse H. 1998. Neuronal synchrony does not represent texture segregation. *Nature*. 396:362-366.
- Liu J, Newsome WT. 2006. Local field potential in cortical area MT: stimulus tuning and behavioral correlations. *J Neurosci*. 26:7779-7790.
- Malach R, Amir Y, Harel M, Grinvald A. 1993. Relationship between intrinsic connections and functional architecture revealed by optical imaging and in vivo targeted biocytin injections in primate striate cortex. *Proc Natl Acad Sci USA*. 90:10469-10473.
- Maldonado PE, Friedman-Hill S, Gray CM. 2000. Dynamics of striate cortical activity in the alert macaque: II. Fast time scale synchronization. *Cereb Cortex*. 10:1117-1131.
- Martínez-Trujillo J, Treue S. 2002. Attentional modulation strength in cortical area MT depends on stimulus contrast. *Neuron*. 35:365-370.
- Matsuda K, Nagami T, Kawano K, Yamane S. 2000. A new system for measuring eye position on a personal computer. Program No. 744.2 in Abstract Viewer/Itinerary Planner. Society for Neuroscience, New Orleans (LA).
- Mitchell JF, Sundberg KA, Reynolds JH. 2007. Differential attention-dependent response modulation across cell classes in macaque visual area V1. *Neuron*. 55:131-141.
- Mitra P, Bokil H. 2008. Observed brain dynamics. New York: Oxford University Press.
- Movshon JA, Adelson EH, Gizzi MS, Newsome WT. 1985. The analysis of moving visual patterns. In: Chagas C, Gattass R, Gross C, editors. *Pattern recognition mechanisms*. Vol. 54. Pontificiae Academiae Scientiarum Scripta Varia. Rome: Vatican Press. p. 117-151.
- Müller MM, Gruber T, Keil A. 2000. Modulation of induced gamma band activity in the human EEG by attention and visual information processing. *Int J Psychophysiol*. 38:283-299.
- Nauhaus I, Benucci A, Carandini M, Ringach DL. 2009. Stimulus contrast modulates functional connectivity in visual cortex. *Nat Neurosci*. 12:70-76.
- Neuenschwander S, Lima B, Singer W. 2008. Stimulus and task-related gamma oscillations in monkey V1 induced by local and global contours. Program No. 769.24 in Abstract Viewer/Itinerary Planner. Society for Neuroscience, Washington (DC).
- Niessing J, Ebisch B, Schmidt KE, Niessing M, Singer W, Galuske RA. 2005. Hemodynamic signals correlate tightly with synchronized gamma oscillations. *Science*. 309:948-951.
- Palanca BJ, Deangelis GC. 2005. Does neuronal synchrony underlie visual feature grouping? *Neuron*. 46:333-346.
- Pesaran B, Pezaris JS, Sahani M, Mitra PP, Andersen RA. 2002. Temporal structure in neuronal activity during working memory in macaque parietal cortex. *Nat Neurosci*. 5:805-811.
- Reynolds JH, Chelazzi L. 2004. Attentional modulation of visual processing. *Ann Rev Neurosci*. 27:611-647.
- Reynolds JH, Pasternak T, Desimone R. 2000. Attention increases sensitivity of V4 neurons. *Neuron*. 26:703-714.
- Roelfsema PR, Lamme VA, Spekreijse H. 2004. Synchrony and covariation of firing rates in the primary visual cortex during contour grouping. *Nat Neurosci*. 7:982-991.
- Rols G, Tallon-Baudry C, Girard P, Bertrand O, Bullier J. 2001. Cortical mapping of gamma oscillations in areas V1 and V4 of the macaque monkey. *Vis Neurosci*. 18:527-540.
- Samonds JM, Bonds AB. 2005. Gamma oscillation maintains stimulus structure-dependent synchronization in cat visual cortex. *J Neurophysiol*. 93:223-236.
- Samonds JM, Zhou Z, Bernard MR, Bonds AB. 2006. Synchronous activity in cat visual cortex encodes collinear and cocircular contours. *J Neurophysiol*. 95:2602-2616.
- Schmidt KE, Castelo-Branco M, Goebel R, Payne BR, Lomber SG, Galuske RA. 2006. Pattern motion selectivity in population responses of area 18. *Eur J Neurosci*. 24:2363-2374.
- Schmidt KE, Kim DS, Singer W, Bonhoeffer T, Löwel S. 1997. Functional specificity of long-range intrinsic and interhemispheric connections in the visual cortex of strabismic cats. *J Neurosci*. 17:5480-5492.
- Schwarz C, Bolz J. 1991. Functional specificity of a long-range horizontal connection in cat visual cortex: a cross-correlation study. *J Neurosci*. 11:2995-3007.
- Schatpour P, Mollholm S, Schwartz TH, Mahoney JR, Mehta AD, Javitt DC, Stanton PK, Foxe JJ. 2008. A human intracranial study of long-range oscillatory coherence across a frontal-occipital-hippocampal brain network during visual object processing. *Proc Natl Acad Sci USA*. 105:4399-4404.
- Siegel M, König P. 2003. A functional gamma-band defined by stimulus-dependent synchronization in area 18 of awake behaving cats. *J Neurosci*. 23:4251-4260.
- Singer W. 1999. Neuronal synchrony: a versatile code for the definition of relations? *Neuron*. 24:49-65,111-125.
- Smith MA, Kohn A. 2008. Spatial and temporal scales of neuronal correlation in primary visual cortex. *J Neurosci*. 28:12591-12603.
- Stettler DD, Das A, Bennett J, Gilbert CD. 2002. Lateral connectivity and contextual interactions in macaque primary visual cortex. *Neuron*. 36:739-750.
- Stoner GR, Albright TD. 1996. The interpretation of visual motion: evidence for surface segmentation mechanisms. *Vision Res*. 36:1291-1310.
- Tallon-Baudry C, Bertrand O. 1999. Oscillatory gamma activity in humans and its role in object representation. *Trends Cogn Sci*. 3:151-162.
- Tamáš G, Somogyi P, Buhl EH. 1998. Differentially interconnected networks of GABAergic interneurons in the visual cortex of the cat. *J Neurosci*. 18:4255-4270.

- Taylor K, Mandon S, Freiwald WA, Kreiter AK. 2005. Coherent oscillatory activity in monkey area V4 predicts successful allocation of attention. *Cereb Cortex*. 15:1424-1437.
- Thiele A, Pooremaeili A, Delicato LS, Herrero JL, Roelfsema PR. forthcoming Additive effects of attention and stimulus contrast in primary visual cortex. *Cereb Cortex*. doi:10.1093/cercor/bhp070.
- Thiele A, Stoner G. 2003. Neuronal synchrony does not correlate with motion coherence in cortical area MT. *Nature*. 421:366-370.
- Thomson DJ. 1982. Spectrum estimation and harmonic analysis. *Proc IEEE*. 70:1055-1096.
- Traub RD, Whittington MA, Colling SB, Buzsáki G, Jefferys JG. 1996. Analysis of gamma rhythms in the rat hippocampus in vitro and in vivo. *J Physiol*. 493:471-484.
- Ts'o DY, Gilbert CD, Wiesel TN. 1986. Relationships between horizontal interactions and functional architecture in cat striate cortex as revealed by cross-correlation analysis. *J Neurosci*. 6:1160-1170.
- Varela F, Lachaux JP, Rodriguez E, Martinerie J. 2001. The brainweb: phase synchronization and large-scale integration. *Nat Rev Neurosci*. 2:229-239.
- Vidal JR, Chaumon M, O'Regan JK, Tallon-Baudry C. 2006. Visual grouping and the focusing of attention induce gamma-band oscillations at different frequencies in human magnetoencephalogram signals. *J Cog Neurosci*. 18:1850-1862.
- Weliky M, Kandler K, Fitzpatrick D, Katz LC. 1995. Patterns of excitation and inhibition evoked by horizontal connections in visual cortex share a common relationship to orientation columns. *Neuron*. 15:541-552.
- Whittington MA, Traub RD, Jefferys JG. 1995. Synchronized oscillations in interneuron networks driven by metabotropic glutamate receptor activation. *Nature*. 373:612-615.
- Woelbern T, Eckhorn R, Frien A, Bauer R. 2002. Perceptual grouping correlates with short synchronization in monkey prestriate cortex. *Neuroreport*. 13:1881-1886.
- Womelsdorf T, Fries P, Mitra PP, Desimone R. 2006. Gamma-band synchronization in visual cortex predicts speed of change detection. *Nature*. 439:733-736.
- Womelsdorf T, Schoffelen JM, Oostenveld R, Singer W, Desimone R, Engel AK, Fries P. 2007. Modulation of neuronal interactions through neuronal synchronization. *Science*. 316:1609-1612.
- Zhou Z, Bernard MR, Bonds AB. 2008. Deconstruction of spatial integrity in visual stimulus detected by modulation of synchronized activity in cat visual cortex. *J Neurosci*. 28:3759-3768.

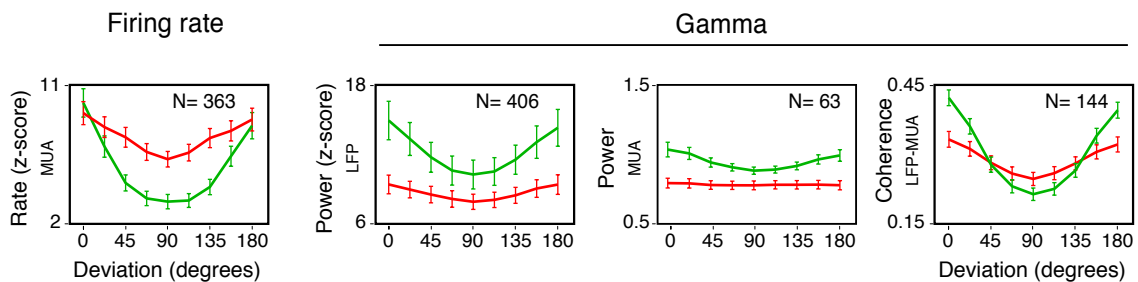
3.8 - SUPPLEMENTARY MATERIAL

In this study most of our analyses have included responses to component 1 at the preferred condition (optimal stimulus orientation and direction). In Supplementary Figure 3.2 we show rate, gamma power and coherence computed for all conditions tested. In the plots, the deviation is expressed relative to the optimal spiking response to component 1. As before, the green and red colors denote responses to single and superimposed components, respectively. Notice, that for a given deviation, component 1 was the same for both stimuli. For responses to component 1 alone, we observed that the rates, gamma power and gamma coherence were strongly dependent on the orientation, as seen from the U-shape of the curves. Modulation was pronounced for the firing rates, indicating that the neurons were generally orientation selective (one-way ANOVA for repeated measures, $F(8, 2896) = 257.6$, $p < 10^{-6}$). Selectivity for gamma was striking for power of the LFP and coherence of the LFP-MUA ($F(8, 3240) = 77.28$, $p < 10^{-6}$; $F(8, 1144) = 310.0$, $p < 10^{-6}$). For the power of MUA, the modulation was weaker but significant ($F(8, 496) = 27.7$, $p < 10^{-6}$). Responses to the two components (plaids), on the other hand, showed clearly less modulation for all measures. For the rates, both curves were similar in shape. The reason is probably that the plaid stimuli were depth-ordered, and component 1 probably dominated the responses. The vigorous responses we see for the non-optimal orientation are probably due to component 2. Another possibility, that we cannot completely exclude in our MUA recordings, is the recruitment of new cells. In any case, the gamma responses were much attenuated for the plaids as compared to the gratings. In the LFP-MUA coherence, the effect was present only for the optimal orientation (0° and 180° deviation). For the non-optimal orientation (90° deviation), we obtained a coherence value significantly higher for the plaids (Fisher's least significant difference test, $df = 2431$, $p < 10^{-6}$). Surprisingly, at this deviation point the gamma power of the LFP and MUA were lower for the plaids ($df = 6885$, $p < 10^{-6}$; $df = 1054$, $p < 10^{-6}$, respectively).

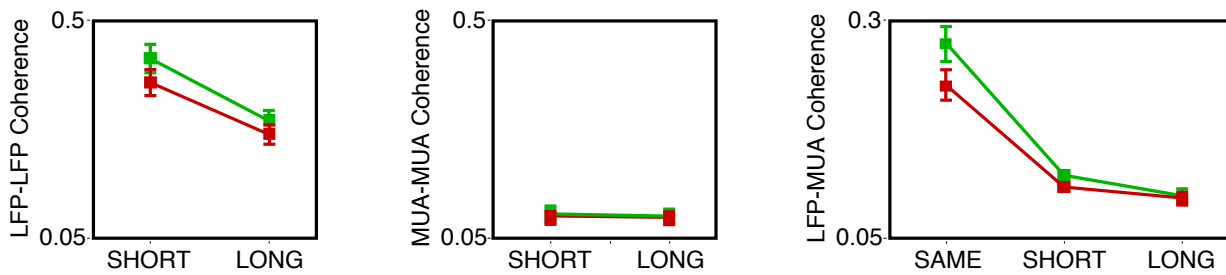
In our study we have obtained simultaneous recordings for sites in the opercular and calcarine sulcus regions. With this novel approach, we could obtain coherence estimates for sites separated by long distances in V1, corresponding to more than 7° of visual angle. In all cases, the cell pairs were stimulated by a single object covering the RFs. In Supplementary Figure 3.3 we show average coherence measures as function of distance between the recording sites for Monkey 1. Short-distance pairs comprised cases where both electrodes were placed in the operculum or in the calcarine sulcus (distances from 1.5 to 3.5 mm). Long-distance pairs, on the other hand, comprised cases where one electrode was placed in the operculum and the other in the calcarine sulcus. From the plots it is clear that recording site distance had a strong impact on coherence, both for gratings and plaids. For the LFP there was a significant attenuation effect, of 31% and of 29%, respectively (paired t-test, $df = 211$, $p < 10^{-6}$ for both stimuli). In general the coherence



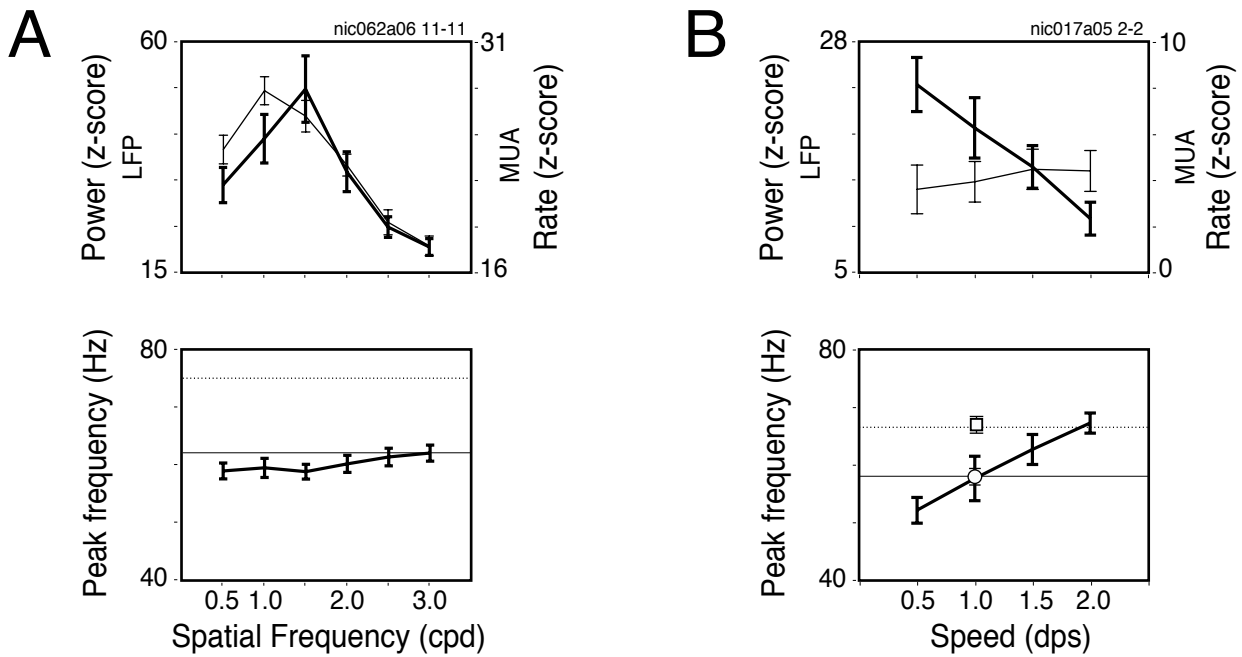
Supplementary Figure 3.1: Control for effects due to component 2 onset transient. LFP and MUA power spectra (left and right plots, respectively) were computed for responses to sequences in which component 2 appeared gradually. Notice the clear reduction in power and shift in oscillation frequency for the LFP. For the MUA, there was a disruption of the response oscillatory patterns. These results are fundamentally the same as the ones shown in Fig. 3.2 (main article). Data obtained from a calcarine site in Monkey 1. Conventions as in Fig. 3.2 (main article).



Supplementary Figure 3.2: Firing rate responses, LFP and MUA spectra, and LFP-MUA coherence for the full range of movement directions tested. Stimulus conditions with increasing deviations from the preferred direction of component 1 (represented by the null deviation) are depicted in the abscissa of all four plots. Green curves stand for component 1 presented alone, while the red curves represent the component 1 superimposed over component 2. The number of sites employed in each of the analysis is given on the top left hand side of the respective plot. Only those sites showing significant activity for component 1 relative to baseline are plotted. The U-shape of the curves representing the responses to component 1 reveal that the sites recorded were predominantly orientation selective. Additionally, it shows that the orientation preference at a given site was shared by all four measures. For the coherence analysis, only responses from LFP-MUA pairs recorded from the same electrode were included. Error bars indicate the 95% confidence interval of the mean. The power and coherence values constitute the average of all bins between 30 and 90 Hz.

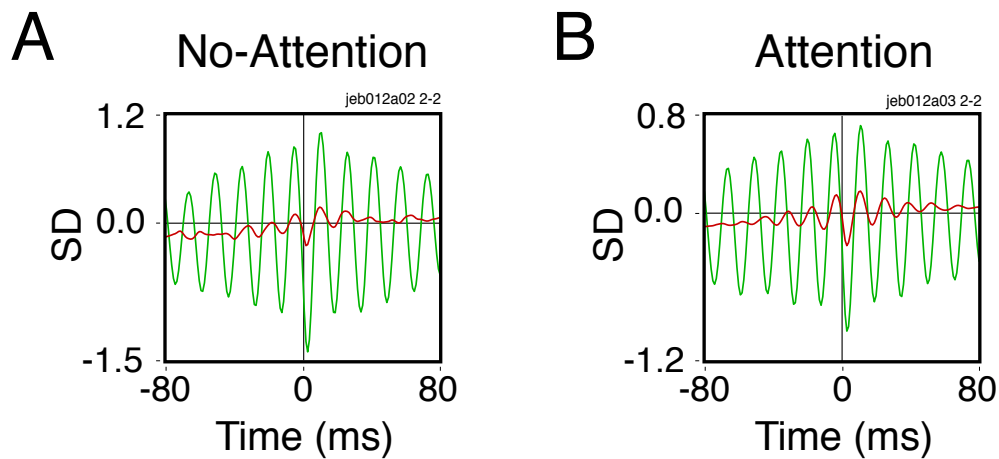


Supplementary Figure 3.3: Decay of the LFP-LFP, MUA-MUA and LFP-MUA gamma coherence with the distance between the sites of a recording pair. Activity recorded between electrode tips standing at a distance of around 3.2 mm or less were considered short (distance), while those with distances above that limit were labeled long. For the LFP-MUA coherence, there was further the possibility of analyzing the LFP and MUA from the same electrode (same). Green curves correspond to the single component grating stimulus, while the red curves correspond to components 1 and 2 superimposed. The numbers of recording pairs analyzed are given beside each data point. Error bars enclose the 95% confidence interval of the mean. The coherence values constitute the average of all bins between 30 and 90 Hz. LFP-LFP and MUA-MUA number of pairs: short, 112; long, 101. LFP-MUA number of pairs: same, 113; short, 224; long, 202.



Supplementary Figure 3.4: Control for effects of spatial frequency and speed on LFP gamma activity. (A) Example of responses to grating stimuli with spatial frequencies ranging between 1.0 and 1.5 cyc/°. The thick curve refers to the LFP gamma power, while the thin curve refers to the firing rate. Despite the strong modulation of the LFP gamma power, the gamma frequency was only marginally affected by varying spatial frequencies of the grating (bottom panel). Continuous and dotted horizontal lines depict the population gamma frequency for the grating and plaid stimuli, respectively. (B) Example of responses to grating stimuli with speed ranging between 0.5 and 2.0°/s. Top panel: the drifting speed of the gratings, while having modest or no effect on the firing rate (thin line), greatly impacted gamma power (thick line). Stronger gamma oscillations were observed for stimuli moving at slower velocities. Concomitantly, the oscillation frequency was higher for increasing speeds (bottom panel). Two individual data points are additionally plotted on the bottom panel. The open circle refers to a grating stimulus as used throughout this study. The filled square refers to a plaid stimulus where component 1 slides over a static and orthogonal component 2. A significant frequency shift is still observed despite the absence of higher resultant velocities for the plaid intersections. Continuous and dotted horizontal lines were plotted to help visualize the respective means of both data points. Error bars enclose the 95% confidence interval of the mean. A drifting speed of 1.0°/s and a spatial frequency of 2.0 cyc/° were used in (A) and (B), respectively.

measured for the MUA was lower than the one for the LFP. For the analysis of LFP-MUA coherence we could include measurements from the same electrode. Notice that coherence assumed high values locally, decaying rapidly with distance. From same-electrode to short-distance pairs, reduction was of 55% and of 52% for grating and plaid stimuli, respectively (Fisher LSD test, $df = 536$, $p < 10^{-5}$ for both stimuli). From short- to long-distance pairs, the reduction was 19% and 11% (Fisher LSD test, $df = 536$, $p < 10^{-5}$ for gratings and $p < 10^{-2}$ for plaids).



Supplementary Figure 3.5: Control for oscillation cycle skipping. (A) Spike triggered average (STA) of the LFP for the same data set presented in Fig. 3.1B of the main article (SUA, cell 1a). The green and red curves represent the STA for the grating and plaid stimuli, respectively. For this case, the monkey responded to a color change of the fixation point. An approximate 5-fold reduction in the amplitude of the LFP is observed for the plaid compared to the grating condition. Thus, skipping of spike events relative to the ongoing LFP gamma oscillations does not explain the attenuation of gamma activity for the plaid condition. (B) Same data as in Fig. 3.10A of the main article (MUA), which corresponds to the site shown in Fig. 3.1A of the main article with attention directed to component 1. The attenuation of gamma oscillation was equivalent in magnitude to the one observed in (A), showing that attending to component 1 did not prevent the attenuation of gamma oscillations that occurred after onset of component 2.

Chapter 4

Gamma responses correlate with temporal expectation in monkey primary visual cortex

I took part in all aspects of this work.

4.1 - ABSTRACT

Gamma oscillations have been linked to selective attention. Here we investigate the effects of expecting a behaviorally relevant event (a change in the fixation point, FP) on the oscillatory patterning of the local field potential (LFP) and spiking responses in V1. Three protocols were used. In the first protocol, FP change occurred at a fixed time point, enabling predictions on task timing. In the second, FP change occurred in trial blocks either early or late in the trial, allowing us to compare responses during epochs of low and high expectation. Finally, we used a cue to indicate the upcoming FP change. All protocols led to an increase in gamma oscillations associated with alpha suppression when the monkeys attended to an event in time. These effects were spatially widespread, since comparable results were observed for both central and peripheral visual field representations. Our findings indicate that temporal expectations have a strong effect on the primary visual cortex, causing a widespread, spatially non-selective modulation of gamma activity.

4.2 - INTRODUCTION

It is well known that the brain is capable of using predictive information about the world. In a stimulus detection task, for example, performance can be considerably improved by previous experience and ongoing expectations. If a cue is used to inform the likely location of a stimulus, reaction time shortens as detection speed increases (Posner *et al.*, 1980). Predictable stimuli are not only detected faster, but also perceived more accurately. Luminance increments are better detected (Hawkins *et al.*, 1990; Müller and Humphreys, 1991), spatial resolution increases (Balz and Hock, *et al.*, 1997; Yeshurun and Carrasco, 1998; Carrasco and Yeshurun, 2009) and contrast sensitivity is enhanced (Carrasco *et al.*, 2000; Cameron *et al.*, 2002). Attention can also influence the subjective experience of contrast, leading to stimulus salience enhancement (Carrasco *et al.*, 2004; see also Schneider and Komlos, 2008).

Spatial cues are not, however, the only predictive information that can be used to improve performance. The temporal structure of the environment can also impact behavior (Nobre *et al.*, 2007; Coull, 2009). Temporal expectation gradually builds-up as a function of elapsed time when the timing of an event can be anticipated. This happens because an event that is expected to occur, but has not yet occurred, must take place in a near future, as conditional probability increases over time (Nobre, 2001; Ghose and Maunsell, 2002). Temporal expectation, as spatial attention, benefits both stimulus detection and discrimination (Coull and Nobre, 1998; Correa *et al.*, 2004; Nobre *et al.*, 2007). For a sequence of events occurring at fixed time points, orientation

discrimination improves when subjects know exactly when to expect the stimulus, suggesting that predictive information may improve object representation (Westheimer and Ley, 1996). In addition, temporal expectation may interact synergistically with predictions about stimulus location (Doherty *et al.*, 2005) and category (Esterman and Yantis, 2009).

Despite the immense efforts in understanding attention, we are still left with an unresolved debate concerning its neural mechanisms (Reynolds and Heeger, 2009; Roelfsema *et al.*, 2007; Reynolds and Chelazzi, 2004). In early visual areas, it is well known that selective attention modulates the firing of neurons (Moran and Desimone, 1985; Motter, 1993; Connor *et al.*, 1997; Luck *et al.*, 1997; Roelfsema *et al.*, 1998; Ito and Gilbert, 1999). The effects of attention on response properties has been described as a gain in contrast (Reynolds *et al.*, 2000; Martinez-Trujillo and Treue, 2002; Reynolds and Desimone, 2003), as a multiplicative scaling of the responses (McAdams and Maunsell, 1999; Treue and Martinez-Trujillo, 1999; Williford and Maunsell, 2006), or as an additive mechanism (Thiele *et al.*, 2009). Recently, Fries and collaborators have proposed an alternative model for attention based on the phase-locking of gamma oscillatory signals (Fries, 2009). The key idea is that stimulus selection depends on stable phase relationships of spiking activity among populations of neurons, which would be responsible for effective channels of communication across processing levels (Fries, 2005; Womelsdorf *et al.*, 2007). In support to his hypothesis, there is now abundant experimental evidence showing that gamma oscillations are modulated by attention both in monkeys (Fries *et al.*, 2001; Bichot *et al.*, 2005; Taylor *et al.*, 2005; Rotermund *et al.*, 2009) and humans (Fell *et al.*, 2002; Doesburg *et al.*, 2007; Garcia-Garcia *et al.*, 2010). Accordingly, theoretical studies have shown that phase-locking of spiking activity may work as a selection mechanism when the networks are engaged in gamma synchronization (Tiesinga *et al.*, 2004; Börgers *et al.*, 2008).

If on the one hand the mechanisms of selective attention have been intensively investigated, the neuronal basis of temporal expectation remains largely unknown. Ghose and Maunsell (2002) have shown that the attentional modulation of spiking responses in monkey V4 depends on task timing. In this study, the effects of attention in firing were stronger whenever the monkeys anticipated the behaviorally relevant stimulus, indicating that temporal expectation influences attentional gain. Similarly, evoked potentials and spiking responses in the inferotemporal cortex were found to be dependent on temporal expectation (Anderson and Sheinberg, 2008). In a visuomotor task in humans where timing could be predicted, measurements of coherence between the motor cortex and the spinal cord have been shown to increase as function of go-signal conditional probability (Schoffelen *et al.*, 2005). Notably, the increase in coherence was restricted to the gamma frequency band. These findings suggest that neuronal interactions mediated by gamma oscillations

may serve as an attentional mechanism during temporal expectation, although direct evidence is lacking.

In the present study we recorded spiking and LFP responses from monkey V1 during a visual detection task. Our results show that allocating attention in time strongly modulates gamma activity. These effects seemed to be widespread in V1. As discussed below, our study suggests that coordinated gamma activity are not only important for selection processes in the brain, but also for building active predictions about the world.

4.3 - EXPERIMENTAL PROCEDURES

4.3.1 - TRAINING AND VISUAL PARADIGM

Two rhesus monkeys (*Macaca mulatta*) participated in this study. Experimental procedures were approved by local authorities (Regierungspraesidium, Hessen, Darmstadt) and were in accordance with the guidelines of the European Community (European Union Directive 86/609/EEC).

Initially the monkeys were trained on a fixation task. A trial started with the appearance of a 0.15° fixation point (4 X 4 pixels; luminance, 10.0 cd/ m²) for which a lever press was required within a window of 700 ms. In a random time point between 2500 and 4000 ms after fixation onset, the color of the FP changed from red to green. To obtain a reward, the monkeys had to maintain their gaze within 1° of the fixation point (FP) during the whole trial, and to release the lever within 500 ms after FP change. Trials were aborted when early or late lever releases occurred, or whenever fixation was interrupted. Eye position was monitored by a search coil system (DNI, Crist Instruments, USA, temporal resolution of 2 ms), or by an infrared camera-based tracking system (Matsuda *et al.*, 2000; temporal resolution of 33 ms). Typically, monkeys performed approximately 1500 correct trials in a 4-hour session, thereby receiving their daily liquid requirement.

Stimuli were generated as sequences of bitmap images using an interface developed by one of the authors (SN; LabVIEW, National Instruments, USA), and were presented as 1024 X 768 pixel resolution movies running at 100 frames/s using a standard graphical board (GeForce 6600-series, NVIDIA, USA) controlled by ActiveStim (www.activestim.com). This software allowed for high timing accuracy. The CRT monitor used for presentation (CM813ET, Hitachi, Japan) was gamma corrected to produce a linear relationship between output luminance and gray values, and subtended a visual angle of 36° X 28°.

At the beginning of each recording session, a bar moving across the screen in 16 different directions was used to map the receptive fields. RF maps were obtained by computing a response matrix with 10 ms resolution (corresponding to 0.2° in visual angle, see examples in Figure 4.2B). The test stimuli consisted of moving gratings or plaid stimuli. The gratings had spatial frequency ranging from 1.25 to 2.0 cycles per degree, velocity ranging from 1.0 to $1.5^\circ/\text{s}$ and a duty cycle of 0.3 (square gratings). These values were chosen because they elicited robust responses in V1. The plaids were constructed by superimposing two gratings with a 135° moving direction offset. The gratings of higher luminance ($\sim 20.0 \text{ cd}/\text{m}^2$) was placed on top of the one of lower luminance ($\sim 8.0 \text{ cd}/\text{m}^2$). The visual stimulus extended from 4° to 16.0° of visual angle and was positioned at the average of the receptive field centers for all recorded neuron.

The monkeys were trained in three protocols: sequence, block, and cue protocols. In all protocols the monkey had to release a lever upon FP color change. In the sequence-protocol, FP change was fixed at 3200 ms relative to trial onset. The stimulus was presented in sequences, gratings-plaids-gratings or plaids-gratings-plaids. Only one of the two sequences was ran during a protocol. Stimulus transitions occurred always at fixed time points (stimulus onset at 800 ms, first stimulus change at 1600 ms, second stimulus change at 2400 ms). Since task timing was fixed, the monkeys could use the various stimulus transitions as a cue for predicting FP change. In the block-protocol, FP change followed two schedules. It could occur early or late in the trial (1600 ms and 3600 ms after trial onset, respectively). The two different schedules were presented in blocks of 50 or 160 trials. In both schedules, 15% of the trials were catch trials in which FP change appeared late for an the early schedule, or early for the late schedule (see diagram in Fig. 4.2A for details). Typically, we ran 6 blocks in an experimental session, where the two schedules were alternated. In this protocol the stimulus remained unchanged along the trial, and consisted of gratings presented at 16 different directions (to obtain tuning curves, blocks of 160 trials) or a single grating presented at the average preferred direction of the cells (blocks of 50 trials). In the cue-protocol, we introduced a cue to indicate the upcoming FP change. This was achieved by a slight increase of FP luminance prior to its change in color. Cueing duration was of 800 ms. Three conditions, randomly presented, were used. In the first and second conditions, cueing and FP color change occurred early or late in the trial (at 1800 ms and 3800 ms), respectively. In the third condition (catch trials), cueing appeared at the beginning of the trial while FP color change occurred only late (3800 ms), at the end of the trial. Condition probabilities were of 45% for the first and second conditions and of 10% for the third condition. Gratings or plaids stimuli were used. As in the block-protocol, the stimulus remained unchanged during the whole trial.

In some experiments we manipulated the value of the reward. To this end banana juice was used instead of water (the monkeys had a clear preference for juice), or the amount of fluid delivered was

increased by a factor of 3. The two schedules were run in alternating blocks of 50 trials (typically a total of 6 blocks was run in a single experiment). Task timing and visual stimulation was the same in the two schedules. Grating stimuli were used with task timing as in the early schedule of the block-protocol.

4.3.2 - PREPARATION AND RECORDING PROCEDURES

Each monkey was surgically implanted with a titanium bolt for fixating the head, a scleral search coil, and a titanium recording chamber. The titanium pieces were fixed to the skull by means of screws (Synthes, Germany). All surgical procedures were conducted under aseptic conditions with isoflurane anesthesia (Baxter, Germany) and assisted by a pressure-controlled ventilation unit (1.8 liters per min N₂O and 0.8 liters per min O₂; Julian station, Dräger Medical, Germany).

Recordings were made from the opercular region of V1 (receptive fields centers, 2.0° to 3.0° eccentricity, central sites) and from the superior bank of the calcarine sulcus (10.0° to 13.0° eccentricity, peripheral sites). Electrodes were inserted independently into the cortex via guide tubes positioned above the dura (diameter, 300 μm; Ehrhardt Söhne, Germany), assembled in a customized recording device. This device comprised five hydraulic microdrives mounted onto an X-Y stage (MO-95, Narishige Scientific Instrument Laboratory, Japan), which was fixed onto the recording chamber by means of a mount adapter. Quartz-insulated tungsten-platinum electrodes (Thomas Recording, Germany; diameter, 80 μm) with impedances ranging from 0.3 to 1.0 MΩ were used to record simultaneously the extracellular activity from 4 to 5 sites in both superficial and deep layers of the cortex.

4.3.3 - DATA COLLECTION AND SPIKE SORTING

Spiking activity of small groups of neurons (MUA) and the local field potential (LFP) were obtained by amplifying (1000X) and band-pass filtering (MUA, 0.7 to 6.0 kHz; LFP, 0.7 to 170 Hz) the recorded signals. For signal amplification and conditioning we used a Plexon pre-amplifier connected to a HST16o25 headset (Plexon Inc., USA). The signals were digitized and stored using a LabVIEW-based acquisition system (SPASS, written by SN). Additional 10X signal amplification was carried out by the acquisition board amplifiers (E-series acquisition boards, National Instruments, USA). Local field potential was acquired with a resolution of 1.0 ms. Spikes were detected by amplitude thresholding, which was set interactively after on-line visualization of the spike waveforms (typically, 2 to 3 standard deviations above noise level). Spike events and corresponding waveforms were sampled at 32 kS/s (spike waveform length, 1.2 ms).

Spike sorting was performed off-line using a dynamic template matching method implemented in a custom software package (developed by Nan-Hui Chen, see details in Lima *et al.*, 2010).

4.3.4 - DATA ANALYSIS

For the sequence-protocol, two 700 ms analysis windows were used. A first window was placed 100 ms after the first stimulus onset (early window), and a second window was placed 100 ms after the last stimulus onset (late window), just before FP change. For the block-protocol, comparisons were made across 400 ms analysis windows placed early in the trial (1200 ms after trial onset) for both the early and the late schedules. In the early schedule, the analysis window was placed just before FP change, during an epoch of high expectation. In the late schedule, on the other hand, the analysis window corresponded to an epoch of low expectation, as FP change occurred only late in the trial. For the cue-protocol, the analysis window was placed 1300 ms after trial onset. In the conditions in which cueing appeared early in the trial (1000 ms after trial onset, cue conditions), the window corresponded to an epoch of high expectation, since it was placed just before FP change. In the conditions in which cueing appeared late in the trial (3000 ms after trial onset, no-cue conditions), however, the analysis window corresponded to an early epoch far from FP change. In this later case, expectation was low.

Our analysis consisted in obtaining estimates of coordinated activity in V1. Autocorrelograms for the spiking responses were computed for each trial (resolution, 1.0 ms; time shift, 80 ms), and averaged over 15 to 20 stimulus repetitions. A damped cosine function was fitted to the correlograms as in König (1994) to obtain the modulation amplitude ratio associated with the first satellite peak in the correlogram, which estimates oscillation strength (see Fig. 4.1A). The peak was measured from the offset of the fitted function, and the confidence limit for the statistical significance of their values was set as follows: the Gabor fits had to account for $\geq 15\%$ of data variance and the z-scores of the peaks in the correlograms had to be > 2 .

Spectral analysis was run both for spike and LFP data using the multitaper method (Thomson, 1982) implemented in Chronux 2.0 (Mitra and Bokil, 2008), an open-source MATLAB toolbox (Mathworks Inc., Natick, USA; available at <http://chronux.org>). Essentially, the multitaper method attempts to reduce the variance of spectral estimates by pre-multiplying the data with several orthogonal tapers known as Slepian functions. The frequency decomposition of multitapered data segments therefore provides a set of independent spectral estimates. Mathematically, the multitapered power spectrum of a time series is defined for a given frequency as an average over all repetitions and tapers:

$$s_x(f) = \frac{1}{K} \sum_{k=1}^K |\tilde{x}_{n,k}(f)|^2$$

where

$$\tilde{x}_{n,k}(f) = \frac{1}{N} \sum_{n=1}^N e^{-i2\pi ft} w_k(t) x_n(t)$$

is the discrete Fourier transform of the product of the measured time series sequence $\{x_n(t), n = 1, 2, \dots, N\}$ with the k^{th} Slepian taper, denoted $w_k(t)$. Numerically, $\tilde{x}_{n,k}(f)$ is computed as the Fast Fourier transform of the product. Data segments were padded with zeros to the length of 1024 (400 ms and 500 ms windows) or 2048 points (700 ms window) before the Fourier transformation. Five Slepian tapers were used for both spike and LFP data. Thus, we obtained a spectral concentration of ± 7.5 Hz, ± 6.0 Hz and ± 4.3 Hz for the data segments of 400 ms, 500 ms and 800 ms, respectively. For computation of the spectrograms, we used windows of 200 ms moved at 50 ms steps. For this case, the spectral concentration was ± 15 Hz.

Estimates of neuronal synchronization were obtained in frequency domain by computing the coherence function, defined as:

$$C_{yx}(f) = \frac{|S_{yx}(f)|}{\sqrt{S_x(f)S_y(f)}}$$

where $S_x(f)$ and $S_y(f)$ are the multitapered power spectrum estimates of the time series $x_n(t)$ and $y_n(t)$ averaged over n repetitions, respectively, and $S_{yx}(f)$ is the cross-power of these two time series. For MUA-MUA and LFP-LFP pairs, coherence measures were computed for data obtained from different electrodes. For LFP-MUA pairs, coherence was computed for data obtained from both the same as well as from different electrodes. Coherence for single trials was estimated using the single-trial coherence pseudovalues (*STCP*), as described in Womelsdorf *et al.* (2006):

$$STCP = N \times C_{all} - (N-1) \times C_{all-i}$$

where N is the total number of trials, C_{all} is the coherence for the entire sample, and C_{all-i} is the coherence for the entire sample with the i^{th} trial left out. The coherence values used to calculate the *STCP* were z-transformed, as described in Kilner *et al.* (2000):

$$Z = \text{arctanh}(C) \times \sqrt{2L}$$

where the C is the coherence value, and L is the number of independent estimates (number of tapers x number of trials).

Baseline activity was estimated using an analysis window positioned before stimulus onset (same length as for stimulus driven activity). The LFP power was expressed in z-score units relative to baseline activity. For this, the power computed for the baseline activity was subtracted from the power computed for stimulus driven activity, and divided by the standard deviation of the baseline activity. Firing rates were also computed in z-score units. Spiking responses were considered significant if the z-score was greater than 1.96 (95% threshold). The bulk of our analysis focused on the preferred conditions, corresponding to the maximal responses. The MUA power spectrum was normalized by the firing rate. The jackknife method was used to select which frequency bins between 30 Hz and 90 Hz (gamma band) were significantly different when comparing the baseline with the stimulus driven activity. Gamma was computed as the average over the selected frequency bins for the power spectrum and coherence functions. Alpha activity was taken as the average power for frequency bins between 8 Hz and 12 Hz. No spectral concentration (multitapers) was used to compute alpha power.

Each site or pair of sites was classified as directional, orientational, pan-directional or non-selective depending on the response to the grating stimuli. This classification was separately performed for the firing rate, gamma power (LFP and MUA), and gamma coherence (LFP-LFP, MUA-MUA and LFP-MUA pairs). The selectivity index was calculated as:

$$SI = (R_{pref} - R_{anti}) / R_{pref}$$

where R_{pref} and R_{anti} represent, respectively, the activity to the preferred and anti-preferred stimulus configurations. To compute the selectivity index for direction, the anti-preferred stimulus was defined as the one with direction 180° away from the preferred stimulus. To determine whether there was a statistically significant relationship between neuronal activity and motion direction, we performed an ANOVA using direction of motion as the main factor. Finally, responses were fit with parametric curves based on the probability function of the von Mises distribution, which is the circular statistics analogue of the normal distribution. As proposed by Swindale *et al.* (2003), the fitting parametric curve for direction selectivity was:

$$M(\Phi) = m + A_1 e^{k_1(\cos(\Phi-\Phi_1)-1)} + A_2 e^{k_2(\cos(\Phi-\Phi_2)-1)}$$

where Φ is the grating direction of motion for which the response is being estimated, m corresponds to the baseline level, A_1 and A_2 represent the maximum heights of the individual

peaks, Φ_1 and Φ_2 are the center directions (in radians) of each peak, and k_1 and k_2 , known as concentration factors, are inversely related to the width of each peak. All parameters were adjusted by a non-linear minimization algorithm provided in the MATLAB Curve Fitting Toolbox (MathWorks, Natick, MA, USA). Fits that accounted for less than 80% of the variance, as determined by R^2 statistics, were rejected. A recording site or pair of sites was classified as direction selective if all of the following criteria were fulfilled: selectivity index > 0.5 , criterion of $p < 0.05$ for the ANOVA, and $R^2 > 0.8$ for the parametric curve fit. In case the site or pair of sites was not classified as direction selective, it was tested for orientation selectivity. To this aim, activity for grating stimuli with opposite directions of motion but same orientation were pooled. The anti-preferred stimulus in this case was defined as the one orthogonal to the preferred stimulus. The parametric curve fitting for orientation selectivity had A_2 constrained to equal 0, which removed the second von Mises function from the equation. The same criteria mentioned above had to be fulfilled in order for the site or pair of sites to be classified as orientation selective.

To estimate the SEM for the power and coherence spectra we used the jackknife method (Efron and Tibshirani, 1993). For visualization purposes in the single case plots, spectral quantities were smoothed with a cubic spline function (smoothing parameter = 0.1). Group data were compared by t -tests (paired and independent samples) and ANOVA. Significant levels were set at 95% ($p < 0.05$).

4.4 - RESULTS

Local field potential (LFP) and multiunit activity (MUA) were recorded from 363 sites in 4 hemispheres of 2 monkeys (Monkey 1, 288 sites; Monkey 2, 75 sites; in a total of 83 experimental sessions). For selected cases, spike sorting was applied to the MUA in order to obtain single unit activity (SUA). Simultaneous recordings were made from the opercular and calcarine regions of V1 corresponding, respectively, to the central ($\sim 3^\circ$ of visual angle; total of 219 sites) and the peripheral ($\sim 10^\circ$ of visual angle; total of 72 sites) representations of the visual field. Our analysis comprised 651 pairs of recording sites, where 427 were central-central, 62 peripheral-peripheral, and 162 central-peripheral pairs.

The monkeys were trained in three protocols: sequence, block, and cue protocols. For all protocols, the monkeys were required to hold their gaze within a window centered on a fixation point (FP), and to respond to a change in FP color by a lever release (see Experimental Procedures).

4.4.1 - BUILDING EXPECTATION IN STIMULUS SEQUENCES

The sequence-protocol consisted in three stimuli presented sequentially along the trial at fixed time points. The first and last stimulus in a sequence were always identical. The sequences could be either gratings-plaids-gratings or plaids-gratings-plaids. Because stimulus events were fixed in time and repeated precisely over hundreds of trials, the monkeys were able to predict task timing, and thus anticipate FP change. With this regime, behavioral performance was high (correct responses, 95% for Monkey 1, 92% for Monkey 2).

An example of oscillatory SUA responses recorded from peripheral V1 during a grating-plaid-grating sequence-protocol is shown in Figure 4.1. In the sequence, the foreground grating component is presented throughout the trial, matching the preferred direction of the cell (indicated by a dot on the tuning curve plot, Fig. 4.1A). In the middle of the sequence, a second component appears (plaid stimuli). The single component stimulus (gratings) induced strong gamma oscillations, as shown in the sliding window autocorrelation analysis and autocorrelograms (see also Lima *et al.*, 2010). Notice the strong increase in gamma for the late as compared to the early stimulus, even though both were physically the same. This increase was even more evident at the LFP level. Fig. 4.1B illustrates spectral analysis of the LFP for both gratings-plaids-gratings and plaids-gratings-plaids sequences for the same recording site. Consistent with the SUA data, the gamma components in the LFP show a dramatic increase for the late stimulus, regardless of stimulus sequence. Observe that the increase in gamma coincides with a decrease in alpha power. Population data is shown in Figure 4.1C. In the plots, data points express z-score values relative to baseline (see Experimental Procedures), split by central (blue) and peripheral (black) sites. Strong effects in the LFP were seen for both gamma (25% increase, paired *t*-test, $df = 299$, $p < 10^{-6}$) and alpha (42% decrease, $df = 299$, $p < 10^{-6}$), in spite of no significant changes in rates ($df = 274$, $p = 0.28$). A similar effect for gamma was also significant in the MUA (32% increase, paired *t*-test, $df = 50$, $p < 10^{-6}$). Notably, there were no considerable differences in gamma (or alpha) modulation between central and peripheral sites (for eccentricities as large as 12°). This is interesting because, although the monkeys were required to direct attention to the FP, the effects proved not to be higher for central sites (closer to the FP representation). On the contrary, the effects in power seemed to be widespread in V1. We conjecture that the key variable here was the allocation of attention in time and not space. It is conceivable that the monkeys used the timing structure of the task to anticipate FP change, the single relevant event to accomplish the task. To investigate this possibility we used a block design protocol where the FP change followed different time schedules.

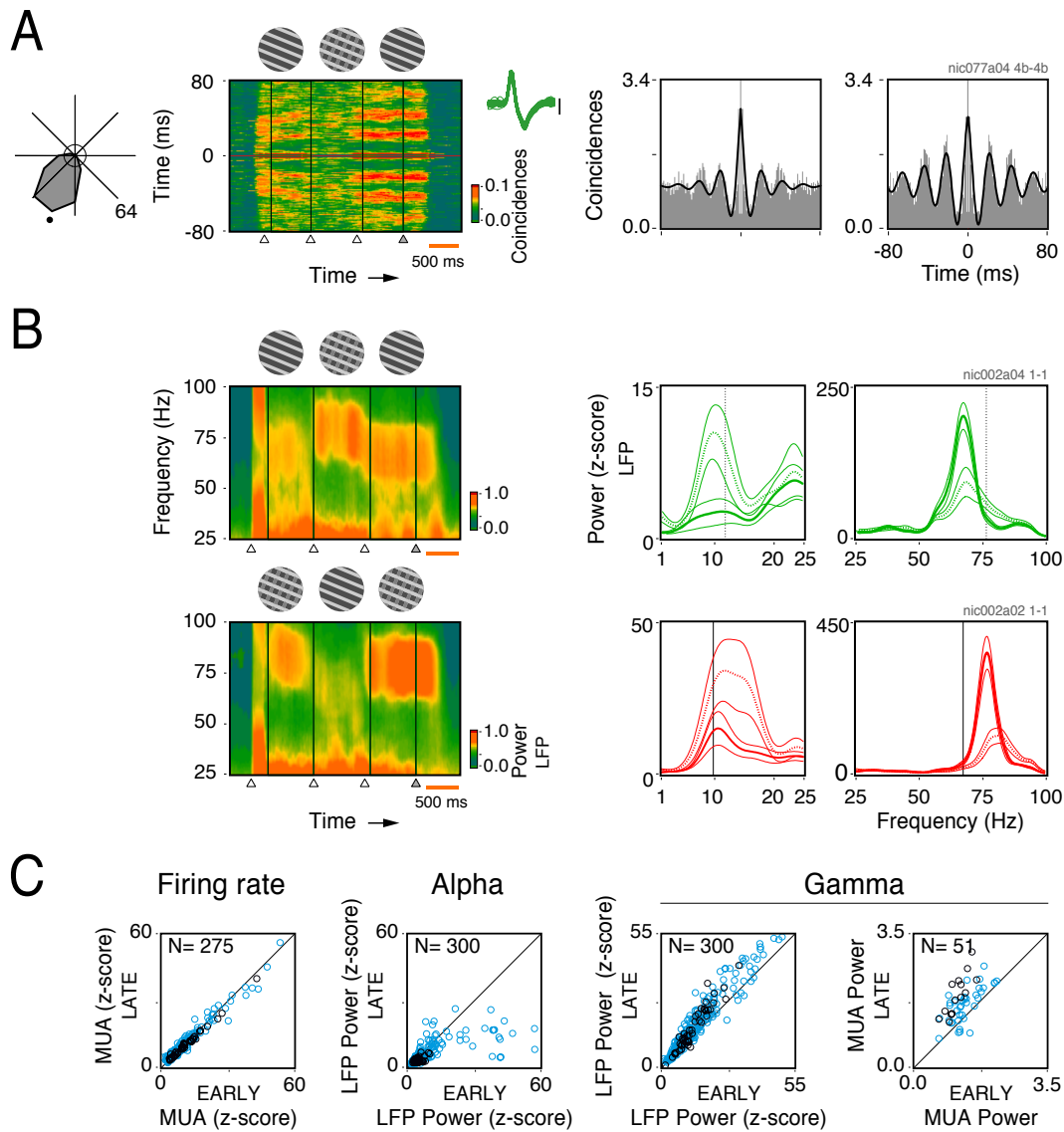


Figure 4.1: Spectral analysis for the sequence-protocol. Comparisons were made for analysis windows placed at the early and late epochs of the trial. Stimuli were strictly the same for the two windows. (A) A grating component matching the preferred direction of an isolated single-unit (black dot in the tuning curve, displayed to the left) is presented throughout the trial. In the middle of the trial, however, a second grating component is presented behind the first, forming a plaid. This forms a chain of stimulus events fixed in time. Sliding window autocorrelogram analysis of a single-unit recorded at 10° eccentricity (spike waveforms displayed to the right) shows that gamma oscillations are more strongly induced for the late as compared to the early grating in the sequence. Autocorrelograms for the early (left) and late (right) gratings show a major enhancement in gamma activity for the grating immediately preceding the change in FP color (modulation amplitudes of 0.75 and 1.60, respectively). Analysis windows are indicated by boxes in (A). The circle in the center of the tuning curve represents the mean spontaneous rate. Stimulus timing events (onset of early grating, onset of plaid, onset of late grating, and FP color change) are indicated by arrow heads at the bottom of the sliding window panel. (B) Time-frequency plots to the left show LFP power along the trial recorded from a single V1 opercular site for the sequences grating-plaid-grating or plaid-grating-plaid. LFP power spectra for the lower (1 - 25 Hz) and higher (25 - 100 Hz) frequency bands are shown to the right. Early versus late comparisons are shown in green for grating stimuli and in red for plaid stimuli (a convention used for all figures). Dotted and continuous lines represent the early and late phases of the trial, respectively. Opposite effects were observed for the low and high frequency bands. For the sequence where early and late gratings are compared, there was a reduction of 84% in alpha power (paired *t*-test, $df = 8$, $p < 10^{-2}$), but an increase of 34% in gamma power ($p < 10^{-2}$) for the late relative to the early grating presentation. A similar result was observed for the plaid-grating-plaid sequence: a 53% decrease in alpha power (paired *t*-test, $df = 8$, $p = 0.04$), but a doubling in gamma power ($p < 10^{-3}$). (C) Population data for rates, LFP alpha power, LFP gamma power and MUA gamma power comparing early and late stimuli. Blue and black circles represent, respectively, sites in the central (opercular region) and peripheral (calcarine sulcus) representations of V1. Number of sites presented in each scatter plot is indicated at the top left hand corner. A total of 300 sites were analyzed. Only those sites showing a significant increase in activity during stimulation are plotted.

4.4.2 - BUILDING EXPECTATION IN TRIAL BLOCKS

In the block-protocol, FP change could occur early or late in the trial. These two different time schedules were run in alternating blocks of 50 or 160 trials. Figure 4.2A summarizes the trial structure for the two schedules. In the expected-late schedule, FP change occurred for most of the cases (85%) late in the trial, at 3600 ms. Only rarely (15% of the cases, catch trials) did the change occur early in the trial, at 1600 ms. Thus the monkeys expected to see a FP change in the late phase of trial. In the expected-early schedule, the probabilities of FP change were reversed (85% early in the trial and 15% late). These two schedules allowed us to compare neuronal responses to the same stimulus during epochs of low and high expectation.

To determine how effective our block-protocol was in building expectation, we compared reaction times for early changes in FP, both when expected or not. An impact on reaction times was seen for Monkey 2 (mean of 403 ms for expected as compared to 429 ms for non-expected trials, paired *t*-test, $df = 9$, $p < 10^{-3}$). For Monkey 1, nevertheless, reaction times were shorter, with no significant differences for expected and non-expected trials (mean of 355 ms, $df = 11$, $p = 0.9$). Despite these differences in performance, both monkeys showed increase in gamma power as a function of expectation, as described for the sequence-protocol.

Figure 4.2B illustrates spectral analysis of the LFP obtained for two sites recorded simultaneously from central and peripheral V1 in Monkey 1. A single moving grating stimulus placed over the RFs was used to co-active all recorded neurons. As for the sequence-protocol, observe the large increase in gamma power for a window placed late in the trial, when change in FP was about to occur, as compared to a window early in the trial (expected-late 85%, solid and dotted lines, respectively). Effects of expectation were also measured by comparing responses during the expected-early schedule with responses during the expected-late schedule for a window placed early in trial (expected and non-expected responses, respectively). This comparison was particularly important because here stimulus timing (onset and duration) was identical for both cases, the only difference being the behavioral context provided by the schedule (expecting early or late). Average increases of 44% and of 37% were measured for the 3° and the 10° sites, respectively (two sample *t*-test, $df = 453$, $p < 10^{-6}$). Notice that, similar to the sequence-protocol, these effects were of comparable magnitudes for central and peripheral recordings, suggesting a widespread effect in V1. Interestingly, for the catch trials in the expected-early schedule, when the FP change did not occur early but late in the trial, gamma increased even further (28% for the 3° site, paired *t*-test, $df = 39$, $p < 10^{-3}$; 34% for the 10° site, $df = 39$, $p < 10^{-2}$). This may have happened because FP change at the end of the trial was highly predictable, given that it had not occurred before (conditional probability at its maximum).

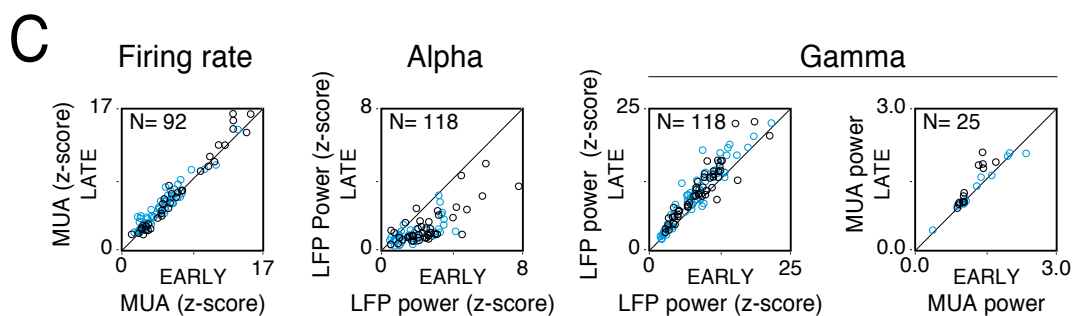
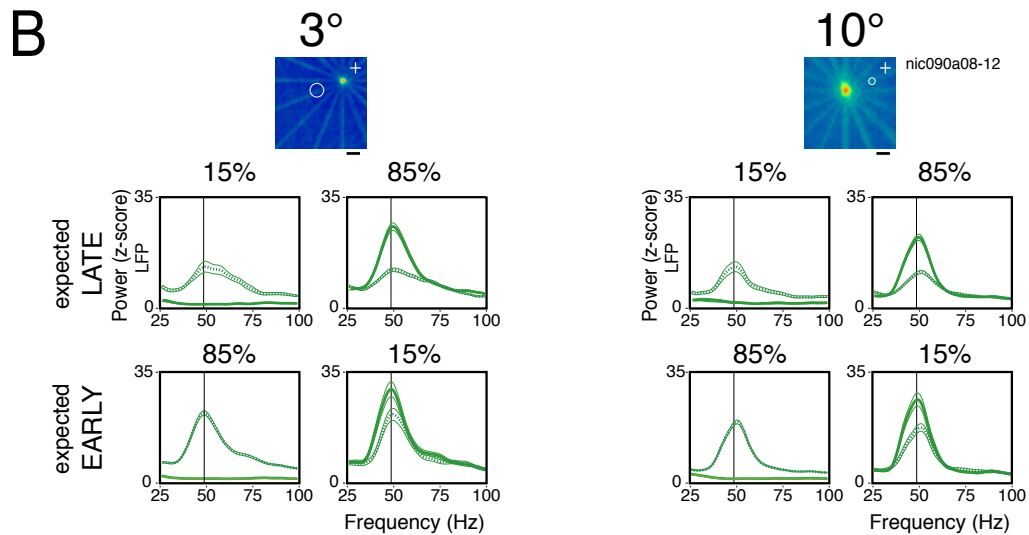
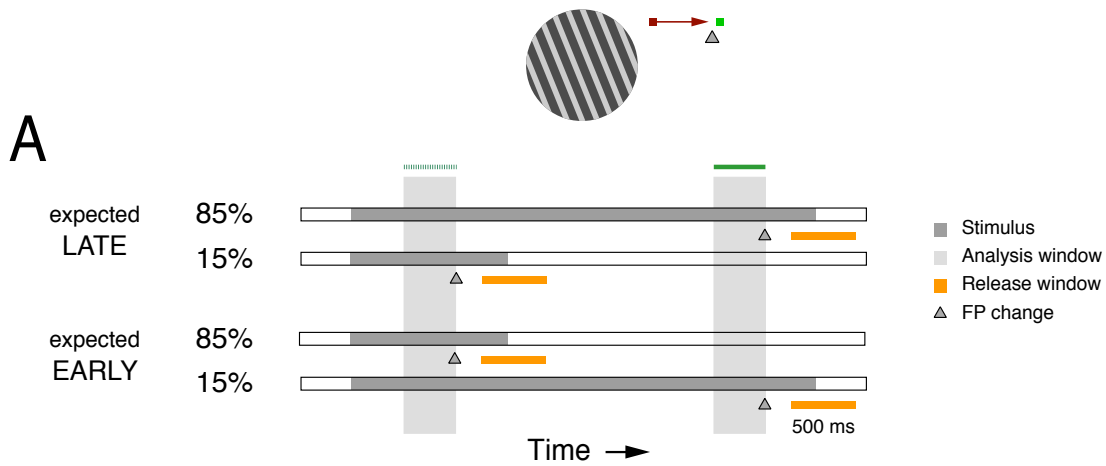


Figure 4.2: Spectral analysis for the block-protocol. (A) General description of the behavioral task. (B) The RF maps for two sites recorded simultaneously from the central (left) and peripheral (right) representations of the visual field are shown at the top (scale bar, 2°). Warmer colors, representing higher firing rates, reflect the center and extent of each RF. The FP position is indicated by a white cross in each map. Below each RF map are the respective LFP power spectra. Dotted and continuous lines represent 400 ms analysis windows positioned early or late in the trial, respectively. Note that both windows end before the FP change event, which takes place at 1600 ms for early changes and at 3600 ms for late changes. Both early and late windows are shown in each spectra plot for the four corresponding conditions. Comparing the spectra for all early windows, note the change in power depending on the probability of an upcoming change in the FP (the dotted lines on the plots above versus the continuous lines on the plots below). (C) Population data for rates, LFP alpha power, LFP gamma power and MUA gamma power comparing non-expected versus expected upcoming changes in the FP for the early windows. Conventions as in Fig. 4.1.

Population data for the block-protocol is presented in Figure 4.2C. From a total of 118 tests for 74 recording sites (41 central and 33 peripheral sites), we observed an average 20% increase in LFP gamma power for expected as compared to non-expected responses (paired t -test, $df = 117$, $p < 10^{-6}$). A significant increase in gamma power could be also observed for the MUA (average increase of 9%, paired t -test, $df = 24$, $p < 10^{-2}$), although only a few sites exhibited significant oscillatory responses. Again, increase in gamma power was associated with a decrease in LFP alpha power (average decrease of 53%, paired t -test, $df = 117$, $p < 10^{-6}$). In contrast to the sequence-protocol, however, we observed a significant increase in firing rates (average increase of 11%, paired t -test, $df = 91$, $p < 10^{-6}$).

Correct responses for the block-protocol were of 95% for Monkey 1 and of 96% for Monkey 2.

4.4.3 - CUEING EFFECTS

Temporal expectation to an event can also be built by means of a cue delivered before event onset. In the cue protocol we used such a strategy by slightly increasing FP luminance for a duration of 800 ms before FP color change (from red to green). Three conditions were used. For the first and second conditions, the cue appeared early or late in the trial, respectively, with an equal probability of 45%. For the remaining 10% of the cases (false-cue condition) the cue appeared early in the trial without being associated, however, with the FP change, which occurred invariably at the end of the trial (see Figure 4.3). The conditions were presented in random order. Notice that, different from the block-protocol, the monkeys relied on an external instruction associated with the FP to anticipate task timing.

The effects of cueing on gamma power are illustrated by the sliding window analysis provided in Figure 4.3. In this example LFP responses were obtained to a plaid stimulus. Recordings were made from central V1 in Monkey 1. In the plots the cueing time is indicated by a red bar (duration of 800 ms). For early cueing, gamma responses in the LFP increased shortly after cue onset. For late cueing, on the other hand, gamma remained low at the beginning and increased only later in the trial. Notice that in this condition gamma power starts to increase before cue onset. We think this happens because expectation, as for the block-protocol, increases towards the end of the trial following a conditional probability function. For the false-cue condition, gamma power increased at the beginning of the trial (cueing effect), decreased after no FP change occurred, and increased once more towards the end of the trial. Here again gamma increases towards the end of the trial following the conditional probability of FP change. These results are consistent with our previous observation for the expected-early schedule of the block-protocol, when the FP change did not occur early but late in the trial (catch trials in Fig. 4.2B).

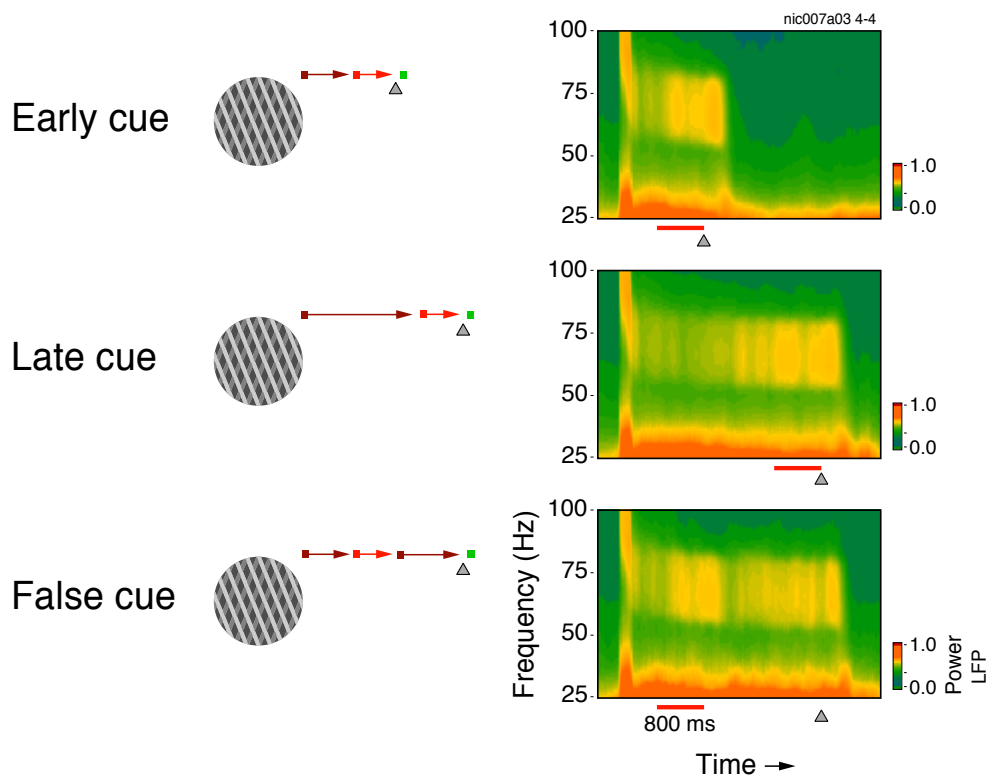


Figure 4.3: Time-frequency analysis of the LFP acquired during a cue-protocol. Illustrated are the three conditions tested (left) with the corresponding LFP spectrogram (right). A plaid was used as visual stimulus. Enhanced LFP gamma power in the early part of the trial occurred only when the cue was presented early (early cue and false cue conditions). For the false cue conditions, gamma oscillations transiently ceased when the cue was turned off, gradually increasing again towards the end of the trial.

The spectral plots in Figure 4.4A give an idea of the size of the cueing effects on LFP gamma and alpha power. Results are shown for responses to gratings (green lines) and to plaids (red lines) recorded from the same site at central V1. Analysis windows (length of 500 ms) were placed at an epoch early in the trial. For the early-cue condition, the window started 300 ms after cue onset and ended just before the FP change event. The same window position was used for the late-cue condition. This allowed us to draw comparisons between epochs with and without cueing (cue and no-cue conditions) for identical stimulus conditions and task timing. As described before, during conditions of high expectation, alpha was suppressed (decrease of 61% for the gratings, two sample t -test, $df = 359$, $p < 10^{-2}$, and decrease of 75% for the plaids, $df = 352$, $p < 10^{-6}$) and gamma power was enhanced (increase of 15% for the gratings, two sample t -test, $df = 359$, $p < 10^{-6}$, and increase of 23% for the plaids, $df = 352$, $p < 10^{-6}$). In accordance with our previous study (Lima *et al.*, 2010), peak frequencies were higher for plaids as compared to gratings stimuli. Note that increase in gamma power is restricted to a narrow band around the peak in the spectrum, with no impact on oscillation frequency. In other words, the temporal expectation effects can be understood as a gain mechanism, affecting the amplitude but not the frequency of the ongoing oscillations.

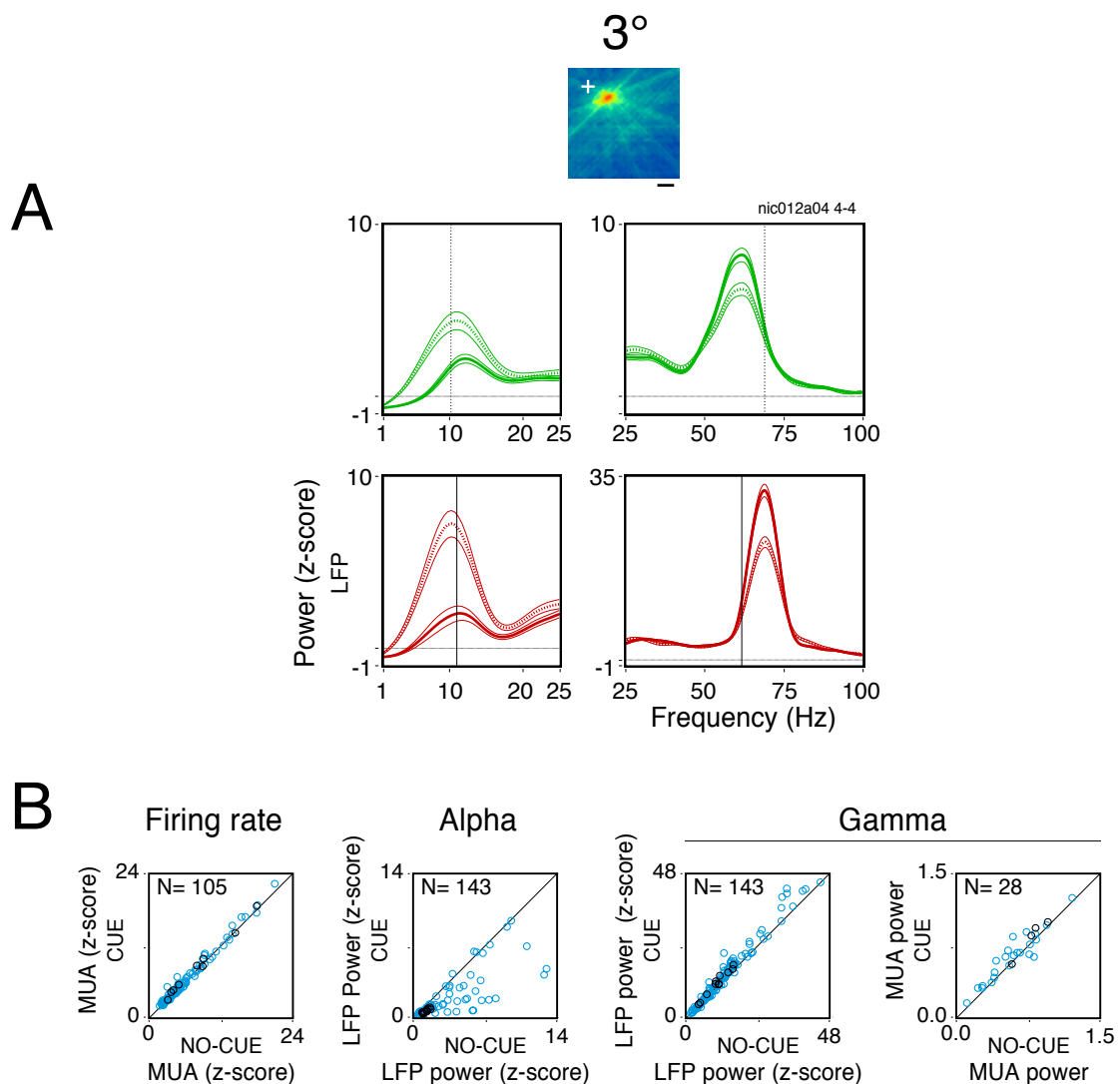


Figure 4.4: Spectral analysis for the cue protocol. (A) RF map of a site in the operculum of Monkey 1 is shown at the top. LFP power spectra for the lower (1-25 Hz) and higher (25-100 Hz) frequency bands are shown below. Dotted and continuous lines represent the no-cue and cue conditions, respectively. As described for the two anterior protocols, opposite effects were observed for the low and high frequency bands. (B) Population data for rates, LFP alpha power, LFP gamma power and MUA gamma power comparing no-cue with cue conditions. Data for 115 sites were acquired (11 sites recorded from the calcarine sulcus). Since some sites were tested for both the grating and plaid stimuli, a total of 144 protocols were analyzed. Blue and black circles represent, respectively, sites recorded from the central (opercular region) and peripheral (calcarine sulcus) representations of V1. Number of sites presented in each scatter plot is indicated at the top left hand corner. Only those sites showing a significant increase in activity during stimulation are plotted. Thin lines in (A) correspond to the SEM.

Population data are given in Figure 4.4B. An average 14% increase in LFP power was observed for cue as compared to no-cue conditions (paired t -test, $df = 142$, $p < 10^{-6}$), while LFP alpha power showed an average decrease of 48% ($df = 142$, $p < 10^{-6}$). MUA gamma power increased 2.3% for the same conditions ($df = 27$, $p < 10^{-2}$). Increase in firing rates was small but significant (6% increase, $df = 104$, $p < 10^{-6}$).

Correct responses for the cue-protocol were of 96% for Monkey 1 and of 92% for Monkey 2.

4.4.4 - NEURONAL COHERENCE

In our analysis so far, we have shown that modulation in gamma power is dependent on expectation level. Power estimates, however, do not provide direct information on time dependencies underlying neuronal interactions. To this end we used coherence measurements, since they express the phase-locking between oscillatory signals, and have been argued to be an important tool for assessing neuronal communication (Fries, 2005). In Figure 4.5 we present the effects of expectation on gamma coherence. In this example, increase in power was associated with a sizable increase in coherence both for LFP-MUA and MUA-MUA pairs (Fig. 4.5A). Data was obtained from two central sites in Monkey 2 during responses to gratings (electrode separation of ~3 mm). Notice that the changes in coherence amplitude are not accompanied by substantial shifts in frequency.

Grand-average results for all protocols are given in Figure 4.5B. Only data exhibiting significant coherence relative to baseline at the gamma-band are shown (jackknife procedure of Arvesen, $p < 0.05$). Observe that the average effects on neuronal coherence, even though highly significant, were comparable to the modulations in power (for LFP-LFP, coherence increase of 6%, paired t -test, $df = 636$, $p < 10^{-6}$; for MUA-LFP, increase of 12%, $df = 789$, $p < 10^{-6}$; for MUA-MUA, increase of 15%, $df = 107$, $p < 10^{-5}$). It is important to emphasize that coherence decreased with separation distances in the cortex. Only a few central-peripheral pairs (red circles in Fig. 4.5B) showed significant coherence during visual stimulation. In these cases, where cortical distances were large, coherence values were lower as compared to those obtained for central-central and peripheral-peripheral pairs. These results are in accord with our previous study (Lima *et al.*, 2010).

Temporal expectation effects on gamma power and coherence depended on visual input. In an additional experiment, we ran the same cue protocol as described above, but with no visual stimulus (Supplementary material and Supplementary Figure 4.3). In this case, the only effect we observed when comparing epochs of low and high expectation was a decrease in alpha power. There was no modulation in gamma power in absence of visual activation of the recorded neurons.

4.4.5 - IMPACT ON ORIENTATION SELECTIVITY

In our study we have mainly used stimuli that best matched the orientation preferences of the neurons. Consequently, our analysis focused on optimal responses when cells are driven maximally. The question remains how strong the expectation effects on gamma are when neuronal responses deviate from maximum. We addressed this question by comparing orientation and direction tuning plots for conditions of both high and low expectation (see details in Experimental Procedures). Examples of tuning curves for firing rates, LFP gamma power and LFP-MUA gamma

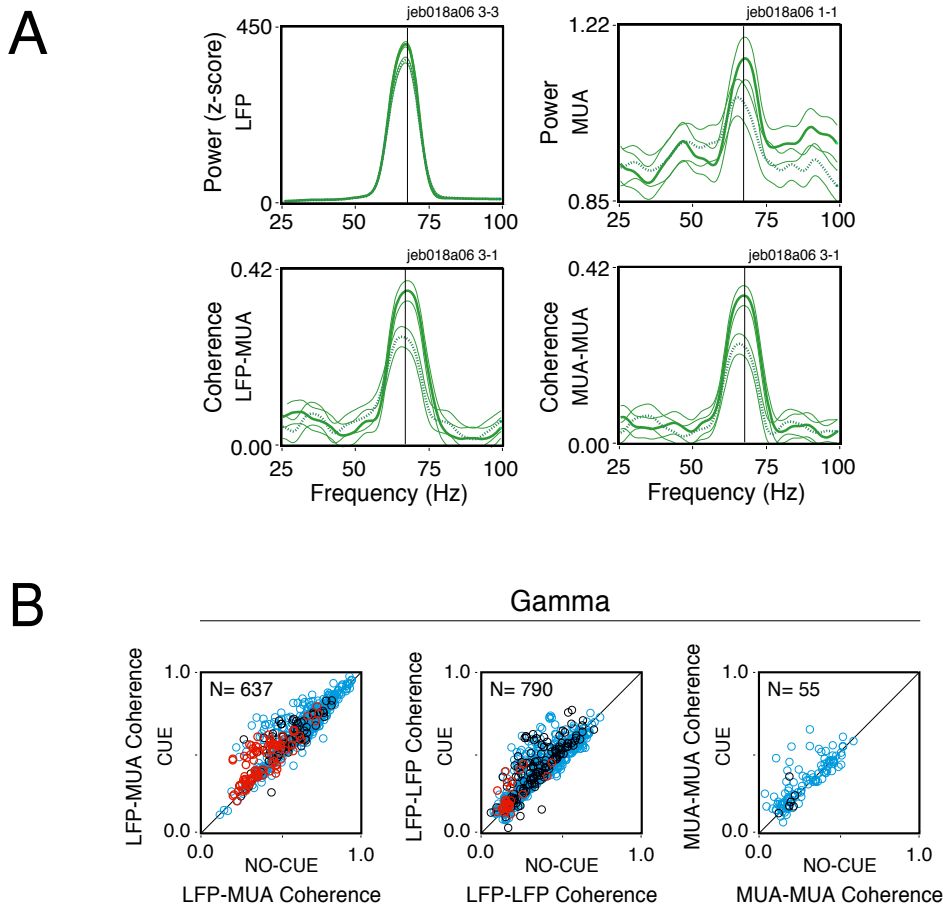


Figure 4.5: Coherence analysis of the gamma activity. (A) LFP-MUA and MUA-MUA coherence for a pair of sites recorded from the operculum of Monkey 2 during a cue-protocol. LFP and MUA gamma spectra for the corresponding sites are shown at the top. Dotted and continuous lines represent the no-cue and cue conditions, respectively. LFP-MUA coherence exhibited an average increase of 47% (two sample t -test, $df = 271$, $p < 10^{-3}$), while MUA-MUA coherence increased 53% ($p < 10^{-3}$), for the cue as compared to the no-cue condition. Only those frequency bins showing a significant increase in coherence during stimulation (jackknife procedure of Arvesen, $p < 0.05$) were selected for analysis: 61 - 74 Hz for the LFP-MUA coherence and 61 - 73 Hz for the MUA-MUA coherence. (B) Population data for the sequence-, block- and cue protocols. LFP-LFP, MUA-LFP and MUA-MUA coherence comparing no-expected versus expected conditions. Blue circles represent pairs recorded exclusively from the operculum, black circles represent pairs recorded exclusively from the calcarine sulcus, and red circles represent pairs that had one site located in the operculum and the other in the calcarine sulcus. Only those sites showing a significant increase in coherence during stimulation are plotted. Thin lines in (A) correspond to the SEM.

coherence are shown in Figure 4.6A. Data were obtained for responses to gratings from the same recording site (peripheral V1, Monkey 1). Interestingly, when LFP gamma power was taken as variable, we could observe a strong effect of expectation on orientation selectivity (increase of orientation index from 0.63 to 0.78). The expectation effects on selectivity were not multiplicative, as in increase in gamma occurred mainly around the preferred orientation, with an important impact on the orientation selectivity index. This effect did not show up for the rates and it was less pronounced for the coherence. Population data confirmed these results (Fig. 4.6B). An average

increase of 17% in selectivity was observed for the LFP gamma (paired t -test, $df = 36$, $p < 10^{-6}$). The LFP-MUA coherence showed a smaller but significant 10% increase in selectivity ($df = 86$, $p < 10^{-3}$). Note that changes in selectivity were comparable for central and peripheral sites (blue and black dots, respectively).

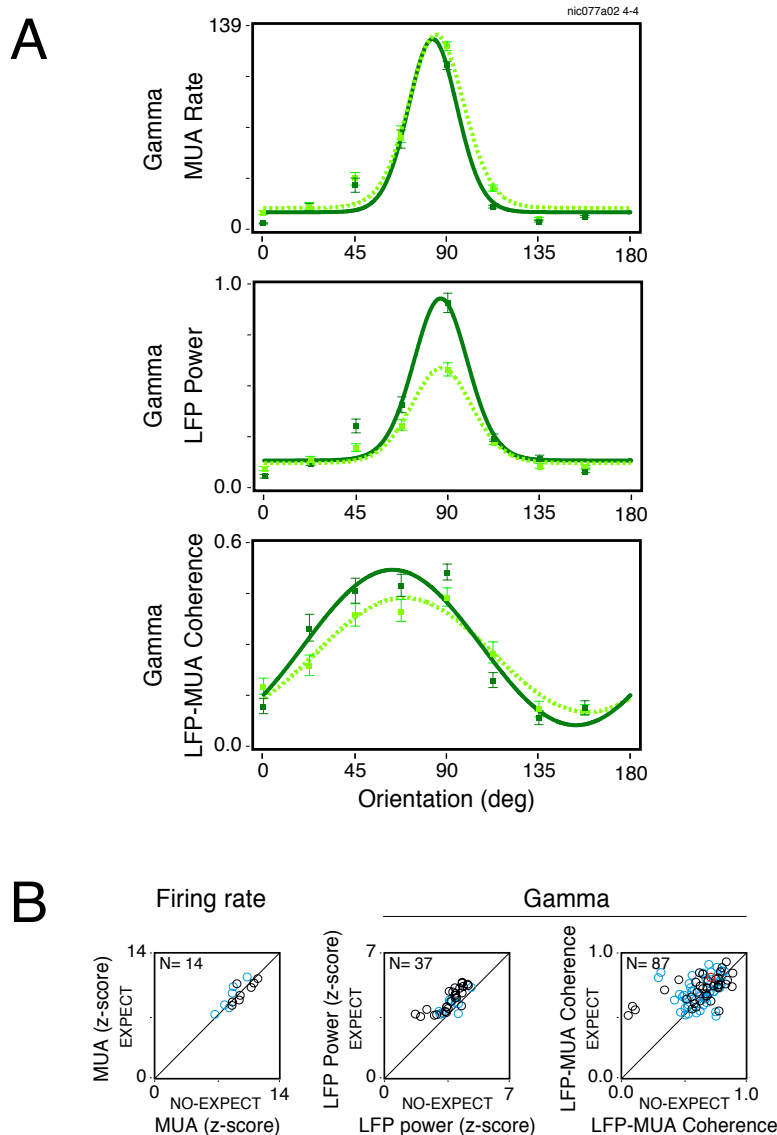


Figure 4.6: Changes in selectivity with temporal expectation. (A) The firing rate, LFP gamma power and LFP-MUA gamma coherence for a site in calcarine sulcus of Monkey 1 during a grating-plaid-grating sequence protocol. Neuronal activity for the various stimulus configurations could be fitted with a single von Mises function in all three analysis, and therefore classified as orientation selective ($R^2 > 0.9$ for all cases). Dotted and continuous lines indicate activity for the early (low expectation) and late (high expectation) analysis windows, respectively. The firing rate responses (A) for the 8 orientations tested were very similar during both periods (orientation index of ~ 0.9 computed from the fitted von Mises function). For the LFP power, however, enhancement in gamma activity during the high expectation period took place predominantly for the preferred orientation ($\sim 90^\circ$). Enhanced gamma phase-locking also occurred mainly for the preferred orientation ($\sim 70^\circ$). The orientation index increased from 0.60 for the early window to 0.77 for the late window. (B) Population data comparing the selectivity indexes during periods of low and high expectation. Analysis for the firing rate, LFP gamma power and LFP-MUA gamma coherence are shown. Only cases where activity significantly increased with expectation are plotted (t -test for the comparison between low and high expectation periods). Blue and black circles represent sites or pairs of sites recorded from the operculum and calcarine sulcus, respectively. Red circles represent pairs where one electrode was placed in the operculum and the other in the calcarine sulcus. Error bars in (A) correspond to the SEM.

4.4.6 - REWARD EFFECTS

In order to examine how motivational context could influence expectation, we manipulated reward value without changing task timing. High and low reward regimes were set by delivering banana juice (high value) instead of water (low value), or by changing the amount of fluid. A block-design was used, with alternating blocks (50 trials) of high and low reward values. Only Monkey 1 was tested in this paradigm (correct responses, 97%). Reaction times were on average 5.5 ms shorter for blocks of high as compared to low reward value (paired t -test, $df = 12$, $p = 0.04$), indicating that our reward schedule was effective in building motivation. Figure 4.7A shows the effects of reward manipulation in alpha and gamma power of LFP.

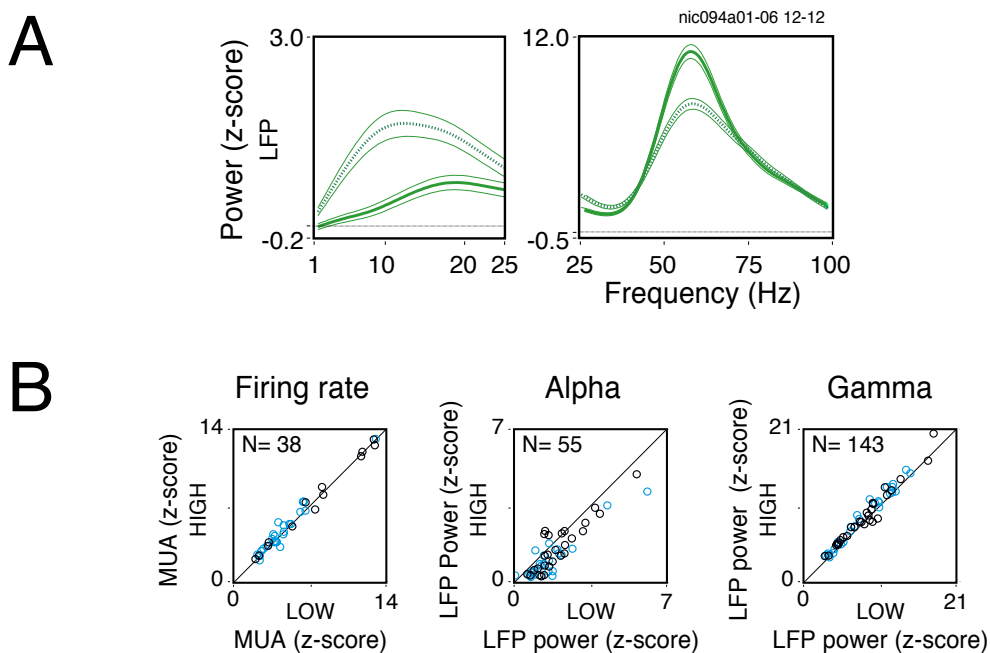


Figure 4.7: Effect of reward value expectation. (A) LFP power recorded from a site in the operculum. Low (1 - 25 Hz) and high (25 - 100 Hz) frequency band spectra responded in opposite ways to the expectation of reward value. Dotted and continuous lines represent conditions where low and high reward value were expected, respectively. Alpha activity decreased on average 86% (two sample t -test, $df = 440$, $p < 10^{-6}$), while gamma activity was enhanced by 17% (two sample t -test, $df = 440$, $p < 10^{-4}$). (B) Population data for rates, LFP alpha power and LFP gamma power comparing low-value and high-value conditions. Blue and black circles represent sites recorded from the central (opercular region) and peripheral (calcarine sulcus) representations of V1, respectively. Number of data points presented in each scatter plot is indicated at the top left hand corner. For some sessions, a second grating stimulus was ran for the same set of recording sites. This gave rise to a total of 55 data points used in the population analysis. Only those sites showing a significant increase in activity during stimulation are plotted. Thin lines in (B) correspond to the SEM.

Responses were obtained to a grating stimulus from a central recording site. In accordance with the results described above, there were clear signs of alpha suppression and of gamma power enhancement. Data from a total of 45 recording sites are shown in Figure 4.7B. There was an average 27% decrease in alpha (paired t -test, $df = 54$, $p < 10^{-6}$) and 7% increase in gamma power ($df = 54$, $p < 10^{-6}$). Firing rates, on the other hand, showed only a small but significant 3% increase

($df = 36$, $p = 0.04$). As before, modulation in power for central and peripheral sites were of comparable magnitude (blue and black circles, respectively).

4.5 - DISCUSSION

Our results provide first evidence that allocating attention in time modulates gamma power and coherence down to the earliest stage of cortical visual processing. These findings suggests that gamma interactions in V1 may contribute to a neuronal mechanism underlying temporal expectation, as it has been shown for spatial and feature attention (Müller *et al.*, 2000; Fries *et al.*, 2001; Bichot *et al.*, 2005; Taylor *et al.*, 2005; Buschman and Miller, 2007; Fries *et al.*, 2008). Overall these results support the notion that oscillatory processes are important for brain activity coordination. Since anticipatory effects on gamma activity exhibits fast dynamics, it may play an important role in perceptual organization.

It is known that in humans attention can modulate visually evoked potentials (reviewed in Eimer, 1998) and induced gamma activity (Gruber *et al.*, 1999; Tallon-Baudry, 2004; Jensen *et al.*, 2007; Wyart and Tallon-Baudry, 2008; Siegel *et al.*, 2008). The mechanistic relations between attention and gamma, however, have only recently been approached by invasive recordings in non-human primates. Fries *et al.* (2001), using a spatial attention paradigm in monkeys, have found strong gamma synchronization in area V4 depending on whether attention was directed to a stimulus inside or outside the RFs of the recorded neurons. In their study, estimates of phase-locking between spiking activity and the LFP (spike-triggered average) showed robust gamma oscillations, which were stronger for the attended condition (see LFP traces in their Fig. 1A and 1B). Posteriorly, Fries *et al.*, 2008 extended these findings providing evidence for spiking activity interactions (spike-spike coherence). The magnitude of the temporal expectation effects on gamma power and coherence we describe here for V1 are comparable to the spatial attention effects described for V4 (see Fig. 7 in Fries *et al.*, 2008). In addition, spatial attention was shown to suppress alpha activity. Our results are also consistent with these findings. Several other reports in monkeys and humans have shown that alpha suppression is involved in a variety of cognitive processes, including attention and memory (see review in Klimesch *et al.*, 2007), suggesting that alpha/gamma imbalance controls information flow in the brain. Contrary evidence, however, has been obtained in V1 for during a spatial attention task, where both alpha and gamma power were reduced for the attended location (Chalk *et al.*, 2010).

As shown in the sliding window analyses presented in Figures 4.1 and 4.3, gamma oscillation strength changes along the trial as a function of the conditional probability of occurrence of the

behaviorally relevant event (hazard rate). We obtained similar results in a paradigm where the monkeys were required to detect Gestalt figures embedded in two-dimensional arrays of Gabor elements (see section “Building expectations: New vistas for gamma oscillations” in the Appendix). In this task, as in our sequence-protocol, the monkeys could predict task timing based on stimulus events. In a time-frequency analysis of Fries *et al.* (2001) data, Liang *et al.* (2005) presented results compatible with our findings, suggesting that hazard rates may correlate with modulation of gamma power. From the plots of their Figure 6 it is clear that power gradually increases along the trial. In principle this effect could be attributed to temporal expectation, although their study was limited to only one time schedule. In our study we used different protocols to build probabilistic time schedules of FP change. While in the sequence and cue-protocols the monkeys could rely on external events to build an internal representation of task timing, in the block-protocol there was no explicit instruction or events available. On the contrary, in the block-protocol information about task timing could only be obtained across trials, after the monkey perceived consistency in the time schedule. All protocols led essentially to the same results, namely an increase in gamma associated with alpha suppression when the monkeys were attending to an event in time. Similar findings were obtained in the study of Schoffelen *et al.* (2005) for cortico-spinal synchronization in humans. In their study, two time schedules were used during a visual detection task requiring a motor response. Macropotential recordings from the motor cortex and from the forearm muscle showed a modulation in coherence for the gamma band which closely followed the hazard rate of stimulus change probability. These results suggest that gamma synchronization may boost neuronal communication during states demanding allocation of resources, as it occurred when subjects were particularly ready to respond. Since there was a strong correlation between reaction time and hazard rate (their Figures 2A and 3A), it is possible that neuronal coherence contributes to improvement in performance. Accordingly, Womelsdorf *et al.* (2006) have shown in V4 that reaction times are shorter for trials with high gamma responses to the spatially attended stimulus. We have also observed a significant shortening of reaction times for conditions of high expectation. Thus, it is likely that gamma synchronization down to V1 allows for efficient stimulus processing, speeding up behavioral responses. It would be interesting to observe whether responses in higher areas exhibit phase-locking to anticipatory gamma activity in V1.

Anticipating a relevant event may also affect the attentional modulation of firing rates. Ghose and Maunsell (2002) trained monkeys to detect a change in stimulus orientation at a cued location (spatial attention task) while using two different time schedules. Depending on the hazard rate of stimulus change the attentional effects on the neuronal responses varied significantly. The higher the perceived probability of stimulus change, the higher was the attentional modulation of the responses. This study was seminal in showing that anticipation can strongly modulate neuronal activity, in parallel to spatial attentional effects. Our study extends these findings by providing

evidence that anticipatory effects exhibit fast dynamics. In the study of Ghose and Maunsell (2002) the monkeys were trained extensively on the first time schedule, and only posteriorly on the second one. Because data was obtained separately for each schedule, one could not compare responses of the same cell for the two conditions. In our block-protocol, on the other hand, the two time schedules were alternated several times during the same recording, with blocks as short as 30 trials. Modulation effects were visible not only in gamma and alpha power, but also in firing rates (Fig. 4.2), indicating that the monkeys could rapidly engage in a new strategy. Our paradigm differed from Ghose and Maunsell (2002) since the task relevant event occurred at fixed points in time, instead of being drawn from probability distributions. This simplification, however, seems to have had little impact on the perceived hazard function, although here evidence is only indirect. As shown in Figure 4.3, modulation in gamma power was not confined to discrete points in time but instead followed a smooth curve as one would expect for a perceived hazard function.

In our results, the anticipatory effects in gamma power and coherence seemed to be dependent on visual input. When the cue-protocol was run without a visual stimulus (Suppl. Fig. 4.3), we detected no significant modulation of gamma activity or firing rates during conditions of high expectation, although an alpha suppression was still visible. Since the total gamma power without visual stimulation was very low, it remains an open question whether the absence of effects on gamma were due to detectability. Contrary to our results, a few studies in monkeys have shown anticipatory effects on neuronal synchronization during epochs without visual stimulation. During a motion discrimination task, de Oliveira *et al.* (1997) have shown an increase in neuronal synchronization in MT for the period before stimulus onset. The authors attribute this effect to expectation, although this interpretation is arguable since the pre-stimulus period was variable. An increase in synchronization was also observed in V1 during a figure-ground discrimination task for activity preceding stimulus onset (Supèr *et al.*, 2003). Besides differences in experimental paradigms, a reason for these discrepancies could be that we investigated synchronization by means of gamma power and coherence (both LFP and MUA), while in the other studies the cross-correlation of spiking activity was used. A recent hemodynamical study in V1 (Sirotin and Das, 2009) has shown anticipatory responses for non-stimulus-driven activity, while the monkeys were expecting a change in the FP. Interestingly, during these epochs, simultaneous recording of neuronal activity revealed no modulation of LFP gamma power or firing rates. Therefore, it is possible that predictive signals are available in V1 even for states of low gamma activity. Overall these studies point to the importance of temporal expectation effects as a potential confounding factor in behavioral studies.

Our results suggest that anticipatory effects on gamma and alpha activity are widespread in V1. In all our experiments the monkeys were trained to attend to a change at the FP, which corresponds

to the central representation of the visual field. If spatial attention were to explain our findings one would observe a consistently higher modulation for central as compared to peripheral sites. Since this was not the case in our results, temporal expectation effects presumably impact V1 as a whole. Figure 4.2 shows a representative example of recordings obtained simultaneously at central and peripheral sites for which the magnitude of the expectation effect was comparable across eccentricities. These findings were consistent for all protocols tested. Attentional modulation of firing rates is known to be weak in early visual areas, increasing in strength over hierarchical levels (Mehta *et al.*, 2000; Maunsell and Cook, 2002). Accordingly, subdural LFP recordings in humans have shown that the effects of spatial attention in V1 are rather small (Yoshor *et al.*, 2007). This could explain why in our results the spatial effects were negligible. Further experiments are needed in order to assess the relative contribution of both attention in space and in time.

It remains to be explained how temporal expectation may influence oscillatory activity over large extensions of cortex in a time scale of seconds or less. A possible explanation could be higher levels of arousal. In accord with this hypothesis, it has been shown that the high amplitude gamma oscillations associated with states of central activation are modulated by ascending cholinergic systems (Herculano-Houzel *et al.*, 1999). Acetylcholine facilitates gamma oscillations *in vitro* (Buhl *et al.*, 1998) and *in vivo* (Rodriguez *et al.*, 2004). Thus, one can hypothesize that the effects of anticipation arise from a non-specific and widespread cholinergic drive acting throughout the cortex. Basal forebrain projections are a possible candidate since they can activate the cortex in a diffuse and global manner (Sarter and Bruno, 2000). During spatial attention, on the other hand, the cholinergic modulation effects would be local. Intracortical injections of acetylcholine enhances attention modulation of the responses (Herrero *et al.*, 2008). Interestingly, in our results, the temporal expectation affected primarily the amplitude of the oscillations, leaving oscillation frequency unaffected. In a previous study we have shown that oscillation frequency was higher for responses to plaids than for gratings stimuli, and that it could be shifted by attending to features of the stimulus (Lima *et al.*, 2010). As shown in Figure 4.4, however, the anticipatory effects did not cause shifts in oscillation frequency. These findings indicate that temporal expectation acts as a gain mechanism predominantly at the main frequency induced by the stimulus. This is important because it shows that gamma modulation was independent of stimulus features or configuration. Moreover, the effects of temporal expectation on gamma power and coherence seemed to impact on orientation selectivity (Figure 4.6). It is known that gamma responses can be selective to stimulus features, such as direction of movement, velocity and contrast (Gray and Singer, 1989; Friedman-Hill *et al.*, 2000; Lima *et al.*, 2010), suggesting that gamma processes may contribute to feature encoding. It is possible that gamma enhancement boosts encoding, explaining why temporal expectation could benefit performance. Imaging experiments in humans have shown that temporal expectation is associated with activation of early visual areas (Coull and Nobre, 1998). Our

results allow us to speculate that these BOLD responses depended on a gamma/ alpha imbalance. Accordingly, Zumer *et al.* (2010) provided further evidence that gamma activity is positively correlated with BOLD while alpha activity is negatively correlated with BOLD.

Our experimental protocols do not allow us to exclude that anticipatory gamma in V1 is somehow related to the preparation of a motor response. An evidence indicating that gamma modulation is independent of motor preparation may be found in the experiments where reward value was manipulated. In this case, motor preparation was the same regardless of reward schedule. Here reward value affected primarily the motivation of the monkey. In cats, association of stimulus with a reward was shown to increase interareal gamma interactions (Salazar *et al.*, 2004). Overall, these results suggests that gamma activity are more related to context dependent coordination processes than the analysis of stimulus features per se.

4.6 - ACKNOWLEDGEMENTS

We thank Michaela Klinkmann and Johanna Klon-Lipok for technical assistance, and Dr. Christiane Kiefert, Yvonne Wenzel and Clemens Sommers for animal care.

This work has been supported by the Max-Planck Society. Bruss Lima was supported during his doctoral studies by the Graduiertenkolleg, J. W. Goethe University - Frankfurt, the Max-Planck Society and the Frankfurt Institute for Advanced Studies (FIAS)

4.7 - REFERENCES

- Anderson B, Sheinberg DL. 2008. Effects of temporal context and temporal expectancy on neural activity in inferior temporal cortex. *Neuropsychologia*. **46**:, 947-957.
- Balz GW, Hock HS. 1997. The effect of attentional spread on spatial resolution. *Vision Res*. **37**: 1499-1510.
- Bichot NP, Rossi AF, Desimone R. 2005. Parallel and serial neural mechanisms for visual search in macaque area V4. *Science*. **308**: 529-534.
- Börgers C, Epstein S, Kopell NJ. 2008. Gamma oscillations mediate stimulus competition and attentional selection in a cortical network model. *Proc. Natl. Acad. Sci. U.S.A.* **105**: 18023-18028.
- Bosman CA, Womelsdorf T, Desimone R, Fries P. 2009. A microsaccadic rhythm modulates gamma-band synchronization and behavior. *J. Neurosci*. **29**: 9471-9480.

- Buhl EH, Tamás G, Fisahn A. 1998. Cholinergic activation and tonic excitation induce persistent gamma oscillations in mouse somatosensory cortex in vitro. *J. Physiol. (London)* **513**: 117-126.
- Buschman TJ, Miller EK. 2007. Top-down versus bottom-up control of attention in the prefrontal and posterior parietal cortices. *Science*. **315**: 1860-1862.
- Cameron EL, Tai JC, Carrasco M. 2002. Covert attention affects the psychometric function of contrast sensitivity. *Vision Res.* **42**: 949-967.
- Carrasco M, Ling S, Read S. 2004. Attention alters appearance. *Nat. Neurosci.* **7**: 308-313.
- Carrasco M, Penpeci-Talgar C, Eckstein M. 2000. Spatial covert attention increases contrast sensitivity across the CSF: support for signal enhancement. *Vision Res.* **40**: 1203-1215.
- Carrasco M, Yeshurun Y. 2009. Covert attention effects on spatial resolution. *Prog. Brain Res.* **176**: 65-86.
- Chalk M, Herrero JL, Gieselmann MA, Delicato LS, Gotthardt S, Thiele A. 2010. Attention Reduces Stimulus-Driven Gamma Frequency Oscillations and Spike Field Coherence in V1. *Neuron*. **66**: 114-125.
- Connor CE, Preddie DC, Gallant JL, Van Essen, DC. 1997. Spatial attention effects in macaque area V4. *J. Neurosci.* **17**: 3201-3214.
- Correa A, Lupiáñez J, Milliken B, Tudela P. 2004. Endogenous temporal orienting of attention in detection and discrimination tasks. *Percept. Psychophys.* **66**: 264-278.
- Coull JT. 2009. Neural substrates of mounting temporal expectation. *PLoS Biol.* **7**: e1000166.
- Coull JT, Nobre AC. 1998. Where and when to pay attention: the neural systems for directing attention to spatial locations and to time intervals as revealed by both PET and fMRI. *J. Neurosci.* **18**: 7426-7435.
- de Oliveira SC, Thiele A, Hoffmann KP. 1997. Synchronization of neuronal activity during stimulus expectation in a direction discrimination task. *J. Neurosci.* **17**: 9248-9260.
- Doesburg SM, Roggeveen AB, Kitajo K, Ward LM. 2007. Large-Scale Gamma-Band Phase Synchronization and Selective Attention. *Cereb. Cortex.* **18**: 386-396.
- Doherty JR, Rao A, Mesulam MM, Nobre AC. 2005. Synergistic effect of combined temporal and spatial expectations on visual attention. *J. Neurosci.* **25**: 8259-8266.
- Efron B, Tibshirani R. 1993. An Introduction to the Bootstrap. New York: Chapman and Hall.
- Eimer M. 1998. Mechanisms of visuospatial attention: Evidence from event-related brain potentials. *Vis. Cogn.* **5**: 257-286.
- Esterman M, Yantis S. 2009. Perceptual Expectation Evokes Category-Selective Cortical Activity. *Cereb. Cortex.* **20**: 1245-1253.
- Fell J, Klaver P, Elger CE, Fernández G. 2002. Suppression of EEG gamma activity may cause the attentional blink. *Conscious. Cogn.* **11**: 114-122.
- Friedman-Hill S, Maldonado PE, Gray CM. 2000. Dynamics of striate cortical activity in the alert macaque: I. Incidence and stimulus-dependence of gamma-band neuronal oscillations. *Cereb. Cortex.* **10**: 1105-1116.

- Fries P. 2005. A mechanism for cognitive dynamics: neuronal communication through neuronal coherence. *Trends Cogn. Sci.* **9**: 474-480.
- Fries P. 2009. Neuronal Gamma-band synchronization as a fundamental process in cortical computation. *Annu. Rev. Neurosci.* **32**: 209-224.
- Fries P, Reynolds JH, Rorie AE, Desimone R. 2001. Modulation of oscillatory neuronal synchronization by selective visual attention. *Science.* **291**: 1560-1563.
- Fries P, Womelsdorf T, Oostenveld R, Desimone R. 2008. The effects of visual stimulation and selective visual attention on rhythmic neuronal synchronization in macaque area V4. *J. Neurosci.* **28**: 4823-4835.
- Garcia-Garcia M, Yordanova J, Kolev V, Domínguez-Borràs J, Escera C. 2010. Tuning the brain for novelty detection under emotional threat: the role of increasing gamma phase-synchronization. *Neuroimage.* **49**: 1038-1044.
- Ghose GM, Maunsell JHR. 2002. Attentional modulation in visual cortex depends on task timing. *Nature.* **419**: 616-620.
- Gray CM, Singer W. 1989. Stimulus-specific neuronal oscillations in orientation columns of cat visual cortex. *Proc. Natl. Acad. Sci. U.S.A.* **86**: 1698-1702.
- Gruber T, Müller MM, Keil A, Elbert T. 1999. Selective visual-spatial attention alters induced gamma band responses in the human EEG. *Clin. Neurophysiol.* **110**: 2074-2085.
- Hawkins HL, Hillyard SA, Luck SJ, Mouloua M, Downing CJ., Woodward DP. 1990. Visual attention modulates signal detectability. *J. Exp. Psychol. Human Percept. Perform.* **16**: 802-811.
- Herculano-Houzel S, Munk MH, Neuenschwander S, Singer W. 1999. Precisely synchronized oscillatory firing patterns require electroencephalographic activation. *J. Neurosci.* **19**: 3992-4010.
- Herrero JL, Roberts MJ, Delicato LS, Gieselmann MA, Dayan P, Thiele A. 2008. Acetylcholine contributes through muscarinic receptors to attentional modulation in V1. *Nature.* **454**: 1110-1114.
- Ito M, Gilbert CD. 1999. Attention modulates contextual influences in the primary visual cortex of alert monkeys. *Neuron.* **22**: 593-604.
- Jensen O, Kaiser J, Lachaux J-P. 2007. Human gamma-frequency oscillations associated with attention and memory. *Trends Neurosci.* **30**: 317-324.
- Kilner JM, Baker SN, Salenius S, Hari R, Lemon RN. 2000. Human cortical muscle coherence is directly related to specific motor parameters. *J. Neurosci.* **20**: 8838-8845.
- Klimesch W, Sauseng P, Hanslmayr S. 2007. EEG alpha oscillations: the inhibition-timing hypothesis. *Brain Res. Rev.* **53**: 63-88.
- König P. 1994. A method for the quantification of synchrony and oscillatory properties of neuronal activity. *J. Neurosci. Methods* **54**: 31-37.
- Liang H, Bressler SL, Buffalo EA, Desimone R., Fries, P. 2005. Empirical mode decomposition of field potentials from macaque V4 in visual spatial attention. *Biol. Cybern.* **92**: 380-392.

- Lima B, Singer W, Chen N-H, Neuenschwander S. 2010. Synchronization Dynamics in Response to Plaid Stimuli in Monkey V1. *Cereb. Cortex.* **20**: 1556-1573.
- Luck SJ, Chelazzi L, Hillyard SA, Desimone R. 1997. Neural mechanisms of spatial selective attention in areas V1, V2, and V4 of macaque visual cortex. *J. Neurophysiol.* **77**: 24-42.
- Martínez-Trujillo J, Treue S. 2002. Attentional modulation strength in cortical area MT depends on stimulus contrast. *Neuron.* **35**: 365-370.
- Matsuda K, Nagami T, Kawano K, Yamane S. 2000. A new system for measuring eye position on a personal computer. Program No. 744.2 in Abstract Viewer/Itinerary Planner. Society for Neuroscience, New Orleans (LA).
- Maunsell JHR, Cook EP. 2002. The role of attention in visual processing. *Philos. Trans. R. Soc. London Ser. B.* **357**: 1063-1072.
- McAdams CJ, Maunsell JH. 1999. Effects of attention on orientation-tuning functions of single neurons in macaque cortical area V4. *J. Neurosci.* **19**: 431-441.
- Mehta AD, Ulbert I, Schroeder CE. 2000. Intermodal selective attention in monkeys. I: distribution and timing of effects across visual areas. *Cereb. Cortex.* **10**: 343-358.
- Mitra P, Bokil H. 2007. Observed Brain Dynamics. Oxford University Press.
- Moran J, Desimone R. 1985. Selective attention gates visual processing in the extrastriate cortex. *Science.* **229**: 782-784.
- Motter BC. 1993. Focal attention produces spatially selective processing in visual cortical areas V1, V2, and V4 in the presence of competing stimuli. *J. Neurophysiol.* **70**: 909-919.
- Müller HJ, Humphreys GW. 1991. Luminance-increment detection: capacity-limited or not? *J. Exp. Psychol. Human Percept. Perform.* **17**: 107-124.
- Müller MM, Gruber T, Keil A. 2000. Modulation of induced gamma band activity in the human EEG by attention and visual information processing. *Int. J. Psychophysiol.* **38**: 283-299.
- Nobre A, Correa A, Coull J. 2007. The hazards of time. *Curr. Opin. Neurobiol.* **17**: 465-470.
- Nobre AC. 2001. Orienting attention to instants in time. *Neuropsychologia.* **39**: 1317-1328.
- Posner MI, Snyder CR, Davidson BJ. 1980. Attention and the detection of signals. *J. Exp. Psychol. Gen.* **109**: 160-174.
- Reynolds JH, Chelazzi L. 2004. Attentional modulation of visual processing. *Annu. Rev. Neurosci.* **27**: 611-647.
- Reynolds JH, Desimone R. 2003. Interacting roles of attention and visual salience in V4. *Neuron.* **37**: 853-863.
- Reynolds JH, Heeger DJ. 2009. The normalization model of attention. *Neuron.* **61**: 168-185.

- Reynolds JH, Pasternak T, Desimone R. 2000. Attention increases sensitivity of V4 neurons. *Neuron*. **26**: 703-714.
- Rodriguez R, Kallenbach U, Singer W, Munk MHJ. 2004. Short- and long-term effects of cholinergic modulation on gamma oscillations and response synchronization in the visual cortex. *J. Neurosci*. **24**: 10369-10378.
- Roelfsema PR, Tolboom M, Khayat PS. 2007. Different Processing Phases for Features, Figures, and Selective Attention in the Primary Visual Cortex. *Neuron*. **56**: 785-792.
- Roelfsema PR, Lamme VA, Spekreijse H. 1998. Object-based attention in the primary visual cortex of the macaque monkey. *Nature*. **395**: 376-381.
- Rotermund D, Taylor K, Ernst UA, Kreiter AK, Pawelzik KR. 2009. Attention improves object representation in visual cortical field potentials. *J. Neurosci*. **29**: 10120-10130.
- Salazar RF, König P, Kayser C. 2004. Directed interactions between visual areas and their role in processing image structure and expectancy. *Eur. J. Neurosci*. **20**: 1391-1401.
- Sarter M, Bruno JP. 2000. Cortical cholinergic inputs mediating arousal, attentional processing and dreaming: differential afferent regulation of the basal forebrain by telencephalic and brainstem afferents. *Neuroscience*. **95**: 933-952.
- Schneider KA, Komlos M. 2008. Attention biases decisions but does not alter appearance. *J. Vis*. **8**: 1-10.
- Schoffelen J-M, Oostenveld R, Fries P. 2005. Neuronal coherence as a mechanism of effective corticospinal interaction. *Science*. **308**: 111-113.
- Siegel M, Donner TH, Oostenveld R, Fries P, Engel AK. 2008. Neuronal synchronization along the dorsal visual pathway reflects the focus of spatial attention. *Neuron*. **60**: 709-719.
- Sirotin YB, Das A. 2009. Anticipatory haemodynamic signals in sensory cortex not predicted by local neuronal activity. *Nature*. **457**: 475-479.
- Supèr H, van der Togt C, Spekreijse H, Lamme VAF. 2003. Internal state of monkey primary visual cortex (V1) predicts figure-ground perception. *J. Neurosci*. **23**: 3407-3414.
- Swindale NV, Grinvald A, Shmuel A. 2003. The spatial pattern of response magnitude and selectivity for orientation and direction in cat visual cortex. *Cereb. Cortex* **13**: 225-238.
- Tallon-Baudry C. 2004. Attention and awareness in synchrony. *Trends Cogn. Sci*. **8**: 523-525.
- Taylor K, Mandon S, Freiwald WA, Kreiter AK. 2005. Coherent oscillatory activity in monkey area V4 predicts successful allocation of attention. *Cereb. Cortex* **15**: 1424-1437.
- Thiele A, Pooresmaeili A, Delicato L, Herrero J, Roelfsema P. 2009. Additive Effects of Attention and Stimulus Contrast in Primary Visual Cortex. *Cereb. Cortex*. **19**: 2970-2981.
- Thomson D. 1982. Spectrum estimation and harmonic analysis. *Proc. IEEE*. **70**: 1055-1096.
- Tiesinga PH, Fellous J-M, Salinas E, José JV, Sejnowski TJ. 2004. Inhibitory synchrony as a mechanism for attentional gain modulation. *J. Phys. (Paris)* **98**: 296-314.

- Treue S, Martínez-Trujillo JC. 1999. Feature-based attention influences motion processing gain in macaque visual cortex. *Nature*. **399**: 575-579.
- Uhlhaas PJ, Pipa G, Lima B, Melloni L, Neuenschwander S, Nikolic D, Singer W. 2009. Neural synchrony in cortical networks: history, concept and current status. *Front. Integr. Neurosci*. **3**: 1-19.
- Westheimer G, Ley E. 1996. Temporal uncertainty effects on orientation discrimination and stereoscopic thresholds. *J. Opt. Soc. Am. A*. **13**: 884-886.
- Williford T, Maunsell JHR. 2006. Effects of spatial attention on contrast response functions in macaque area V4. *J. Neurophysiol*. **96**: 40-54.
- Womelsdorf T, Fries P, Mitra PP, Desimone R. 2006. Gamma-band synchronization in visual cortex predicts speed of change detection. *Nature*. **439**: 733-736.
- Womelsdorf T, Schoffelen J-M., Oostenveld R., Singer W, Desimone R, Engel AK, Fries P. 2007. Modulation of neuronal interactions through neuronal synchronization. *Science*. **316**: 1609-1612.
- Wyart V, Tallon-Baudry C. 2008. Neural dissociation between visual awareness and spatial attention. *J. Neurosci*. **28**: 2667-2679.
- Yeshurun Y, Carrasco M. 1998. Attention improves or impairs visual performance by enhancing spatial resolution. *Nature*. **396**: 72-75.
- Yoshor D, Ghose GM, Bosking WH, Sun P, Maunsell JHR. 2007. Spatial attention does not strongly modulate neuronal responses in early human visual cortex. *J. Neurosci*. **27**: 13205-13209.
- Zumer JM, Brookes MJ, Stevenson CM, Francis ST, Morris PG. 2010. Relating BOLD fMRI and neural oscillations through convolution and optimal linear weighting. *Neuroimage*. **49**: 1479-1489.

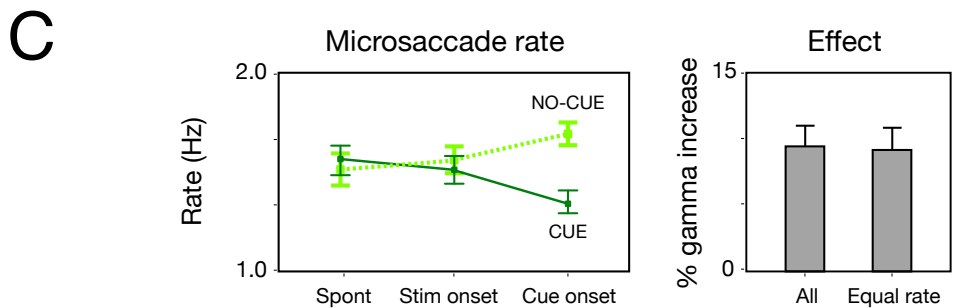
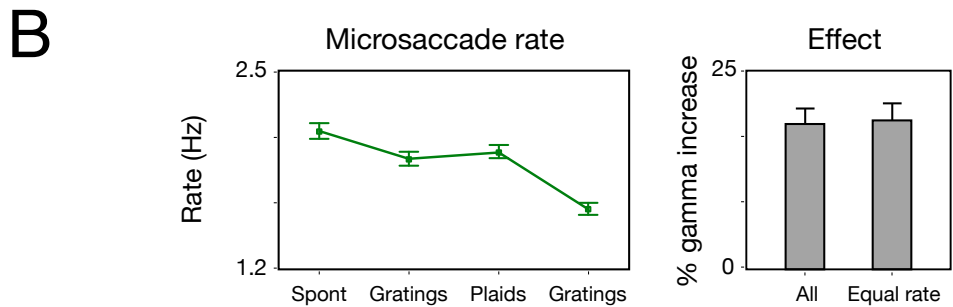
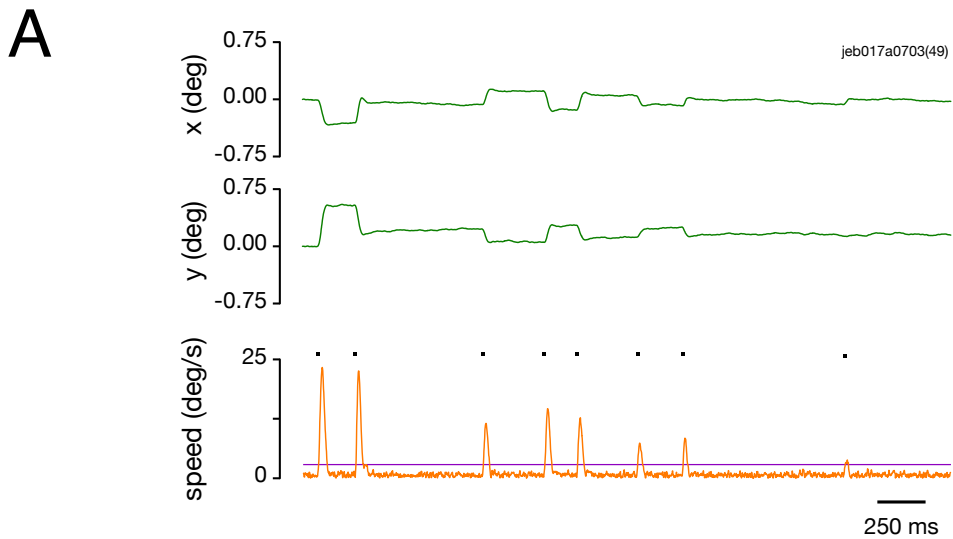
4.8 - SUPPLEMENTARY MATERIAL

A concern in our results was that the observed modulation of gamma responses could be actually explained by different patterns of microsaccades across the conditions being compared. Analysis is provided here to rule out this confounding effect. In addition, we provide results for effects of temporal expectation during the absence of visual stimulation and effects of cueing the value of the reward.

4.8.1 - CONTROL FOR MICROSACCADES

Recently Bosman *et al.* (2009) have shown that during fixation microsaccadic eye movements are capable of modulating ongoing gamma oscillations in the visual cortex. We were therefore concerned that the modulation effects described here could simply result from different microsaccade patterns for the epochs of high and low expectation.

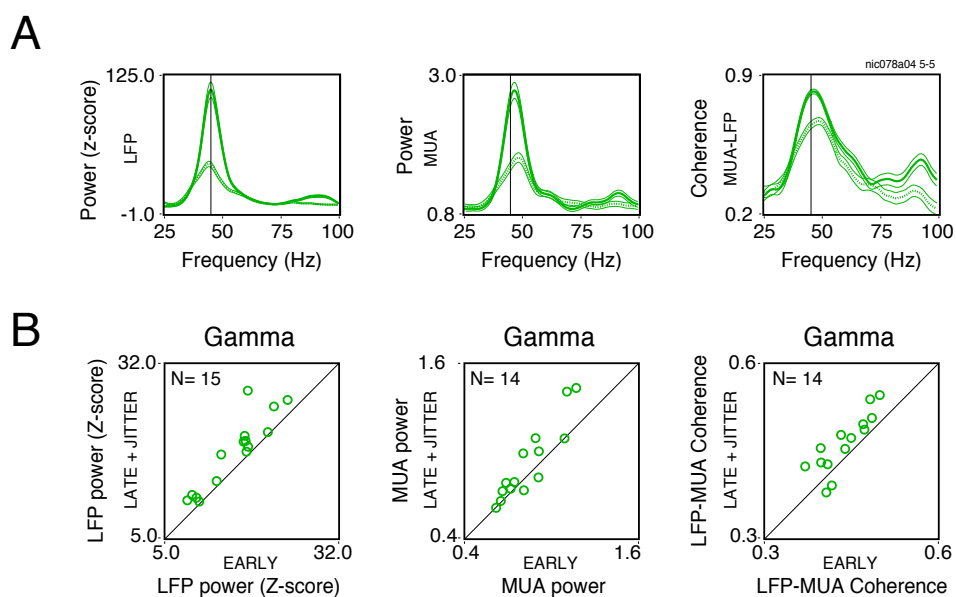
In our study, eye position was usually monitored with an infrared eye tracker system (Matsuda *et al.*, 2000). For a few control sessions, however, eye position was acquired at higher temporal and spatial resolution by using a search coil system (DNI, Crist Instruments). To detect microsaccadic events, the horizontal and vertical eye position signals were first low-pass filtered (<15 Hz) to remove high frequency noise. In order to obtain the speed of eye movement, the filtered signals were differentiated in time and then combined to give overall eye velocity. If eye velocity exceeded 4 standard deviations of the baseline signal mean, but the eye position still remained within 1° of the fixation point, it was considered a microsaccadic event. Supplementary Figure 4.1A shows the eye movement trace acquired using the search coil system. Supplementary Figure 4.1B compares the frequency of microsaccadic eye movements during the different periods of the grating-plaid-grating sequence protocol. There was a significant decrease in the frequency of microsaccades for the late window as compared to all preceding trial intervals (paired *t*-test, $df = 527$, $p < 10^{-6}$). We assumed this was due to the attentional state during the late window, when the monkey anticipated an upcoming FP color change. The next question we asked was if the change in microsaccadic pattern could explain the modulation in LFP gamma power. To address this point we selected trials having the same number of microsaccadic events for the early and late windows (195 out of 528 trials). We then computed the expectation effect (increase in gamma power for the late as compared to the early window), both for the original set of trials as well as for the subset where the number of microsaccadic events during early and late windows were matched. Power increased approximately 18% for both groups, indicating that microsaccadic eye movements could not explain the expectation effects we have described. The same procedure was applied to the cue protocols (Supplementary Figure 4.1C). A significant difference in the frequency of



Supplementary Figure 4.1: Microsaccadic pattern and gamma power. (A) Horizontal and vertical components of a single-trial eye movement trace. Data acquired from Monkey 2 while performing a grating-plaid-grating sequence protocol. Eye movement velocity is plotted on the graph below. The horizontal line represents the detection threshold for microsaccadic events (dots). (B) Frequency of microsaccadic events for grating-plaid-grating sequence protocols (data from 528 trials performed over 3 experimental sessions). The bar plot on the right compares the expectation effect for all trials ($N = 528$) with the expectation effect for a subset of trials ($N = 195$) having the same number of microsaccadic events during the early and late windows. No significant difference in the expectation effect, as measured by the LFP gamma power, was observed between them (paired t -test, $df = 44$, $p = 0.62$). (C) The same analysis as in (B) but applied to the cue-protocol (data from 542 trials performed over 2 experimental sessions). The continuous and dotted curves represent the cue and no-cue conditions, respectively. Before cue onset (spontaneous and stimulus-onset periods), the frequency of microsaccadic events was statistically the same during the no-cue and cue conditions (two sample t -test, $df = 25$, $p > 0.6$). A significant divergence occurred, however, during the cue-onset period (two sample t -test, $df = 527$, $p < 10^{-4}$). The frequency of microsaccades increased for the no-cue condition and decreased for the cue condition. As in (A), the bar plot on the right compares the expectation effect for all trials with the expectation effect for a subset of trials where the number of microsaccades were matched during both conditions. No significant difference was found between the them (two sample t -test, $df = 9$, $p = 0.2$).

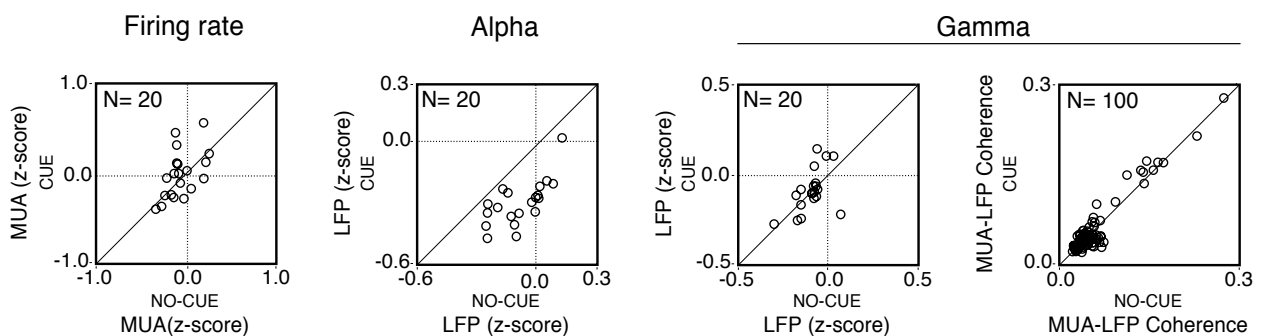
microsaccadic events was observed for the initial part of the trial depending if the cue was displayed or not. The incidence of microsaccades decreased for the cue condition and increased for the no-cue condition, analogous to the pattern described for the sequence-protocol where fixation was more stable during periods of higher expectation. To account for the effect of microsaccades on LFP power, we again selected a subset of trials where the number of microsaccadic events was the same for the no-cue and cue conditions. No significant change in the expectation effect was observed between the original 542 trials and the 446 subset matched for the number of microsaccadic events.

We indeed found significant task-dependent differences in the pattern of microsaccades. The frequency of microsaccadic events was consistently lower for periods before a FP color change event, where we assumed the monkeys had higher levels of expectation. However, after accounting for the frequency of microsaccadic events, it became clear that the expectation effect could not be explained by eye movements alone.



Supplementary Figure 4.2: The impact of stimulus spatial jitter on gamma activity. The last stimulus in the grating-plaid-grating sequence protocol had its position jittered on the computer screen. (A) The LFP power, MUA power and LFP-MUA coherence for a single site recorded from Monkey 1. Dotted and continuous lines represent the activity for the early (no jitter) and late (jitter) gratings in the sequence. An enhancement in gamma power and coherence was still observed despite the jitter. There was an average increase of 63% for the LFP gamma power, of 34% for the MUA gamma power, and of 17% for the LFP-MUA coherence (paired *t*-test, *df* = 104, *p* < 10⁻⁶ for all three analysis). Only those frequency bins showing significant increase in activity during stimulation were selected for analysis: 30 - 90 Hz for the LFP power, 38 - 57 Hz for the MUA power, and 30 - 90 Hz for the LFP-MUA coherence. (B) Population data for LFP gamma power, MUA gamma power and LFP-MUA gamma coherence comparing the activity for the early (no jitter) and the late (jitter) stimuli. For the coherence analysis, only LFP and MUA signals acquired from the same electrode are plotted. Number of sites presented in each scatter plot is indicated at the top left hand corner. Only those sites showing a significant increase in activity during stimulation are plotted. Thin lines in (A) correspond to the SEM. Data acquired from Monkey 1.

Corroborating this finding, Supplementary Figure 4.2 illustrates an experiment where we used a modified version of the grating-plaid-grating sequence protocol. In this experiment, the decreased frequency of microsaccades for the late window was compensated by spatially jittering the position of the grating stimulus on the computer screen. Therefore, while the first grating of the sequence had no jitter, the last grating was jittered at a frequency of approximately 3 Hz with random displacements of up to 0.56° (average displacement of 0.28°). Despite the jitter added to the last grating stimulus, the gamma activity induced for the late window was still significantly higher than the one induced for the early window. This result was also evident in the population data. A total of 15 sites were tested with the jitter protocol. For each experimental session (N = 3), a single moving grating was chosen and positioned so as to jointly stimulate all recorded receptive fields. There was an enhancement in both LFP gamma power (18%, paired *t*-test, *df* = 14, *p* < 10⁻³) and in MUA gamma power (11%, paired *t*-test, *df* = 13, *p* = 0.02), as well an increase in LFP-MUA gamma coherence (6%, paired *t*-test, *df* = 13, *p* < 10⁻²). Overall, the results shown in Supplementary Figures 4.1 and 4.2 indicate that the expectation effect we describe here cannot be explained by the pattern of microsaccades elicited by temporal expectation.

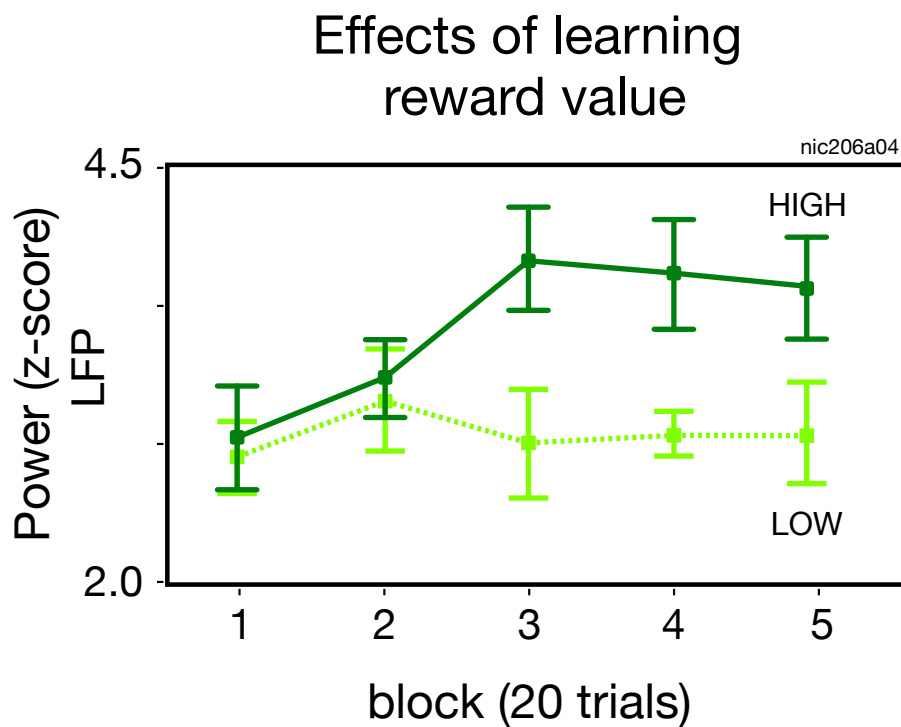


Supplementary Figure 4.3: Effects of temporal expectation on neuronal activity when no stimulus was presented over the receptive fields of the recorded neurons. Population data comparing firing conditions with low (no-cue) and high (cue) expectation for the cue-protocol. Analysis were performed for the firing rate, LFP alpha power, LFP gamma power and LFP-MUA coherence. For the coherence analysis, LFP-MUA pairs acquired from the same as well as from different electrodes are plotted. No significant differences in firing rate (paired *t*-test, *df* = 19, *p* = 0.2), LFP gamma power (paired *t*-test, *df* = 19, *p* = 0.9) or LFP-MUA gamma coherence (paired *t*-test, *df* = 99, *p* = 0.4) were observed. The LFP alpha power, however, showed a significant suppression for the cue, as compared to the no-cue condition (paired *t*-test, *df* = 19, *p* < 10⁻⁶). All recorded sites (N = 20) and LFP-MUA pairs (N = 100) were included in the analysis. The frequency bands of 8 - 12 Hz and 30 - 90 Hz were taken as alpha and gamma activity, respectively. Data was acquired from Monkeys 1 and 2.

4.8.2 - EXPECTATION EFFECT WITHOUT VISUAL STIMULATION

For all the experiments described so far, either a grating or a plaid stimulus was used to drive neuronal activity. In this additional experiment we investigated if temporal expectation could still modulate neuronal activity when no stimulus was presented over the receptive field of the recorded neurons. Supplementary Figure 4.3 shows the population data acquired during cue protocols

when no stimulus was presented. Only for the LFP alpha power did we find any significant effect. There was a two-fold suppression in alpha power for the condition of higher expectation (cue), as compared to the condition of lower expectation (no-cue). This suggests that for the expectation effect to be fully revealed in the LFP, spiking activity or coherence, it is necessary to drive neuronal activity with visual stimulation.



Supplementary Figure 4.4: Learning the association between reward value and a cue along an experimental session. Reward value was indicated to the monkey by the brightness of the FP. Continuous and dotted lines represent conditions with high and low reward value, respectively. The x-scale represents time bin along the session, where each bin encompasses 20 consecutive trials. The y-scale represents LFP gamma activity (30 - 90 Hz) averaged over 5 recording sites. The monkey gradually learnt along the session which brightness of the FP corresponded to which reward value. After around 60 trials (3rd time bin), the LFP gamma power in response to the low and high value conditions began to statistically differentiate from each other (paired *t*-test, *df* = 4, *p* < 10⁻²). For the time bins 3, 4 and 5, there was an average 34% increase in LFP power for the high as compared to the low value condition.

4.8.3 - LEARNING REWARD VALUE

Finally, we observed the changes in gamma power along a session while the monkey learnt to associate the brightness of the FP with the value of the upcoming reward. Therefore, while trial timing was kept constant, reward value changed as a function of a cue. The FP brightness, and consequently the value of the reward, changed randomly for each trial. The visual stimulus (moving grating) was displayed at 400 ms, and the FP color change event occurred at 2000 ms after the beginning of the trial. Supplementary Figure 4.4 shows an experiment where reward value (short versus long) was indicated by the brightness of the FP along the trial (dark or bright red,

respectively). The monkey did not know beforehand which brightness level indicated which upcoming reward. After around 60 trials, however, gamma activity for the two conditions (low and high reward value) diverged significantly from each other, where the average power for the high-reward-value condition was approximately 35% higher as compared to the low-reward-value condition.

4.9 - SUPPLEMENTARY REFERENCES

Bosman CA, Womelsdorf T, Desimone R, Fries P. 2009. A microsaccadic rhythm modulates gamma-band synchronization and behavior. *J. Neurosci.* 29: 9471-9480.

Matsuda K, Nagami T, Kawano K, Yamane S. 2000. A new system for measuring eye position on a personal computer. Program No. 744.2 in Abstract Viewer/Itinerary Planner. Society for Neuroscience, New Orleans (LA).

Chapter 5

Gamma-phase shifting in awake monkey visual cortex

Reprint of Vinck M, Lima B, Womelsdorf T, Oostenveld R, Singer W, Neuenschwander S and Fries P. (2010). *J. Neurosci.* 30: 1250-1257.

This work was done in collaboration with the Donders Institute for Brain, Cognition and Behaviour, Nijmegen, The Netherlands.

I performed the experimental part of this work.

Gamma-Phase Shifting in Awake Monkey Visual Cortex

Martin Vinck,^{1*} Bruss Lima,^{2*} Thilo Womelsdorf,¹ Robert Oostenveld,¹ Wolf Singer,^{2,3} Sergio Neuenschwander,² and Pascal Fries^{1,4}

¹Donders Institute for Brain, Cognition, and Behaviour, Radboud University Nijmegen, 6525 EN Nijmegen, The Netherlands, ²Max Planck Institute for Brain Research, 60528 Frankfurt, Germany, ³Frankfurt Institute for Advanced Studies, Johann Wolfgang Goethe University, 60438 Frankfurt, Germany, and ⁴Ernst Strüngmann Institute in Cooperation with Max Planck Society, 60528 Frankfurt, Germany

Gamma-band synchronization is abundant in nervous systems. Typically, the strength or precision of gamma-band synchronization is studied. However, the precise phase with which individual neurons are synchronized to the gamma-band rhythm might have interesting consequences for their impact on further processing and for spike timing-dependent plasticity. Therefore, we investigated whether the spike times of individual neurons shift systematically in the gamma cycle as a function of the neuronal activation strength. We found that stronger neuronal activation leads to spikes earlier in the gamma cycle, i.e., we observed gamma-phase shifting. Gamma-phase shifting occurred on very rapid timescales. It was particularly pronounced for periods in which gamma-band synchronization was relatively weak and for neurons that were only weakly coupled to the gamma rhythm. We suggest that gamma-phase shifting is brought about by an interplay between overall excitation and gamma-rhythmic synaptic input and has interesting consequences for neuronal coding, competition, and plasticity.

Introduction

Neuronal gamma-band synchronization has been found in several different species, in many different brain structures, and under numerous stimulation, motor, or cognitive conditions (Gray et al., 1989; Bragin et al., 1995; Fries et al., 2001, 2008a; Brosch et al., 2002; Pesaran et al., 2002; Schoffelen et al., 2005; Hoogenboom et al., 2006). Correspondingly, gamma-band synchronization has been implicated in several functions (Gray et al., 1989; Bragin et al., 1995; Wehr and Laurent, 1996; Fries et al., 2001; Fell et al., 2001; Pesaran et al., 2002; Buschman and Miller, 2007). Models that try to explain how gamma-band synchronization subserves different functions typically focus on the precision or strength of gamma-band synchronization (Singer and Gray, 1995; Engel et al., 2001; Salinas and Sejnowski, 2001; Börgers and Kopell, 2008), but the phase of gamma-band synchronization might be another important aspect, as has been proposed numerous times (Buzsáki and Chrobak, 1995; Maass and Natschläger, 1997; Börgers et al., 2005; Schneider et al., 2006; Nikolić, 2007; Fries et al., 2007; Tiesinga et al., 2008; Quian Quiroga and Panzeri, 2009) but so far not yet demonstrated (Ray et al., 2008).

Gamma-band synchronization within a local group of neurons entails rhythmic inhibition through the local inhibitory interneuron network (Csicsvari et al., 2003; Hasenstaub et al., 2005; Vida et al., 2006; Buzsáki, 2006; Bartos et al., 2007; Morita et al., 2008). The gamma-rhythmic inhibition constitutes a gamma cy-

cle that might impact neuronal processing (Fries et al., 2007). Neurons that are strongly activated might spike early in the gamma cycle, i.e., there might be gamma-phase shifting. The spike phase in the gamma cycle would thereby provide an instantaneous analog representation of neuronal excitation. Gamma-phase shifting could have important consequences, endowing early spikes with enhanced impact on postsynaptic neurons (Börgers et al., 2005; Börgers and Kopell, 2008) and with an enhanced chance to potentiate synapses through spike timing-dependent plasticity (STDP) (Markram et al., 1997; Bi and Poo, 1998; Caporale and Dan, 2008) (for more details, see Discussion).

Therefore, as a first step, we set out here to test whether gamma-phase shifting exists in awake monkey visual cortex. We recorded spikes and local field potentials (LFPs) simultaneously from several electrodes in monkey primary visual cortex during stimulation with gratings of different orientations. We found strong evidence for gamma-phase shifting and some indication that it is brought about by the interplay between overall neuronal excitation and gamma-rhythmic synaptic input.

Materials and Methods

Experimental procedures. Experiments were performed on three adult rhesus monkeys (*Macaca mulatta*) and followed the guidelines of the European Community for the care and use of laboratory animals (European Union Directive 86/609/EEC) with approval by the appropriate local committee on animal welfare (Regierungspräsidium Hessen, Darmstadt, Germany). After an initial training period, each monkey was surgically implanted with a titanium bolt for stabilizing head position, a scleral search coil for measuring eye position, and a titanium recording chamber (internal diameter, 6 mm) that allowed microelectrode access to primary visual cortex V1. The titanium pieces were fixed to the skull by means of orthopedic screws (Synthes). All surgical procedures were conducted under aseptic conditions with isoflurane anesthesia (Baxter) assisted by a pressure-controlled ventilation unit (1.8 L/min N₂O and 0.8 L/min O₂; Julian unit; Dräger Medical). Recordings were made from the opercular region of V1 (receptive field centers: 2.0–5.0° of eccentricity)

Received April 4, 2009; revised Nov. 20, 2009; accepted Nov. 28, 2009.

This research was supported by The European Science Foundation European Young Investigator Award Program (P.F.), The Netherlands Organization for Scientific Research (P.F.), Max Planck Society, and the Ernst Strüngmann Institute. We thank C. Bosman for helpful comments.

*M.V. and B.L. contributed equally to this work.

Correspondence should be addressed to Pascal Fries, Ernst Strüngmann Institute in Cooperation with Max Planck Society, Deutschordenstraße 46, 60528 Frankfurt, Germany. E-mail: pascal.fries@esi-frankfurt.de.

DOI:10.1523/JNEUROSCI.1623-09.2010

Copyright © 2010 the authors 0270-6474/10/301250-08\$15.00/0

and, in some occasions, from the superior bank of the calcarine sulcus (8.0–12.0° of eccentricity). Electrodes were inserted independently into the cortex via transdural guide tubes (diameter: 300 μm; Ehrhardt Söhne), assembled in a customized recording device (designed by one of the authors, SN). This device comprised five precision hydraulic micro-drives mounted onto an x–y stage (MO-95; Narishige), which was secured onto the recording chamber by means of a threaded adapter, providing high recording stability. Quartz-insulated tungsten–platinum electrodes (diameter: 80 μm; Thomas Recording) with impedances from 0.3 to 1.0 MΩ were used to record simultaneously the extracellular activity from three to five sites. Spiking activity of small groups of neurons [multiunit activity (MUA)] and the LFP were obtained by amplifying (1000×) and bandpass filtering (MUA: 0.7–6.0 kHz; LFP: 0.7–170 Hz) the recorded signals using a customized 32 channel head stage and pre-amplifier (head stage HST16025; head stage and preamplifier from Plexon). Additional 10× signal amplification was done by on-board amplifiers (E-series acquisition boards; National Instruments). The signals were digitized and stored using a LabVIEW-based acquisition system developed in our laboratory (SPASS, written by SN). Local field potentials were acquired with a resolution of 1.0 ms. Spikes were detected by amplitude thresholding, which was set interactively after online visualization of the spike waveforms (typically 2 to 3 SDs above the noise). Spike events and corresponding waveforms were sampled at 32 kHz, and spike waveforms were recorded for a duration of 1.2 ms.

Visual stimulation. Stimuli were presented as movies at 100 or 120 frames per second using a standard graphical board (GeForce 6600-series; NVIDIA). The cathode ray tube monitor used for presentation (CM813ET; Hitachi) was gamma corrected to produce a linear relationship between output luminance and gray values and subtended a visual angle of 36° × 28° (1024 × 768 pixels). At the beginning of each recording session, receptive fields were mapped using an automatic procedure, in which a bar was moved across the screen in 16 different directions ($n = 160$ trials). Receptive field position was estimated from the global maximum of a response matrix, at a resolution of ~6 min of arc. Subsequently, monkeys passively viewed drifting gratings during fixation of a small central fixation spot. Gratings had spatial frequencies ranging from 0.5 to 2.0 cycles/° and velocities ranging from 0.5 to 3.0°/s. Grating drift directions were generated randomly from a total of 16 directions (steps of 22.5°). The stimuli were centered over the receptive fields within a circular aperture of ~8.0°. After the monkey acquired fixation, there was a prestimulus baseline of 800–1000 ms after which the stimulus was presented for a duration of 800–1500 ms. For the present analysis, we used only data from this time period. If not mentioned otherwise, we excluded the first 250 ms after stimulus onset because of response onset transients. Monkeys were required to hold stable gaze for 3000 ms, during which additional test stimuli were shown (plaids composed of two grating components) and to respond to a color change of the fixation point. To obtain a reward, monkeys had to release the lever within 500 ms after the color change of the fixation point. Trials were aborted when early or late lever releases occurred or whenever fixation was interrupted and were followed by a blank screen period. Eye position was monitored continuously by a search coil system (DNI; Crist Instruments) with a temporal resolution of 2 ms.

Spike sorting. Offline spike sorting was performed using principal component analysis (Offline Sorter; Plexon). We used the following criteria to include a single unit in our sample: it had to be well isolated from the multiunit (MUA) on at least one of the first two principal component analysis scores of the waveforms, its isolation had to be stable across time, and a clear refractory period had to be visible in the interspike interval distribution.

Spike–LFP phase locking and spike phase analysis. Around each spike recorded from one electrode, a 150 ms data segment of the LFPs recorded on other electrodes was cut out. Each LFP data segment was multiplied by a Hanning window before Fourier transforming it, giving the spike-triggered LFP spectrum, as follows:

$$X_i(f) = \sum_t w(t) X_i(t) e^{-2\pi jft}, \quad (1)$$

where $x_i(t)$ is the time series of the LFP data segment around the spike i , $i = 1, 2, \dots, N$, and $w(t)$ the Hanning window. The 150 ms segment length

allowed a frequency resolution of 6.67 Hz. We averaged across the M LFPs from the other electrodes (i.e., not the one on which the spike was recorded) by the following:

$$\bar{X}_i(f) = \frac{1}{M} \sum_{m=1}^M \frac{X_i^m(f)}{|X_i^m(f)|}, \quad (2)$$

where $\bar{X}_i(f)$ is now a complex number. By means of Equation 2, the magnitude of the spike-triggered LFP spectrum is ignored in the computation of the spike phase. The spike phase is now simply given by $\theta_i = \arg(\bar{X}_i(f))$. We measured phase consistency by means of the spike–LFP phase-locking value, which is defined as follows:

$$P(f) = \left| \frac{1}{N} \sum_{i=1}^N \frac{\bar{X}_i(f)}{|\bar{X}_i(f)|} \right|. \quad (3)$$

The spike–LFP phase-locking value is a biased measure with respect to the number of spikes that are entered in the computation. Therefore, we always entered the same fixed number of spikes into Equation 3 when we compared between samples with a different number of elements. Furthermore, we reduced the statistical variance of our spike–LFP phase-locking value by means of a bootstrapping procedure. For every repetition, we drew the fixed number of spikes without replacement from all the spikes that were in the sample. For each bootstrapped sample drawn, we determined the spike–LFP phase-locking value. Subsequently, we averaged these spike–LFP phase-locking values across all bootstrapped samples, giving our “unbiased” phase-locking value. The statistical significance of the “biased” phase-locking value was assessed by means of the Rayleigh test ($\alpha = 0.001$).

Relationship of spike phase and orientation. We investigated whether stimulus orientation determines the spike phase in the gamma cycle. Nonpreferred orientations typically have a small number of spikes that are only weakly gamma-band phase locked. Thus, the estimate of their mean spike phase suffers from high variance. To reduce this variance, at the potential cost of a reduced effect size, we determined the four orientations with the lowest firing rate and pooled these together as the nonpreferred orientations. Similarly, we pooled together the two orientations with the highest firing rate together as the preferred orientations. This ensured that both conditions had a sufficiently large number of spikes. In addition, we only included neurons for which each condition contained >30 spikes.

Relation between spike density and spike phase. To estimate neuronal activation on short timescales, we determined for each individual spike the density of temporally neighboring spikes by convolving the spike train with a Gaussian kernel with a length of ±125 ms and an SD of 50 ms. Importantly, spike density is a linear predictor variable, whereas spike phase is a circular variable. Hence, their relationship cannot be studied properly with the standard linear regression model, because this model minimizes a linear error term and not a circular one. To address the linear–circular case, we used a linear–circular regression model (Fisher and Lee, 1992). In this model, an arc-tangens link function maps the linear predictor variable to the circle, giving the following model:

$$\theta_i = \mu + 2 * \tan^{-1}(\beta X_i) + \varepsilon_i, \quad (4)$$

where X_i , $i = 1, 2, \dots, N$, is the independent variable containing N data points, β is the regression coefficient we wanted to estimate, and ε_i is described by a von Mises distribution $VM(\mu, \kappa)$. To determine the parameter set (β, μ, κ), we maximized the likelihood as follows:

$$L = -n \log I(\kappa) + \kappa \sum_{i=1}^n \cos(\theta_i - \mu - g(\beta X_i)), \quad (5)$$

using an iterative least-squares algorithm. An SE of our regression parameter was computed, and a p value was obtained by comparing the t statistic, as follows:

$$T_\beta = \frac{\hat{\beta}}{\sqrt{\text{var}(\hat{\beta})}}, \quad (6)$$

against the standardized normal distribution. To directly determine the spike phases associated with different spike densities at the group level,

we binned spike densities into nonoverlapping bins and calculated the corresponding mean spike phases, averaged across all neurons, for every bin. We only included neurons that had at least 30 spikes in every spike density percentile. The relationship between spike density percentile and spike phase was statistically quantified using linear–circular regression.

Relationship between strength of phase locking and gamma-phase shifting. To quantify the relationship between the degree of gamma-phase shifting and the strength of phase locking, we removed several potential confounds from our data.

(1) An obvious confound is that weak and strong phase-locked neurons might have different spike numbers. Therefore, we used the bootstrapping bias-correction procedure as explained above, choosing a fixed number (100) of spikes to determine our spike–LFP phase-locking value.

(2) A more complicated potential confound is that stronger gamma-phase shifting will correspond to a higher dispersion of spike phases and will thus result in a lower spike–LFP locking by definition. Therefore, we introduced a new measure of phase locking, which measures the spike dispersion relative to the estimated phase shift or, in other words, which subtracts the phase shift and then estimates the phase locking as the resultant length of residual error terms (Eq. 3). This new phase-locking value is now calculated on the error terms as follows:

$$P(f) = \left| \frac{1}{N} \sum_{i=1}^N \exp(j * \varepsilon_i) \right|, \quad (7)$$

where ε_i is derived from Equation 4. This procedure removed the shifting mean phase in the gamma cycle from the data.

(3) Different animals might have different distributions of the strength of spike–field phase locking. To normalize for this, we used a Z-score standardization for our phase-locking values relative to the mean phase locking within each animal.

After removing these potential confounds, we then sorted neurons into weakly and strongly locked units by using a Z-score value of 0 as our cutoff value. For these two groups, we calculated the corresponding mean spike phases in the gamma cycle, averaged across all neurons. The relationship between spike density percentile and mean phase was quantified by means of linear–circular regression.

Relationship between LFP gamma-band power and phase shifting. We obtained an indirect measure of the strength of gamma-rhythmic synaptic input by determining the gamma-band power of the spike-triggered LFP spectra. We then used this gamma power to sort, for each neuron, the trials into low-, medium-, and high-gamma trials. Within those three groups of trials, we then determined the dependency of spike phase in the gamma cycle on the spike density percentile. It is expected that trials with a higher LFP gamma-band power will correspond to a higher degree of gamma-band phase locking.

Results

In three monkeys (monkeys J, L, and N), we recorded a total of 106 visually responsive isolated single neurons (25 from monkey J, 23 from monkey L, and 58 from monkey N). The spikes of each of the single units were then related to the average LFP recorded simultaneously from separate electrodes spaced at 1–3 mm distance. During visual stimulation, these spike–LFP pairs showed clear phase locking in the gamma-frequency band (Fig. 1). The gamma-frequency band was different in the three monkeys, peaking at ~67 Hz in monkey J and ~40 Hz in monkeys L and N. These three bands are within the range of gamma frequencies described in previous studies in monkeys (Friedman-Hill et al., 2000; Maldonado et al., 2000; Fries et al., 2008a,b) and humans (Hoogenboom et al., 2006; Wyart and Tallon-Baudry, 2008; Muthukumaraswamy et al., 2009). These monkey-specific peak frequencies were used for further analyses, unless full spectra are shown. Further analyses were restricted to those units that showed significant gamma-band spike–LFP phase locking (62 of the 106 units).

Spikes could be locked to different phases of the gamma cycle. Early phases occurred when the neuron was strongly activated

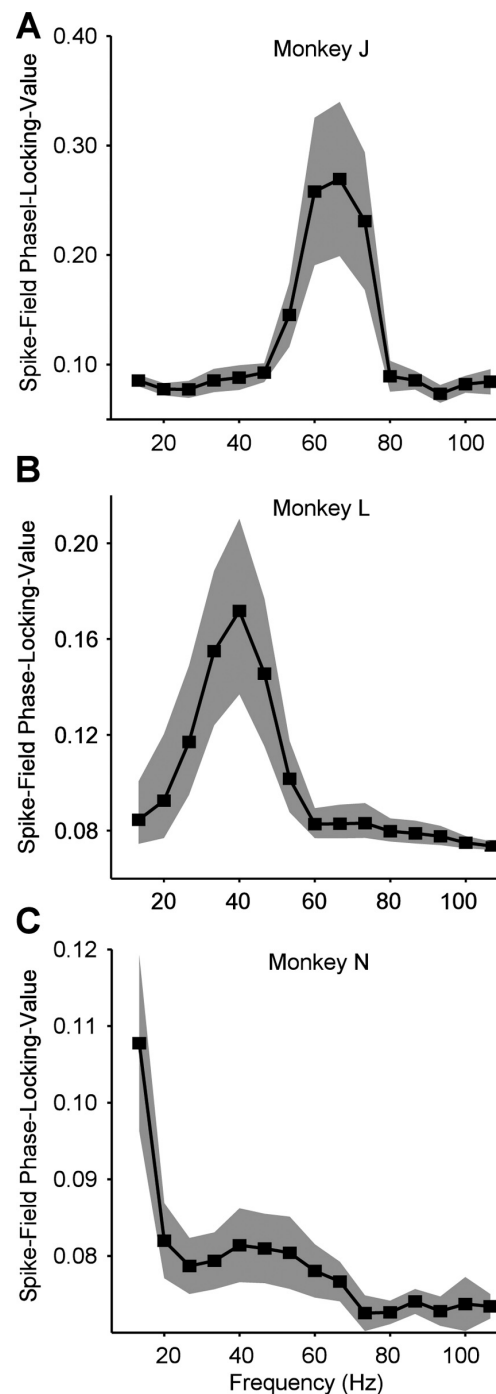


Figure 1. Spike–LFP phase-locking spectra. **A**, Monkey J. Average spike–LFP phase-locking value plotted as function of frequency. Shaded regions indicate 95% confidence intervals around the mean. A gamma-band peak is visible at ~67 Hz. **B**, Monkey L. Same conventions as in **A**. A gamma-band peak is visible at ~40 Hz. **C**, Monkey N. Same conventions as in **A**. A gamma-band peak is visible at ~40–53 Hz.

(example shown in Fig. 2A). Neuronal activation was strongly determined by stimulus orientation. Correspondingly, stimulus orientation determined spike phases in the gamma cycle. The spikes of the example neuron (Fig. 2A,B) shifted from $205.6 \pm 11.3^\circ$

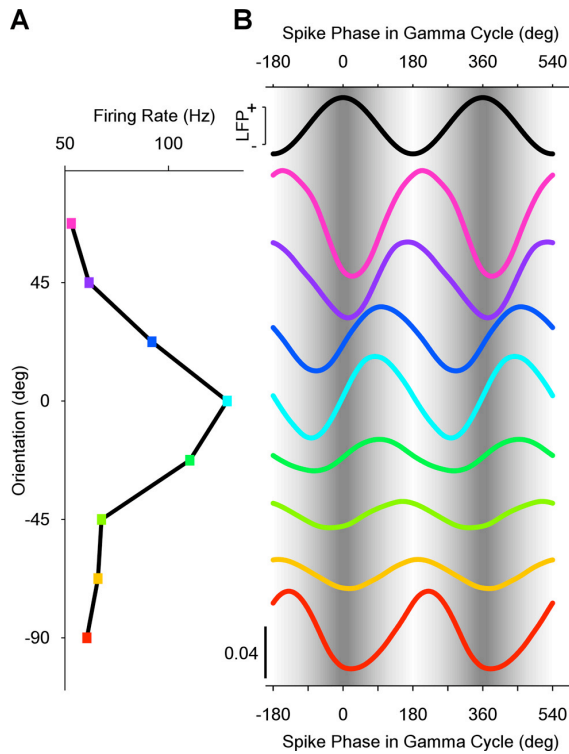


Figure 2. Match between stimulus orientation and neuronal orientation preference determines spike phase in the gamma cycle. **A, B**, Data from one example neuron. **A**, Firing rate as a function of stimulus orientation. **B**, The black sine wave at the top and the sinusoidal gray shading in the background illustrate the LFP gamma phase. The colored lines show spike densities as a function of phase in the gamma cycle. The colors correspond to the colors used in the firing rate panel on the left. All spike density curves are probability densities, normalized such that the mean value of each curve is $1/2\pi$ (bottom left calibration bar applies to all curves, and curves are offset along the *y*-axis to correspond to **A**).

[95% confidence interval (c.i.)] for the nonpreferred orientation to $91.0 \pm 11.3^\circ$ (95% c.i.) for the preferred orientation. Such orientation-dependent gamma-phase shifting was significant across the population of neurons ($p = 0.0027$, two-sided paired-sample sign test), although the orientation-dependent shift was smaller in the average than in the example (Fig. 3). On average, spikes shifted from $158.5 \pm 14.3^\circ$ (95% c.i.) for nonpreferred orientations to $137.22 \pm 17.9^\circ$ (95% c.i.) for preferred orientations.

Neuronal activation was not only determined by stimulus orientation but also by other factors. One such factor was the time after stimulus onset. Stimulus onset typically induces initial strong activation that then declines gradually. Furthermore, time after stimulus onset determined the exact position of the drifting grating over the receptive field of the recorded neuron. The corresponding dynamic modulations in neuronal activation modulated the spike phase in the gamma cycle (Fig. 4).

The rapid dynamics visible in Figure 4 suggest that the spike phase in the gamma cycle is determined by neuronal activation on short timescales. To estimate neuronal activation on short timescales, we determined for each individual spike the density of temporally neighboring spikes by convolving the spike train with a Gaussian kernel with an SD of 50 ms. The example neuron in Figure 5A demonstrates that high spike densities led to early (low) phases in the gamma cycle. This is evident in the negative linear–circular regression slope. Negative slopes were observed

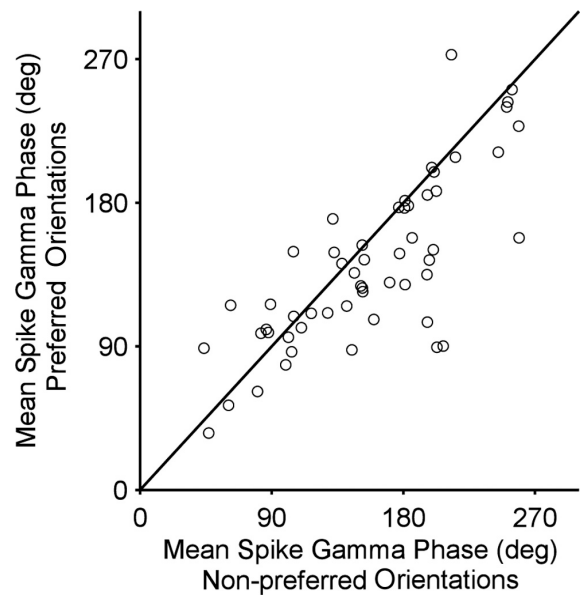


Figure 3. Population results for orientation-dependent phase shift. Scatter plot of mean spike phase for the four least preferred orientations (*x*-axis) versus mean spike phase for the two most preferred orientations (*y*-axis). Every dot represents a single unit.

for the majority of neurons (80.65% negative slopes, of which 42% individually significant at $\alpha = 0.05$) (Fig. 5B). The average slope was $-0.60 \pm 0.13^\circ/\text{Hz}$ of spike density ($p = 1.8e^{-06}$, Wilcoxon’s signed-rank test). This finding was consistent for monkey J (average slope: -0.76 ± 0.21 ; average *t* statistic: -1.6 ± 0.37 ; $p = 2.6e^{-04}$), monkey L (average slope: -0.48 ± 0.14 ; average *t* statistic: -1.65 ± 0.69 ; $p = 0.01$), and monkey N (average slope: -0.56 ± 0.29 ; average *t* statistic: -0.76 ± 0.28 ; $p = 0.01$). The dependence of spike phase on spike density was specific for the respective gamma-frequency bands of the three monkeys (Fig. 5C–E).

To directly determine the spike phases associated with different spike densities, we binned spike densities and calculated the corresponding mean spike phases in the gamma cycle, averaged across all neurons. Those mean spike phases are shown as a function of the spike density percentile in Figure 6A. On average, spikes shifted from $157.2 \pm 13.3^\circ$ for the lowest spike density percentile to $127.1 \pm 17.8^\circ$ for the highest spike density percentile. This is reflected in a clear negative linear–circular regression (regression slope, $-0.37 \pm 0.10^\circ/\text{spike density percentile}$; $p = 0.0010$, two-sided *t* test).

Together, the results so far show that, within the gamma cycle, spikes occur earlier when the neurons are more strongly activated. The overall neuronal excitation level appears to interact with the gamma-rhythmic component of synaptic input such that higher excitation levels surpass rhythmic membrane potential modulation earlier. If this model is correct, then one might hypothesize that stronger rhythmic input constrains spike times more, i.e., stronger rhythmic input might lead to less activation-dependent shifting of spikes in the gamma cycle, because it might focus the spikes on the peaks of the depolarization cycle. We tested this hypothesis in three ways.

First, we tested whether the amount of phase shifting is related to the strength of rhythmic input in a given trial. We estimated the strength of gamma-rhythmic synaptic input indirectly by determining the gamma-band power of the LFP (Frost, 1967;

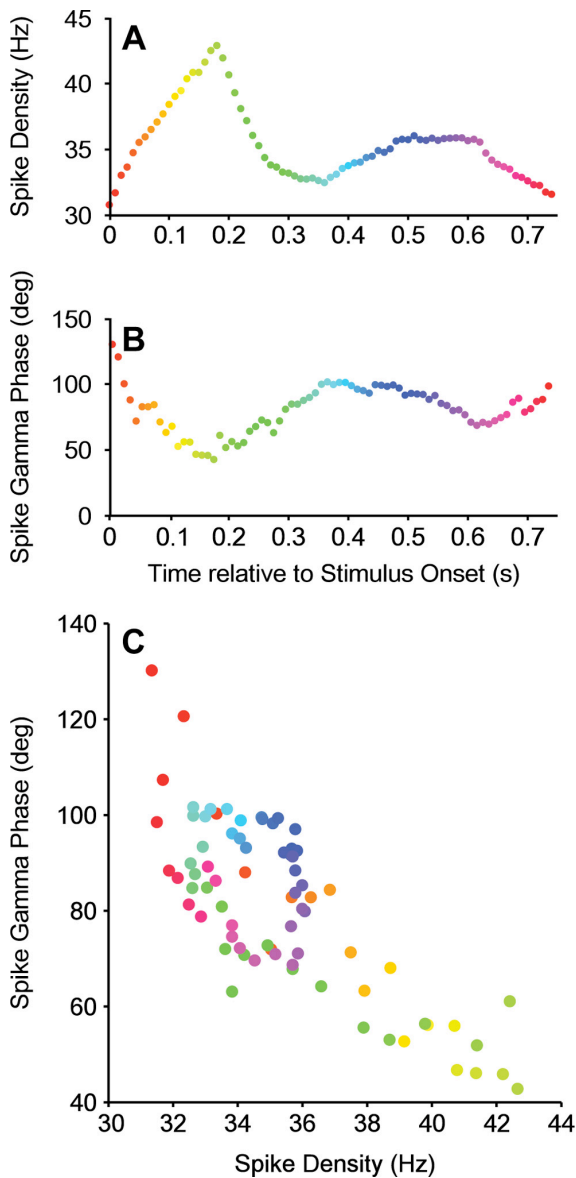


Figure 4. Temporal evolution of spike density and spike phase during the trial. *A–C*, Data from one example neuron. *A*, Spike density as a function of time after stimulus onset, calculated in 250 ms rectangular windows. The fluctuations in spike density are predominantly driven by the onset transient and the position of the drifting grating over the receptive field of the neuron. *B*, Same analysis but for the spike phase in the gamma cycle. *C*, Same data as in *A* and *B* but now showing spike phase directly as a function of spike density.

Mitzdorf, 1985; Schroeder et al., 1995). We then used the gamma power to sort, for each neuron, the trials into low-, medium-, and high-gamma trials. Within those three groups of trials, we then determined the dependence of spike phase in the gamma cycle on the spike density percentile. Figure 6*B* shows that strong neuronal activation shifted spike phases less during high compared with low gamma-band power. Regression slopes were more negative during low gamma-band power than high gamma-band power (two-sided paired-sign test, $p = 0.0396$).

Second, we tested whether the activation-dependent phase shift was larger when gamma-band power was very weak in the

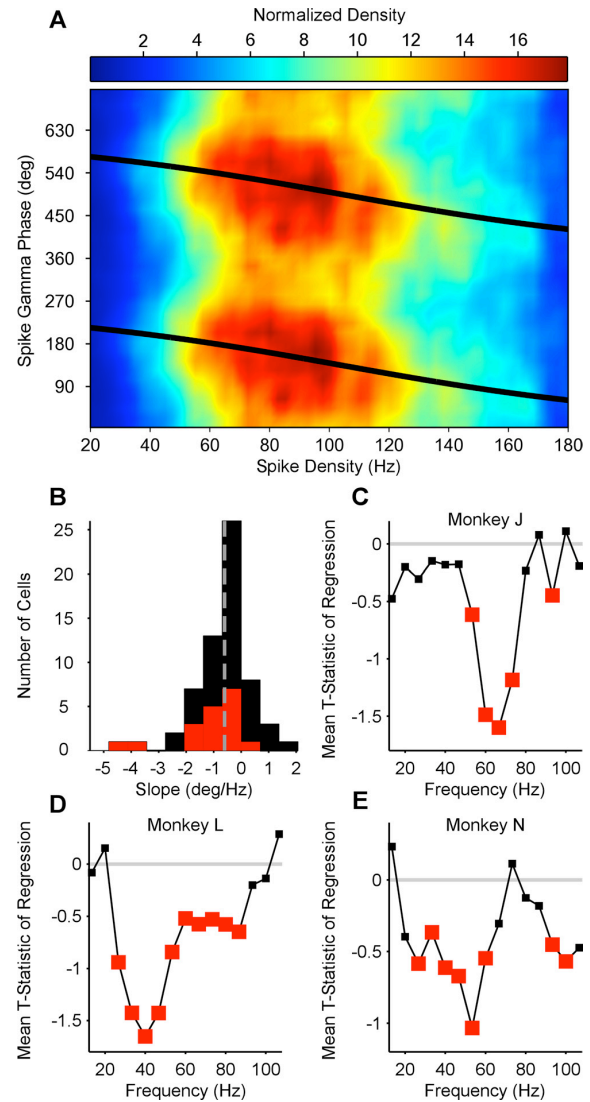


Figure 5. The relationship between spike density and spike phase. *A*, Example neuron. Spike phase in the gamma cycle plotted as a function of spike density. Colors represent normalized density. *B*, Group result. Distribution of linear–circular phase-shift regression parameter across neurons. Red bars indicate significant regression weights. Distribution is clearly skewed to the left. *C–E*, Comparison of frequencies. Average t statistic of spike phase onto spike density regression plotted as a function of frequency. For each monkey, gamma-phase shifting is most significant in that monkey's individual gamma-frequency band (compare with Fig. 1). Red squares indicate significant mean t statistic values (two-sided t test).

absence of visual stimulation, during the fixation baseline. We analyzed the baseline period and confirmed that the average spike phase shift as a function of spike density was much larger during the baseline than during visual stimulation (Fig. 6*C*) ($-7.72 \pm 3.0999^\circ$ /spike density percentile; $p = 0.0064$, two-sided t test).

Third, we used the fact that different neurons phase lock to the gamma rhythm to widely varying degrees. This variation might be attributable to either differences in how strongly a neuron is targeted by gamma-rhythmic input or how responsive to this input it is. We determined for each neuron how strongly it was, on average, phase locked to the gamma rhythm. For this particular analysis, we used a phase-locking measure that compensated

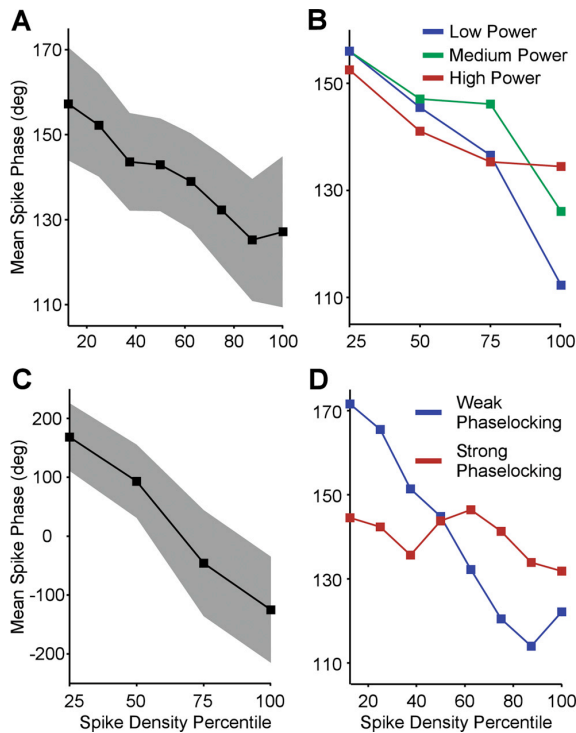


Figure 6. Relationship between strength of rhythmic input and gamma-phase shifting. **A**, Group result. Mean spike phase in gamma cycle averaged across all neurons plotted as a function of spike density percentile. Filled region indicates 95% confidence intervals. **B**, Group result. Relationship between spike density percentile and spike phase in gamma cycle for trials with high power (red) versus trials with low power (blue). **C**, Mean spike phase in gamma cycle during fixation baseline period averaged across all neurons plotted as a function of spike density percentile. Filled region indicates 95% confidence intervals. **D**, Relationship between spike density percentile and spike phase in gamma cycle separate for neurons with strong phase locking (red) versus weak phase locking (blue).

for the effects of phase shifting on phase locking by essentially subtracting the estimated phase shift (for details, see Materials and Methods). We then used this shift-corrected metric of gamma-phase locking to sort neurons into weakly and strongly locked units. Figure 6D shows that activation-dependent gamma-phase shifts were much bigger in weakly ($-0.71 \pm 0.16^\circ/\text{spike density percentile}$; $p = 6.55e^{-06}$, two-sided t test) compared with strongly gamma-locked units ($-0.10 \pm 0.125^\circ/\text{spike density percentile}$; $p = 0.21$, two-sided t test).

Discussion

To summarize, we found that neurons spike earlier in the gamma cycle of the LFP when they are more strongly activated, i.e., we observed gamma-phase shifting. We observed gamma-phase shifting first for different activation levels induced by different stimulus orientations. It held true when the activation level around each spike was estimated by the immediately surrounding spike density. We hypothesized that this gamma-phase shifting is brought about by the interaction of varying excitation levels with gamma-rhythmic synaptic input. In support of this, we found that gamma-phase shifting was particularly strong (1) during conditions when LFP gamma-band power was weak and (2) for neurons that were only loosely locked to the gamma rhythm. These latter results are consistent with the hypothesis that weak phase shifting is caused by strong gamma-rhythmic synaptic in-

put, although the correlative evidence does not prove a causal relation.

One potential concern is that the observed changes in spike phase are trivial byproducts of changes in neuronal activation. Neuronal activation is measured by determining postsynaptic spike density, and increased spike numbers will reduce the variance of the phase estimate. However, spike number will not affect the mean of the phase estimate. Increased neuronal activation is also often associated with enhanced LFP power and improved spike–LFP locking (Friedman-Hill et al., 2000; Frien and Eckhorn, 2000; Frien et al., 2000), but the same reasoning holds: whereas the variance of the phase estimate is affected, the mean is not.

Another concern relates to the sorting of neurons into groups with weak and strong gamma-band phase locking. We found that neurons with weak locking shift more. It might be argued that this finding reflects a circularity, because neurons that shift much would have a low phase locking, by definition. We accounted for this by first estimating the phase shift with a regression and then determining the phase locking from the residual errors around the shifting mean phase (for a more elaborate account, see Materials and Methods). Thereby, the shifting mean phase is removed from the data before the phase locking is determined. Even with this correction, low phase-locking was related to large phase shifts.

Our findings complement the work on theta phase precession in the hippocampus (O’Keefe and Recce, 1993; Mehta et al., 2002; Harris et al., 2002) by demonstrating phase shifting for the gamma-frequency band in the awake monkey visual cortex. However, we emphasize one important difference: in hippocampal theta-phase precession, as spikes shift to earlier phases, the precision of theta-band synchronization decreases (Mehta et al., 2002). In contrast, in visual cortical gamma-phase shifting, spikes shift to earlier phases during stronger neuronal activation, and this enhanced activation is typically correlated with an enhanced precision of gamma-band synchronization (Friedman-Hill et al., 2000; Frien and Eckhorn, 2000; Frien et al., 2000). The reason for this discrepancy might be the more local generation of cortical gamma compared with hippocampal theta (Buzsáki, 2006). The theta-rhythmic inhibition that impinges on a given hippocampal neuron stems, at least to a substantial part, from distant and/or widespread neuronal networks (Buzsáki, 2002) whose activation is relatively independent of the local network of the respective neuron. Increased activation of the local network will therefore lift excitation such that it exceeds inhibition not only earlier but also longer in the theta cycle. Longer firing during the theta cycle gives more spike dispersion relative to the theta cycle, i.e., less precise spike–LFP theta phase locking. In contrast, the gamma-rhythmic input that impinges on a given cortical neuron stems predominantly from the local neuronal network whose activation is influenced and highly correlated with the activation of the respective neuron. Thus, increased activation of the local network will not only lift excitation, but it will also increase gamma rhythmic input. This increased rhythmic input will constrain neuronal spiking and thereby lead to stronger spike–LFP gamma phase locking.

It should be noted that, in rat hippocampus, neuronal spiking is locked not only to the theta rhythm but also to the gamma rhythm (Bragin et al., 1995). One study described different classes of hippocampal pyramidal cells that are locked to different phases of the gamma cycle (Senior et al., 2008). These phases differ for different phases of the theta rhythm, but the study did not investigate whether there is a systematic gamma-phase shifting.

One previous study investigated fine time shifts between MUAs recorded from electrodes in primary visual cortex of anesthetized cats (König et al., 1995). Cats were stimulated with drifting bars of varying orientation that activated different MUAs to different degrees. Strongly driven MUAs fired few milliseconds before weakly driven MUAs. These findings are consistent with ours, but our present results extend them in several respects. First, rather than relating two MUAs to each other, we related isolated single neurons to the LFP. This latter approach is used for the investigation of hippocampal theta-phase precession and thereby makes the two phenomena comparable. Second, König et al. studied the position of the central peak in cross-correlograms. This demonstrates a lead or lag in time, but it does not establish a frequency-specific phase shift, i.e., the earlier analysis could not establish gamma-phase shifting. Third, the spectral specificity attained through our approach enabled us to make a close link to models of gamma-band synchronization that prominently entail gamma-rhythmic inhibition (Bartos et al., 2007; Börgers and Kopell, 2008; Morita et al., 2008). Finally, our data were obtained in the awake monkey, demonstrating that gamma-phase shifting exists in the awake state and in the best available invasive model for the human brain.

One recent study investigated spike and LFP recordings from awake monkey secondary somatosensory cortex during tactile stimulation with varying levels of intensity (Ray et al., 2008). The authors set out to test the hypothesis put forward by us previously, stating that stronger activation of cortical neurons should lead to gamma-phase shifting (Fries et al., 2007). In short, the study failed to find evidence for this hypothesis, but this failure is most likely explained by a confound in the recorded signals. The study used spikes and LFPs recorded through the same electrode. The rapid extracellular potential fluctuations associated with action potentials are spectrally broad and therefore contribute also to the LFP. For this reason, previous studies that used spikes and LFPs from the same electrode explicitly removed the spike contribution to the LFP (Pesaran et al., 2002; Jacobs et al., 2007). These spike contributions to the LFP rise with frequency with the same spectral profile as the spectral energy that Ray et al. (2008) take as gamma-band activity (their Fig. 4). Thus, the signal components of the LFP, which Ray et al. consider to be gamma-band activity, reflect the spike itself. They record the spike also in the conventional way, i.e., through high-pass filtering and thresholding, and find that these conventionally recorded spikes have a fixed phase to their high-frequency LFP components. Because both signals reflect the same spiking events, it is self-evident that they do not shift relative to each other.

The potential consequences of gamma-phase shifting are at least twofold (Fries et al., 2007). (1) Excitatory neurons will likely have a bigger impact on their target neurons when they spike early in the gamma cycle. Gamma-rhythmic output typically entrains neuronal target groups (Börgers and Kopell, 2008). Those target groups are therefore undergoing rhythmic inhibition. This rhythmic inhibition will affect inputs least that arrive particularly early in the cycle. The precise arrival time of synaptic inputs depends also on the conduction delays, which, for distant neuronal groups, might be large relative to the phase shift. Therefore, the detailed sequence of neuronal firing in two (distant) interacting neuronal groups is an interesting issue for future research. Regardless of the precise timing relation between synaptic inputs and the phase of the ongoing gamma rhythm of the target group, early input spikes are in the position to trigger additional inhibition in the target group that will in any case diminish the impact of later spikes, thereby exerting a winner takes all mechanism.

(2) Activity-dependent changes of synaptic efficacy are sensitive to the precise relative timing of presynaptic and postsynaptic activity, a phenomenon that is called spike timing-dependent plasticity (Markram et al., 1997; Bi and Poo, 1998; Caporale and Dan, 2008). It has been proposed that STDP might be enabled by gamma-band synchronization because the latter focuses neuronal activity in sufficiently short time windows (Wespatat et al., 2004). However, simple cofiring of presynaptic and postsynaptic neurons within short time windows does not lead to systematic STDP. Rather, STDP requires that the presynaptic neuron is either leading or lagging the postsynaptic neuron by a few milliseconds. This is achieved through gamma-phase shifting, because it translates different neuronal activation levels into different spike times during the gamma cycle. Intriguingly, during high-gamma states, spikes shifted less. Such small shifts should lead to maximal synaptic changes, because STDP is stronger for shorter delays between presynaptic and postsynaptic spiking. These predicted consequences of gamma-phase shifting should in principle apply to any two neuronal groups that are gamma-band synchronized, whether they are located within the same or different brain areas/structures (Womelsdorf et al., 2007).

To conclude, gamma-phase shifting is clearly present in awake monkey V1. It will be an important target for future research to test whether it leads to the predicted consequences. If so, gamma-phase shifting could be a very important phenomenon given the widespread occurrence of gamma-band synchronization in different species and brain regions and its relation to numerous cognitive functions (Fries, 2009).

References

- Bartos M, Vida I, Jonas P (2007) Synaptic mechanisms of synchronized gamma oscillations in inhibitory interneuron networks. *Nat Rev Neurosci* 8:45–56.
- Bi GQ, Poo MM (1998) Synaptic modifications in cultured hippocampal neurons: dependence on spike timing, synaptic strength, and postsynaptic cell type. *J Neurosci* 18:10464–10472.
- Börgers C, Kopell NJ (2008) Gamma oscillations and stimulus selection. *Neural Comput* 20:383–414.
- Börgers C, Epstein S, Kopell NJ (2005) Background gamma rhythmicity and attention in cortical local circuits: a computational study. *Proc Natl Acad Sci U S A* 102:7002–7007.
- Bragin A, Jandó G, Nádasdy Z, Hetke J, Wise K, Buzsáki G (1995) Gamma (40–100 Hz) oscillation in the hippocampus of the behaving rat. *J Neurosci* 15:47–60.
- Brosch M, Budinger E, Scheich H (2002) Stimulus-related gamma oscillations in primate auditory cortex. *J Neurophysiol* 87:2715–2725.
- Buschman TJ, Miller EK (2007) Top-down versus bottom-up control of attention in the prefrontal and posterior parietal cortices. *Science* 315:1860–1862.
- Buzsáki G (2002) Theta oscillations in the hippocampus. *Neuron* 33:325–340.
- Buzsáki G (2006) *Rhythms of the brain*. Oxford: Oxford UP.
- Buzsáki G, Chrobak JJ (1995) Temporal structure in spatially organized neuronal ensembles: a role for interneuronal networks. *Curr Opin Neurobiol* 5:504–510.
- Caporale N, Dan Y (2008) Spike timing-dependent plasticity: a Hebbian learning rule. *Annu Rev Neurosci* 31:25–46.
- Csicsvari J, Jamieson B, Wise KD, Buzsáki G (2003) Mechanisms of gamma oscillations in the hippocampus of the behaving rat. *Neuron* 37:311–322.
- Engel AK, Fries P, Singer W (2001) Dynamic predictions: oscillations and synchrony in top-down processing. *Nat Rev Neurosci* 2:704–716.
- Fell J, Klaver P, Lehnertz K, Grunwald T, Schaller C, Elger CE, Fernández G (2001) Human memory formation is accompanied by rhinal-hippocampal coupling and decoupling. *Nat Neurosci* 4:1259–1264.
- Fisher NI, Lee AJ (1992) Regression models for an angular response. *Biometrics* 48:665–677.
- Friedman-Hill S, Maldonado PE, Gray CM (2000) Dynamics of striate cor-

- tical activity in the alert macaque. I. Incidence and stimulus-dependence of gamma-band neuronal oscillations. *Cereb Cortex* 10:1105–1116.
- Frien A, Eckhorn R (2000) Functional coupling shows stronger stimulus dependency for fast oscillations than for low-frequency components in striate cortex of awake monkey. *Eur J Neurosci* 12:1466–1478.
- Frien A, Eckhorn R, Bauer R, Woelbern T, Gabriel A (2000) Fast oscillations display sharper orientation tuning than slower components of the same recordings in striate cortex of the awake monkey. *Eur J Neurosci* 12:1453–1465.
- Fries P (2009) Neuronal gamma-band synchronization as a fundamental process in cortical computation. *Annu Rev Neurosci* 32:209–224.
- Fries P, Reynolds JH, Rorie AE, Desimone R (2001) Modulation of oscillatory neuronal synchronization by selective visual attention. *Science* 291:1560–1563.
- Fries P, Nikolić D, Singer W (2007) The gamma cycle. *Trends Neurosci* 30:309–316.
- Fries P, Scheeringa R, Oostenveld R (2008a) Finding gamma. *Neuron* 58:303–305.
- Fries P, Womelsdorf T, Oostenveld R, Desimone R (2008b) The effects of visual stimulation and selective visual attention on rhythmic neuronal synchronization in macaque area V4. *J Neurosci* 28:4823–4835.
- Frost JD Jr (1967) Comparison of intracellular potentials and ECoG activity in isolated cerebral cortex. *Electroencephalogr Clin Neurophysiol* 23:89–90.
- Gray CM, König P, Engel AK, Singer W (1989) Oscillatory responses in cat visual cortex exhibit inter-columnar synchronization which reflects global stimulus properties. *Nature* 338:334–337.
- Harris KD, Henze DA, Hirase H, Leinekugel X, Dragoi G, Czurkó A, Buzsáki G (2002) Spike train dynamics predicts theta-related phase precession in hippocampal pyramidal cells. *Nature* 417:738–741.
- Hasenstaub A, Shu Y, Haider B, Kraushaar U, Duque A, McCormick DA (2005) Inhibitory postsynaptic potentials carry synchronized frequency information in active cortical networks. *Neuron* 47:423–435.
- Hoogenboom N, Schoffelen JM, Oostenveld R, Parkes LM, Fries P (2006) Localizing human visual gamma-band activity in frequency, time and space. *Neuroimage* 29:764–773.
- Jacobs J, Kahana MJ, Ekstrom AD, Fried I (2007) Brain oscillations control timing of single-neuron activity in humans. *J Neurosci* 27:3839–3844.
- König P, Engel AK, Roelfsema PR, Singer W (1995) How precise is neuronal synchronization? *Neural Comput* 7:469–485.
- Maass W, Natschläger T (1997) Networks of spiking neurons can emulate arbitrary Hopfield nets in temporal coding. *Netw Comput Neural Syst* 8:355–372.
- Maldonado PE, Friedman-Hill S, Gray CM (2000) Dynamics of striate cortical activity in the alert macaque. II. Fast time scale synchronization. *Cereb Cortex* 10:1117–1131.
- Markram H, Lübke J, Frotscher M, Sakmann B (1997) Regulation of synaptic efficacy by coincidence of postsynaptic APs and EPSPs. *Science* 275:213–215.
- Mehta MR, Lee AK, Wilson MA (2002) Role of experience and oscillations in transforming a rate code into a temporal code. *Nature* 417:741–746.
- Mitzdorf U (1985) Current source-density method and application in cat cerebral cortex: investigation of evoked potentials and EEG phenomena. *Physiol Rev* 65:37–100.
- Morita K, Kalra R, Aihara K, Robinson HP (2008) Recurrent synaptic input and the timing of gamma-frequency-modulated firing of pyramidal cells during neocortical “UP” states. *J Neurosci* 28:1871–1881.
- Muthukumaraswamy SD, Edden RA, Jones DK, Swettenham JB, Singh KD (2009) Resting GABA concentration predicts peak gamma frequency and fMRI amplitude in response to visual stimulation in humans. *Proc Natl Acad Sci U S A* 106:8356–8361.
- Nikolić D (2007) Non-parametric detection of temporal order across pairwise measurements of time delays. *J Comput Neurosci* 22:5–19.
- O’Keefe J, Recce ML (1993) Phase relationship between hippocampal place units and the EEG theta rhythm. *Hippocampus* 3:317–330.
- Pesaran B, Pezaris JS, Sahani M, Mitra PP, Andersen RA (2002) Temporal structure in neuronal activity during working memory in macaque parietal cortex. *Nat Neurosci* 5:805–811.
- Quian Quiroga R, Panzeri S (2009) Extracting information from neuronal populations: information theory and decoding approaches. *Nat Rev Neurosci* 10:173–185.
- Ray S, Hsiao SS, Crone NE, Franaszczuk PJ, Niebur E (2008) Effect of stimulus intensity on the spike-local field potential relationship in the secondary somatosensory cortex. *J Neurosci* 28:7334–7343.
- Salinas E, Sejnowski TJ (2001) Correlated neuronal activity and the flow of neural information. *Nat Rev Neurosci* 2:539–550.
- Schneider G, Havenith MN, Nikolić D (2006) Spatiotemporal structure in large neuronal networks detected from cross-correlation. *Neural Comput* 18:2387–2413.
- Schoffelen JM, Oostenveld R, Fries P (2005) Neuronal coherence as a mechanism of effective corticospinal interaction. *Science* 308:111–113.
- Schroeder CE, Steinschneider M, Javitt DC, Tenke CE, Givre SJ, Mehta AD, Simpson GV, Arezzo JC, Vaughan HG Jr (1995) Localization of ERP generators and identification of underlying neural processes. *Electroencephalogr Clin Neurophysiol Suppl* 44:55–75.
- Senior TJ, Huxter JR, Allen K, O’Neill J, Csicsvari J (2008) Gamma oscillatory firing reveals distinct populations of pyramidal cells in the CA1 region of the hippocampus. *J Neurosci* 28:2274–2286.
- Singer W, Gray CM (1995) Visual feature integration and the temporal correlation hypothesis. *Annu Rev Neurosci* 18:555–586.
- Tiesinga P, Fellous JM, Sejnowski TJ (2008) Regulation of spike timing in visual cortical circuits. *Nat Rev Neurosci* 9:97–107.
- Vida I, Bartos M, Jonas P (2006) Shunting inhibition improves robustness of gamma oscillations in hippocampal interneuron networks by homogenizing firing rates. *Neuron* 49:107–117.
- Wehr M, Laurent G (1996) Odour encoding by temporal sequences of firing in oscillating neural assemblies. *Nature* 384:162–166.
- Wespapat V, Tennigkeit F, Singer W (2004) Phase sensitivity of synaptic modifications in oscillating cells of rat visual cortex. *J Neurosci* 24:9067–9075.
- Womelsdorf T, Schoffelen JM, Oostenveld R, Singer W, Desimone R, Engel AK, Fries P (2007) Modulation of neuronal interactions through neuronal synchronization. *Science* 316:1609–1612.
- Wyart V, Tallon-Baudry C (2008) Neural dissociation between visual awareness and spatial attention. *J Neurosci* 28:2667–2679.

Chapter 6

General discussion

6.1 - THE DIFFERENT PERSPECTIVES OF OBSERVED BRAIN FUNCTION

It is no wonder that we keep returning to two basic parameters when trying to investigate how the brain works, namely time and space (Singer, 1999a; Harris, 2005). How precise can neuronal processing be, or how precise is it required to be, in order to account for our cognitive capabilities? Is it sufficient to have integration windows of tens of milliseconds for the post-synaptic neuron, or is millisecond precision crucial? Alternatively, how localized is the representation of complex objects? Can it go down to the level of single neurons (Gross *et al.*, 1969; Desimone *et al.*, 1984) or single columns (Wang *et al.*, 1996) in the temporal cortex? Or are complex representations manifested in long range, distributed interactions across various brain areas? Due to the complexity of the brain, it can sometimes be impossible to understand its activation pattern by simple exploratory observation. One needs to conceive an initial hypothesis which is both robust but comprehensive before performing experiments and trying to interpret the results. And still, a good correlation between model and data is not enough to infer about brain function. The hypothesis needs to survive exhaustive retesting of the model predictions. In many cases, brain complexity is so high that it can easily accommodate conflicting hypothesis trying to explain the same phenomenon. Main stream neuroscience has long assumed that neurons summate post-synaptic potentials over long integration windows (Barlow, 1972). Therefore, analyzing neuronal responses based on the firing rate of single cells has given rise to countless success stories. Among them are concepts such as receptive field and feature selectivity (Hubel and Wiesel, 1979). So why search for an alternative coding mechanism? The use of the time domain is specially attractive, since it hugely expands the coding space available for neuronal processing. Exploring distributed operations adds further flexibility to the representation of new patterns (Singer, 1993). Synchronous oscillations is a potential mechanism capable of supporting both precise timing and distributed representations in the brain. How can oscillatory activity support long-range interactions during distributed neuronal processing? Does it engage long stretches of brain tissue into a continuous neuronal ensemble, or does the activation pattern resemble a patchwork?

Here, oscillatory activity was measured using intracortical microelectrode recordings. Synchronous, subthreshold rhythmic activity of small cell populations around the electrode tip were revealed in the local field potential (LFP). The LFP is a more localized signal than the electroencephalogram measured from the scalp (Logothetis, 2003). In order to increase sampling over cortical surface, we recorded from multiple electrodes simultaneously (usually 5 electrodes; maximum 10 electrodes). This strategy is limited in spatial coverage when compared to the EEG or MEG, which can sample from a large surface of the brain with high temporal resolution. Alternatively, it also does not allow direct observation of processes taking place inside the cell or at single channels. It therefore misses a variety of complex computations taking place along the dendritic trees (London and Häusser,

2005). This mesoscopic scale of analysis, however, provides a level of spatial resolution which is arguably the most adequate to investigate cooperative processes in the brain. Alternative methods such as the functional magnetic resonance imaging (fMRI) have higher spatial resolution when compared to the EEG, but rely on slow hemodynamic responses that typically require several seconds. From the same electrode tip that acquired the LFP, we also obtained multi- and single unit spiking activity. Therefore, both sub- and suprathreshold neuronal activity could be simultaneously compared. We performed control experiments to measure the leakage of spike responses into the LFP signal recorded from the same electrode. This was done by simulating spike waveforms, feeding them into the amplifier, and low-pass filtering the compound signal as in the original experiment. We observed that a leakage into the low-pass signal (the LFP signal) did in fact exist, but its magnitude was several times smaller than the real LFP signal (data not shown). Therefore, in our analysis, we included correlation measures obtain both within and between electrodes. Correlation between spiking activity and LFP acquired from the same electrode was typically much higher than the one obtained across electrodes (see Chapter 3, Supplementary Fig. 3.3). However, the spectral profile (such as peak frequency and bandwidth) of intra- and inter-electrode correlations were very similar. This led us to believe that spiking activity at the gamma frequency band was indeed more correlated with the local as compared to more distant LFP signals. We also recorded systematically from regions of V1 representing different eccentricities in the visual field. Simultaneous recordings from the operculum ($\sim 3^\circ$ eccentricity) and from the calcarine sulcus ($\sim 10^\circ$ eccentricity) provided a further opportunity to observe correlated gamma activity across long distances in V1. Visual stimulus was chosen so as to optimally and jointly activate both sites. LFP-LFP correlations were frequently found, but had lower magnitude as compared to signal pairs acquired from nearby sites in the cortex. LFP-spike correlations were rare, and spike-spike correlations were never found between distant sites. Thus, correlation measurements which included the LFP signal were much more likely to reach significance. One possible reason for these results maybe selective sampling. The LFP reflects the activity of a population of neurons, while single-cell discharges are much more prone to skip cycles in the oscillatory process. Indeed, the incidence of oscillatory activity was clearly more visible in the LFP than in the spikes. Gamma rhythmic activity in the spiking responses was always associated, for the same electrode, with strong LFP oscillations at the same frequency. Strong LFP gamma oscillations, however, were no guarantee of rhythmic discharges in the spikes. Several other studies in the primary visual cortex have also reported a decay in correlation with increasing distances (Gray *et al.*, 1989; Engel *et al.*, 1990; Maldonado *et al.*, 2000). How can high frequency oscillations still support distributed representations in the brain when they are only locally correlated? The primary visual cortex is a large area which has a very precise representation of the visual field (Gattass *et al.*, 1987). It might be specialized in providing higher centers in the brain with

a faithful map of the world. Correlations between distant parts of the visual field would thereby be left to higher visual areas, which are smaller and more interconnected. It might also be the case that the LFP suffers from under-sampling when compared to techniques such as the EEG. Rodriguez *et al.* (1999), using EEG measurements in humans, were able to find long range interactions at the gamma frequency band across several associative areas.

The visual stimulus is another key factor influencing gamma processes in area V1. It is well described that neurons in the primary visual cortex respond selectively to orientated contours (Hubel and Wiesel, 1959). Moving gratings not only provide oriented contours, but are able to engage V1 neurons into sustained activation. For this reason, gratings have been systematically used to study gamma processes in early visual areas (Eckhorn *et al.*, 1988; Roelfsema *et al.*, 1994, 1997; Fries *et al.*, 1997; Herculano-Houzel *et al.*, 1999; Friedman-Hill *et al.*, 2000; Maldonado *et al.*, 2000; Niessing *et al.*, 2005). By using gratings we were also able to find robust, sustained gamma oscillations in monkey V1. The spatial frequency and the speed of the grating stimulus were determinants of the strength of the gamma oscillations induced both in the spiking activity and in the LFP. Synchronization throughout our data set was invariably associated with phase locking of gamma oscillatory activity between the respective sites. Accordingly, synchronous oscillations between sites were only found when the individual sites also exhibited oscillatory activity. Finally, synchronization between spike trains, whenever they occurred, were precise to the millisecond time scale and were not phase-locked to stimulus onset.

We increased the complexity of the visual stimulus by superimposing a second moving grating on top of the first. This was enough to profoundly reduce the strength of spike gamma oscillations. Gray *et al.* (1990) found similar results using bars instead of gratings. Recently proposed techniques to study correlated activity between two signals, such as the coherency method, explicitly disregard overall oscillatory power by normalizing the cross-spectrum by both individual spectra (Fries *et al.*, 2001; Jarvis and Mitra, 2001; Pesaran *et al.*, 2002). In this way, coherence measures are particularly sensitive to the phase-locking of oscillatory activity across trials. Fries (2005) proposed that coherent activity among neuronal groups can be a fundamental mechanism by which different brain regions communicate with each other. Coherence measures for the superimposed grating stimuli in area V1, however, were still significantly lower than those observed for the gratings alone. As it will be discussed below, the nature of the neuronal interactions that we observed in area V1 were very sensitive to the physical characteristics of the stimulus but not to their global properties.

Anesthesia causes profound changes in the spatiotemporal organization of ongoing cortical activity (Greenberg *et al.*, 2008). Brain states under general anesthesia have been compared to brain states during natural sleep, specially due to their common thalamic deactivation (Franks, 2008).

Therefore, one has to be careful when drawing parallels between results obtained in the anesthetized and in the awake preparations. Most of the basic properties of gamma oscillations that have been described for the anesthetized cat (Gray and Singer, 1989; Engel *et al.*, 1990; Gray *et al.*, 1990), however, have been confirmed in the awake monkey (Friedman-Hill *et al.*, 2000; Maldonado *et al.*, 2000). But it has been reported that gamma activity obtained in the awake cat usually exhibits larger amplitude than the one recorded from the anesthetized preparation (Gray and Di Prisco, 1997). All the data shown in the previous chapters were obtained from the awake brain. For some of the tasks, the animal was actively engaged in making predictions of upcoming trial events, or selectively attending to a particular surface of the visual stimulus.

As a technical remark, it is important to note that gamma oscillations in V1 are very sensitive to infection in the brain. One of our monkeys acquired an accidental infection which we believed evolved to an encephalitis. After the monkey's recovery, spiking activity revealed clear receptive fields and tuning curves for motion direction. We were, however, unable to detect any gamma activity in the spikes nor in the LFP for the remaining years that the cylinder remained implanted.

The initial motivation for carrying out this work was to test the binding-by-synchronization (BBS) hypothesis using a motion integration paradigm. To this aim, we used plaid stimuli in conditions of perceptual segmentation or perceptual binding while recording neuronal activity in monkey V1. In a parallel work which also employed plaid stimuli, we tested how individual neurons in the visual wulst of the awake owl integrate motion.

6.2 - MOTION INTEGRATION: A COMPARATIVE STUDY IN THE OWL

We investigated whether single neurons in the visual wulst of the awake owl are capable of signaling global stimulus motion. In these experiments we used plaid stimuli in a paradigm similar to the one described by Movshon *et al.* (1985). Studies on humans have shown that additive plaids, constructed by superimposing two non-parallel sinusoidal gratings, can lead to different percepts depending on the physical characteristics of the component grating stimuli (Adelson and Movshon, 1982). When both grating components had the same contrast, speed and spatial frequency, subjects predominantly perceived a single rigidly moving plaid pattern (pattern motion). By using this stimulus configuration we assumed that owls, as humans, would also perceive pattern motion. Even though perception was made biased to pattern motion, we had different predictions as to how neurons in the visual wulst of the owl would respond. Neurons in the primary visual cortex of the cat and the monkey, due to the small size of their receptive fields, are believed to not resolve the aperture problem (Movshon *et al.*, 1985). Therefore, having only a small aperture

to analyze the visual object, V1 neurons respond predominately to the single grating components of the plaid. Only neurons at higher cortical areas, such area MT in the monkey, have been reported to signal global motion direction (but see Guo *et al.*, 2004). Neurons in the visual wulst of the owl also have small receptive fields. The visual wulst, like area V1, is the first region of the telencephalon to receive projections from the retinotalamofugal pathway (Shimizu and Bowers, 1999). Therefore, investigating how neurons in the wulst integrate motion provides a valuable comparison between the visual systems of birds and mammals. In our data set, a large proportion of the neurons in the visual wulst were found to be direction selective (66%). This population was further classified on the basis of whether they responded preferentially to the motion of each component grating or to the motion of the plaid as a whole. Curiously, none of the neurons responded to the global motion of the plaid. Similar to what has been described in the striate cortex of the anesthetized mammal (Movshon *et al.*, 1985), 80% of the direction selective neurons in the wulst responded to the direction of the component gratings. Specially intriguing was the fact that only a few neurons in the visual wulst were unclassifiable (20%). Therefore, the majority of cells were capable of filtering out the single motion components of the plaid stimulus. Global motion perception in the owl brain may be carried out by a pathway that includes the wulst as an initial processing stage. Further work will be necessary to address which areas of the owl's brain are capable of integrating global stimulus motion.

6.3 - THE VARIABILITY OF GAMMA PROCESSES IN MONKEY V1

Oscillatory activity has been implicated in numerous neuronal processes including the coding and integration of sensory input (Singer and Gray, 1995; Singer, 1999b; Buzsáki and Draguhn, 2004; Lakatos *et al.*, 2005; Fries, 2005; Fries, 2009). These various proposals, however, impose different constraints on how rhythmic activity in the brain should perform these functions. Here, we assumed that the temporal characteristics of the oscillation should be, to some extent, uncoupled from stimulus timing (Singer, 1999b). To serve as a relational code, its time frame needs to be referenced to the internal dynamics of the brain. Additionally, we assumed that the frequency of the oscillation has to be faster than the average rhythmic fluctuations of the incoming input so as to still contribute with an extra coding dimension. We found robust gamma oscillations comprising frequencies that were at least one order of magnitude higher than the temporal frequency of the stimulus. Furthermore, the occurrence of gamma oscillations was highly dependent on visual stimulation. The incidence of high frequency oscillations during non-stimulation periods (fixation only) was very low. Finally, the phase of the oscillations was largely independent of stimulus onset, suggesting that they are indeed timed to the internal dynamics of the brain. As a matter of fact,

oscillatory processes were more linked to the intrinsic organization and dynamics of the brain than we had initially anticipated. We made systematic recordings from the two hemispheres of 3 monkeys. For equal stimulation conditions, we observed that each one of the individuals had a specific peak oscillation frequency in the gamma band, a phenomenon we referred to as “gamma signature”. Despite the inter-individual differences, however, the spectral profile within the same individual was incredibly consistent. This consistency was observed not only across recording sessions but also across hemispheres. Other features of the spectrum, such as the peak-frequency bandwidth and power at low-frequency bands, also differed across individuals but were similar for recording obtained from the same monkey. Recently, similar results have been described for human subjects (Muthukumaraswamy *et al.*, 2010). This inter-subject variability may be linked to certain aspects of cortical architecture, such as the size and shape of orientation columns (Kaschube *et al.*, 2002), or the width of ocular dominance columns (Horton and Adams, 2005). The concentration of the inhibitory neurotransmitter GABA has also been correlated with peak gamma frequency (Muthukumaraswamy *et al.*, 2009). Future investigations should address the neural basis for this phenomenon. Genetic polymorphism, age and gender are possible contributing factors (Linkenkaer-Hansen *et al.*, 2007; Muthukumaraswamy *et al.*, 2010).

We generally used large grating stimuli in order to stimulate extensive portions of area V1. This enabled us to investigate the peak oscillation frequency across sites representing different eccentricities in the visual field (from $\sim 2^\circ$ to $\sim 13^\circ$ of visual angle). Our expectation was that the peak oscillation frequency for the gamma band would be similar throughout area V1. This assumption was based on the idea that interactions between spatially distributed neuronal groups are optimally carried out when they oscillated at similar frequencies (Fries, 2005; Schoffelen *et al.*, 2005; Womelsdorf *et al.*, 2007). Curiously, that is not what we observed. Oscillation frequency was inversely related to eccentricity, in a way that peak frequency systematically decreased for sites representing more peripheral portions of the visual field. Several reports have shown that peak oscillation frequency increases with respect to stimulus velocity (Eckhorn *et al.*, 1988; Gray *et al.*, 1990; Friedman-Hill *et al.*, 2000). We also observed this trend in our data (see Chapter 3, Supplementary Fig. 3.4). We used this finding to interpret the shifts in oscillation frequency across eccentricity. The cortical magnification factor decreases for portions of V1 representing the peripheral visual field (Daniel and Whitteridge, 1961). Therefore, the representation of a single grating stimulus will move at different velocities relative to the cortical surface in area V1. It will move faster at the foveal, as compared to the peripheral representation of the visual field. If velocity relative to cortical surface is the crucial factor determining oscillation frequency, this would explain why sites recorded in the calcarine sulcus exhibited lower frequency. If this explanation is correct, it supports the notion that cortical architecture plays a fundamental role in shaping oscillatory processes.

The activation pattern of the orientation columns in area V1 was also an important factor determining the gamma oscillation frequency. As mentioned above, gratings are capable of strongly activating neurons in primary visual areas. Furthermore, they activate a very specific population of neurons, namely the columns selective to the orientation presented. Superimposing two gratings with different orientations significantly reduced gamma oscillatory power. This finding suggested that the heterogeneous activation of area V1 gave rise to competitive interactions among columns having different selectivities. A complementary phenomena occurred for the oscillation frequency. Superimposing two gratings led to a systematic increase in the gamma oscillation frequency as compared to when a single grating was presented alone. We thereby investigated if the power and frequency changes were arising due to competitive mechanisms induced by the different grating components. We performed two experiments where we parametrically tested the disturbance induced by component 2 (background grating) on the ongoing oscillations induced by component 1 (foreground grating) alone (see Chapter 3, Figs. 3.4 and 3.5). In the first experiment, we increased the contrast of component 2 relative to component 1. The oscillation frequency increased and power decreased for increasing contrast values. In a second experiment, the same trend was observed when the angle between the two components was increased. Both experiments argue in favor of a competitive mechanism. The most intriguing result, however, was when both gratings had the same orientation but moved in opposite directions. In this case, oscillation frequency and power were comparable to the single grating condition. Most of the selective neurons that we encountered in V1 were selective for orientation and not for direction of motion. Therefore, we believe that two gratings with the same orientation and moving in opposite directions still activate a homogeneous population of neurons, explaining why oscillation frequency does not increase and the power does not reduce as compared to a grating presented alone. We can only speculate why the gamma oscillation gets faster for more heterogeneous patterns of V1 activation. Inhibitory interneurons have been implicated in the generation of high frequency oscillations in both the neocortex and the hippocampus (Csicsvari *et al.*, 2003; Hasenstaub *et al.*, 2005). It is thereby likely that the intrinsic connections in V1 differentially impact the inhibitory network depending on the pattern of visual stimulation. Intracellular recordings combined with pharmacological manipulations *in vivo* would be the most adequate approach to investigate this issue.

Finally, attention alone was also capable of modulating oscillation frequency. We trained a monkey to selectively pay attention to one of the surfaces of the plaid (i.e. to one of the grating components). Depth-ordered plaids were used for this experiment (Thiele and Stoner, 2003). The stimulus was built so as to be perceived as one surface sliding over the other (component motion). This was made possible because the uppermost grating was brighter. Additionally, it occluded the darker bars of the underlying grating. When the monkey paid attention to the uppermost grating,

the oscillation frequency decreased and approached the value obtained for the single grating condition. When the monkey paid attention to the underlying grating, oscillation frequency increased, as in the experiment described above where the contrast of the background grating was made higher.

Overall, results discussed above suggest that gamma oscillations in monkey V1 are strongly dependent on cortical architecture (Lamme and Spekreijse, 1998; Palanca and DeAngelis, 2005). Despite this fact, it is interesting to observe that oscillation frequency in V1 can be modulated by selective attention. More specifically, it can be modulated by orienting attention to a particular surface of the stimulus. In another set of experiments, we observed that gamma power, but not oscillation frequency, could be strongly modulated by orienting attention in time.

6.4 - ORIENTATING ATTENTION IN TIME

Studies have shown that directing attention in space or to specific stimulus features can modulate both power and coherence of gamma activity in monkey area V4 (Fries *et al.*, 2001; Bichot *et al.*, 2005; Taylor *et al.*, 2005). We investigated if gamma activity could also be modulated by orienting attention in time. We recorded, however, from area V1, which is the primary stage of visual processing in the cortex. Investigations in this field have been primarily done using functional imaging in humans (Coull and Nobre, 1998; Nobre, 2001). Ghose and Maunsell (2002), however, analyzed firing rate activity in area V4 while monkeys changed their expectations with respect to the timing of relevant trial events. Indeed, V4 neurons increased their firing rate during trial periods where expectation was high.

Here, the monkeys were trained in three types of protocols (sequence-, block- and cue-protocol; see also Appendix for results on a figure detection task). The common feature to all protocols was that they had predictable time schedules. More specifically, the monkeys could predict in time when the behaviorally relevant trial event (change in fixation point color) would occur. In order for the monkey to receive the liquid reward, it had to release the lever immediately after the fixation point changed color. In this way, the monkeys created expectations of future trial events. For some of the protocols, we occasionally presented catch-trials. As a result, the change in fixation point color changed earlier than usual in the trial. For these cases, reaction time was significantly slower, demonstrating that the monkey's expectation was frustrated (i.e. it was caught by surprise). The frequency of microsaccades was another behavioral measure that reflected the monkey's expectation. Microsaccade rate decreased during periods where the probability of fixation point change increased, suggesting that the monkey selectively engaged attention in time. For all three

protocols the monkey was required to perform a detection task (detect a color change). Since this took place at the fixation point, it consisted in a foveal detection task. We recorded from receptive fields with visual representation near ($\sim 2^\circ$) and far away ($\sim 13^\circ$) from the fovea. Therefore, we were able to evaluate changes in neuronal activity for regions in the visual field that were spatially near and distant from the monkey's focus of attention. We observed robust and systematic increases in gamma power for trial periods where expectation was high. Correlations in the gamma band, as measured by coherence methods, also increased with expectation. Interactions remained relatively local, however, following the pattern already described above. Associated with gamma enhancement, we found simultaneous suppression of alpha activity. Interestingly, the observed modulation in firing rates by temporal expectation was small or non-existent. An important aspect of these results is that, contrary to the effects of selective attention discussed above, orientating attention in time induced no systematic changes in oscillation frequency. We believe this has to do with the influence of stimulus features on oscillation frequency. Selective attention to certain features acts by further enhancing this influence on neuronal activity. Orientating attention in time, however, does not explicitly direct attention to any feature of the stimulus.

Since the monkey performed a foveal task, we hypothesized that the modulation of oscillatory activity would be high for receptive fields recorded near the fovea, and would be attenuated or non-existent for cortical regions representing the periphery. The results clearly indicated that this assumption was wrong. The magnitude of the effects were comparable throughout the eccentricities recorded. This is specially intriguing when one considers the V1 magnification factor. That means that at least half of area V1 is being modulated by expectation, in a condition where only the foveal representation is relevant for the task. Not only did gamma activity increase with expectation, it was differentially modulated depending on the orientation of the grating stimulus. We observed that the strongest enhancement in gamma activity took place for the preferred orientation. Therefore, for measures of LFP gamma power, the orientation selectivity of local groups of neurons increased. This phenomenon was also observed for the gamma coherence measured between the LFP and the spiking activity. Since firing rates were poorly modulated by expectation, changes in selectivity for the spiking responses could not be truly revealed. Finally, we observed that oscillatory activity could also be modulated by more abstract concepts such as reward value. When the monkey was able to predict the value of the reward that would be given at the end of the trial, oscillatory activity was accordingly modulated.

Gamma band synchronization has been associated with activated brain states (Munk *et al.*, 1996; Herculano-Houzel *et al.*, 1999). Therefore, it is possible that orienting attention in time uses a neural substrate similar to the one responsible for shifting the brain between different states of activation. There are at least two similarities between the results presented here and the ones reported by

Munk *et al.* (1996) and Herculano-Houzel *et al.* (1999). First, activated brain states were associated with enhanced gamma synchronization and concomitant power suppression at lower frequencies. This was also the pattern we observed for states of high expectation. Second, both in their work and in the results presented here, modulation of oscillatory activity was widespread in the primary visual cortex. It is unclear from the results of Herculano-Houzel *et al.* (1999) of how fast the brain can switch between different states. The authors studied either spontaneous fluctuation of brain states, or the effects of lengthy periods of MRF stimulation. Both events take place in the order of minutes or hours. In our results, modulation of oscillatory activity could occur in a relatively fast time scale. In the cue-protocol, for example, changes in oscillatory activity took place within a few hundreds of milliseconds. Rodriguez *et al.* (2004) demonstrated that activated cortical states require the action of muscarinic receptors in the cortex. It would be interesting to see if the expectation effect we describe in V1 is also dependent on this receptor type.

In our results, orienting attention in time was only able to modulate V1 gamma activity when a visual stimulus was displayed over the receptive fields. In the absence of visual stimulation (blank screen), only a weak suppression of alpha power could be observed. A recent work investigating a very similar phenomenon in monkey V1 arrived at somewhat curious results (Sirotin and Das, 2009). The authors studied the hemodynamic response when monkeys anticipated upcoming trial events. The experiments, however, were performed with only a small fixation point in an otherwise dark room. Despite strong hemodynamic modulation in regard to temporal expectation, no changes in firing rates or gamma activity were observed. Moore and Cao (2008) have suggested that alterations in blood perfusion can take place prior to changes in neuronal activity. Hemodynamic responses could thereby serve a modulatory role, instead of a simple supportive role to brain activation. Tasks involving expectation may prove particularly useful when devising experiments to address this hypothesis.

6.5 - BINDING-BY-SYNCHRONIZATION (BBS) IN V1 OF THE BEHAVING MONKEY

Oscillations should depend on stimulus properties, but in a very special way (Gray *et al.*, 1989; Singer and Gray, 1995; Singer, 1999b). The activity of single cells, for example, can be well characterized by events taking place within its classical receptive field. In this way, single unit activity essentially reflects the local properties of the visual stimulus. Oscillations too will be influenced by local features, specially if measurements are made from small groups of neurons. But as a candidate for a relational code, oscillatory activity from larger populations should necessarily reflect the global properties of the stimulus. This hypothesis has been successfully addressed

several times before (Gray *et al.*, 1989; Engel *et al.*, 1991; Kreiter and Singer, 1996; Castelo-Branco *et al.*, 2000). Recent work, however, has not been able to confirm earlier findings (Lamme and Spkreijse, 1998; Thiele and Stoner, 2003; Palanca and DeAngelis, 2005). We decided to address this issue in monkey area V1 using plaid stimuli. As discussed above, physical manipulations of the grating components making up a plaid can bias perception to component motion (two objects sliding over each another) or to pattern motion (a single moving object). Recording from pairs of sites that selectively respond to either of the component gratings provides an ingenious method for testing the BBS hypothesis (Castelo-Branco *et al.*, 2000). V1 is an interesting area to test the BBS hypothesis because, based on the analysis of firing rates, only a few of its neurons are capable of integrating stimulus motion (Guo *et al.*, 2004). Synchronous activity in V1, converging onto single neurons in downstream areas, could thereby explain the pattern-motion sensitivity of single MT cells (Movshon *et al.*, 1985). The tests we performed were basically two. If the V1 sites respond to the same grating, they should remain synchronizing their activity regardless of whether the plaid is perceived as having component or pattern motion. As a matter of fact, they should remain synchronizing regardless if the second component is present at all. This is because, in any of the cases, the pair of sites are responding to the same object. The second test deals with the case where each site responds to one of the two grating components. They should synchronize their activity only when presented with pattern motion, since only in this condition do they respond to the same object. Our results did not comply with the predictions of neither of the two tests. As already discussed above, superimposing two grating stimuli considerably decreased the power and coherence of gamma oscillations. The first test predicted otherwise, that synchronization should not be affected when adding the second grating. The second test was generally more difficult to carry out. This was because it required a special combination of orientation selectivities during the session, where each recording site matched one of the grating components. For these experiments, results involving the spiking activity were systematically negative, whereas correlations involving the LFP were inconsistent.

A major concern during our experiments was that the monkey was not attending to the visual stimulus, thereby explaining our negative results. Ideally, we should have trained the monkeys to report whether they perceived component or pattern motion while simultaneously recording in V1. This we did not do. We did, however, train one monkey to pay attention to one of the surfaces of a component plaid stimulus. Therefore, we could repeat our first test but now making sure that the monkey was indeed perceiving that surface. There were no major differences in gamma activity between the tasks with and without attention, except for the changes in oscillation frequency already discussed. Similar experiments, but using Gestalt figures made up of Gabor patches, were also performed in order to test the BBS hypothesis in V1. They also yielded negative results (data not shown).

Once again, our results indicate that gamma activity in area V1 is very sensitive to the local but not to the global properties of the stimulus. This might be related to the finding that gamma interactions in V1 are rather local and heavily dependent on cortical architecture. Alternatively, it might indeed be the case that area V1 is more concerned with representing the external world in fine detail rather than establishing links between the various stimulus features. Accordingly, binding would be left to higher level areas capable of better integrating information across space. Another possibility is that our analysis methods were inadequate for detecting fast and non-stationary epochs of synchronous activity in area V1. A recent work in the primary visual cortex suggests that this may indeed be the case. Maldonado *et al.* (2008) recorded spiking activity from multiple sites in area V1 of the freely viewing monkey. The authors observed that synchronization events took place shortly after the monkey fixated, and lasted only a few tens of milliseconds. It is therefore likely that future investigations on this issue will require more sophisticated analysis tools than the ones employed here.

6.6 - THE BRAIN AS AN ANALOGUE OPERATOR

The initial description of the hippocampal theta phase precession by O'Keefe and Recce (1993) introduced a new framework of how the timing of the all-or-none spike event could encode information. More specifically, the precise timing of the spike event relative to the ongoing theta cycle could provide graded information regarding the rat's position within the place field. Harris *et al.* (2002) generalized these findings by demonstrating that phase precession is not unique to spatial tasks, but is a general property of neuronal activity. Hence, higher discharge rates are systematically associated with earlier firing relative to the theta cycle. In this way, phase precession is a potential mechanism capable of transforming a rate code into a temporal code (Mehta *et al.*, 2002).

While theta activity is a prominent rhythm in rodent hippocampus (Burgess and O'Keefe, 2005), gamma oscillations are ubiquitous in the mammalian neocortex (Fries, 2009). Could gamma activity in the early visual cortex subservise a similar type of phenomenon as the theta phase precession described for the hippocampus? We investigated this issue by recording LFP and spiking activity from area V1 of the fixating monkey. While fixating, monkeys were presented with moving gratings in 8 different orientations. The timing of the spike relative to the LFP gamma oscillation shifted as a function of the neuronal activation strength. Neurons that were strongly activated spiked earlier in the gamma cycle, a phenomenon we called gamma-phase shifting. The phase of the spike in the gamma cycle provided thereby an instantaneous analog representation of neuronal excitation.

Looking into the mechanisms of how gamma oscillations are generated in the cortex provides insight into how gamma-phase shifting may impact neuronal processing. The gamma cycle can be viewed as rhythmic waves of inhibition imposed by the local network of interneurons on groups of pyramidal cells (Csicsvari *et al.*, 2003; Hasenstaub *et al.*, 2005). An equally relevant feature of the gamma cycle, however, is that the excitatory drive to the inhibitory interneurons is mainly provided by the pyramidal cells (Fries *et al.*, 2007). The reciprocal interactions between the two classes of neurons enable a mechanism capable of increasing the signal-to-noise ratio in the following way. Spikes arising from strong activation occur earlier on the gamma cycle. By providing subsequent excitatory input to the interneurons, they would contribute to the initiation of the next inhibitory wave. In this way, inhibition prevents neurons with weaker excitatory drive (i.e. arriving later in the gamma cycle) from firing. For the same reasons, spikes occurring earlier in the gamma cycle will have enhanced impact on postsynaptic neurons.

Gamma-phase shifting in V1 seems to result from the interplay between neuronal excitation and gamma-rhythmic synaptic input. Potentially, it could assist neuronal processing by selecting only those inputs with the strongest excitatory drive. This property fits well with the finding that gamma processes are rather local in V1. It therefore provides a different perspective on the role of gamma activity in the brain. Acting locally, this mechanism does not necessarily require correlations of gamma activity among spatially distributed sites. We tested gamma-phase shifting in conditions where excitatory drive changed considerably (i.e. different stimulus orientations). It would be interesting to investigate if selective attention can also bias neuronal processing through mechanisms of gamma-phase shifting. Namely, to verify if attention to a stimulus feature could force spikes to fire earlier in the gamma cycle thereby increasing their impact on downstream neurons. This hypothesis could have been tested in the selective attention paradigm where the monkey paid attention to one of the two plaid surfaces. As mentioned, we did not find any modulation in gamma power as a function of attended surface. However, neurons that responded to the grating representing the attended surface could have had its spikes pushed to earlier phases of the gamma cycle. In this way, attention could still modulate neuronal processing but without any changes in firing rate nor gamma power.

6.7 - CONCLUDING REMARKS

We performed an extensive set of experiments to investigate the role of gamma processes in monkey area V1. Experiments on surface segmentation were carried out using different configurations of plaid stimuli. Based on the binding-by-synchronization hypothesis, we made

predictions on how neurons in area V1 should synchronize their activity depending on stimulus configuration and, therefore, on perception. None of our predictions held, regardless of whether the monkey passively viewed the stimulus or actively attended to one of its surfaces. Consequently, gamma activity was predominantly dependent on the local properties of the stimulus, and not on its global properties as we had initially hypothesized. On the other hand, we observed that gamma activity in the primary visual cortex seems to be highly dependent on cortical architecture. We described several stimulus parameters capable of modulating both gamma power and gamma oscillation frequency. In all cases, the nature of the modulation could be satisfactorily explained by the functional organization of the early visual cortex.

In accordance with several recently published studies, we found that attention can strongly modulate gamma activity. We here describe that directing attention in time impacts both gamma power and coherence in monkey V1. Gamma activity was systematically enhanced during conditions of higher temporal expectation. Concomitant to gamma increases, we observed an associated alpha power suppression. Additionally, modulation of oscillatory activity was shown to be widespread in V1. Finally, similar to the hippocampal theta phase precession, we report gamma-phase shifts in V1. We argue that this phenomenon may be a potentially important mechanism for neuronal processing.

6.8 - REFERENCES

- Adelson EH, Movshon JA. 1982. Phenomenal coherence of moving visual patterns. *Nature*. **300**: 523-525.
- Barlow HB. 1972. Single units and sensation: A neuron doctrine for perceptual psychology? *Perception*. **1**: 371-394.
- Bichot NP, Rossi AF, Desimone R. 2005. Parallel and serial neural mechanisms for visual search in macaque area V4. *Science*. **308**: 529-534.
- Burgess N, O'Keefe J. 2005. The theta rhythm. *Hippocampus*. **15**: 825-826.
- Buzsáki G, Draguhn A. 2004. Neuronal oscillations in cortical networks. *Science*. **304**: 1926-1929.
- Castelo-Branco M, Goebel R, Neuenschwander S, Singer W. 2000. Neural synchrony correlates with surface segregation rules. *Nature*. **405**: 685-689.
- Coull JT, Nobre AC. 1998. Where and when to pay attention: the neural systems for directing attention to spatial locations and to time intervals as revealed by both PET and fMRI. *J. Neurosci*. **18**: 7426-7435.
- Csicsvari J, Jamieson B, Wise KD, Buzsáki G. 2003. Mechanisms of gamma oscillations in the hippocampus of the behaving rat. *Neuron*. **37**: 311-322.

- Daniel PM, Whitteridge D. 1961. The representation of the visual field on the cerebral cortex in monkeys. *J. Physiol. (London)* **159**: 203-221.
- Desimone R, Albright TD, Gross CG, Bruce C. 1984. Stimulus-selective properties of inferior temporal neurons in the macaque. *J. Neurosci.* **4**: 2051-2062.
- Eckhorn R, Bauer R, Jordan W, Brosch M, Kruse W, Munk M, Reitboeck HJ. 1988. Coherent oscillations: a mechanism of feature linking in the visual cortex? Multiple electrode and correlation analyses in the cat. *Biol. Cybern.* **60**: 121-130.
- Engel AK, König P, Gray CM, Singer W. 1990. Stimulus-Dependent Neuronal Oscillations in Cat Visual Cortex: Inter-Columnar Interaction as Determined by Cross-Correlation Analysis. *Eur. J. Neurosci.* **2**: 588-606.
- Engel AK, König P, Singer W. 1991. Direct physiological evidence for scene segmentation by temporal coding. *Proc. Natl. Acad. Sci. U.S.A.* **88**: 9136-9140.
- Franks N. 2008. General anaesthesia: from molecular targets to neuronal pathways of sleep and arousal. *Nat. Rev. Neurosci.* **9**: 370-386.
- Friedman-Hill S, Maldonado PE, Gray CM. 2000. Dynamics of striate cortical activity in the alert macaque: I. Incidence and stimulus-dependence of gamma-band neuronal oscillations. *Cereb. Cortex.* **10**: 1105-1116.
- Fries P. 2005. A mechanism for cognitive dynamics: neuronal communication through neuronal coherence. *Trends. Cogn. Sci.* **9**: 474-480.
- Fries P. 2009. Neuronal gamma-band synchronization as a fundamental process in cortical computation. *Annu. Rev. Neurosci.* **32**: 209-224.
- Fries P, Nikolic D, Singer W. 2007. The gamma cycle. *Trends Neurosci.* **30**: 309-316.
- Fries P, Reynolds JH, Rorie AE, Desimone R. 2001. Modulation of oscillatory neuronal synchronization by selective visual attention. *Science.* **291**: 1560-1563.
- Fries P, Roelfsema PR, Engel AK, König P, Singer W. 1997. Synchronization of oscillatory responses in visual cortex correlates with perception in interocular rivalry. *Proc. Natl. Acad. Sci. U.S.A.* **94**: 12699-12704.
- Gattass R, Sousa APB, Rosa MGP. 1987. Visual topography of V1 in the *Cebus* monkey. *J. Comp. Neurol.* **259**: 529-548.
- Ghose GM, Maunsell JHR. 2002. Attentional modulation in visual cortex depends on task timing. *Nature.* **419**: 616-620.
- Gray CM, Di Prisco GV. 1997. Stimulus-dependent neuronal oscillations and local synchronization in striate cortex of the alert cat. *J. Neurosci.* **17**: 3239-3253.
- Gray CM, Engel AK, König P, Singer W. 1990. Stimulus-Dependent Neuronal Oscillations in Cat Visual Cortex: Receptive Field Properties and Feature Dependence. *Eur. J. Neurosci.* **2**: 607-619.
- Gray CM, König P, Engel AK, Singer W. 1989. Oscillatory responses in cat visual cortex exhibit inter-columnar synchronization which reflects global stimulus properties. *Nature.* **338**: 334-337.

- Gray CM, Singer W. 1989. Stimulus-specific neuronal oscillations in orientation columns of cat visual cortex. *Proc. Natl. Acad. Sci. U.S.A.* **86**: 1698-1702.
- Greenberg DS, Houweling AR, Kerr JN. 2008. Population imaging of ongoing neuronal activity in the visual cortex of awake rats. *Nat. Neurosci.* **11**: 749-751.
- Gross CG, Bender DB, Rocha-Miranda CE. 1969. Visual receptive fields of neurons in inferotemporal cortex of the monkey. *Science.* **166**: 1303-1306.
- Guo K, Benson PJ, Blakemore C. 2004. Pattern motion is present in V1 of awake but not anaesthetized monkeys. *Eur. J. Neurosci.* **19**: 1055-1066.
- Harris KD. 2005. Neural signatures of cell assembly organization. *Nat. Rev. Neurosci.* **6**: 399-407.
- Harris KD, Henze DA, Hirase H, Leinekugel X, Dragoi G, Czurkó A, Buzsáki G. 2002. Spike train dynamics predicts theta-related phase precession in hippocampal pyramidal cells. *Nature.* **417**: 738-741.
- Hasenstaub A, Shu Y, Haider B, Kraushaar U, Duque A, McCormick DA. 2005. Inhibitory postsynaptic potentials carry synchronized frequency information in active cortical networks. *Neuron.* **47**: 423-435.
- Herculano-Houzel S, Munk MH, Neuenschwander S, Singer W. 1999. Precisely synchronized oscillatory firing patterns require electroencephalographic activation. *J. Neurosci.* **19**: 3992-4010.
- Horton JC, Adams DL. 2005. The cortical column: a structure without a function. *Philos. Trans. R. Soc. London Ser. B.* **360**: 837-862.
- Hubel DH, Wiesel TN. 1959. Receptive fields of single neurones in the cat's striate cortex. *J. Physiol. (London)* **148**: 574-591.
- Hubel DH, Wiesel TN. 1979. Brain mechanisms of vision. *Sci. Am.* 150-162.
- Jarvis MR, Mitra PP. 2001. Sampling properties of the spectrum and coherency of sequences of action potentials. *Neural Comput.* **13**: 717-749.
- Kaschube M, Wolf F, Geisel T, Löwel S. 2002. Genetic influence on quantitative features of neocortical architecture. *J. Neurosci.* **22**: 7206-7217.
- Kreiter AK, Singer W. 1996. Stimulus-dependent synchronization of neuronal responses in the visual cortex of the awake macaque monkey. *J. Neurosci.* **16**: 2381-2396.
- Lakatos P, Shah AS, Knuth KH, Ulbert I, Karmos G, Schroeder CE. 2005. An oscillatory hierarchy controlling neuronal excitability and stimulus processing in the auditory cortex. *J. Neurophysiol.* **94**: 1904-1911.
- Lamme VA, Spekreijse H. 1998. Neuronal synchrony does not represent texture segregation. *Nature.* **396**: 362-366.
- Linkenkaer-Hansen K, Smit DJ, Barkil A, van Beijsterveldt TE, Brussaard AB, Boomsma DI, van Ooyen A, de Geus EJ. 2007. Genetic contributions to long-range temporal correlations in ongoing oscillations. *J. Neurosci.* **27**: 13882-13889.
- Logothetis NK. 2003. The underpinnings of the BOLD functional magnetic resonance imaging signal. *J. Neurosci.* **23**: 3963-3971.

- London M, Häusser M. 2005. Dendritic computation. *Annu. Rev. Neurosci.* **28**: 503-532.
- Maldonado P, Babul C, Singer W, Rodriguez E, Berger D, Grun S. 2008. Synchronization of Neuronal Responses in Primary Visual Cortex of Monkeys Viewing Natural Images. *J. Neurophysiol.* **100**: 1523-1532.
- Maldonado PE, Friedman-Hill S, Gray CM. 2000. Dynamics of striate cortical activity in the alert macaque: II. Fast time scale synchronization. *Cereb. Cortex.* **10**: 1117-1131.
- Mehta MR, Lee AK, Wilson MA. 2002. Role of experience and oscillations in transforming a rate code into a temporal code. *Nature.* **417**: 741-746.
- Moore CI, Cao R. 2008. The hemo-neural hypothesis: on the role of blood flow in information processing. *J. Neurophysiol.* **99**: 2035-2047.
- Movshon JA, Adelson EH, Gizzi MS, Newsome WT. 1985. The analysis of moving visual patterns. In *Study Week on Pattern Recognition Mechanisms*, ed. C Chagas, R Gattass, C Gross, 54: 117-151. Pont. Acad. Scient. Scrip. Varta. Vatican Press.
- Munk MH, Roelfsema PR, König P, Engel AK, Singer W. 1996. Role of reticular activation in the modulation of intracortical synchronization. *Science.* **272**: 271-274.
- Muthukumaraswamy SD, Edden RA, Jones DK, Swettenham JB, Singh KD. 2009. Resting GABA concentration predicts peak gamma frequency and fMRI amplitude in response to visual stimulation in humans. *Proc. Natl. Acad. Sci. U.S.A.* **106**: 8356-8361.
- Muthukumaraswamy SD, Singh KD, Swettenham JB, Jones DK. 2010. Visual gamma oscillations and evoked responses: variability, repeatability and structural MRI correlates. *Neuroimage.* **49**: 3349-3357.
- Niessing J, Ebisch B, Schmidt KE, Niessing M, Singer W, Galuske RA. 2005. Hemodynamic signals correlate tightly with synchronized gamma oscillations. *Science.* **309**: 948-951.
- Nobre AC. 2001. Orienting attention to instants in time. *Neuropsychologia.* **39**: 1317-1328.
- O'Keefe J, Recce ML. 1993. Phase relationship between hippocampal place units and the EEG theta rhythm. *Hippocampus.* **3**: 317-330.
- Palanca BJ, DeAngelis GC. 2005. Does neuronal synchrony underlie visual feature grouping? *Neuron.* **46**: 333-346.
- Pesaran B, Pezaris JS, Sahani M, Mitra PP, Andersen RA. 2002. Temporal structure in neuronal activity during working memory in macaque parietal cortex. *Nat. Neurosci.* **5**: 805-811.
- Rodriguez E, George N, Lachaux JP, Martinerie J, Renault B, Varela FJ. 1999. Perception's shadow: long-distance synchronization of human brain activity. *Nature.* **397**: 430-433.
- Rodriguez R, Kallenbach U, Singer W, Munk MHJ. 2004. Short- and long-term effects of cholinergic modulation on gamma oscillations and response synchronization in the visual cortex. *J. Neurosci.* **24**: 10369-10378.
- Roelfsema PR, Engel AK, König P, Singer W, 1997. Visuomotor integration is associated with zero time-lag synchronization among cortical areas. *Nature.* **385**: 157-161.

- Roelfsema PR, König P, Engel AK, Sireteanu R, Singer W. 1994. *Eur. J. Neurosci.* **6**: 1645-1655.
- Schoffelen JM, Oostenveld R, Fries P. 2005. Neuronal coherence as a mechanism of effective corticospinal interaction. *Science.* **308**: 111-113.
- Shimizu T, Bowers AN. 1999. Visual circuits of the avian telencephalon: evolutionary implications. *Behav. Brain Res.* **98**: 183-191.
- Singer W. 1993. Synchronization of cortical activity and its putative role in information processing and learning. *Annu. Rev. Physiol.* **55**: 349-374.
- Singer W. 1999a. Time as coding space? *Curr. Opin. Neurobiol.* **9**: 189-194.
- Singer W. 1999b. Neuronal synchrony: a versatile code for the definition of relations? *Neuron.* **24**: 49-65, 111-125.
- Singer W, Gray CM. 1995. Visual feature integration and the temporal correlation hypothesis. *Ann. Rev. Neurosci.* **18**: 555-586.
- Sirotin YB, Das A. 2009. Anticipatory haemodynamic signals in sensory cortex not predicted by local neuronal activity. *Nature.* **457**: 475-479.
- Taylor K, Mandon S, Freiwald WA, Kreiter AK. 2005. Coherent oscillatory activity in monkey area v4 predicts successful allocation of attention. *Cereb. Cortex.* **15**: 1424-1437.
- Thiele A, Stoner G. 2003. Neuronal synchrony does not correlate with motion coherence in cortical area MT. *Nature.* **421**: 366-370.
- Wang G, Tanaka K, Tanifuji M. 1996. Optical imaging of functional organization in the monkey inferotemporal cortex. *Science.* **272**: 1665-1668.
- Womelsdorf T, Schoffelen JM, Oostenveld R, Singer W, Desimone R, Engel AK, Fries P. 2007. Modulation of neuronal interactions through neuronal synchronization. *Science.* **316**: 1609-1612.

Appendix

Reprint of Uhlhass PJ, Pipa G, Lima B, Melloni L, Neuenschwander S, Nikolic D, Singer W. (2009). Neural synchrony in cortical networks: history, concept and current status. *Front. Integr. Neurosci.* **3**: 1-19.

For this work I participated in the section entitled: “Building expectations: new vistas for gamma oscillations”.



Neural synchrony in cortical networks: history, concept and current status

Peter J. Uhlhaas^{1,2}, Gordon Pipa^{1,3}, Bruss Lima¹, Lucia Melloni¹, Sergio Neuenschwander¹, Danko Nikolić^{1,3} and Wolf Singer^{1,3*}

¹ Department of Neurophysiology, Max Planck Institute for Brain Research, Frankfurt am Main, Germany

² Laboratory for Neurophysiology and Neuroimaging, Department of Psychiatry, Johann Wolfgang Goethe Universität, Frankfurt am Main, Germany

³ Frankfurt Institute for Advanced Studies, Johann Wolfgang Goethe Universität, Frankfurt am Main, Germany

Edited by:

Rui M. Costa, Champalimaud
Neuroscience Programme, Instituto
Gulbenkian de Ciência, Portugal

Reviewed by:

Miles A. Whittington, Newcastle
University, UK
Shih-Chieh Lin, Duke University
Medical Center, USA

*Correspondence:

Wolf Singer, Department of
Neurophysiology, Max Planck Institute
for Brain Research, Deutschordenstr.
46, Frankfurt am Main 60528,
Germany.
e-mail: singer@mpih-frankfurt.mpg.de

Following the discovery of context-dependent synchronization of oscillatory neuronal responses in the visual system, the role of neural synchrony in cortical networks has been expanded to provide a general mechanism for the coordination of distributed neural activity patterns. In the current paper, we present an update of the status of this hypothesis through summarizing recent results from our laboratory that suggest important new insights regarding the mechanisms, function and relevance of this phenomenon. In the first part, we present recent results derived from animal experiments and mathematical simulations that provide novel explanations and mechanisms for zero and non-zero phase lag synchronization. In the second part, we shall discuss the role of neural synchrony for expectancy during perceptual organization and its role in conscious experience. This will be followed by evidence that indicates that in addition to supporting conscious cognition, neural synchrony is abnormal in major brain disorders, such as schizophrenia and autism spectrum disorders. We conclude this paper with suggestions for further research as well as with critical issues that need to be addressed in future studies.

Keywords: synchrony, oscillations, gamma, cortex, cognition

INTRODUCTION

NEURAL SYNCHRONY IN CORTICAL NETWORKS

The cerebral cortex is a highly distributed system in which numerous areas operate in parallel, exchange their results via reciprocal recurrent connections and through self-organizing dynamics create coherent states that are equivalent with representations of sensory objects, decisions and programs for motor acts. The topology of the connectivity shares properties with small world networks which implies that there are certain areas which sustain more connections than others (hubs) but that there is no singular center where all information converges and which would be in a position to serve as a supraordinate coordinating center. This raises a number of important questions: i) how are the numerous computations occurring simultaneously in spatially segregated processing areas coordinated and bound together to give rise to coherent percepts and actions, ii) how are input signals selected for further processing and how are the results of sensory processes routed selectively across the densely connected network to executive structures and finally, iii) how are the often graded relations between simultaneously represented contents encoded. In principle, there are two different solutions to these problems. First, devoted architectures of connections that assume coordinating and binding functions through convergence and divergence of labelled lines, and second, dynamics that allow for the self-organization of ever changing spatio-temporal activity patterns on the backbone of fixed anatomical connections. These two strategies are not mutually exclusive but can coexist and complement one another. In the review we shall concentrate on the second strategy and here, in particular, on coordinating mechanisms that rely on the temporal patterning of neuronal activity and

comprise phenomena such as self-generated network oscillations, synchronization and phase locking.

An important link between temporal patterning of neuronal activity and cortical computations was the discovery that oscillatory rhythms in the beta/gamma range (20–80 Hz) serve to establish precise and context dependent temporal relations – in this case synchrony – between distributed neural discharges. Gray et al. (1989) showed that action potentials generated by cortical cells align with the oscillatory rhythm which has the consequence that neurons phase locked to synchronized oscillations, synchronize their discharges with high precision. More recent evidence indicates that these oscillations are not only instrumental for the synchronization of neuronal discharges but can support also other consistent temporal relations by establishing systematic phase lags between the discharges of distributed neurons. *In-vitro* studies (Volgushev et al., 1998) and multi-site recordings in the visual cortex of cats (Fries et al., 2001b) provided evidence, that the oscillatory patterning of neuronal activity is an efficient mechanism to adjust the precise timing of spikes and is potentially a versatile mechanism to convert rate coded input to cells into a temporal code defined by the time of occurrence of spikes relative to the oscillation cycle (see also Fries et al., 2007).

Following the initial descriptions of context dependent synchronization in the visual cortex, numerous studies have been initiated in order to investigate the functional role of this phenomenon. These have demonstrated that response synchronization is a ubiquitous phenomenon in cortical networks and likely to serve a variety of different functions in addition to feature binding at early levels of sensory processing.

Studies in the motion sensitive area MT of the visual cortex of awake monkeys (Kreiter and Singer, 1996), the optic tectum of pigeons (Neuenschwander et al., 1996), other cortical areas in the cat (Engel et al., 1991) and the retina (Neuenschwander and Singer, 1996) provided evidence that the oscillatory patterning of neuronal responses and the synchronization of these oscillations is highly sensitive to context. Combining multi-site recordings with the sectioning of the corpus callosum (Engel et al., 1991) and with developmental studies (König et al., 1993; Löwel and Singer, 1992) indicated that the long distance synchronization of oscillatory responses is mediated to a substantial extent by the network of reciprocal cortico-cortical connections. Multi-site recordings also provided evidence that synchronization occurs between widely distributed structures, such as the primary visual cortex, the optic tectum and the suprasylvian cortex (Brecht et al., 1998) and that it plays a role in the coordination of widely distributed functions as is required e.g. in sensory-motor processing (Roelfsema et al., 1997). This latter study indicated further that synchronized oscillatory activity is not only stimulus driven but also generated in anticipation of a visual discrimination task requiring fast motor responses. This observation led to the hypothesis that self-generated oscillatory activity in the beta- and gamma frequency range could be a correlate of focused attention and serve both modality specific selection of stimuli and the coordination of sensory and executive subsystems required for the execution of the anticipated task. A close relation between synchronization and input selection has also been found in experiments on binocular rivalry (Fries et al., 2001a).

The notion of an involvement of synchronized beta- and gamma oscillations in attention dependent processes agrees also with the evidence that there is a close relation between arousal, activated cortical states and the occurrence of high frequency oscillations. Gamma oscillations occur only with activated cortical states and require for their expression activation of muscarinic receptors in the cortex (Herculano-Houzel et al., 1999; Munk et al., 1996).

Taken together, the results suggested that synchronization enhances the saliency of the synchronized responses which can in turn be used for a variety of different operations. Joint increases of saliency favour joint selection and processing of signals which can in principle support attention dependent stimulus selection and feature binding.

The notion that the saliency of responses can be enhanced in a complementary way either by increases of discharge rate or by synchronization has later received direct support from experiments on apparent brightness perception (Biederlack et al., 2006).

THE GENERATION OF NEURAL SYNCHRONY

The discovery of synchronized oscillations has motivated a large number of *in-vitro* studies searching for the mechanisms that would generate these oscillations and this led to a re-evaluation of the functional role of inhibitory interneurons. Classically, inhibition has been considered as a mechanism for gain control, contrast enhancement and improvement of signal to noise ratios. *In-vitro* investigations of oscillating networks demonstrated, however, that the network of inhibitory interneurons plays a crucial role in the rhythmic pacing of neuronal activity. Through this additional function they assume a pivotal role in the temporal structuring and

coordination of neuronal responses (Cardin et al., 2009; Sohal et al., 2009; for a review see Bartos et al., 2007).

These experimental results on oscillatory neuronal networks have motivated a large number of theoretical studies investigating the functional properties of networks capable of engaging in oscillations and stimulus dependent synchronization patterns. These studies provided deep insights into both the mechanisms that sustain oscillations and their synchronization as well as the putative functions of the temporal coding strategies that can be implemented in networks of coupled oscillators with essentially non-linear dynamics (Traub et al., 2004).

STUDIES IN HUMAN SUBJECTS

Non invasive electrophysiological methods such as EEG and MEG recordings register preferentially if not exclusively synchronized neuronal activity because they average over large populations of neurons. Thus, non-synchronized sources of activity tend to cancel out and synchronized signals are enhanced. This, together with the ease to perform demanding psychophysical experiments, is one of the reasons why investigations on synchronized oscillations and their putative function have been particularly rewarding in human subjects. These studies provided rapidly growing evidence for a close relation between synchronous oscillatory activity in the beta- and gamma frequency range and a variety of cognitive functions such as perceptual grouping, focused attention, maintenance of contents in short term memory, poly-sensory integration, formation of associative memories and sensory motor coordination (for review see Singer, 2004; Tallon-Baudry, 2009).

THE SCOPE OF THE PRESENT REVIEW

Despite the abundant evidence for close correlations between oscillatory activity and a wide range of physiological and psychological phenomena, we are still far from understanding the full implications of the complex dynamics expressed in networks capable of engaging in oscillatory activity in various frequency bands. Numerous observations support the hypothesis that oscillations and synchrony are the backbone of temporal coding strategies but most of the evidence is still correlative in nature. Therefore, search for the functional implications of self-organized temporal patterning of neuronal activity is pursued by an increasing number of laboratories both at the experimental and theoretical level.

In the present review, we provide an update of results obtained in our lab that suggest novel mechanisms for the temporal coordination of distributed neuronal-responses and extend the scope of functions subserved by synchronized oscillatory activity. In this context we present results derived from animal experiments and mathematical simulations that provide explanations for the conundrum that nerve nets with finite conduction delays can synchronize with zero-phase lag (see 'Theoretical Approach' by Pipa). In addition, we discuss evidence that suggests that small delays between spikes occurring in synchrony with gamma oscillations contain stimulus related information (see 'Novel Empirical Results on Temporal Coding' by Nikolić). Next we present novel data on the relationship between attention, expectancy and gamma oscillations (see 'Building Expectations: New Vistas for Gamma Oscillations' by Lima and Neuenschwander) and the relation between phase locking of high frequency oscillations and consciousness (see 'Neural

Synchrony as a Mechanism for Conscious Perception?' by Melloni). Finally, we investigate the relevance of synchronous oscillations in the context of psychiatric syndromes and report recent data which indicate that neural synchrony is abnormal in major psychiatric diseases such as schizophrenia and autism spectrum disorders that are associated with altered states of consciousness and dysfunctional cognition (see 'Neural Synchrony in Schizophrenia and Autism Spectrum Disorders' by Uhlhaas).

In the final part of the paper, we provide a perspective on open questions and challenges regarding the role of oscillations and synchrony and propose some empirical and theoretical strategies to cope with these questions.

MECHANISM AND CODING PROPERTIES OF SYNCHRONIZATION

One of the central problems regarding neural synchrony is the questions of how neurons can synchronise their responses with zero or near-zero phase lag synchrony. Early studies showed that zero-phase lag synchronization can occur even between distant neuronal assemblies, raising the question of the mechanistic implementation of such phenomena. This is particularly relevant as the conduction delays in cortex make the occurrence of zero-phase lag synchrony difficult to accomplish.

In the following two sections, we will summarise recent work that has used computer simulations and mathematical approaches as well as multi-unit recordings to reveal novel mechanisms of zero lag and near-zero phase synchronization. We begin this section with what is known today about the low-level mechanisms responsible for generation of neuronal synchrony and for coding information by synchronized groups of neurons. The first section 'Theoretical Approach' is mostly an overview of the theoretical work, which revealed a number of counterintuitive phenomena that could not be detected without the efforts based on mathematical analyses and computer simulations. The second section 'Novel Empirical Results on Temporal Coding' describes empirical work that helped elucidate the fundamentals of the synchrony-related operations within the neocortex.

THEORETICAL APPROACH

Mechanisms for zero lag synchrony

A special and challenging case of synchronization is zero time lag or zero phase synchronization in which the activity is modulated synchronously and either without any temporal delay or delay much smaller than the conduction delays ('near zero time lag' or 'near zero phase'). Remarkably, most neuronal synchrony was found to occur with such small phase lags between periodic or quasi-periodic dynamics (Roelfsema et al., 1997). For simplicity, the first part focuses on zero time lag synchronization exclusively. Near time zero lag synchronization is covered in later sections. However, so far only very few and highly specialized models have been able to account for zero lag synchrony in networks coupled with delay. Especially in neuronal networks these delays can be substantial due to conduction times, synaptic delays and electrotonic propagation.

Maybe the simplest mechanism to induce zero phase synchronization is entrainment via common drive from a single source, i.e. from other cortical and sub-cortical areas (Steriade et al., 1993), that synchronizes the respective target cells. In local networks, pacemaker cells with intrinsic oscillatory activity can entrain the

network activity in certain frequency range, i.e. chattering cells that have been discussed to be involved in generating stimulus driven gamma oscillations (Gray and McCormick, 1996). It is important to note that entrainment determines both the rhythm and the synchronization among the target cells. To study the limits of this simple mechanism in complex networks we modelled common drive and entrainment by an unidirectional coupling with an auxiliary hub (Huang and Pipa, 2007). The remarkable and generalizable finding was that entrainment via an auxiliary hub can always synchronize activity, and this occurs for any arbitrary coupling, e.g. linear or non-linear, for any network topology, and for a wide range of intrinsic properties of the neurons of the network. In addition, a lower bound was identified for the minimal coupling strength necessary for synchronization by entrainment. This minimal coupling strength was a function of the type of coupling between the hub and the network, but also of the properties of the network itself. Thus, the occurrence of synchronization can be controlled either by modifying the coupling of the auxiliary hub and therefore the strength of the entrainment and/or by modifications of the intrinsic properties of the neurons in the synchronized network or the coupling within this network. This suggests that even for a simple mechanism such as entrainment, the synchronization can be very dynamic, depending both on the strength of the entrainment and on numerous parameters of the complete system.

Another class of mechanisms for zero phase synchrony is emerging synchronization by network effects. This mechanism is very different from entrainment, since emerging properties are arising by the interaction of the elements in the network and cannot be explained by a single element or a subset of isolated elements alone. For zero phase synchronization based on such network effects several mechanisms have been proposed. Among these are recurrent inhibition, mutual excitation, mutual inhibition, gap junction coupling and synaptic spike doublet based coupling (Kopell et al., 2000; Ritz and Sejnowski, 1997; Van Vreeswijk et al., 1994). Especially for the biologically relevant case of non-instantaneous coupling and heterogeneous networks, the recurrent inhibition between excitatory and inhibitory sub networks was found to stabilize and induce zero phase synchronization reliably and quickly (Kopell et al., 2000; Van Vreeswijk et al., 1994). In addition, synchronization via recurrent inhibition can synchronize neuronal activity without changing the overall firing rate of the neurons (Tiesinga and Sejnowski, 2004; Buia and Tiesinga, 2006), as it was reported by many experimental studies. In contrast, instantaneous excitatory coupling was shown to favor desynchronization rather than synchrony for a broad class of models and parameter regimes (Kopell et al., 2000; Ritz and Sejnowski, 1997).

Compared to chemical coupling, the gap junction coupling is electrical and almost instantaneous. Its importance for generating oscillatory and synchronous activity was highlighted in experimental studies that demonstrated that fast oscillations can be observed even if chemical synaptic transmission is blocked (Buzsaki and Draguhn, 2004). The nature of gap junction coupling is diffusive and essentially homogenizes the membrane potential fluctuations in the network. This homogenization was shown to lead to complementary effects of electrical and chemical coupling for networks that comprises both types at the same time. It was shown that electrical and chemical coupling act similarly and add up linearly when the

coupling of both types is weak. However, due to homogenization of fluctuations of the membrane potential, even weak gap junction coupling can boost the effect of the much stronger chemical coupling (Kopell and Ermentrout, 2004). This suggests that more than a single mechanism may contribute to zero phase synchronization and demonstrates that modifications of individual mechanisms can substantially alter the synchronization patterns.

Another class of mechanisms that support zero phase synchrony is based on spikes in rapid succession, e.g. doublets of spikes (Kopell et al., 2000). The model was confirmed by experimental findings in rat hippocampus slices, which linked the firing of spike doublets by interneurons to gamma oscillations that are synchronized over several millimeters (Traub et al., 1996). However, for long range synchronization across different regions and especially across hemispheres, none of the above mentioned local mechanisms is general enough. Synchronization via spike doublets breaks down for gamma frequencies when conduction delays become large and recurrent inhibition with or without gap junction coupling is only plausible for local networks due to the topology that is dominated by local neuronal coupling.

In addition, the topology of complex networks turns out to be another very important parameter for the establishment of local and long-range synchronization. Entrainment via an auxiliary hub can be seen as an extreme case (Huang and Pipa, 2007) but topologies also play an essential role in cases of emergent synchrony. Thus, hubs in the network were proposed to shorten the path length between elements and therefore to foster fast and stable synchrony (Arecchi et al., 1999; Grinstein and Linsker, 2005). An alternative approach to study dynamical properties and to infer functionality of the topology of complex networks is the decomposition of a network in principle building blocks, i.e. motifs that are repeated connectivity patterns within the network (Milo et al., 2002; Sporns and Kotter, 2004). However, a generalizing framework that describes synchrony in complex networks has not been found yet.

Finally, several authors have suggested that the reciprocal coupling of cortical areas with the different thalamic nuclei may support the coordination of distributed cortical processing (Llinas and Pare, 1998; Sherman and Guillery, 2002). The thalamus with its bidirectional and radial connectivity to the neo-cortex represents a simple network motif. It consists of a V-shaped configuration composed of three populations, two of which are bidirectionally coupled with the third. The special role of this third central population is that it redistributes common activity to the two other populations in a symmetrical way (Fischer et al., 2006). We could recently demonstrate that the dynamics in this network motif can naturally induce and stabilize zero phase lag synchronization between the outer populations for any conduction delay between the populations (Vicente et al., 2008).

The principle behind this mechanism is that relaying the activity of the outer two neuronal populations via a central mediator redistributes identical information to both outer elements and therefore allows for self-organized lag-free synchronization among the outer pools (see **Figure 1**). It is important to emphasize that the central element is the key for the communication among the populations, but does not dictate the dynamics as in the case of a master-slave system. Therefore, zero phase synchronization via relaying is an emergent property of all three populations. Remarkably, dynamical

relaying has also been demonstrated to be an effective mechanism for inducing and stabilizing zero time lag synchronization between chaotic elements (Fischer et al., 2006). Regarding the temporal precision and the time the system needs to synchronize, the mechanism proved to be compatible with experimentally observed millisecond precise synchronization that is established within tens of milliseconds or very few oscillation cycles. The mechanism also overcomes the problems posed by long axonal delays and high frequencies that cannot be coped with by other synchronizing mechanisms. Thus, dynamical relaying based synchronization might provide a general solution for the establishment of long range neuronal synchrony, irrespective of whether the V-motif is implemented via cortico-thalamic or purely cortico-cortical connections.

Near zero-phase synchronization

In addition to zero-phase synchronization, oscillations also display synchronization with consistent phase differences of fractions of an oscillation cycle (see below). A special case of near zero phase synchrony are delays that are additive. In this case the relative phase difference between pairs of neurons can also be expressed as a relative delay compared to a single global synchronized dynamics of the network.

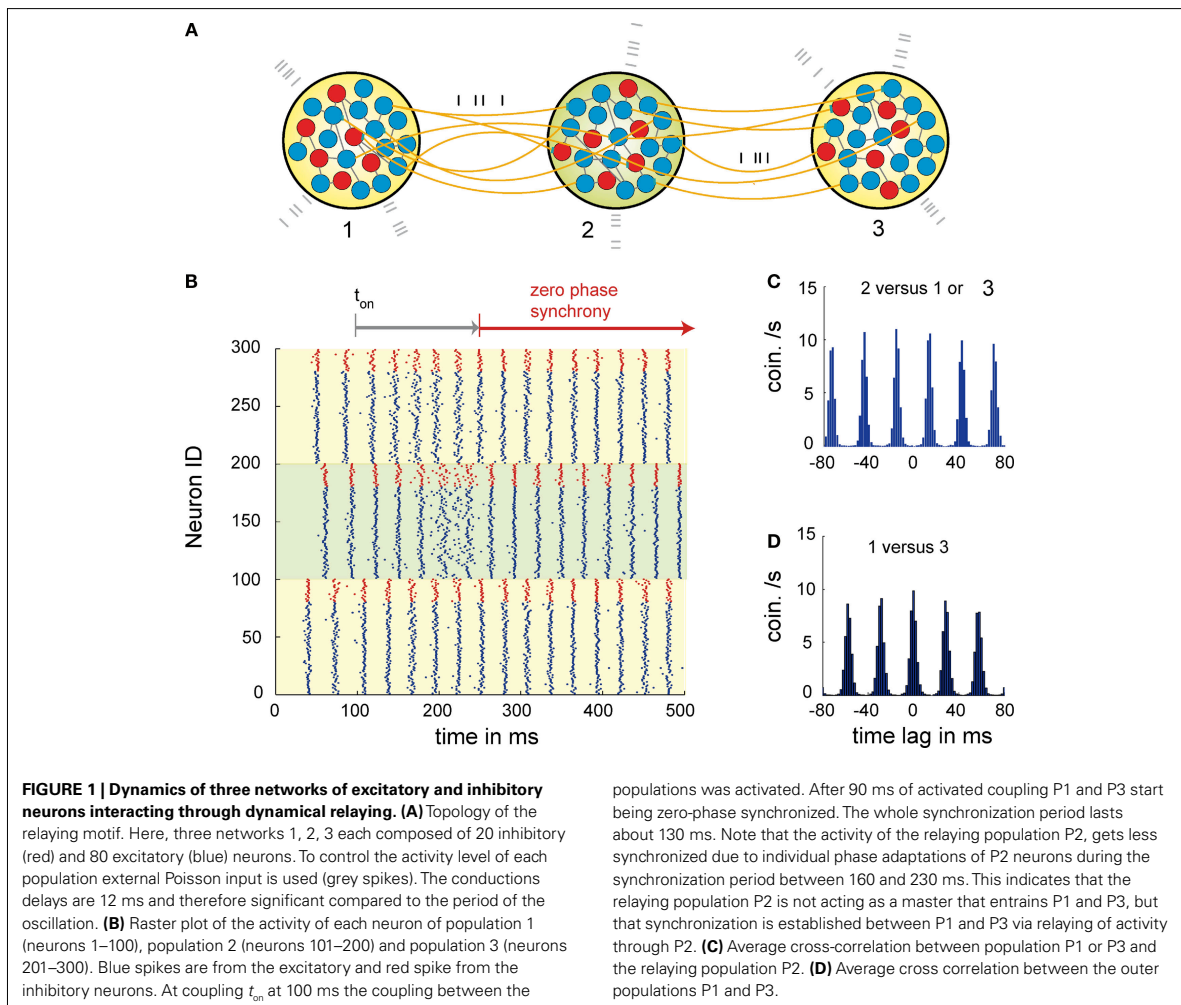
One possibility to explain near zero phase synchrony is detuning. In heterogeneous networks individual elements can have different intrinsic properties such as the resonant frequencies. When coupling of the intrinsically different elements leads to globally synchronized activity, the activity of each individual element needs to be adjusted to match global dynamics. For systems that are composed of oscillatory or excitable elements with different resonant frequencies it is well known that the adaptation to a single and global rhythm requires individual adjustments of phase advances and lags (Pikovsky et al., 2001; Schuster and Wagner, 1989). Therefore, detuning naturally leads to phase differences among the elements of the network. For oscillatory activity and global synchronization detuning even leads to additive phase differences, that can be expressed for each individual as a phase difference to a single global dynamics. Additive phase relations were also discussed to be caused by small differences in conduction delays from a common drive. Regarding the encoding of information (see 'Novel Empirical Results on Temporal Coding'), both the detuning but also the common drive hypothesis open the possibility to encode information in the relative timing of the discharges of individual neurons through a temporal code that is based on phase relations.

NOVEL EMPIRICAL RESULTS ON TEMPORAL CODING

Function of near zero phase lags in synchrony

The early work on synchronized cortical events indicated that many of these phenomena do not result from stimulus locked synchronization but from internally generated temporal patterning based on gamma and beta oscillatory activity. Meanwhile, it became apparent that systematic phase-lags occurring with sub-millisecond precision may enable the cortex to exploit temporal relationship between action potentials for information coding in sensory systems.

A coding mechanism based on phase lags has been already discovered in the hippocampus and is supported by the internally generated oscillations in the theta range (5–8 Hz) (O'Keefe and Recce, 1993) and in the neo-cortex for oscillations in the gamma range (>40 Hz). These oscillations are not locked to the stimuli but

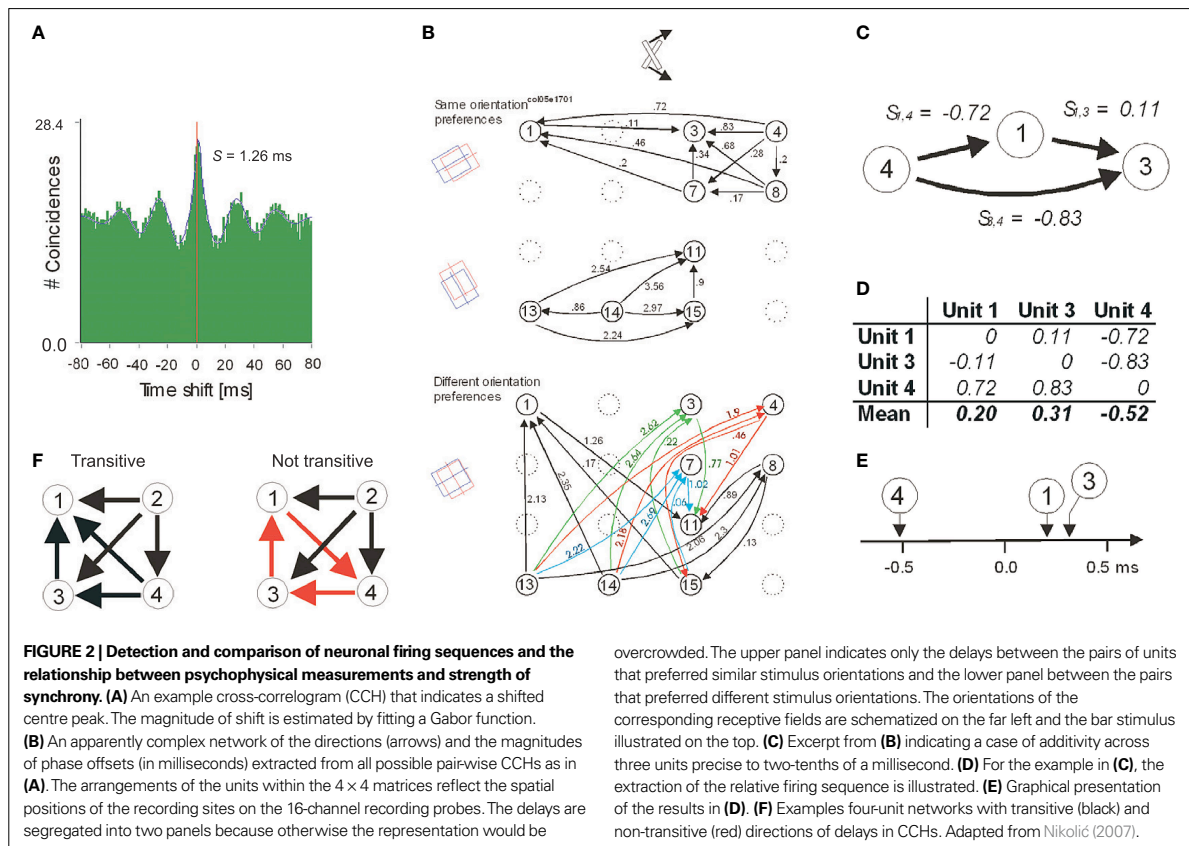


are generated by internal mechanisms independently of stimulus timing. The neurons discharge during particular phases of the oscillation cycle whereby the relative phase of spike generation varies in a context dependent way. In the hippocampus cells fire progressively earlier in the theta-cycle as the animal traverses the cell's place field, a phenomenon called phase precession (Buzsaki, 2002; O'Keefe and Recce, 1993). Consequently, neurons that follow the same rhythm generate also action potentials in precise temporal relationships relative to each other. Oscillations in the theta frequency range are also observed in the neocortex where they coexist with much faster oscillations in the beta and gamma bands, i.e. >20 Hz.

These high frequency oscillations are important for the generation of precise temporal relations and neuronal synchrony. Two neurons are said to synchronize their discharges when the likelihood that they will both fire action potentials within a small time window (up to several milliseconds wide) is much higher than what is expected by chance. The chance level is determined from the overall firing rates of the neurons. For a pair of neurons,

synchronization is commonly assessed from the narrow centre-peaks in cross-correlation histograms (CCH) (see example in Figure 2A) but recently also methods have been developed that can detect synchrony simultaneously across a large number of neurons (Pipa et al., 2007, 2008). These methods overcome certain limitations of pair-wise CCH analysis and permit rate corrected detection of higher order correlations.

There are two ways how neuronal synchrony may support the encoding of information about stimuli. The first and the most extensively investigated is the modulation of the strength of synchronization. The degree to which neurons synchronize their discharges can vary and depends on many variables, such as the similarity of the feature preferences of neurons and the spatial distance between them. Neurons in the visual cortex are more likely to synchronize their responses the more their orientation preferences are similar and the closer their receptive fields are in space (Betsch et al., 2004). These and other results (Gray et al., 1989) have led to the hypothesis that the strength of neuronal synchrony serves to signal information



about the relatedness between the visual features that activate those neurons (Singer, 1999).

The second principle for coding information by neuronal synchrony is similar to that in hippocampus and utilizes the delays or phase-offsets among the discharges of neurons that are participating in synchronized assemblies. In the neocortex, neurons are rarely synchronized with exact zero delays. Instead, CCHs usually reveal small but highly stable and significant delays (Havenith et al., 2009; König et al., 1995; Nikolić, 2007; Roelfsema et al., 1997; Schneider and Nikolić, 2006). These delays may extend up to ~ 15 ms (Schneider and Nikolić, 2006) and do not reflect conduction delays as they change as a function of stimulus properties. They also vary systematically for different pairs of simultaneously recorded units, which allows one to extract a one-dimensional representation of the relative firing times for all coupled, i.e. synchronized neurons (Figures 2B–E). Thus, cortical neurons exhibit systematic differences in their firing times relative to some internal reference. Systematicity can be formally conceived as additivity of phase delays (e.g., Figure 2C), which allows parametric analysis based on ANOVA (Schneider et al., 2006). Alternatively, the directions of phase offsets can be investigated without considering their magnitudes in which case they are treated as mathematical transitivity and can be subjected to non-parametric analysis (Figure 2F) (Nikolić, 2007).

Unpublished observations support the notion that the internal reference signal for the rank ordering of phase offsets are the—often stimulus induced—oscillations in the high frequency range (beta and gamma). Most importantly, these delays, and thus also the relative firing times, change dynamically as a function of stimulus properties (König et al., 1995; Nikolić, 2007; Schneider et al., 2006). This led to the hypothesis that the relative time at which a neuron sends action potentials could be exploited to encode stimulus-related information (Nikolić et al., 2004). One possible encoding principle is a conversion of an amplitude code to a temporal code, such that more strongly depolarized neurons generate action potentials earlier than the less optimally stimulated ones (Fries et al., 2007).

In Figure 3A we show a firing sequence determined from the spike-trains obtained from 14 units in area 17 of a cat. Figure 3B indicates that this sequence is reliable when the same stimuli are presented twice and Figure 3C that the sequence changes if stimulus properties are changed. The extent to which this putative code can be used for computations in the brain and the accuracy with which it can carry information are yet to be investigated. Our results suggest that the trial-to-trial variability of firing sequences can be comparable to that of neurons' firing rates, the pre-condition for such a remarkable coding precision being the presence of strong beta/gamma oscillations (Havenith et al., 2007).

In future, the spatial extent to which neurons can engage into this distributed code and its possible specificity for certain cortical layers or for given cortical areas will need to be determined. There are several options how this information can be read out by individual neurons. Simple integrate-and-fire neurons with sufficiently short integration time constants have been shown to be sensitive to information encoded in the precise stimulus-induced temporal relations of neuronal discharges (Nikolić et al., 2007). It remains to be seen how these properties and the implementation of additional computational capabilities through active dendritic mechanisms improve the readout of the rich temporal relations resulting from internal patterning of response timing. The available evidence suggests that the biophysical properties of the dendritic processes are well suited for such readout of coincident events (Williams and Atkinson, 2008) and temporally ordered information. The exquisite sensitivity of spike timing dependent plasticity (STDP) for the sequence order of pre- and post-synaptic activity indicates that precise temporal relations matter in neuronal processing and can be read out efficiently (Markram et al., 1997).

The main motivation for the present studies is that the firing sequences driven by beta/gamma activity and defined within a single oscillation cycle may constitute a mechanism for the encoding and exchange of information in the cortex. Thus, in addition to the firing rates, precise timing of individual discharges may be used to gate transmission and synaptic plasticity, to selectively route activity across the densely interconnected cortical network and to define particular relations in distributed activity patterns. This hypothesis is directly related to the present research and needs to be pursued. If supported by further data it will have profound implications for our understanding of brain function. Temporal sequences may be

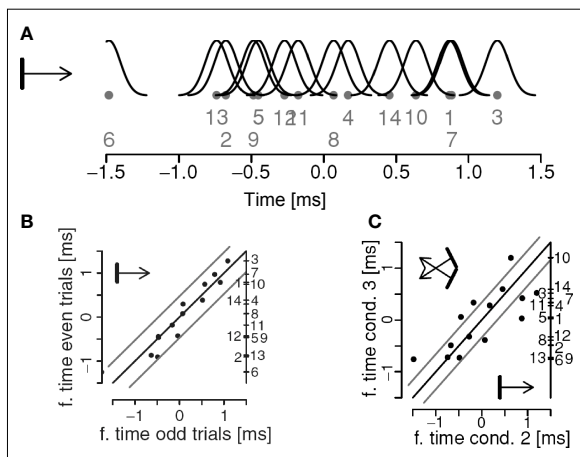


FIGURE 3 | (A) A firing sequence extracted for a network of 14 units. The dots denote the estimated positions of the units, the number their identities, and the black curves indicate the localization errors. **(B)** The relative firing sequence in **(A)** estimated for two repetitions of the same stimuli. Gray lines parallel to the diagonal indicate error limits of two standard deviations. Unit identities are indicated on the right side of the panel. **(C)** Changes in firing sequences as a function of a change in stimulus properties. Stimuli are sketched in the corners of the graph. Units outside the error lines change significantly their preferred firing times. Adapted from Schneider et al. (2006).

a fundamental mechanism by which the nervous system achieves its function. Likewise, beta/gamma oscillations could serve not only to adjust the timing of action potentials but they could also provide an internal temporal reference for the extraction of this information.

Complementary rate and temporal code

In addition to studying putative principles of temporal coding, it is necessary to collect evidence for a functional role of synchrony. One indication comes from a study in which we related changes in synchrony to a perceptual phenomenon called apparent brightness (Biedlerlack et al., 2006). With multisite recordings in the cat visual cortex we compared directly the changes in discharge rate and synchrony with stimulus modifications that lead to changes in apparent brightness. This revealed a close match between a psychophysical function describing the magnitude of the visual illusion on the one hand, and the change in the strength of synchronization between the neurons responding to the stimulus, on the other (Figures 4A,B). Moreover, by comparing changes in discharge rate and synchrony for different stimulus configurations the study indicated that an

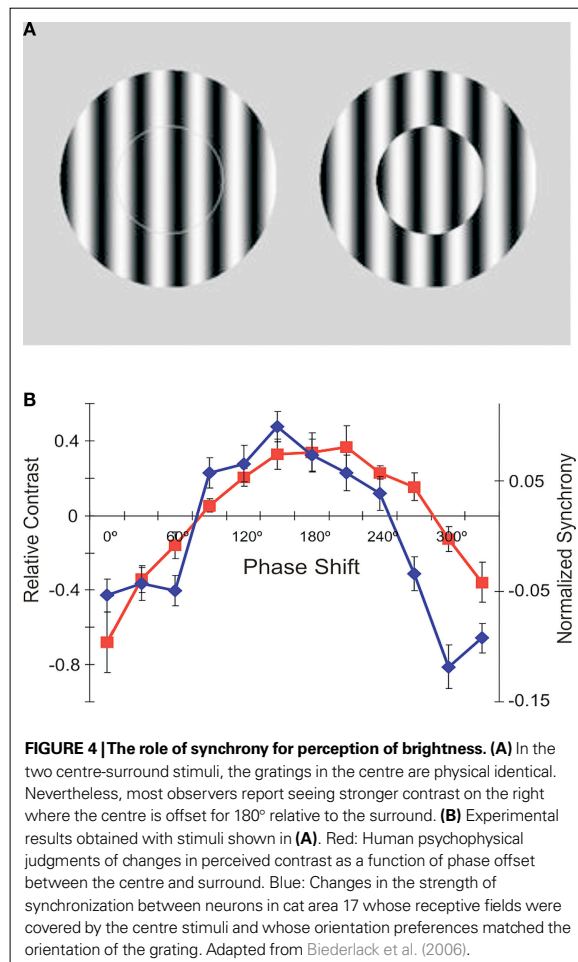


FIGURE 4 | The role of synchrony for perception of brightness. (A) In the two centre-surround stimuli, the gratings in the centre are physical identical. Nevertheless, most observers report seeing stronger contrast on the right where the centre is offset for 180° relative to the surround. **(B)** Experimental results obtained with stimuli shown in **(A)**. Red: Human psychophysical judgments of changes in perceived contrast as a function of phase offset between the centre and surround. Blue: Changes in the strength of synchronization between neurons in cat area 17 whose receptive fields were covered by the centre stimuli and whose orientation preferences matched the orientation of the grating. Adapted from Biedlerlack et al. (2006).

increase in synchrony produces a perceptual effect that is equivalent to an increase in firing rates. That is, if neurons synchronize more strongly, the stimulus is perceived more intensively. The significance of this study is that conclusions are based on a close match between complete physiological and psychological functions, which were determined for the entire spectrum of stimulus properties, exceeding thus the usual correlative evidence based only on extreme values (e.g., minimum and maximum stimulus intensities).

This type of analysis allows one to falsify theories even when the analyses of extreme values support them and are correlated perfectly. In our case, this allowed us to falsify an alternative hypothesis that synchrony accounted for figure-ground segregation, which, besides the extremes, showed otherwise completely uncorrelated measures (Biedlerlack et al., 2006). At the same time, by showing a close match between increased perceived brightness and either increased synchrony or increased discharge rate, the results showed the perceptual equivalence of raising the saliency of responses either by increasing discharge rate or synchrony.

CONCLUDING REMARKS

In conclusion, in this section we have first presented a theoretical framework for synchronization among neurons with delays smaller than the conduction delays. Next, we have reviewed empirical evidence for the existence of such delays and for their functional role in brain computations. These studies are at the very beginning of the search for temporal codes and we expect the research in this direction to expand. It will be a great challenge to provide direct causal proof that changes in firing sequences affect behavior or psychological experience (e.g., perception). However, this applies equally to all other codes that have been investigated in the attempt to bridge the brain-mind gap.

BUILDING EXPECTATIONS: NEW VISTAS FOR GAMMA OSCILLATIONS

As argued above, a critical step in understanding perceptual organization is to find out how the brain builds stable relationships among sensory inputs. For this, however, it is not only important to know about encoding principles, but also to probe ongoing states of expectancy and attention. Beyond a purely sensory-driven approach to perception, this view focuses on top-down mechanisms which are related to large-scale dynamics at multiple scales. The mechanisms underlying these processes are still largely unknown. As discussed before, an attractive hypothesis is that precise temporal patterning of neuronal activity provides a framework for contextual links (Engel et al., 2001; Singer, 1999). In this model, sensory inputs interact with internally generated signals necessary for building predictions about the world.

Evidence in support of the neuronal synchronization hypothesis was initially obtained in anesthetized animals, and later extended to waking and conscious states, as described in cats (Gray and Viana Di Prisco, 1997; Roelfsema et al., 1997; von Stein et al., 2000), non-human (Eckhorn et al., 1993; Fries and Eckhorn, 2000; Gail et al., 2000; Kreiter and Singer, 1992, 1996; Maldonado et al., 2000) and human primates (Palva and Palva, 2007; Rodriguez et al., 1999; Tallon-Baudry et al., 1997). Notwithstanding these findings, after two decades of research, the role of gamma in feature binding remains a matter of dispute and controversy (Ghose and Maunsell,

1999; Roelfsema, 2006; Shadlen and Movshon, 1999; Singer, 1999). In monkeys, several studies designed to test for perceptual grouping failed to support the synchronization hypothesis (Dong et al., 2008; Lamme and Spekreijse, 1998; Palanca and DeAngelis, 2005; Roelfsema et al., 2004; Thiele and Stoner, 2003).

More recently, however, evidence became available that synchronization of gamma oscillatory responses are closely linked to more general cognitive functions such as selective attention (Doesburg et al., 2008; Dong et al., 2008; Fan et al., 2007; Fries et al., 2001a; Lakatos et al., 2008; Roy et al., 2007; Steinmetz et al., 2000; Taylor et al., 2005; Womelsdorf and Fries, 2006; Womelsdorf et al., 2007), short- and long-term memory (Herrmann et al., 2004; Pesaran et al., 2002; Wu et al., 2008) and multisensory integration (Lakatos et al., 2007), suggesting that gamma-oscillations may have a much wider relevance in cortical networks for behavioral and cognitive phenomena.

In this section, we present new experimental evidence supporting this hypothesis by showing that, in addition to selective attention, preparation to respond or perceptual readiness also leads to a selective increase in the gamma components of the responses. Since the modulation in gamma power associated with readiness exhibits very fast dynamics, it may play a particularly important role in perceptual organization, as briefly discussed below.

It is well established that arousal and attention are of general relevance for visual processing (Posner, 1980). Studies in monkeys and humans have shown that attention can selectively enhance processing of image features (Desimone and Duncan, 1995; Reynolds and Desimone, 2000; Sheinberg and Logothetis, 2001; Spitzer et al., 1988). Directing attention to a stimulus at a particular location leads to an increase in its effective contrast (Carrasco et al., 2004; Reynolds and Chelazzi, 2004) and can modulate tuning properties (Roberts et al., 2007; Spitzer et al., 1988). Given the central role of attention in perception, Fries and collaborators, decided to investigate whether gamma oscillations could also serve as a selection mechanism. In recordings from area V4, they have found strong phase-locking between spiking activity and ongoing LFP oscillations confined to the gamma band (Fries et al., 2001a, 2008; Womelsdorf et al., 2006, 2007). Based on these findings, a mechanism was proposed in which effective communication within distributed neuronal networks relies essentially on the precise temporal relationships (Fries, 2005; Fries et al., 2007, 2008). According to this hypothesis, attentional enhancement of neuronal synchronization would facilitate selectively the communication among synchronized assemblies, which is thought to be important for a large number of operations underlying cortical processing (Azouz and Gray, 2003; Salinas and Sejnowski, 2000; Sejnowski and Paulsen, 2006).

In order to investigate the dependency of gamma oscillations on attentional preparation, or readiness, we have trained macaque monkeys to respond to a variety of stimuli, such as gratings, plaids and Gabor patches (Lima et al., 2006, 2007; Neuenschwander et al., 2008). In all these paradigms the monkeys were required to detect a stimulus change at fixed time points within the trial. Here we present results obtained for responses to Gestalt figures embedded in 2D-arrays of Gabor patch elements (Neuenschwander et al., 2008). During this task, the Gabor elements changed their orientation randomly every 400 ms. At a fixed time point (3200 ms), a subset of neighboring Gabors were aligned to form a closed

figure. The appearance of the figure required a motor response, and therefore, implicitly carried a behavioral relevance. Thus, in anticipation of the stimulus, the monkeys were likely to build up expectancy, or response readiness along the course of the trial.

Neuronal responses were recorded at multiple sites in area V1. The embedded figures were constructed as a function of the position and properties of the receptive fields of the neurons. In this way, a unique figure was designed for every new set of recording sites. Within the trial, the changes in the orientation of the Gabor elements were set to match the preference of the cells at fixed epochs, coinciding or not with the appearance of the figure. Thus, we could study the same local responses in two contexts: in one case associated with a global percept (Figure 5), and in the other not. Figure 5A shows the average peri-stimulus time histogram (PSTH) obtained for a single cell. Robust responses to the matching

orientation of the Gabor element are readily visible in the histogram as brief transient peaks followed by a sustained component. The last epoch of orientation match was the one associated with the figure. At this very moment the monkey was required to respond within 500 ms with a lever release. Notice that response levels were similar for all epochs in which the stimulus orientation matched the orientation preference of the neurons.

A dramatic difference, however, was revealed in the temporal structure of the responses. As shown by the sliding autocorrelation analysis of the spiking activity (Figure 5B), there was a marked increase of gamma oscillatory components developed prior to the behavioral response. Accordingly, the spectral analysis of the LFP and single cell spiking activity showed a peak at around 50 Hz, which was more pronounced for the window associated with the behavioral response (Figure 5C). Controls were also made for behavioral responses without the appearance of an embedded figure (not shown). In those cases the monkey had to report a color change of the fixation point. Surprisingly, we have found no significant differences in gamma modulation between the conditions with and without the embedded figure, indicating that the stimulus per se was not responsible for the enhancement. Thus, there was no simple relation between gamma synchronization and the binding of elements into a figure.

Taken together, our results suggest that gamma activity is strongly modulated by central states, probably related to perceptual readiness or readiness to act. A potential explanation could be higher levels of arousal associated with the anticipation of behavioral responses. States of central activation are associated with cholinergic facilitation of gamma activity (Herculano-Houzel et al., 1999; Rodriguez et al., 2004). It remains to be clarified, however, whether there is a direct link between the motor response preparation per se and the modulation of gamma activity in V1. The fast modulation of gamma power in the present experiments could be mediated by top-down influences or ascending cholinergic mechanisms controlling the intrinsic dynamics of the cortical networks. In either case, the anticipatory entrainment of the visual cortex in highly synchronous gamma oscillations is likely to be instrumental for the expected processing of sensory signals and their propagation towards executive structures. Recently it has been shown that coherence between motor cortex and spinal motor neurons increases as function of readiness to respond (Schiffman et al., 2005), similar to our results in V1. These corticospinal interactions have been interpreted as evidence for a role of gamma synchronization in neuronal communication (Fries, 2005). It would be interesting to see, whether more anterior cortical regions also engage in anticipatory gamma activity and whether there are any consistent temporal relationships.

NEURAL SYNCHRONY AS A MECHANISM FOR CONSCIOUS PERCEPTION?

The distributed organization of the primate brain poses particular challenges for understanding the integrative aspect of cognition, of which consciousness is the utmost example. The 'intentional' feature of consciousness, the fact that our experience always refers to something, suggests that understanding how the content of cognition is represented in the brain, and how unified experience can emerge out of distributed brain activity might be particularly informative

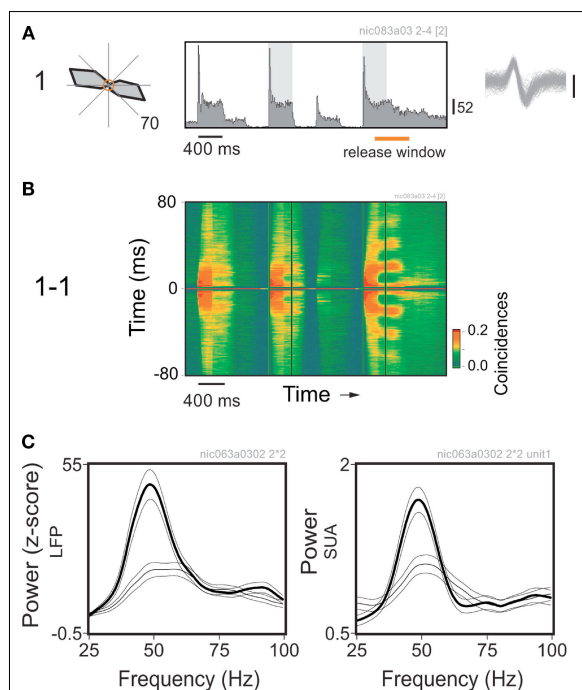


FIGURE 5 | Perceptual readiness modulates gamma power in V1 of the monkey. (A) Average response histogram for a single cell to a Gabor element centered over its receptive field. The orientation of the Gabor element changes at 400 ms steps. Notice the strong responses for the epochs of orientation match. Analysis windows are indicated by the shadowed rectangles on the plot. Direction tuning is shown on the left. Spontaneous activity is represented by the central circle, maximum average rate is indicated at the bottom right of the plot. **(B)** Sliding window autocorrelation for the responses shown above. Plots are aligned in time. Autocorrelation functions were computed for 200 ms windows at steps of 50 ms. **(C)** Corresponding power spectra obtained for the local field potential (LFP) and spiking activity recorded from the same electrode. Thin line: window of match in the middle of the trial. Thick line: window of match prior to the behavioral response (in this example, coincides with the appearance of the embedded figure). Multitaper spectral analysis was obtained using the Chronux analysis software. Power was normalized by the firing rate. Thin lines around the mean indicate 95% confidence intervals.

in the quest for the neuronal correlates of consciousness (NCC)¹. Thus, theories of binding and large-scale integration have recently come into the focus of the research on consciousness (Engel and Singer, 2001; Thompson and Varela, 2001).

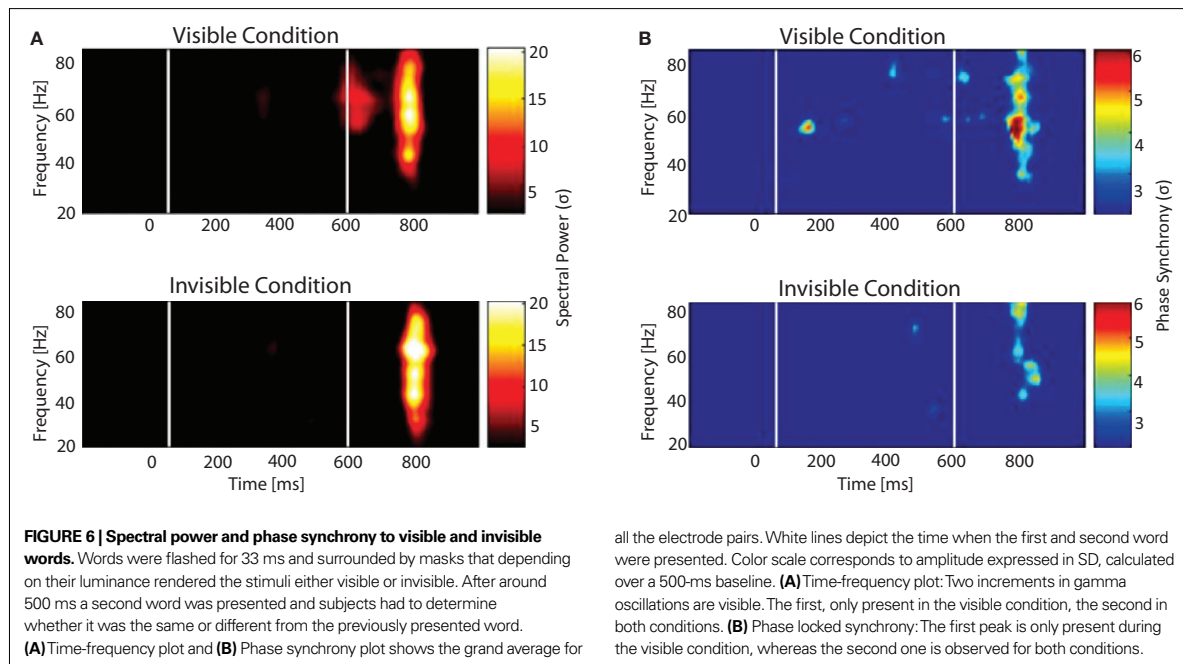
One candidate mechanism for dynamic sub-system integration is the precise synchronization between the participating neuronal assemblies (Varela et al., 2001). Several properties make neuronal synchrony worth considering in the context of the NCC. Besides offering a mechanism to link elementary features together and thus allowing for the representation of composite perceptual objects, binding by neuronal synchrony could confer the brain with a vast and economical representational space (Singer, 2002). Considered at a large scale, synchronization of distant neuronal assemblies could allow for subsystem integration and thus account for the unified aspect of conscious experience (e.g., where different sources of information are bound in an integrative cognitive moment). However, processes explaining how the unity of conscious experience is achieved do not suffice alone as a potential mechanism for consciousness. Any given theory of the NCC should also at least explain how different percepts dynamically map into different states, and how the system dynamically selects subsets of neuronal responses for conscious representation. Importantly, given that a considerable amount of cognitive and executive operations can be performed without being aware of them (Dehaene et al., 1998, 2001; Sergent et al., 2005), it is also necessary to distinguish between these two types of processing (conscious and non-conscious) at the neural level. Evidence suggests that changes in neuronal synchrony could account for these two processing modes. First, regular changes in the content of consciousness can be represented when considering that groups of neurons can take part or drop off from the dynamically linked network. The formation of assemblies would be only limited by the time needed to establish stable states between them. This property could then account for the transitoriness and temporal flow of experience (Varela, 1999). Second, due to the coincidence sensitivity of cortical neurons synchronized inputs enhance the probability of response in target neurons (Salinas and Sejnowski, 2001), and this in turn would allow for the amplification of neuronal responses and selection of subpopulations of responses based on the strength and propagation of their activity (Jensen et al., 2007). Third, the required switch between conscious and unconscious processing could be achieved by varying the spatial scale of the synchronized neuronal assemblies. Conscious cognition would involve long-distance coordination between distributed neuronal groups, whereas unconscious cognition would be instantiated by local coordination (Dehaene et al., 2006; Thompson and Varela, 2001). Small world networks, of which the brain seems to be one example (Yu et al., 2008), combine these two processing modes: local modularity and long-range connectivity. Thus, depending on dynamic shifts in coupling, the same anatomical network can support both local and global – or subconscious and conscious – operations (Buzsaki, 2007).

¹In the context of this review consciousness will be understood as the subjects' ability to detect (report the presence or absence) or identity (discrimination) a particular stimulus. In contrast, failure to detect or to identify will be taken as indication of unawareness. Thus, awareness refers to the representation of internal or sensory changes that are accessible to introspection or direct report. An NCC will be defined as the minimal set of neuronal events that are necessary and/or sufficient for perceptual awareness (Chalmers, 2000; Kanwisher, 2001).

Long range synchronization in the beta and gamma range has been observed with scalp as well as with intracranial recordings when a coherent and unified percept emerges in response to a given stimulus (Lutz et al., 2002; Rodriguez et al., 1999; Sehatpour et al., 2008). For instance, Sehatpour et al. (2008), using intracranial electrodes, reported robust coherence in the beta-band between the hippocampal formation, occipitotemporal cortex, and lateral prefrontal cortex when participants recognized fragmented images. In contrast, when scrambled versions of the same images were presented significantly lower coherence was observed. These results suggest that transient oscillatory coupling between distributed cortical regions may underlie effective communication during visual object processing. Furthermore, in conditions of competition such as in binocular rivalry selection of responses for further processing appears to be achieved via increases in neuronal synchronization of groups of neurons in the primary visual cortex of the cat (Fries et al., 1997, 2002), while discharge rate of neurons does not distinguish between the dominant (perceived) and non-dominant (suppressed) pattern. Studies employing MEG and EEG in humans yielded similar results (Cosmelli et al., 2004; Doesburg et al., 2005; Srinivasan et al., 1999; Tononi et al., 1998): Perceived stimuli correlate with increased synchronization in the gamma range between distal cerebral areas (occipital and frontal regions) (Cosmelli et al., 2004). Similar results have been obtained in the attentional blink paradigm. Successful detection of stimuli was accompanied by increased synchronization in the beta range. Source analysis revealed, as in the case of binocular rivalry, dynamical coordination in the beta range between frontal, parietal, and temporal regions for detected targets (Gross et al., 2004).

Recently, in order to directly explore the relation between neuronal synchrony and conscious perception, we designed a paradigm in which the electrophysiological signatures related to conscious and unconscious processing of visual stimuli were directly compared (Melloni et al., 2007). Subjects had to detect and identify a briefly exposed word (33 ms) presented between masking stimuli. The strength of the masks was adjusted such that in half of the trials subjects had no conscious recollection of having seen the word. After a delay of ~500 ms a second word was presented, always visible, and the subject had to decide whether the two words were the same or different. Importantly, in an attempt to study the processes related to conscious perception dissociated from other cognitive processes such as decision making and motor response, the first stimulus over which visibility was manipulated was separated in time from a second stimuli over which subject had to respond.

To study the neuronal signatures related to conscious processing and how they evolve over time we simultaneously recorded electroencephalographic activity (EEG) and subsequently analyzed different measures of neuronal responses: time resolved power changes of local signals, the precision of phase synchronization across recording sites over a wide frequency range, and event-related potentials. The first electrophysiological event that distinguished seen from unseen words was an early and transient burst of long-distance synchronization observed in the gamma frequency. Regional distributions of gamma spectral power and phase revealed that the amplitude and patterns of gamma oscillations were spatially homogeneous and similar for the two conditions, while the patterns of phase synchrony were markedly different (Figure 6). Significant



phase locking within and across hemispheres, between occipital, parietal and frontal site was observed only for the visible condition and was absent in the invisible condition.

After this transient period of synchronization, an increase in amplitude of the P300 component was observed, which has been interpreted as a correlate of the transfer of information into working memory. Furthermore, we observed increases in amplitude of theta oscillations over frontal electrodes during the interval in which visible words had to be kept in memory, in accordance with the assigned role of frontal theta oscillations in the maintenance of short term memories (Jensen and Tesche, 2002; Schack et al., 2005). The specificity of long-distance synchronization for conscious perception was further supported in an additional experiment controlling for the depth of processing (Melloni and Rodriguez, 2007). Altogether our results show that the precise phase locking across a widely distributed cortical network, and not the power of the local stimulus induced gamma oscillation, is the earliest signature of conscious processing. This suggests that conscious processing requires a particular dynamical state of the cortical network. We propose that this transient synchronization might enhance the saliency of the activation patterns not only allowing for contents to get access to consciousness but also triggering a cascade of processes such as perceptual stabilization, maintenance in working memory, and generation of expectations, all aspects intimately related with conscious awareness. It is at present unknown whether the early large-scale synchronization is already the neuronal correlate of phenomenal awareness or whether awareness emerges only from the entirety of the processes following this coordinated state. In addition, it remains to be clarified whether the large scale synchronization transfers contents into awareness and/or maintains them. The transient nature of the effect argues in favour of the first possibility.

The subsequent theta oscillations might then support maintenance. The rapid update of new contents might be instantiated by the short periods of long-distance synchronization in the gamma band, while the slower pace of theta oscillations might relate to sustained integration and maintenance of local results. The interplay between these two frequency bands might underlie the phenomenon of continuous but ever changing conscious experience.

NEURAL SYNCHRONY IN SCHIZOPHRENIA AND AUTISM SPECTRUM DISORDERS

In addition to the putative role of neural synchrony in temporal coding, top-down modulation of sensory signals and large-scale integration of distributed neural assemblies, there is increasing evidence suggesting that abnormal neural synchrony is a pathophysiological mechanism in neuropsychiatric disorders. Accordingly, in the following section, we will examine the evidence for a relationship between alterations in neural synchrony and the pathophysiology of schizophrenia and autism spectrum disorders (ASD)². These results suggest that there are fundamental changes in neural synchrony that may underlie the cognitive dysfunctions associated with these disorders as well as certain symptoms.

Testing this hypothesis may have important implications both for the potential understanding and treatment of the disorders as these belong to the most costly public health problems. Furthermore, research into brain disorders also holds the potential to gain novel insights into the functional relevance of neural synchrony during normal brain functioning by establishing close correlations between

²Alterations in neural synchrony are not confined to these disorders (see Uhlhaas and Singer, 2006, for a review). Alterations in neural synchrony are also involved in Epilepsy, Parkinson's Disease and Alzheimer's Disease, for example.

abnormal synchronization and specific cognitive deficits in a variety of neuropsychiatric disorders.

SCHIZOPHRENIA

From its earliest beginnings, the pathophysiology of schizophrenia has been described as a disorder involving a deficit in the integration and coordination of neural activity that leads to dysfunctions in cognition. Thus, Bleuler (1911) chose the word 'schizophrenia' to highlight the fragmentation of mental functions. Given the fundamental role of neural synchrony in establishing coherent mental contents (see 'Neural Synchrony as a Mechanism for Conscious Perception?' by Melloni), it can therefore be proposed that impaired neural synchrony underlies the fragmentation of mental functions in schizophrenia.

Indeed, current theories of schizophrenia (Friston, 1999; Phillips and Silverstein, 2003) converge on the notion that core aspects of the pathophysiology are due to deficits in the coordination of distributed neural processes that involve multiple cortical areas. This perspective contrasts with earlier views that emphasized a regionally specific pathophysiological process as the underlying cause for the signs and symptoms of schizophrenia. Some of the cognitive deficits in schizophrenia concern functions, such as working memory, attention, and perceptual organization, have been proposed to involve synchronization of oscillatory activity in the beta- and gamma-band band (see Phillips and Silverstein, 2003, for a review).

A substantial body of EEG³/MEG-studies now support the hypothesis that cognitive deficits are related to impaired neural synchrony. Examination of auditory and visual steady-state responses to repetitive stimulation in patients with schizophrenia has revealed a specific reduction in the power of the stimulus-locked response in the beta- and gamma-frequency range, but not in the lower frequencies (Krishnan et al., 2005; Kwon et al., 1999). Reductions in evoked oscillatory activity have been reported for tasks involving visual binding (Spencer et al., 2003, 2004), for backward-masking (Wynn et al., 2005), in auditory oddball-paradigms (Gallinat et al., 2004) and during TMS-evoked activity over frontal regions (Ferrarelli et al., 2008). These results suggest selective deficiencies in the ability of cortical networks or cortico-thalamo-cortical loops to engage in precisely synchronized high-frequency oscillations.

Recently, we have tested the involvement of high-frequency oscillations with MEG in chronic-schizophrenia patients during the perception of Mooney faces (Tillmann et al., 2008) (see **Figure 7**). Mooney faces consist of degraded pictures of human faces where all shades of gray are removed, thus leaving only black and white contours. MEG signals were analysed for spectral changes in oscillatory activity in the frequency range of 25–200 Hz. Compared to healthy controls, schizophrenia patients showed a highly significant reduction in high-frequency gamma-band activity (60–120 Hz) over parieto-occipital sensors which was accompanied by a significant deficit in the ability to detect upright Mooney faces. Thus, these findings suggest a comprehensive deficit in the regulation of

gamma-band oscillations across a wide frequency range during perceptual organization in schizophrenia.

In addition to analyses of spectral power, several studies have also examined phase synchrony between distributed neuronal populations while patients performed cognitive tasks (Slewa-Younan et al., 2004; Spencer et al., 2003; Uhlhaas et al., 2006). Overall, these studies conclude that patients with schizophrenia are characterised by reduced phase-locking of oscillations in the beta- and lower gamma-band range highlighting that in addition to abnormalities in local circuits, large-scale integration of neural activity is impaired. It is currently, unclear, however to what extent impairments in local circuits contribute to long-range synchronization impairments or whether these represent two independent phenomena.

Correlations between cognitive dysfunctions and alterations in neural synchrony are furthermore accompanied by relationships between the positive symptoms of schizophrenia and changes in the amplitude of beta- and gamma-band oscillations. Specifically, patients with auditory hallucinations are characterised by an increase in oscillatory activity in temporal regions relative to patients without hallucinations (Lee et al., 2006; Spencer et al., 2008), suggesting that the abnormal generation of internal experiences is related to increased beta- and gamma-band activity. These observations are also corroborated by the finding that auditory hallucinations in schizophrenia are associated with enhanced white matter connectivity in temporal regions as disclosed by recent DTI-studies (Hubl et al., 2004), indicating a possible link between pathological oscillatory activity and anatomical hyperconnectivity.

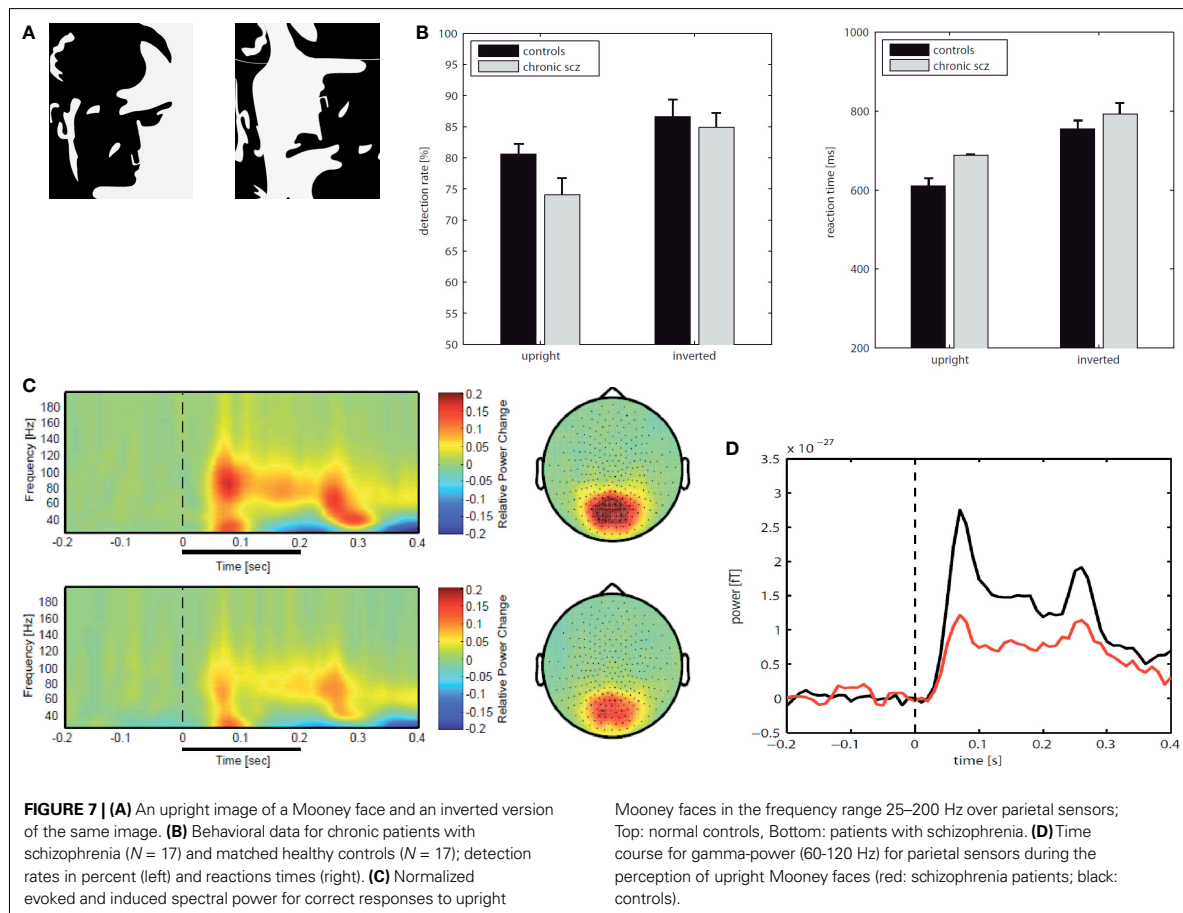
The observed deficits in neural synchrony in schizophrenia are consistent with impairments in neurotransmitter systems as well as altered anatomical parameters that are fundamental to establishing synchronised oscillations at high frequencies in cortical networks. One prominent candidate mechanism for the changes in neural synchrony are dysfunctions in GABAergic interneurons (see Lewis et al., 2005, for a review). For example, there is consistent evidence for reduced GABA (γ -aminobutyric acid) synthesis in the parvalbumin-(PV) containing subpopulation of inhibitory GABA neurons in schizophrenia which are critically involved in the generation of cortical and hippocampal oscillatory activity (see 'The Generation of Neural Synchrony').

In addition, impairments in long-range synchronization in schizophrenia can be related to changes in white matter volume and organisation as long distance synchronization of oscillatory responses is mediated by reciprocal cortico-cortical connections (König et al., 1993; Löwel and Singer, 1992). This possibility is supported by *in-vivo* anatomical examinations with diffusion tensor imaging (DTI) that have revealed white matter anomalies throughout cortical and subcortical structures (for a review see Kubicki et al., 2007).

AUTISM SPECTRUM DISORDERS (ASDs)

ASDs constitute a heterogeneous neurodevelopmental syndrome that is characterized by a triad of impairments that affect social interaction, verbal and nonverbal communication, and the repertoire of interests and activities (APA, 2000). Similar to recent work in schizophrenia, theories that account for the pervasive cognitive dysfunctions associated with ASDs converge on the notion that the pathophysiological mechanisms in ASDs involve a deficit in

³Recently, it has been proposed that scalp recorded gamma-band oscillations in EEG-data reflect miniature saccades instead of cognitive or neuronal processes (Yuval-Greenberg et al., 2008). For a critical evaluation of this claim see Melloni et al. (2009).



the temporal coordination of distributed neural activity (Uhlhaas and Singer, 2007).

Parallels between the pathophysiology of schizophrenia and ASDs extend to cognitive impairments and certain symptoms. Thus, both disorders are characterised by abnormal perceptual integration during auditory and visual perception (Happé and Frith, 2006; Uhlhaas and Silverstein, 2005), for example, suggesting similar mechanisms that account for cognitive dysfunctions. Furthermore, clinical symptoms, such as the disorganization of thought and language as well as negative symptoms can be found in both disorders (Konstantareas and Hewitt, 2001), suggesting an overlap in the clinical phenotype.

Recent fMRI and EEG/MEG studies have supported the potential role of dysfunctional temporal coordination of neural responses in ASDs. Just et al. (2004) examined functional connectivity by measuring the covariance of BOLD signals during sentence comprehension in high-functioning individuals with autism. The study showed systematic differences between groups with respect to the distribution of brain activation and functional connectivity. Compared to controls, subjects with autism were characterized by a marked reduction in functional connectivity throughout the

cortical language system that was most pronounced during comprehension of sentences. A number of additional fMRI studies have supported the concept of reduced functional connectivity in ASDs (Castelli et al., 2002; Koshino et al., 2005; Villalobos et al., 2005).

In analogy to the findings in schizophrenia patients, these data predict that autism should be associated with reduced neural synchrony. Similar to patients with schizophrenia, ASDs are characterised by impaired auditory steady-state (ASS) potentials to stimulation in the 40 Hz range. Wilson et al. (2007) examined entrainment to 40 Hz stimulation in MEG-data in healthy controls and children and adolescent participants with ASDs. Participants with ASDs showed a marked reduction in gamma-band power that was particularly pronounced in the left hemisphere. Impairments in gamma-band activity elicited by auditory stimulation were also observed in first-degree relatives of proband with ASDs (Rojas et al., 2008), suggesting that dysfunctions in gamma-band activity are a potential endophenotype.

In addition, there is also evidence for impairments in task-related oscillations in ASDs. Milne et al. (2009) investigated visuo-perceptual integration in 20 individuals with ASD and 20 control subjects with EEG. Visual evoked potentials elicited by Gabor

patches were compared in participants with and without ASD and a source-localisation algorithm was employed to identify the generators of oscillatory activity. In those components located near the striate or extrastriate cortex, variations in the spatial frequency of stimuli exerted a smaller effect on induced increases in alpha- and gamma-band power in participants with ASD, suggesting abnormal modulation and recruitment of alpha- and gamma-band oscillations during perception integration in ASDs.

Finally, resting state EEG-data suggest a relationship between neural synchrony and aberrant brain development in ASDs. Thus, an excess of gamma-band activity has been reported in children with ASDs (Orekhova et al., 2007). In contrast, in adult participants reduced long-range coherence in resting-state EEG has been observed (Murias et al., 2007), suggesting that during later developmental stages, there is faulty maturation of cortico-cortical connections that leads to a disconnection syndrome (Geschwind and Levitt, 2007). This evidence is in agreement with anatomical data that indicate that during early development, white matter increases significantly more in ASDs than in normal children (Herbert et al., 2003). Evidence for a transient hypertrophy of white matter has also been found in previous studies (Courchesne et al., 2001) and later complemented by results suggesting exaggerated pruning to subnormal levels consistent with evidence for anatomical hypo-connectivity (Just et al., 2004; McCaffery and Deutsch, 2005).

Anatomical abnormalities are accompanied by alterations in neurotransmitter systems that may lead to an imbalance between excitation and inhibition, and in turn to hyperexcitability and unstable cortical networks (Hussman, 2001; Rubenstein and Merzenich, 2003). This hypothesis is consistent with abnormalities in GABAergic and glutamatergic transmitter systems in ASDs (for a review see DiCicco-Bloom et al., 2006).

NEURAL SYNCHRONY IN BRAIN DISORDERS

In summary, the potential role of neural synchrony in schizophrenia and ASDs is supported by close correlations between alterations in neural synchrony and cognitive impairments as well as through dysfunctions in transmitter-systems and anatomical parameters that are critical for neural synchrony to occur in cortical networks. Accordingly, we believe that further investigations into the role of neural synchrony in schizophrenia and ASDs are likely to be crucial for establishing valid pathophysiological models of these disorders.

This perspective is based on the fact that efforts to identify specific cortical regions that can account for the diverse impairments in cognition and explain the heterogeneous symptoms have so far been fruitless. Instead, the more plausible assumption is that different syndromes are related to distinct but overlapping pathologies in the coordination of distributed neuronal activity patterns that are revealed by the systematic investigation of the temporal and spatial organisation of neural synchrony across different frequency bands. This is undoubtedly a challenging task but such a research program will ultimately lead to better diagnostic tools for early diagnosis and intervention.

CONCLUDING REMARKS

In this paper, we have attempted to give an overview on the history and current status of concepts about the role of oscillations and

synchrony in neuronal networks. Initially discovered in the visual system and conceptualized as a possible mechanism for dynamically binding perceptual elements into coherent object representations, it is becoming more and more evident that this discovery has wider implications for the understanding of neural codes and integrated brain functions than originally assumed. However, we also wish to emphasize that many open questions remain that are fundamental to our understanding of this phenomenon and need to be addressed by future research.

THE BINDING BY SYNCHRONY HYPOTHESIS

A still much debated issue is the role of neural synchrony in perceptual grouping and feature binding. Evidence regarding the binding hypothesis is heterogeneous. Numerous studies support the initial interpretation while others report negative evidence. Most studies agree that synchronization in the retina or early visual cortex reflects well some of the Gestalt criteria for perceptual grouping such as continuity of contours, similarity in feature space (colinearity, similar orientation) and common fate. However, it is clear that synchronization at early stages of processing tends to be restricted to closely spaced (a few millimetres at most) groups of neurons and does not generalize to all neurons engaged in the encoding of an extended object (for citations see main text). Because multisite recordings in higher visual areas are rare, little is known as to whether cells in inferotemporal cortex participating in the distributed representation of an object exhibit signs of object specific synchronization. The one study that has specifically addressed that issue indicates that this might indeed be the case (Hirabayashi and Miyashita, 2005). When monkeys recognize that component features of a face (mouth, nose, eyes etc.) actually form a face rather than a scrambled collection of features, neurons responding to the features transiently synchronize their responses. Thus, when investigating relations between perceptual grouping and synchronization, it is important to make educated guesses as to which binding functions are expected to occur at which level of processing. We consider it as likely that binding functions are realized at many different scales, whereby early processing stages can support only very local grouping operations while global, object specific grouping takes place only in the late, non-retinotopically organized areas. It may be that some of the negative findings are the result of the probably inappropriate assumption that all binding should be achieved at once already at low processing levels. Another difficulty in the testing of the binding by synchrony hypothesis is the transitory nature of synchronization. Numerous studies indicate, especially when performed in awake behaving animals, that epochs of synchronous firing may be very short (in the range of tens of milliseconds). This is in perfect agreement with the evidence that scene segmentation, perceptual grouping and object recognition can be achieved in less than 200 ms which leaves only a few tens of milliseconds per processing stage to accomplish its operations. Short episodes of synchronous firing may, however, not be detectable with conventional cross correlation techniques, especially if discharge rates are low as is the case under natural viewing conditions. In this case other methods such as the unitary event analysis (Gruen et al., 2002a,b) or its refined version Neuroxidence (Pipa et al., 2008) need to be applied. These methods can detect individual events of coincident firing and distinguish them from spurious

coincidences even if the discharge rates of the neurons are not stationary. If grouping operations are based on brief episodes of synchronous firing, they would have passed undetected because so far all experiments on feature binding have relied on conventional cross correlation analysis. Since these novel methods have been tested successfully on experimental and simulated data, they can now be applied to clarify the question whether synchronization serves to tag responses to groupable features as related and to thereby support perceptual grouping and scene segmentation.

In designing these future studies it will have to be considered that synchronization is state and attention dependent and that different binding functions are likely to be accomplished at different levels of the processing hierarchy. Thus, the challenge is to design tests that are appropriate for the investigated processing stage.

FURTHER CHALLENGES

Ideally, in all investigations of the functional role of synchronized oscillations, one would of course like to obtain causal evidence. This would require manipulations of oscillations and synchrony without interfering with other response variables. First attempts to achieve this with pharmacological and genetic manipulations of synchronizing mechanisms have been made but much more work is needed. So far, the large majority of studies have provided only correlative evidence for the involvement of neural synchrony in cognitive and executive functions. Although the same problem exists for the relation between changes in firing rates and behavioural functions, the possibility needs to be considered that changes in neural synchrony are in part an epiphenomenon of neuronal dynamics and are not exploited further. At present we consider this as highly unlikely because of the numerous findings from normal and abnormal brains that demonstrated close relationships between alterations in behaviour and cognition and associated modulations in the synchronization and amplitude of oscillatory activity in a wide range of frequencies. Also, there is abundant evidence from studies on synaptic plasticity and memory formation that emphasizes the importance of precise timing relations between the discharges of interconnected neurons for use dependent synaptic modifications (Markram et al., 1997). As timing relations are crucial in this context for the definition of relations, it follows that they must be of similar importance in signal processing because signatures of relatedness must be the same in signal processing and learning. As the timing relations relevant for determining the polarity of use dependent synaptic plasticity are defined on the scale of milliseconds, similarly precise temporal relations must be realized in signal processing in order to define the relatedness of neuronal responses.

Another important and unresolved question is related to the coexistence of oscillations in different frequency bands. We are only at the beginning of understanding their mutual interactions and spatial organization. Neuronal synchrony is found on different temporal and spatial scales. The spatial scale of synchrony can range from local synchronization of small numbers of neurons within a single cortical column to the synchronization of large populations that are distributed across different cortical regions and even across both hemispheres (Singer, 1999). The temporal scales of neuronal synchrony range from very precise sub-millisecond spike-spike synchronization to the synchronization of slow oscillatory activity as low as <0.1 Hz. Remarkably, synchronization is

not confined to oscillations of the same frequency band but occurs across different frequencies as $n:m$ synchrony (Palva et al., 2005; Tognoli and Kelso, 2009). This allows for the concatenation of rhythms and for the establishment of partial correlations (Roozun et al., 2008). An attractive hypothesis is that this could serve as a mechanism to encode nested relations – an indispensable function for the neuronal representation of composite objects and movements. Yet, so far there is no evidence that the observed concatenation of rhythms is used for the encoding of graded, hierarchically organized relations.

Yet another conundrum of neural synchrony is that it can be stable and long lasting, e.g. in sleep or drowsiness, but also very dynamic and transient in awake and attentive brains, as it was reported for perceptual grouping and the control of focused attention (Fries et al., 2001a; Taylor et al., 2005). While stable synchrony can be explained by fixed coupling based on the connectivity of the network, the very transient switches between synchronized and unsynchronized dynamics are much more challenging properties regarding the underlying mechanism.

To explain the fast dynamical modulation of synchrony remains a theoretical challenge. The fast time scale of switches between synchronized and de-synchronized states observed in the data seems to be incompatible with the speed of changes in the functional topology or the coupling strength that can be achieved with conventional mechanisms of synaptic plasticity. The same holds for putative mechanisms that could cause changes in transmission delays. Thus, the most likely option for the modulation of synchrony is to change the dynamical states of the coupled neuronal populations, such as the balance between excitation and inhibition (Brunel, 2000; Destexhe et al., 1999). Such state changes can achieve fast and flexible modulations of effective coupling among populations of neurons or areas of the brain. They can be induced by rate changes of sub populations, by changes in the balance of excitation and inhibition, and also by changes of the level of noise (Melloni et al., 2007; Ullner et al., 2009). To distinguish between these mechanisms will require close cooperation between theoreticians and experimentalists for the formulation of predictions and their testing.

Thus, much further work is required for the exploration of the various functions of oscillations and neural synchrony. Since the discovery of stimulus and context dependent synchronization of gamma oscillations some 20 years ago, we keep being intrigued by the growing variety of cognitive and executive functions that seem to exploit this mechanism. As far as prognoses are possible in basic research, we predict that application of massively parallel multisite recordings techniques – electrical or optical – and evaluation of temporal relations among distributed neuronal responses will continue to provide us with data that we consider indispensable for a deeper understanding of integrated cerebral functions.

ACKNOWLEDGMENTS

This work was supported by the Max Planck Society, the Hertie Foundation, an EU grant Project “Global Approach to Brain Activity: From Cognition to Disease” (GABA) Contract No. 043309, a grant from Deutsche Forschungsgemeinschaft (NI 708/2-1), and by the German Federal Ministry of Education and Research (BMBF) within the “Bernstein Focus: Neurotechnology” through research grant 01GQ0840.

REFERENCES

- American Psychiatric Association (2000). Diagnostic and Statistical Manual of Mental Disorders, Fourth Edn, Text Revision. Washington, DC, American Psychiatric Association.
- Arecchi, F. T., Boccaletti, S., and Ramazza, P. (1999). Pattern formation and competition in nonlinear optics. *Phys. Rep. Rev. Sect. Phys. Lett.* 318, 1–83.
- Azouz, R., and Gray, C. M. (2003). Adaptive coincidence detection and dynamic gain control in visual cortical neurons *in vivo*. *Neuron* 37, 513–523.
- Bartos, M., Vida, I., and Jonas, P. (2007). Synaptic mechanisms of synchronized gamma oscillations in inhibitory interneuron networks. *Nat. Rev. Neurosci.* 8, 45–56.
- Betsch, B. Y., Einhäuser, W., Körding, K. P., and König, P. (2004). The world from a cat's perspective – statistics of natural videos. *Biol. Cybern.* 90, 41–50.
- Biedlerlack, J., Castelo-Branco, M., Neuenchwander, S., Wheeler, D. W., Singer, W., and Nikolić, D. (2006). Brightness induction: rate enhancement and neuronal synchronization as complementary codes. *Neuron* 52, 1073–1083.
- Bleuler, E. (1950). *Dementia Praecox or the Group of Schizophrenias*. New York, International University Press. (Original work published in 1911).
- Brecht, M., Singer, W., and Engel, A. K. (1998). Correlation analysis of corticocortical interactions in the cat visual system. *J. Neurophysiol.* 79, 2394–2407.
- Brunel, N. (2000). Dynamics of sparsely connected networks of excitatory and inhibitory spiking neurons. *J. Comput. Neurosci.* 8, 183–208.
- Buia, C., and Tsieng, P. H. (2006). Attentional modulation of firing rate and synchrony in a model cortical network. *J. Comput. Neurosci.* 20, 247–264.
- Buzsáki, G. (2002). Theta oscillations in the hippocampus. *Neuron* 33, 325–340.
- Buzsáki, G. (2007). The structure of consciousness. *Nature* 446, 267.
- Buzsáki, G., and Draguhn, A. (2004). Neuronal oscillations in cortical networks. *Science* 304, 1926–1929.
- Cardin, J. A., Carlén, M., Meletis, K., Knoblich, U., Zhang, F., Deisseroth, K., Tsai, L. H., and Moore, C. I. (2009). Driving fast-spiking cells induces gamma rhythm and controls sensory responses. *Nature* 459, 663–667.
- Carrasco, M., Ling, S., and Read, S. (2004). Adaptive coincidence detection and dynamic gain control in visual cortical neurons *in vivo*. *Nat. Neurosci.* 7, 308–313.
- Castelli, F., Frith, C., Happe, F., and Frith, U. (2002). Autism, Asperger syndrome and brain mechanisms for the attribution of mental states to animated shapes. *Brain* 125, 1839–1849.
- Chalmers, D. J. (2000). What is a neural correlate of consciousness? In *Neural Correlates of Consciousness: Empirical and Conceptual Questions*, T. Metzinger, ed. (Cambridge, MA, MIT Press), pp. 17–40.
- Cosmelli, D., David, O., Lachaux, J. P., Martinerie, J., Garnero, L., Renault, B., and Varela, F. (2004). Waves of consciousness: ongoing cortical patterns during binocular rivalry. *Neuroimage* 23, 128–140.
- Courchesne, E., Karns, C. M., Davis, H. R., Ziccardi, R., Carper, R. A., Tigue, Z. D., Chisum, H. J., Moses, P., Pierce, K., Lord, C., Lincoln, A. J., Pizzo, S., Schreibman, L., Haas, R. H., Akshoof, N. A., and Courchesne, R. Y. (2001). Unusual brain growth patterns in early life in patients with autistic disorder: an MRI study. *Neurology* 57, 245–254.
- Dehaene, S., Changeux, J. P., Naccache, L., Sackur, J., and Sergent, C. (2006). Conscious, preconscious, and subliminal processing: a testable taxonomy. *Trends Cogn. Sci.* 10, 204–211.
- Dehaene, S., Naccache, L., Cohen, L., Bihan, D. L., Mangin, J. F., Poline, J. B., and Riviere, D. (2001). Cerebral mechanisms of word masking and unconscious repetition priming. *Nat. Neurosci.* 4, 752–758.
- Dehaene, S., Naccache, L., Le Clec, H. G., Koehlin, E., Mueller, M., Dehaene-Lambertz, G., van de Moortele, P. F., and Le Bihan, D. (1998). Imaging unconscious semantic priming. *Nature* 395, 597–600.
- Desimone, R., and Duncan, J. (1995). Neural mechanisms of selective visual attention. *Annu. Rev. Neurosci.* 18, 193–222.
- Destexhe, A., Contreras, D., and Steriade, M. (1999). Cortically-induced coherence of a thalamic-generated oscillation. *Neuroscience* 92, 427–443.
- DiCicco-Bloom, E., Lord, C., Zwaigenbaum, L., Courchesne, E., Dager, S. R., Schmitz, C., Schultz, R. T., Crawley, J., and Young, L. J. (2006). The developmental neurobiology of autism spectrum disorder. *J. Neurosci.* 26, 6897–6906.
- Doesburg, S. M., Kitajo, K., and Ward, L. M. (2005). Increased gamma-band synchrony precedes switching of conscious perceptual objects in binocular rivalry. *Neuroreport* 16, 1139–1142.
- Doesburg, S. M., Roggeveen, A. B., Kitajo, K., and Ward, L. M. (2008). Large-scale gamma-band phase synchronization and selective attention. *Cereb. Cortex* 18, 386–396.
- Dong, Y., Mihalas, S., Qiu, F., von der Heydt, R., and Niebur, E. (2008). Synchrony and the binding problem in macaque visual cortex. *J. Vis.* 8, 1–16.
- Eckhorn, R., Frien, A., Bauer, R., Woelbern, T., and Kehr, H. (1993). High frequency (60–90 Hz) oscillations in primary visual cortex of awake monkey. *Neuroreport* 4, 243–246.
- Engel, A. K., Fries, P., and Singer, W. (2001). Dynamic predictions: oscillations and synchrony in top-down processing. *Nat. Rev. Neurosci.* 2, 704–716.
- Engel, A. K., König, P., Kreiter, A. K., and Singer, W. (1991). Stimulus-dependent neuronal oscillations in cat visual cortex: inter-columnar interactions as determined by cross-correlation analysis. *Eur. J. Neurosci.* 2, 588–606.
- Engel, A. K., and Singer, W. (2001). Temporal binding and the neural correlates of sensory awareness. *Trends Cogn. Sci.* 5, 16–25.
- Fan, J., Byrne, J., Worden, M. S., Guise, K. G., McCandless, B. D., Fossella, J., and Posner, M. I. (2007). The relation of brain oscillations to attentional networks. *J. Neurosci.* 27, 6197–6206.
- Ferrarelli, F., Massimini, M., Peterson, M. J., Riedner, B. A., Lazar, M., Murphy, M. J., Huber, R., Rosanova, M., Alexander, A. L., Kalin, N., and Tononi, G. (2008). Reduced evoked gamma oscillations in the frontal cortex in schizophrenia patients: a TMS/EEG study. *Am. J. Psychiatry* 165, 996–1005.
- Fischer, I., Vicente, R., Buldu, J. M., Peil, M., Mirasso, C. R., Torrent, M. C., and Garcia-Ojalvo, J. (2006). Zero-lag long-range synchronization via dynamical relaying. *Phys. Rev. Lett.* 97, 123902.
- Frien, A., and Eckhorn, R. (2000). Functional coupling shows stronger stimulus dependency for fast oscillations than for low-frequency components in striate cortex of awake monkey. *Eur. J. Neurosci.* 12, 1466–1478.
- Fries, P. (2005). A mechanism for cognitive dynamics: neuronal communication through neuronal coherence. *Trends Cogn. Sci.* 9, 474–480.
- Fries, P., Reynolds, J. H., Rorie, A. E., and Desimone, R. (2001a). Modulation of oscillatory neuronal synchronization by selective visual attention. *Science* 291, 1560–1563.
- Fries, P., Neuenschwander, S., Engel, A. K., Goebel, R., and Singer, W. (2001b). Rapid feature selective neuronal synchronization through correlated latency shifting. *Nature Neurosci.* 4, 194–200.
- Fries, P., Nikolić, D., and Singer, W. (2007). The gamma cycle. *Trends Neurosci.* 30, 309–316.
- Fries, P., Roelfsema, P. R., Engel, A. K., König, P., and Singer, W. (1997). Synchronization of oscillatory responses in visual cortex correlates with perception in interocular rivalry. *Proc. Natl. Acad. Sci. U.S.A.* 94, 12699–12704.
- Fries, P., Schröder, J. H., Roelfsema, P. R., Singer, W., and Engel, A. K. (2002). Oscillatory neuronal synchronization in primary visual cortex as a correlate of stimulus selection. *J. Neurosci.* 22, 3739–3754.
- Fries, P., Womelsdorf, T., Oostenveld, R., and Desimone, R. (2008). The effects of visual stimulation and selective visual attention on rhythmic neuronal synchronization in macaque area V4. *J. Neurosci.* 28, 4823–4835.
- Friston, K. J. (1999). The disconnection hypothesis. *Schizophr. Res.* 30, 115–125.
- Gail, A., Brinksmeier, H. J., and Eckhorn, R. (2000). Contour decouples gamma activity across texture representation in monkey striate cortex. *Cereb. Cortex* 10, 840–850.
- Gallinat, J., Winterer, G., Herrmann, C. S., and Senkowski, D. (2004). Reduced oscillatory gamma-band responses in unmedicated schizophrenic patients indicate impaired frontal network processing. *Clin. Neurophysiol.* 115, 1863–1874.
- Geschwind, D. H., and Levitt, P. (2007). Autism spectrum disorders: developmental disconnection syndromes. *Curr. Opin. Neurobiol.* 17, 103–111.
- Ghose, G. M., and Maunsell, J. (1999). Specialized representations in visual cortex: a role for binding? *Neuron* 24, 79–85, 111–125.
- Gray, C. M., Koenig, P., Engel, A. K., and Singer, W. (1989). Oscillatory responses in cat visual cortex exhibit inter-columnar synchronization which reflects global synchrony properties. *Nature* 23, 334–337.
- Gray, C. M., and McCormick, D. A. (1996). Chattering cells: superficial pyramidal neurons contributing to the generation of synchronous oscillations in the visual cortex. *Science* 274, 109–113.
- Gray, C. M., and Viana Di Prisco, G. (1997). Stimulus-dependent neuronal oscillations and local synchronization in striate cortex of the alert cat. *J. Neurosci.* 17, 3239–3253.
- Grinstein, G., and Linsker, R. (2005). Synchronous neural activity in scale free network models versus random network models. *Proc. Natl. Acad. Sci. U.S.A.* 102, 9948–9953.
- Gross, J., Schmitz, F., Schnitzler, I., Kessler, K., Shapiro, K., Hommel, B., and Schnitzler, A. (2004). Modulation of long-range neural synchrony reflects temporal limitations of visual attention in humans. *Proc. Natl. Acad. Sci. U.S.A.* 101, 13050–13055.
- Gruen, S., Diesmann, M., and Aertsen, A. M. H. J. (2002a). Unitary

- events in multiple single-neuron spiking activity: I. Detection and significance. *Neural Comput.* 14, 43–80.
- Gruen, S., Diesmann, M., and Aertsen, A. M. H. J. (2002b). Unitary events in multiple single-neuron spiking activity: II. Nonstationary data. *Neural Comput.* 14, 81–119.
- Happé, F., and Frith, U. (2006). The weak coherence account: detail-focused cognitive style in autism spectrum disorders. *J. Autism. Dev. Dis.* 36, 5–25.
- Havenith, M. N., Yu, S., Chen, N., Biedlerack, J., Singer, W., and Nikolic, D. (2007). Millisecond delays in neuronal spiking activity carry information as accurately as firing rates. *Soc. Neurosci. Abstr.* 615.7 2007. Society for Neuroscience 37th Annual Meeting, San Diego, USA.
- Havenith, M. N., Zemmar, A., Yu, S., Baudrexel, S. M., Singer, W., and Nikolic, D. (2009). Measuring sub-millisecond delays in spiking activity with millisecond time-bins. *Neurosci. Lett.* 450, 296–300.
- Herbert, M. R., Ziegler, D. A., Deutsch, C. K., O'Brien, L. M., Lange, N., Bakardjiev, A., Hodgson, J., Adrien, K. T., Steele, S., Makris, N., Kennedy, D., Harris, G. J., and Caviness, V. S. (2003). Dissociations of cerebral cortex, subcortical and cerebral white matter volumes in autistic boys. *Brain* 126, 1182–1192.
- Herculano-Houzel, S., Munk, M. H., Neuenschwander, S., and Singer, W. (1999). Precisely synchronized oscillatory firing patterns require electroencephalographic activation. *J. Neurosci.* 19, 3992–4010.
- Herrmann, C. S., Munk, M. H. J., and Engel, A. K. (2004). Cognitive functions of gamma-band activity: memory match and utilization. *Trends Cogn. Sci.* 8, 347–355.
- Hirabayashi, T., and Miyashita, Y. (2005). Dynamically modulated spike correlation in monkey inferior temporal cortex depending on the feature configuration within a whole object. *J. Neurosci.* 25, 10299–10307.
- Huang, D., and Pipa, G. (2007). Achieving synchronization of networks by an auxiliary hub. *Europhys. Lett.* 77, 50010.
- Hubl, D., Koenig, T., Strik, W., Federspiel, A., Kreis, R., Boesch, C., Maier, S. E., Schroth, G., Lovblad, K., and Dierks, T. (2004). Pathways that make voices: white matter changes in auditory hallucinations. *Arch. Gen. Psychiatry* 61, 658–668.
- Hussman, J. P. (2001). Suppressed GABAergic inhibition as a common factor in suspected etiologies of autism. *J. Autism Dev. Disord.* 31, 247–248.
- Jensen, O., Kaiser, J., and Lachaux, J. P. (2007). Human gamma-frequency oscillations associated with attention and memory. *Trends Neurosci.* 30, 317–324.
- Jensen, O., and Tesche, C. D. (2002). Frontal theta activity in humans increases with memory load in a working memory task. *Eur. J. Neurosci.* 15, 1395–1399.
- Just, M. A., Cherkassky, V. L., Keller, T. A., and Minshew, N. J. (2004). Cortical activation and synchronization during sentence comprehension in high-functioning autism: evidence of underconnectivity. *Brain* 127, 1811–1821.
- Kanwisher, N. (2001). Neural events and perceptual awareness. *Cognition* 79, 89–113.
- König, P., Engel, A. K., Löwel, S., and Singer, W. (1993). Squint affects synchronization of oscillatory responses in cat visual cortex. *Eur. J. Neurosci.* 5, 501–508.
- König, P., Engel, A. K., Roelfsema, P. R., and Singer, W. (1995). How precise is neuronal synchronization? *Neural Comput.* 7, 469–485.
- Konstantareas, M. M., and Hewitt, T. (2001). Autistic disorder and schizophrenia: diagnostic overlaps. *J. Autism Dev. Disord.* 31, 19–28.
- Kopell, N., and Ermentrout, B. (2004). Chemical and electrical synapses perform complementary roles in the synchronization of interneuronal networks. *Proc. Natl. Acad. Sci. U.S.A.* 101, 15482–15487.
- Kopell, N., Ermentrout, G. B., Whittington, M. A., and Traub, R. D. (2000). Gamma rhythms and beta rhythms have different synchronization properties. *Proc. Natl. Acad. Sci. U.S.A.* 97, 1867–1872.
- Koshino, H., Carpenter, P. A., Minshew, N. J., Cherkassky, V. L., Keller, T. A., and Just, M. A. (2005). Functional connectivity in an fMRI working memory task in high-functioning autism. *NeuroImage* 24, 810–821.
- Kreiter, A. K., and Singer, W. (1992). Oscillatory neuronal responses in the visual cortex of the awake macaque monkey. *Eur. J. Neurosci.* 4, 369–375.
- Kreiter, A. K., and Singer, W. (1996). Stimulus-dependent synchronization of neuronal responses in the visual cortex of the awake macaque monkey. *J. Neurosci.* 16, 2381–2396.
- Krishnan, G. P., Vohs, J. L., Hetrick, W. P., Carroll, C. A., Shekhar, A., Bockbrader, M. A., and O'Donnell, B. F. (2005). Steady state visual evoked potential abnormalities in schizophrenia. *Clin. Neurophysiol.* 116, 614–624.
- Kubicki, M., McCarley, R., Westin, C. F., Park, H. J., Maier, S., Kikinis, R., Jolesz, F. A., and Shenton, M. E. (2007). A review of diffusion tensor imaging studies in schizophrenia. *J. Psychiatr. Res.* 41, 15–30.
- Kwon, J. S., O'Donnell, B. F., Wallenstein, G. V., Greene, R. W., Hirayasu, Y., Nestor, P. G., Hasselmo, M. E., Potts, G. F., Shenton, M. E., and McCarley, R. W. (1999). Gamma frequency-range abnormalities to auditory stimulation in schizophrenia. *Arch. Gen. Psychiatry* 56, 1001–1005.
- Lakatos, P., Chen, C. M., O'Connell, M. N., Mills, A., and Schroeder, C. E. (2007). Neuronal oscillations and multisensory interaction in primary auditory cortex. *Neuron* 53, 279–292.
- Lakatos, P., Karmos, G., Mehta, A. D., Ulbert, I., and Schroeder, C. E. (2008). Entrainment of neuronal oscillations as a mechanism of attentional selection. *Science* 320, 110–113.
- Lamme, V. A., and Spekreijse, H. (1998). Neuronal synchrony does not represent texture segregation. *Nature* 396, 362–366.
- Lee, S. H., Wynn, J. K., Green, M. F., Kim, H., Lee, K. J., Nam, M., Park, J. K., and Chung, Y. C. (2006). Quantitative EEG and low resolution electromagnetic tomography (LORETA) imaging of patients with persistent auditory hallucinations. *Schizophr. Res.* 83, 111–119.
- Lewis, D. A., Hashimoto, T., and Volk, D. W. (2005). Cortical inhibitory neurons and schizophrenia. *Nat. Rev. Neurosci.* 6, 312–324.
- Lima, B., Chen, N., Singer, W., and Neuenschwander, S. (2006). Strength of stimulus-induced gamma oscillations in monkey V1 depend on attention and expectancy. *Soc. Neurosci. Abstr.* 32.4. Society for Neuroscience 36th Annual Meeting, Washington, DC, USA.
- Lima, B., Singer, W., and Neuenschwander, S. (2007). Distributed gamma oscillations induced by expectancy in monkey V1 and V4. *Soc. Neurosci. Abstr.* 33.8.5. Society for Neuroscience 37th Annual Meeting, Washington, DC, USA.
- Llinas, R., and Pare, D. (1998). Coherent oscillations in specific and nonspecific thalamo-cortical networks and their role in cognition. In *Thalamus*, E. G. Jones, ed. (Amsterdam, Elsevier), pp. 501–516.
- Löwel, S., and Singer, W. (1992). Selection of intrinsic horizontal connections in the visual cortex by correlated neuronal activity. *Science* 255, 209–212.
- Lutz, A., Lachaux, J. P., Martinerie, J., and Varela, F. J. (2002). Guiding the study of brain dynamics by using first-person data: synchrony patterns correlate with ongoing conscious states during a simple visual task. *Proc. Natl. Acad. Sci. U.S.A.* 99, 1586–1591.
- Maldonado, P. E., Friedman-Hill, S., and Gray, C. M. (2000). Dynamics of striate cortical activity in the alert macaque: II. Fast time scale synchronization. *Cereb. Cortex* 10, 1117–1131.
- Markram, H., Lübke, J., Frotscher, M., and Sakmann, B. (1997). Regulation of synaptic efficacy by coincidence of postsynaptic APs and EPSPs. *Science* 275, 213–215.
- McCaffery, P., and Deutsch, C. K. (2005). Macrocephaly and the control of brain growth in autistic disorders. *Prog. Neurobiol.* 77, 38–56.
- Melloni, L., Molina, C., Pena, M., Torres, D., Singer, W., and Rodriguez, E. (2007). Synchronization of neural activity across cortical areas correlates with conscious perception. *J. Neurosci.* 27, 2858–2865.
- Melloni, L., and Rodriguez, E. (2007). Non-perceived stimuli elicit local but not large-scale neural synchrony. *Perception* 36, (EVP Abstract Supplement).
- Melloni, L., Schwiedrzik, C. M., Rodriguez, E., and Singer, W. (2009). (Micro)Saccades, corollary activity and cortical oscillations. *Trends Cogn. Sci.* 3, 239–245.
- Milne, E., Scope, A., Pascalis, O., Buckley, D., and Makeig, S. (2009). Independent component analysis reveals atypical electroencephalographic activity during visual perception in individuals with autism. *Biol. Psychiatry* 65, 22–30.
- Milo, R., Shen-Orr, S., Itzkovitz, S., Kashtan, N., Chklovskii, D., and Alon, U. (2002). Network motifs: simple building blocks of complex networks. *Science* 298, 824–827.
- Munk, M. H., Roelfsema, P. R., König, P., Engel, A. K., and Singer, W. (1996). Role of reticular activation in the modulation of intracortical synchronization. *Science* 272, 271–274.
- Murias, M., Webb, S. J., Greenson, J., and Dawson, G. (2007). Resting state cortical connectivity reflected in EEG coherence in individuals with autism. *Biol. Psychiatry* 62, 270–273.
- Neuenschwander, S., Engel, A. K., König, P., Singer, W., and Varela, F. J. (1996). Synchronization of neuronal responses in the optic tectum of awake pigeons. *Vis. Neurosci.* 13, 575–584.
- Neuenschwander, S., Lima, B., and Singer, W. (2008). Stimulus and task-related gamma oscillations in monkey V1 induced by local and global contours. *Soc. Neurosci. Abstr.* 2008-S-112007-SfN. Society for

- Neuroscience 38th Annual Meeting, Washington, DC, USA.
- Neuenschwander, S., and Singer, W. (1996). Long-range synchronization of oscillatory light responses in the cat retina and lateral geniculate nucleus. *Nature* 379, 728–732.
- Nikolić, D. (2007). Non-parametric detection of temporal order across pairwise measurements of time delays. *J. Comput. Neurosci.* 22, 5–19.
- Nikolić, D., Häusser, S., Singer, W., and Maass, W. (2007). Temporal dynamics of information content carried by neurons in the primary visual cortex. *Adv. Neural Inf. Process. Syst.* 19.
- Nikolić, D., Schneider, G., Havenith, M. N., and Singer, W. (2004). Short time delays in neuronal activity depend on stimulus properties. *Soc. Neurosci. Abstr.* 490.8. 2004: Society for Neuroscience 34th Annual Meeting, San Diego, USA.
- O'Keefe, J., and Recce, M. L. (1993). Phase relationship between hippocampal place units and the EEG theta rhythm. *Hippocampus* 3, 317–330.
- Orekhova, E. V., Stroganova, T. A., Nygren, G., Tsetlin, M. M., Posikera, I. N., Gillberg, C., and Elam, M. (2007). Excess of high frequency electroencephalogram oscillations in boys with autism. *Biol. Psychiatry* 62, 1022–1029.
- Palanca, B. J., and DeAngelis, G. C. (2005). Does neuronal synchrony underlie visual feature grouping? *Neuron* 46, 333–346.
- Palva, J. M., Palva, S., and Kaila, K. (2005). Phase synchrony among neuronal oscillations in the human cortex. *J. Neurosci.* 25, 3962–3972.
- Palva, S., and Palva, J. M. (2007). New vistas for alpha-frequency band oscillations. *Trends Neurosci.* 30, 150–158.
- Pesaran, B., Pezaris, J. S., Sahani, M., Mitra, P. P., and Andersen, R. A. (2002). Temporal structure in neuronal activity during working memory in macaque parietal cortex. *Nat. Neurosci.* 5, 805–811.
- Phillips, W. A., and Silverstein, S. M. (2003). Convergence of biological and psychological perspectives on cognitive coordination in schizophrenia. *Behav. Brain Sci.* 26, 65–138.
- Pikovsky, A., Rosenblum, M., and Kurths, J. (2001). Synchronization. Cambridge, Cambridge University Press.
- Pipa, G., Riehle, A., and Grün, S. (2007). Validation of task-related excess of spike coincidences based on NeuroXidence. *Neurocomputing* 70, 2064–2068.
- Pipa, G., Wheeler, D. W., Singer, W., and Nikolić, D. (2008). NeuroXidence: reliable and efficient analysis of an excess or deficiency of joint-spike events. *J. Comput. Neurosci.* 25, 64–88.
- Posner, M. I. (1980). Orienting of attention. *Q. J. Exp. Psychol.* 32, 3–25.
- Reynolds, J. H., and Chelazzi, L. (2004). Attentional modulation of visual processing. *Annu. Rev. Neurosci.* 27, 611–647.
- Reynolds, J. H., and Desimone, R. (2000). The role of neural mechanisms of attention in solving the binding problem. *Neuron* 24, 19–29, 111–125.
- Ritz, R., and Sejnowski, T. J. (1997). Synchronous oscillatory activity in sensory systems: new vistas on mechanisms. *Curr. Opin. Neurobiol.* 7, 536–546.
- Roberts, M., Delicato, L. S., Herrero, J., Gieselmann, M. A., and Thiele, A. (2007). Attention alters spatial integration in macaque V1 in an eccentricity-dependent manner. *Nat. Neurosci.* 10, 1483–1491.
- Rodriguez, E., George, N., Lachaux, J. P., Martinerie, J., Renault, B., and Varela, F. J. (1999). Perception's shadow: long-distance synchronization of human brain activity. *Nature* 397, 430–433.
- Rodriguez, R., Kallenbach, U., Singer, W., and Munk, M. H. J. (2004). Short- and long-term effects of cholinergic modulation on gamma oscillations and response synchronization in the visual cortex. *J. Neurosci.* 24, 10369–10378.
- Roelfsema, P. R. (2006). Cortical algorithms for perceptual grouping. *Annu. Rev. Neurosci.* 29, 203–227.
- Roelfsema, P. R., Engel, A. K., König, P., and Singer, W. (1997). Visuomotor integration is associated with zero time-lag synchronization among cortical areas. *Nature* 385, 157–161.
- Roelfsema, P. R., Lamme, V. A., and Spekreijse, H. (2004). Synchrony and covariation of firing rates in the primary visual cortex during contour grouping. *Nat. Neurosci.* 7, 982–991.
- Rojas, D. C., Maharajh, K., Teale, P., and Rogers, S. J. (2008). Reduced neural synchronization of gamma-band MEG oscillations in first-degree relatives of children with autism. *BMC Psychiatry* 8, 66.
- Roopun, A. K., Kramer, M. A., Carracedo, L. M., Kaiser, M., Davies, C. H., Traub, R. D., Kopell, N. J., and Whittington, M. A. (2008). Period concatenation underlies interactions between gamma and beta rhythms in neocortex. *Front. Cell. Neurosci.* 2, 1.
- Roy, A., Steinmetz, P. N., Hsiao, S. S., Johnson, K. O., and Niebur, E. (2007). Synchrony: a neural correlate of somatosensory attention. *J. Neurophysiol.* 98, 1645–1661.
- Rubenstein, J. L., and Merzenich, M. M. (2003). Model of autism: increased ratio of excitation/inhibition in key neural systems. *Genes Brain Behav.* 2, 255–267.
- Salinas, E., and Sejnowski, T. J. (2000). Impact of correlated synaptic input on output firing rate and variability in simple neuronal models. *J. Neurosci.* 20, 6193–6209.
- Salinas, E., and Sejnowski, T. J. (2001). Correlated neuronal activity and the flow of neural information. *Nat. Rev. Neurosci.* 2, 539–550.
- Schack, B., Klimesch, W., and Sauseng, P. (2005). Phase synchronization between theta and upper alpha oscillations in a working memory task. *Int. J. Psychophysiol.* 57, 105–114.
- Schneider, G., Havenith, M. N., and Nikolić, D. (2006). Spatio-temporal structure in large neuronal networks detected from cross-correlation. *Neural Comput.* 18, 2387–2413.
- Schneider, G., and Nikolić, D. (2006). Detection and assessment of near-zero delays in neuronal spiking activity. *J. Neurosci. Meth.* 152, 97–106.
- Schoffelen, J. M., Oostenveld, R., and Fries, P. (2005). Neuronal coherence as a mechanism of effective corticospinal interaction. *Science* 308, 111–113.
- Schuster, H. G., and Wagner, P. (1989). Mutual entrainment of two limit cycle oscillators with time delayed coupling. *Prog. Theor. Phys.* 81, 939–945.
- Sehatpour, P., Molholm, S., Schwartz, T. H., Mahoney, J. R., Mehta, A. D., Javitt, D. C., Stanton, P. K., and Foxe, J. J. (2008). A human intracranial study of long-range oscillatory coherence across a frontal-occipital-hippocampal brain network during visual object processing. *Proc. Natl. Acad. Sci. U.S.A.* 105, 4399–4404.
- Sejnowski, T. J., and Paulsen, O. (2006). Network oscillations: emerging computational principles. *J. Neurosci.* 26, 1673–1676.
- Sergent, C., Baillet, S., and Dehaene, S. (2005). Timing of the brain events underlying access to consciousness during the attentional blink. *Nat. Neurosci.* 8, 1391–1400.
- Shadlen, M. N., and Movshon, J. A. (1999). Synchrony unbound: a critical evaluation of the temporal binding hypothesis. *Neuron* 24, 67–77, 111–125.
- Sheinberg, D. L., and Logothetis, N. K. (2001). Noticing familiar objects in real world scenes: the role of temporal cortical neurons in natural vision. *J. Neurosci.* 21, 1340–1350.
- Sherman, S. M., and Guillery, R. W. (2002). The role of the thalamus in the flow of information to the cortex. *Philos. Trans. R. Soc. Lond., B, Biol. Sci.* 357, 1695–1708.
- Singer, W. (1999). Neuronal synchrony: a versatile code for the definition of relations? *Neuron* 24, 49–65, 111–125.
- Singer, W. (2002). Phenomenal awareness and consciousness from a neurobiological perspective. In *Neural Correlates of Consciousness*, T. Metzinger, ed. (Cambridge, MA, MIT Press), pp. 121–137.
- Singer, W. (2004). Time as coding space in the cerebral cortex. In *Functional Neuroimaging of Visual Cognition. Attention and Performance XX*, N. Kanwisher and J. Duncan, eds (Oxford, Oxford University Press), pp. 99–123.
- Slewa-Young, S., Gordon, E., Harris, A. W., Haig, A. R., Brown, K. J., Flor-Henry, P., and Williams, L. M. (2004). Sex differences in functional connectivity in first-episode and chronic schizophrenia patients. *Am. J. Psychiatry* 161, 1595–1602.
- Sohal, V. S., Zhang, F., Yizhar, O., and Deisseroth, K. (2009). Parvalbumin neurons and gamma rhythms enhance cortical circuit performance. *Nature* 459, 698–702.
- Spencer, K. M., Nestor, P. G., Niznikiewicz, M. A., Salisbury, D. F., Shenton, M. E., and McCarley, R. W. (2003). Abnormal neural synchrony in schizophrenia. *J. Neurosci.* 23, 7407–7411.
- Spencer, K. M., Nestor, P. G., Perlmuter, R., Niznikiewicz, M. A., Klump, M. C., Frumin, M., Shenton, M. E., and McCarley, R. W. (2004). Neural synchrony indexes disordered perception and cognition in schizophrenia. *Proc. Natl. Acad. Sci. U.S.A.* 101, 17288–17293.
- Spencer, K. M., Salisbury, D. F., Shenton, M. E., and McCarley, R. W. (2008). Gamma-band auditory steady-state responses are impaired in first episode psychosis. *Biol. Psychiatry* 64, 369–375.
- Spitzer, H., Desimone, R., and Moran, J. (1988). Increased attention enhances both behavioral and neuronal performance. *Science* 240, 338–340.
- Sporns, O., and Kotter, R. (2004). Motifs in brain networks. *PLoS Biol.* 2, 1910–1918.
- Srinivasan, R., Russell, D. P., Edelman, G. M., and Tononi, G. (1999). Increased synchronization of neuromagnetic responses during conscious perception. *J. Neurosci.* 19, 5435–5448.
- Steinmetz, P. N., Roy, A., Fitzgerald, P. J., Hsiao, S. S., Johnson, K. O., and Niebur, E. (2000). Attention modulates synchronized neuronal firing in primate somatosensory cortex. *Nature* 404, 187–190.
- Steriade, M., McCormick, D. A., and Sejnowski, T. J. (1993). Thalamocortical oscillations in the sleeping and aroused brain. *Science* 262, 679–685.
- Tallon-Baudry, C. (2009). The roles of gamma-band oscillatory synchrony in human visual cognition. *Front. Biosci.* 14, 321–332.

- Tallon-Baudry, C., Bertrand, O., Delpeuch, C., and Pernier, J. (1997). Oscillatory gamma-band (30–70 Hz) activity induced by a visual search task in humans. *J. Neurosci.* 17, 722–734.
- Taylor, K., Mandon, S., Freiwald, W. A., and Kreiter, A. K. (2005). Coherent oscillatory activity in monkey area V4 predicts successful allocation of attention. *Cereb. Cortex* 15, 1424–1437.
- Thiele, A., and Stoner, G. (2003). Neuronal synchrony does not correlate with motion coherence in cortical area MT. *Nature* 421, 366–370.
- Thompson, E., and Varela, F. J. (2001). Radical embodiment: neural dynamics and consciousness. *Trends Cogn. Sci.* 5, 418–425.
- Tiesinga, P. H., and Sejnowski, T. J. (2004). Rapid temporal modulation of synchrony by competition in cortical interneuron networks. *Neural Comput.* 16, 251–275.
- Tillmann, C., Wibral, M., Leweke, M., Kohler, A., Singer, W., Koethe, D., Kranaster, L., Maurer, K., and Uhlhaas, P. J. (2008). High-frequency gamma-band oscillations during perceptual organisation in chronic and first-episode schizophrenia patients. *Soc. Neurosci. Abstr.* 34, 2. Society for Neuroscience 38th Annual Meeting, Washington, D.C., USA.
- Tognoli, E., and Kelso, J. A. (2009). Brain coordination dynamics: true and false faces of phase synchrony and metastability. *Prog. Neurobiol.* 87, 31–40.
- Tononi, G., Srinivasan, R., Russell, D. P., and Edelman, G. M. (1998). Investigating neural correlates of conscious perception by frequency-tagged neuromagnetic responses. *Proc. Natl. Acad. Sci. U.S.A.* 95, 3198–3203.
- Traub, R. D., Bibbig, A., LeBeau, F. E., Buhl, E. H., and Whittington, M. A. (2004). Cellular mechanisms of neuronal population oscillations in the hippocampus *in vitro*. *Annu. Rev. Neurosci.* 27, 247–278.
- Traub, R. D., Whittington, M. A., Stanford, I. M., and Jefferys, J. G. R. (1996). A mechanism for generation of long-range synchronous fast oscillations in the cortex. *Nature* 383, 621–624.
- Uhlhaas, P. J., Linden, D. E. J., Singer, W., Haenschel, C., Lindner, M., Maurer, K., and Rodriguez, E. (2006). Dysfunctional long-range coordination of neural activity during Gestalt perception in schizophrenia. *J. Neurosci.* 26, 8168–8175.
- Uhlhaas, P. J., and Silverstein, S. M. (2005). Perceptual organization in schizophrenia spectrum disorders: a review of empirical research and associated theories. *Psychol. Bull.* 131, 618–632.
- Uhlhaas, P. J., and Singer, W. (2006). Neural synchrony in brain disorders: relevance for cognitive dysfunction and pathophysiology. *Neuron* 52, 155–168.
- Uhlhaas, P. J., and Singer, W. (2007). What can neural synchrony tell us about autism? *Biol. Psychiatry* 62, 190–191.
- Ullner, E., Vicente, R., Pipa, G., and Garcia-Ojalvo, J. (2009). Contour integration and synchronization in neuronal networks of the visual cortex. *Springer Lect. Notes Comput. Sci. Artif. Neural Netw.* 5164, 703–712.
- Van Vreeswijk, C., Abbott, L. F., and Ermentrout, G. B. (1994). When inhibition not excitation synchronizes neural firing. *J. Comput. Neurosci.* 1, 313–321.
- Varela, F., Lachaux, J. P., Rodriguez, E., and Martinerie, J. (2001). The brainweb: phase synchronization and large-scale integration. *Nat. Rev. Neurosci.* 2, 229–239.
- Varela, F. J. (1999). The specious present: a neurophenomenology of time consciousness. In *Naturalizing Phenomenology*, J. Petitot, F. J. Varela, J.-M. Roy, and B. Pachoud, eds. (Stanford, CA, Stanford University Press), pp. 266–314.
- Vicente, R., Gollo, L. L., Mirasso, C. R., Fischer, I., and Pipa, G. (2008). Dynamical relaying can yield zero time lag neuronal synchrony despite long conduction delays. *Proc. Natl. Acad. Sci. U.S.A.* 105, 17157–17162.
- Villalobos, M. E., Mizuno, A., Dahl, B. C., Kemmotsu, N., and Muller, R. A. (2005). Reduced functional connectivity between V1 and inferior frontal cortex associated with visuomotor performance in autism. *NeuroImage* 25, 916–925.
- Volgushev, M., Chistiakova, M., and Singer, W. (1998). Modification of discharge patterns of neocortical neurons by induced oscillations of the membrane potential. *Neuroscience* 83, 15–25.
- von Stein, A., Chiang, C., and König, P. (2000). Top-down processing mediated by interareal synchronization. *Proc. Natl. Acad. Sci. U.S.A.* 97, 14748–14753.
- Williams, S. R., and Atkinson, S. (2008). Dendritic synaptic integration in central neurons. *Curr. Biol.* 22, R1045–R1047.
- Wilson, T. W., Rojas, D. C., Reite, M. L., Teale, P. D., and Rogers, S. J. (2007). Children and adolescents with autism exhibit reduced MEG steady-state gamma responses. *Biol. Psychiatry* 62, 192–197.
- Womelsdorf, T., and Fries, P. (2006). Neuronal coherence during selective attentional processing and sensory-motor integration. *J. Physiol. (Paris)* 100, 182–193.
- Womelsdorf, T., Fries, P., Mitra, P., and Desimone, R. (2006). Gamma-band synchronization in visual cortex predicts speed of change detection. *Nature* 439, 733–736.
- Womelsdorf, T., Schoffelen, J.-M., Oostenveld, R., Singer, W., Desimone, R., Engel, A. K., and Fries, P. (2007). Modulation of neuronal interactions through neuronal synchronization. *Science* 316, 1609–1612.
- Wu, W., Wheeler, D. W., Staedtler, E. S., Munk, M. H., and Pipa, G. (2008). Behavioral performance modulates spike field coherence in monkey prefrontal cortex. *Neuroreport* 19, 235–238.
- Wynn, J. K., Light, G. A., Breitmeyer, B., Nuechterlein, K. H., and Green, M. F. (2005). Event-related gamma activity in schizophrenia patients during a visual backward-masking task. *Am. J. Psychiatry* 162, 2330–2336.
- Yu, S., Huang, D., Singer, W., and Nikolic, D. (2008). A small world of neuronal synchrony. *Cereb. Cortex* 18, 2891–2901.
- Yuval-Greenberg, S., Tomer, O., Keren, A. S., Nelken, I., and Deouell, L. Y. (2008). Transient induced gamma-band response in EEG as a manifestation of miniature saccades. *Neuron* 58, 429–441.

Conflict of Interest Statement: The authors declare that the research was conducted in the absence of any commercial or financial relationships that could be construed as a potential conflict of interest.

Received: 04 March 2009; paper pending published: 20 March 2009; accepted: 11 July 2009; published online: 30 July 2009.

Citation: Uhlhaas PJ, Pipa G, Lima B, Melloni L, Neuenschwander S, Nikolić D and Singer W (2009) Neural synchrony in cortical networks: history, concept and current status. *Front. Integr. Neurosci.* 3:17. doi: 10.3389/fneuro.07.017.2009

Copyright © 2009 Uhlhaas, Pipa, Lima, Melloni, Neuenschwander, Nikolić and Singer. This is an open-access article subject to an exclusive license agreement between the authors and the Frontiers Research Foundation, which permits unrestricted use, distribution, and reproduction in any medium, provided the original authors and source are credited.

Detailed summary

Introduction: Visual neuroscience has accumulated a large amount of information regarding the analytical capabilities of the nervous system. The advent of single unit recordings enabled a detailed description of receptive field properties throughout the visual pathway. The concentric receptive fields in the retina respond optimally to luminance contrast across its ON and OFF sub-regions. Response attributes gradually evolve to extract increasingly more complex features of the visual stimulus. The pioneering studies by David Hubel and Torsten Wiesel first described the orientation and direction selectivities of neurons in the early visual cortex. Subsequently, single cells in the medial temporal lobe have been shown to respond to complex objects such as hands and faces. Mainstream neuroscience has therefore assumed that the representation of complex objects is a natural unfolding of convergence taking place along the visual pathway. Cells responding to elementary features of the stimulus gradually create, through their pattern of anatomical connections, the specialized neurons observed in higher areas. This proposal, however, is not without limitations. A pertinent criticism generally applied to the single unit doctrine is the one commonly referred to as the “combinatorial problem”. We are constantly confronted with unlimited combinations of elements and features and yet we face no problem in recognizing patterns and objects presented in our visual scene. Is it possible that each one of our percepts is coded by the response of a single highly specialized neuron in the brain? If not, which mechanism could serve as a relational code capable of integrating activity across different neuronal ensembles? The requirement for such a mechanism is made further evident by the distributed nature of visual processing. Feature extraction by neurons along the visual pathway inevitably leads to spatially scattered representations. Additionally, parallel pathways of neuronal processing are common in the brain. We lack, however, a general theory capable of explaining how distributed information can be efficiently integrated into single percepts. The working hypothesis here is that the brain uses the time domain in order to integrate and process visual information. More specifically, neuronal ensembles would signal relations present in the stimulus by selectively synchronizing their spiking responses. Synchronization is generally associated with oscillatory activity in the brain. Gamma oscillations in particular have been linked to various integrative processes in the visual system. Studies in anesthetized animals have shown a conspicuous increase in power for the gamma frequency band (30 to 60 Hz) in response to visual stimuli. Recently, these observations have been extended to behavioral studies which addressed the role of gamma activity in cognitive processes demanding selective attention. The initial motivation for carrying out this work was to test the binding-by-synchronization (BBS) hypothesis as proposed by Wolf Singer and collaborators. This was addressed by recording the response of V1 neurons to a pair of superimposed gratings (plaid stimulus). Physical manipulations of the plaid stimulus can bias perception to component motion

(two objects sliding over one another) or to pattern motion (a single moving object). Recordings from pairs of sites selectively responding to either of the grating stimuli allowed us to test two predictions of the BBS hypothesis. First, if the V1 sites respond to the same grating, the BBS hypothesis predicts that the neurons should synchronize their activity regardless of whether the plaid is perceived as having component or pattern motion. This is because the pair of sites is responding to the same object. The second test deals with the case where each site responds to one of the two grating components. In this case the BBS hypothesis predicts that they should synchronize their activity only when presented with pattern motion since only in this condition do they respond to the same object.

While testing the binding-by-synchronization hypothesis we performed various experiments which addressed the role of both stimulus and cortical architecture on the properties of gamma oscillations. Additionally, gamma oscillations have been associated with visual processes demanding selective spatial attention. Here we investigated whether gamma activity could also be modulated by allocating attention in time. Finally, we report on gamma-phase shifts in area V1 and how they depend on the level of neuronal activation.

Methods: We recorded neuronal activity in area V1 of four Rhesus monkeys (*Macaca mulatta*). Recordings were performed with multiple electrodes (average of 5 electrodes) in the central (~3°) and parafoveal (~10°) representations of the visual field. The compound signal acquired from each electrode was submitted to filtering procedures which isolated different frequency components of the neuronal activity. The low frequencies (0.7-170 Hz) gave rise to the local field potential (LFP) while high frequencies (700-6000 Hz) contained the spiking activity of multiple neurons (MUA). For selected cases, offline spike sorting further isolated single unit activity from the MUA.

Neuronal activity was obtained while the monkeys were awake and engaged in several sorts of behavioral tasks. The monkeys were trained to come to the laboratory on a daily basis, either for training or for participating in a recording session. In their home cage, the animals lived in social groups composed of 2-5 individuals. Upon instruction, they learnt to approach and sit on a primate chair. Once in the lab, they were positioned in front of a monitor screen which displayed visual stimulation during the experiment. In order to stabilize the visual image on the retina, monkeys were trained to fixate a small red point (fixation point, FP) on the screen. Fixation was monitored either with a scleral search coil or with an infrared camera. A typical trial started when the monkey fixated and pressed a lever. Throughout the trial, fixation had to remain within 1° of the FP. Upon color change of the FP (from red to green), the monkey was required to immediately release the lever in order to obtain a liquid reward (fruit juice). Trials were aborted for early or late lever releases, or when fixation was interrupted during the trial. No reward was delivered in these cases. Typically,

monkeys performed between 700 and 1500 correct trials in 5 hour sessions thereby receiving their daily liquid requirement.

At the beginning of each recording session, V1 receptive fields were mapped using an automatic procedure in which a bar was moved across the screen in 16 different directions. Both the center and the extend of the receptive fields were estimated by interpolating the spiking activity elicited by all 16 directions of motion. Direction tuning curves for each site were subsequently obtained with square-wave grating stimuli, also moving in 16 different directions. The grating was positioned so as to simultaneously activate all recorded neurons. The other visual stimulus employed during this study was the moving plaid. Plaids are bi-stable stimuli capable of eliciting different percepts depending on their physical characteristics. They were built by superimposing two gratings with an offset of 135° in their moving direction (45° orientation offset). Plaid transparency was manipulated by varying the luminance of the individual components and their intersections. In this way, they could be perceived either as a single moving surface (pattern plaids) or as two segregated surfaces drifting in different directions (component plaids).

Different types of behavioral tasks were used during this study. The most simple consisted in the FP-change detection task (explained above). For this case, stimuli presented over the receptive fields were passively viewed by the monkey while it detected a color-change event at the fovea. This task was used to study the receptive field properties and to investigate changes in the ongoing activity while single and superimposed grating stimuli were presented along the same trial. Additionally, this task was used to orient the attention of the monkey in time. This was done by making the relevant trial events predictable. Fixed stimuli sequences, where the FP-change event occurred invariably at the end of the sequence, were used to build temporal expectation (sequence protocols). For the block protocol, the FP-change event could take place early or late in the trial. Trials with the same time schedule were presented in blocks of approximately 50 repetitions, making task timing predictable. Finally, the proximity of the FP-change event could be indicated by a luminance cue presented at the FP itself (cue protocols). Neuronal activity was compared for trial segments where temporal expectation was either low or high.

One monkey was trained to direct attention to one of the plaid surfaces. For this experiment, the configuration of the plaid stimulus was highly biased to the perception of two surfaces sliding over each other. The monkey was required to respond to a luminance change in the cued grating component and to ignore changes taking place at the distractor component. In this task, the FP remained unchanged and served only to hold the monkey's gaze.

The analysis employed here consisted in obtaining measures of temporal patterning for local (MUA and SUA) and global (LFP) neuronal activity in V1. Both time and frequency domain approaches

were used. For assessment of synchronous oscillations in the spiking responses, auto- and cross-correlograms were computed on a trial-by-trial basis (resolution of 1 ms), and then averaged over all repetitions for each condition. Spectral quantities were estimated for both spike and LFP signals using the multitaper method. The power spectrum was computed in z-score units relative to the spontaneous activity. The degree of phase-locking between pairs of time series was evaluated by computing coherence measures.

Results and Discussion: Experiments on surface segmentation were carried out using different configurations of plaid stimuli. Based on the binding-by-synchronization hypothesis, we made predictions on how neurons in area V1 should synchronize their activity depending on stimulus configuration and, therefore, on perception. None of our predictions held, regardless of whether the monkey passively viewed the stimulus or actively attended to one of its surfaces. Consequently, gamma activity was predominantly dependent on the local properties of the stimulus, and not on its global properties as we had initially hypothesized.

To better understand the negative results described above, we performed an extensive set of experiments in order to investigate which main factors determine the properties of gamma activity in monkey area V1. Drifting gratings with optimal orientation, speed and spatial frequency are known to induce strong gamma oscillations in the primary visual cortex. Due to the columnar organization of V1 and to the pattern of horizontal projections which connect neurons with similar selectivity, single gratings are believed to activate a selective population of cells. Indeed, gamma oscillations induced by a single grating were strong and sustained, and generally gave rise to single peaks in the power spectrum. Adding a second grating to the stimulus profoundly changed the dynamics of neuronal activity. Namely, gamma power (specially for the spiking activity) was greatly attenuated while the LFP oscillation frequency systematically shifted to higher values. We believe that the main effect of adding a second grating to the stimulus was to activate two neuronal populations with different selectivity properties. We thereby investigated whether the power and frequency changes observed were arising due to competitive mechanisms induced by the different grating components. We performed two experiments where we parametrically tested the disturbance induced by component 2 (background grating) on the ongoing oscillations induced by component 1 (foreground grating) alone. In the first experiment, we increased the contrast of component 2 relative to component 1. The oscillation frequency increased and power decreased for increasing contrast values. In a second experiment, the same trend was observed when the angle between the two components was increased. Both experiments argued in favor of a competitive mechanism.

The second important finding was the spatial extent of correlated gamma activity in area V1. We recorded spiking activity and LFP from three different spatial scales: signals obtained from the

same electrode, signals obtained from separate but nearby sites in the cortex, and signals obtained from sites in the cortex representing distant eccentricities (3° versus 10°). We were therefore able to observe the decay of correlated gamma activity as a function of cortical distance. Correlation between spiking activity and LFP acquired from the same electrode was typically much higher than the one obtained across electrodes. LFP-LFP correlations between distant electrodes were frequently found but had lower magnitude as compared to signal pairs acquired from nearby sites in the cortex. LFP-spike correlations were rare, and spike-spike correlations were never found between distant sites. Thus, correlation measurements which included the LFP signal were much more likely to reach significance. One possible reason for these results may be due to sampling. The LFP reflects the activity of a population of neurons while single-cell discharges are much more prone to skip cycles in the oscillatory process. Indeed, the incidence of oscillatory activity was clearly more visible in the LFP than in the spikes. We conclude that the limited extent in which gamma interactions take place in V1 may restrict their role as a mechanism capable of integrating information across spatially distributed sites.

The oscillation frequency of gamma activity in V1 was found to be modulated by several factors. The pattern of cortical activation (single versus superimposed gratings) was one of them. The second factor was the eccentricity of the recording site. Oscillation frequency was inversely related to eccentricity in a way that peak frequency systematically decreased for sites representing more peripheral portions of the visual field. A third factor was selective attention. Oscillation frequency depended on which surface of the plaid stimulus the monkey attended to. Finally, inter-individual variability also played a role. For equal stimulation conditions, we observed that each of the monkeys had a specific peak oscillation frequency in the gamma band. Despite the inter-individual differences, the spectral profile within the same individual was incredibly consistent, as revealed by measurements across hemispheres and different recording sessions.

In accordance with several recently published studies, we found that attention can strongly modulate gamma activity. Here, we report that directing attention in time modulates gamma processes in monkey V1. Temporal expectation led to enhancement of gamma oscillations (30 to 90 Hz) in the LFP and occasionally in the spiking activity, and it was typically associated with an alpha suppression, as generally seen in studies on selective attention. Phase-locking between spiking activity and LFP also increased for gamma components as estimated from spike-field coherence measurements. These effects were spatially widespread. Even though the focus of attention was directed to the FP, we observed comparable magnitudes of change for both central (3°) and parafoveal (10°) receptive fields. Gamma enhancement occurred in a frequency-specific, stimulus-dependent manner. Previously, we reported that superimposed gratings induced gamma oscillations at higher frequencies as compared to those induced by the individual gratings. Here,

we show that expectation affects the strength of the oscillations without shifts in the main frequency components induced by a particular stimulus. Our results support the existence of a gain mechanism capable of widespread, spatially non-selective modulation of gamma activity. It is possible that internal states, such as expectation, are capable of gain-controlling the frequency-specific rhythms induced by features of the stimulus.

Finally, similar to the hippocampal theta phase precession, we report gamma-phase shifts in area V1. The timing of the spike relative to the gamma oscillation cycle shifted as a function of the neuronal activation strength. Neurons that were strongly activated spiked earlier in the gamma cycle. The phase of the spike in the gamma cycle thereby provided an instantaneous analog representation of neuronal excitation.

Conclusions: Gamma activity in the primary visual cortex seems to be highly dependent on cortical architecture. We described several stimulus parameters capable of modulating both gamma power and gamma oscillation frequency. In all cases, the nature of the modulation could be satisfactorily explained by the functional organization of the early visual cortex. Additionally, we observed that temporal expectation can strongly modulate gamma power and coherence in monkey area V1.

Zusammenfassung

Einleitung: Die visuelle Hirnforschung hat eine große Informationsmenge über die analytischen Fähigkeiten des Nervensystems zusammengetragen. Die Einführung von Einzelzelleitungen ermöglichte eine detaillierte Beschreibung der Eigenschaften rezeptiver Felder im Sehsystem. Konzentrische rezeptive Felder in der Netzhaut antworten optimal auf einen Luminanzkontrast in ihren On- und Off-Regionen. Antworteigenschaften entwickeln sich schrittweise entlang der Sehbahn, indem zunehmend komplexere Eigenschaften des visuellen Reizes extrahiert werden. Die Pionierarbeiten von David Hubel und Torsten Wiesel beschrieben zunächst Orientierungs- und Richtungsselektivität von Neuronen in frühen visuellen Kortexarealen. Später fand man Einzelzellen im medialen Temporallappen, die auf komplexe Objekte wie Hände und Gesichter antworten. Die Hirnforschung ist daher lange davon ausgegangen, dass die Repräsentation komplexer Objekte eine natürliche Entfaltung von Konvergenz entlang der Sehbahn darstellt. Zellen, welche auf elementare Merkmale des Stimulus antworteten, bildeten so durch ihr Muster anatomischer Verbindungen schrittweise die spezialisierten Neurone in höheren visuellen Arealen. Diese Sichtweise zeigt allerdings Limitationen auf. Eine beständige Kritik, die an der „Einzelzeldoktrin“ geübt wird, ist das sogenannte kombinatorische Problem. Obwohl wir ständig mit einer unbegrenzten Fülle an Kombinationen verschiedener Elemente und Merkmale konfrontiert sind, laufen wir selten Gefahr, Muster und Objekte in einer visuellen Szene nicht zu erkennen. Ist es überhaupt möglich, dass jedes unserer möglichen Perzepte durch die Antwort eines einzelnen hoch spezialisierten Neurons im Hirn kodiert wird? Falls nicht, welcher Mechanismus könnte einen relationalen Code darstellen, der es ermöglicht, die Aktivität verschiedener neuronaler Ensembles zu integrieren? Die Anforderungen an einen solchen Mechanismus treten besonders hervor, wenn man sich die verteilte Struktur der visuellen Verarbeitung verdeutlicht. Die Merkmalsextraktion entlang der Sehbahn führt unvermeidbar zu einer räumlich verstreuten Repräsentation eines visuellen Reizes. Zusätzlich kommen parallele Bahnen neuronaler Verarbeitung im Hirn häufig vor. Es fehlt eine universale Theorie darüber, wie die verteilte Information effizient in eine einzige Wahrnehmung integriert wird. Die Arbeitshypothese hier lautet, dass das Hirn die Zeitdomäne benutzt, um visuelle Informationen zu integrieren und zu verarbeiten. Konkret würden neuronale Ensembles die aus dem Stimulus hervorgehenden Beziehungen durch eine selektive Synchronisation ihrer Aktionspotenziale signalisieren. Synchronisation ist normalerweise mit oszillatorischer Hirnaktivität assoziiert. Besonders die Oszillationen im Gamma Frequenzband sind mit verschiedensten integrativen Prozessen im Sehsystem in Verbindung gebracht worden. Arbeiten an anästhesierten Tieren haben einen auffälligen Anstieg von Energie im Gamma Frequenzband (30-60 Hz) unter visueller Stimulation gezeigt. Kürzlich sind diese Beobachtungen auf Verhaltensstudien ausgeweitet worden, welche die Rolle von Gamma Aktivität bei der für

kognitive Prozesse erforderlichen gerichteten Aufmerksamkeit untersuchen. Die ursprüngliche Motivation dieser Arbeit war es, die von Wolf Singer und Mitarbeitern formulierte „binding-by-synchronization (BBS)“ Hypothese zu testen. Dies wurde durch die Ableitung neuronaler Antworten in V1 bei Darbietung eines Paares übereinander gelegter Balkengitter („Plaid“ Stimulus) angegangen. Physikalische Manipulationen der Luminanz in Unterregionen des Plaid-Stimulus können die Wahrnehmung zugunsten der Bewegung der Einzelkomponenten (zwei Objekte, die sich übereinander schieben) oder der Bewegung des Gesamtmusters (ein einziges sich in eine gemeinsame Richtung bewegendes Objekt) beeinflussen. Die gleichzeitige Ableitung von zwei Neuronen, die jeweils nur selektiv auf eines der beiden Balkengitter antworteten, ermöglichte es uns, zwei Vorhersagen der BBS Hypothese zu testen. Falls beide V1 Neurone auf dasselbe Balkengitter antworteten, sollten sie ihre Aktivität unabhängig davon, ob das Plaid in Einzelkomponenten oder als Gesamtmuster wahrgenommen würde, synchronisieren. Der Grund dafür wäre, dass beide Neurone auf dasselbe Objekt reagierten. Im zweiten Fall antworten beide Ableitstellen auf jeweils eine der beiden Balkengitterkomponenten. Hier sagt die BBS Hypothese voraus, dass beide ihre Aktivität nur bei Gesamtmusterbewegung synchronisieren würden, da sie nur in dieser Bedingung auf dasselbe Objekt antworten würden.

Um die BBS Hypothese zu belegen, unternahmen wir verschiedene Experimente, in denen wir sowohl die Rolle des Sehreizes als auch die der kortikalen Architektur auf die Eigenschaften von Gamma Oszillationen untersuchten. Außerdem wurden Gamma Oszillationen mit der visuellen Verarbeitung bei selektiver räumlicher Aufmerksamkeit in Verbindung gebracht. In der vorliegenden Arbeit untersuchten wir, ob Gamma Aktivität auch durch zeitlich strukturierte Aufmerksamkeitsprozesse moduliert wird.

Zuletzt beschreiben wir Phasenverschiebungen von Gamma Oszillationen in V1, und wie diese vom allgemeinen Niveau neuronaler Aktivität abhängen.

Methoden: Wir leiteten die neuronale Aktivität in V1 von vier Rhesusaffen ab (*Macaca mulatta*). Die Ableitungen wurden mit mehreren Elektroden gleichzeitig (im Mittel 5 Elektroden) in der zentralen (~3°) und parafovealen (~10°) Gesichtsfeldrepräsentation durchgeführt. Das Gesamtsignal jeder Elektrode wurde gefiltert, um unterschiedliche Frequenzanteile der neuronalen Aktivität zu isolieren. Die niedrigen Frequenzen (0.7-170 Hz) ergaben das lokale Feldpotenzial (LFP), während die hohen Frequenzen (700-6000 Hz) die Aktionspotenzialaktivität mehrerer Neurone (MUA) enthielten. Für ausgewählte Fälle isolierten wir Einzelzellaktivität von Multizellaktivität mittels eines „offline“ Spikesortieralgorithmus.

Die neuronale Aktivität wurde registriert, während die Affen wach und mit verschiedenen kurzen Aufgaben beschäftigt waren. Die Affen wurden trainiert für Trainings- oder Ableitsitzungen täglich

ins Labor zu kommen. In ihrem Heimatkäfig lebten die Affen in sozialen Gruppen bestehend aus 2 bis 5 Individuen. Sie wurden angelernt zu einem Primatenstuhl zu kommen und sich dort hinein zu setzen. Im Labor wurden sie mit dem Stuhl vor einen Computermonitor gesetzt, auf dem die Sehreize während der Experimente gezeigt wurden. Um das Bild auf der Netzhaut zu stabilisieren, wurden die Affen trainiert, einen kleinen roten Punkt auf dem Bildschirm zu fixieren (Fixierpunkt, FP). Die Fixierung wurde mittels einer Skleradrahtspule oder einer Kamera verifiziert. Ein typischer Versuchsdurchgang startete dann, wenn der Affe richtig fixierte und einen Hebel drückte. Während eines gültigen Versuchsdurchgangs durfte die Fixierung nicht mehr als 1° vom FP abweichen. Auf eine Farbänderung des FP hin (von rot zu grün) musste der Affe unmittelbar den Hebel loslassen, um eine flüssige Belohnung (Fruchtsaft) zu erhalten. Versuchsdurchgänge wurden dann verworfen, wenn der Affe den Hebel zu früh oder zu spät losließ, oder die Fixierung während des Durchgangs unterbrach. In diesen Fällen gab es keine Belohnung. Normalerweise erreichten die Affen 700 bis 1500 korrekte Versuchsdurchgänge in fünfstündigen Sitzungen, während derer sie ihren täglichen Flüssigkeitsbedarf deckten.

Zu Beginn einer Ableitsitzung wurden die rezeptiven Felder in V1 automatisch mit Hilfe eines in 16 verschiedene Richtungen über den Monitor bewegten Balkens charakterisiert. Sowohl das Zentrum als auch das Ausmaß der rezeptiven Felder wurden durch Interpolieren der in allen 16 Richtungen hervorgerufenen Aktionspotenzialaktivität abgeschätzt. Richtungstuningkurven wurden für jeden Ableitort mit Rechteck-Balkenmustern, die sich ebenfalls in 16 Richtungen bewegten, ermittelt. Das Balkenmuster wurde dabei so positioniert, dass alle abgeleiteten Neurone gleichzeitig stimuliert wurden. Der andere während dieser Arbeit angewandte Sehreiz war das bewegte „Plaid“. Plaids sind bistabile Sehreize und können daher in Abhängigkeit ihrer physikalischen Charakteristik (Luminanzverteilung) zu verschiedenen Wahrnehmungen führen. Dazu wurden zwei Balkenmuster mit einer Winkeldifferenz von 135° in ihrer Bewegungsrichtung (45° Winkeldifferenz in ihrer Orientierung) übereinandergelegt. Die Transparenz des Plaids wurde durch Änderung der Luminanz der einzelnen Komponenten und ihrer Schnittstellen manipuliert. So wurden sie entweder als einzige bewegte Oberfläche (Musterplaids) oder als zwei getrennte in verschiedene Richtungen driftende Oberflächen (Komponentenplaids) wahrgenommen.

Verschiedene Verhaltensaufgaben wurden in dieser Arbeit benutzt. Die einfachste bestand darin, die Änderung des FPs anzuzeigen (siehe oben). In diesem Fall wurden Sehreize auf den rezeptiven Feldern dargeboten und passiv vom Affen wahrgenommen, während er die Farbänderung des FP in der Fovea erkennen sollte. Mit dieser Aufgabe wurden die Eigenschaften der rezeptiven Felder, sowie Änderungen der laufenden Aktivität bei Darbietung einzelner und überlagerter Balkengitter während des Versuchsdurchgangs gemessen. Zusätzlich wurde diese Aufgabe dazu verwendet, die Aufmerksamkeit des Affen entlang der Zeitachse zu lenken. Dazu wurden relevante Zeitpunkte

vorhersagbar gemacht. Festgelegte Stimulusabfolgen, in denen die FP-Änderung unveränderlich am Ende der Sequenz auftrat, dienten zum Aufbau zeitlicher Erwartung (Sequenzprotokolle). Beim Blockprotokoll konnte die FP-Änderung entweder früh oder spät im Versuchsdurchgang auftreten. Durchgänge mit derselben Abfolge wurden in Blöcken präsentiert und 50-mal wiederholt, so dass der zeitliche Ablauf der Aufgabe vorhersagbar wurde. Weiter konnte die bevorstehende FP-Änderung durch ein Luminanzsignal am FP selbst angezeigt werden (Signalprotokolle). Die neuronalen Aktivitäten in Zeitabschnitten mit niedriger und hoher zeitlicher Erwartung wurden miteinander verglichen.

Ein Affe wurde trainiert, seine Aufmerksamkeit auf eine der beiden Plaidoberflächen zu richten. Für dieses Experiment wurde der Plaidmuster dergestalt konstruiert, die Wahrnehmung zugunsten zweier übereinander gleitender Oberflächen zu beeinflussen. Der Affe bekam die Aufgabe, auf Luminanzänderungen in der beobachteten Balkengitterkomponente zu antworten und Änderungen in der anderen, ablenkenden Komponente zu ignorieren. In dieser Aufgabe blieb der FP unverändert und diente nur dazu, den Blick des Affen festzuhalten.

Messungen der zeitlichen Muster der lokalen (MUA und SUA) und globalen (LFP) neuronalen Aktivität in V1 wurden vorgenommen. Sowohl zeit- als auch frequenzdomänenbasierte Analysen wurden durchgeführt. Zur Erkennung synchroner Oszillationen in den Aktionspotenzialantworten berechneten wir Auto- und Kreuzkorrelogramme für jeden Versuchsdurchgang einzeln (1 ms Auflösung) und mittelten dann über alle Wiederholungen der jeweiligen Reizbedingung. Spektrale Anteile wurden für sowohl MUA als auch LFP Signale mittels der Multitaper-Methode ermittelt. Das Powerspektrum wurde in Z-Werteinheiten (z-score) relativ zur Spontanaktivität ausgedrückt. Der Grad der Phasenübereinstimmung wurde durch Messungen der Kohärenz ermittelt.

Ergebnisse und Diskussion: Experimente zur Oberflächentrennung wurden mit verschiedenen Plaid Konfigurationen durchgeführt. Mithilfe der BBS Hypothese machten wir Voraussagen darüber, wie Neurone in V1 in Abhängigkeit von der Sehreizeanordnung und damit der Wahrnehmung synchronisieren sollten. Keine dieser Voraussagen bewahrheitete sich, unabhängig davon, ob der Affe den Reiz passiv anschaute oder aktiv seine Aufmerksamkeit auf eine der Oberflächen richtete. Folglich hing die Gamma Aktivität hauptsächlich von lokalen und weniger – wie ursprünglich angenommen - von globalen Stimuluseigenschaften ab.

Um die oben beschriebenen negativen Ergebnisse besser zu verstehen, unternahmen wir eine ausgedehnte Experimentreihe, um die Hauptfaktoren, welche Gamma-Aktivität in V1 vom Affen bestimmen, zu identifizieren.

Es ist bekannt, dass bewegte Balkengitter optimaler Orientierung, Geschwindigkeit und Ortsfrequenz ausgeprägte Gamma-Oszillationen in der primären Sehrinde hervorrufen. Wegen der kolumnären Organisation von V1 und dem Muster horizontaler Verbindungen, welche Neurone ähnlicher Antwortselektivitäten miteinander verknüpfen, ist davon auszugehen, dass einzelne Balkengitter eine ausgewählte Population von Zellen aktivieren. Tatsächlich waren die durch einzelne Balkengitter erzeugten Gamma Oszillationen groß und lang anhaltend, und führten in der Regel zu einzelnen Signalgipfeln im Powerspektrum. Fügten wir ein zweites Balkengitter zum Stimulus hinzu, so änderte sich die Dynamik der neuronalen Aktivität deutlich. Energie im Gamma-Frequenzbereich wurde besonders für Aktionspotenzialaktivität stark abgeschwächt, während LFP Oszillationsfrequenzen systematisch höhere Werte annahmen. Wir nehmen an, dass der Haupteffekt des Hinzufügens des zweiten Balkengitters der war, zwei neuronale Populationen mit unterschiedlichen Antwortigenschaften anzusprechen. Dabei untersuchten wir, ob die beobachteten Power- und Frequenzänderungen aus einem Wettstreit zwischen den verschiedenen Balkengitterkomponenten herrührten. Wir führten zwei Experimente durch, in denen wir die durch das zweite Balkengitter (Hintergrundgitter) hervorgerufene Störung auf die durch das erste Balkengitter (Vordergrundgitter) erzeugten laufenden Oszillationen parametrisch testeten. Im ersten Experiment erhöhten wir den Kontrast der zweiten relativ zur ersten Komponente. Für zunehmende Kontraste nahm die Oszillationsfrequenz zu und die Power ab. Im zweiten Experiment zeigte sich derselbe Trend, wenn der Winkel zwischen den beiden Komponenten vergrößert wurde. Beide Ergebnisse sprechen für einen kompetitiven Mechanismus.

Das zweite wichtige Ergebnis dieser Arbeit war das räumliche Ausmaß korrelierter Gamma-Aktivität in V1. Wir leiteten Aktionspotenzialaktivität und LFPs auf drei verschiedenen räumlichen Skalen ab: von derselben Elektrode, von verschiedenen aber nahe beieinander liegenden Orten im Kortex, und von verschiedenen, aber weit voneinander entfernte Exzentrizitäten (3° und 10°) repräsentierenden Kortex orten. Dabei konnten wir einen Abfall korrelierter Gamma-Aktivität als Funktion des kortikalen Abstands beobachten. Die Korrelationen zwischen Aktionspotenzialen und LFPs derselben Elektrode waren gewöhnlich höher als die zwischen verschiedenen Elektroden. LFP-LFP Korrelationen zwischen weit voneinander entfernten Elektroden traten häufig auf, aber mit einer niedrigeren Amplitude als zwischen Signalpaaren, welche von nebeneinander liegenden Kortexorten abgeleitet worden waren. LFP-Aktionspotenzial Korrelationen waren selten, und Aktionspotenzial-Aktionspotenzial Korrelationen traten nie zwischen weiter voneinander entfernten Orten auf. Deshalb erreichten Korrelationsmaße, welche das LFP mit einschlossen, mit größerer Wahrscheinlichkeit Signifikanzniveau. Eine mögliche Erklärung für dieses Ergebnis bietet die unterschiedliche Abtastrate der neuronalen Aktivität durch die beiden Signale. Während das LFP die Aktivität einer Neuronen Population widerspiegelt, sind Aktionspotenziale einzelner Zellen eher dafür anfällig, Oszillationszyklen zu überspringen. Tatsächlich trat oszillatorische Aktivität im LFP

häufiger auf als in den Aktionspotenzialen. Folglich kamen wir zu dem Schluss, dass der begrenzte Rahmen, in dem Interaktionen im Gammaband in V1 erfolgen, ihre Rolle als ein Information integrierender Mechanismus zwischen räumlich verstreuten Ableitorten einschränkt.

Die Oszillationsfrequenz von Gamma-Aktivität in V1 wurde von mehreren Faktoren beeinflusst. Das Muster kortikaler Aktivierung (einzelne im Vergleich zu überlagerten Balkengittern) war einer davon. Der zweite Faktor war die Exzentrizität des Ableitortes. Die Oszillationsfrequenz verhielt sich umgekehrt zur Exzentrizität dergestalt, dass die Frequenz am Amplitudengipfel des Powerspektrums systematisch für die die peripheren Gesichtsfeldanteile abbildenden Orte abnahm. Ein dritter Faktor war gerichtete Aufmerksamkeit. Die Oszillationsfrequenz hing davon ab, auf welche Oberfläche des Plaid-Reizes der Affe seine Aufmerksamkeit richtete. Schließlich spielte auch interindividuelle Variabilität eine Rolle. Bei gleichen Reizbedingungen beobachteten wir einen für jeden Affen spezifischen Oszillationsfrequenzgipfel im Gamma-Band. Trotz der interindividuellen Unterschiede war das spektrale Profil über Messungen in beiden Hemisphären und verschiedene Ableitsitzungen hinweg sehr konsistent.

In Übereinstimmung mit anderen kürzlich veröffentlichten Studien fanden wir, dass Gamma-Aktivität durch Aufmerksamkeit sehr stark beeinflusst wird. In der vorliegenden Arbeit zeigen wir, wie die gezielte Lenkung von Aufmerksamkeit entlang der Zeitachse Gamma-Prozesse in V1 von Affen moduliert. Zeitliche Erwartung führte zu einer Zunahme von Gamma-Oszillationen (30 bis 90 Hz) im LFP und gelegentlich in der Aktionspotenzialaktivität. Diese Zunahme wurde meistens von einer Alpha-Abnahme begleitet, wie es auch in Studien über selektive Aufmerksamkeit gewöhnlich der Fall ist. Wie Kohärenzmessungen zeigten, nahm die Übereinstimmung der Phasen zwischen Aktionspotenzialen und LFPs ebenfalls für Gamma-Komponenten zu. Diese Effekte waren räumlich sehr weit ausgedehnt. Obwohl der Fokus der Aufmerksamkeit auf den FP gerichtet war, beobachteten wir vergleichbar große Änderungen für sowohl zentrale (3°) als auch parafoveale (10°) rezeptive Felder. Der Anstieg von Gamma trat in einer frequenzspezifischen und reizabhängigen Art und Weise auf. Zuvor hatten wir berichtet, dass überlagerte, zusammengesetzte Balkengitter Gamma-Oszillationen bei höheren Frequenzen als die einzeln gezeigten individuellen Balkengitter hervorriefen. Hier stellten wir nun fest, dass Erwartung die Stärke der Oszillation beeinflusst, ohne die Hauptfrequenzkomponenten, die durch einen bestimmten Sehreiz induziert wurden, zu verschieben. Unsere Ergebnisse deuten somit auf einen Verstärkungsmechanismus hin, der in der Lage ist, Gamma-Aktivität ausgedehnt und räumlich unselektiv zu modulieren. Möglicherweise kontrollieren interne Hirnzustände wie Erwartung die Amplitude der durch bestimmte Stimulusmerkmale ausgelösten frequenzspezifischen Rhythmen.

Als letztes berichten wir über Gamma-Phasenverschiebungen in V1, ähnlich der Präzession von Theta Phasen im Hippocampus. Der relative Zeitpunkt eines Aktionspotenzials zum Gamma-Zyklus

verschob sich als Funktion der Stärke neuronaler Aktivierung. Stark aktivierte Neurone feuerten früher im Gamma-Zyklus. Somit liefert die Phase der Aktionspotenziale im Gamma-Zyklus eine unmittelbare analoge Repräsentation neuronaler Erregung.

Schlussfolgerungen: Gamma-Aktivität im primären visuellen Kortex wird in starkem Maße von der kortikalen Architektur beeinflusst. Wir beschrieben mehrere Stimulusparameter, die sowohl Gamma Power als auch Gamma Oszillationsfrequenz modulieren können. In allen Fällen konnte die Art und Weise der Modulation zufriedenstellend durch die funktionelle Organisation der frühen Sehrinde erklärt werden. Zusätzlich beobachteten wir, dass zeitliche Erwartung Power und Kohärenz im Gammabereich in V1 beim Affen sehr stark modulieren kann.

Acknowledgements

Sergio Neuenschwander has provided me during all of these years with valuable and dedicated supervision. He shared with me all his experience in visual neuroscience, which resulted in countless discussions, insights and pleasurable moments. Most importantly, he shared with me his personal stories, which have so importantly guided my own path. Without his expertise in all aspects of this work, none of this would have become possible. I would like to specially thank him for inviting me to Germany, and for always including me in all aspects of the lab.

Wolf Singer heads a department alike few in the world. The originality of his work and his insights into the unknown mechanisms of brain function are ingredients that make his department such an outstanding environment to be in. As a director, he is able to create an atmosphere which is both stimulating and multidisciplinary. And despite his very busy schedule, he always finds time for the graduate students in his group. I would like to thank him for his generosity and his continuous support throughout these years.

This work was only possible due to the exceptional technical assistance provided by Michaela Klinkmann, Hanka Klon-Lipok and Clemens Sommer. I would like to acknowledge their skills, dedication and commitment.

I was lucky to work in a center which provided support for every aspect of my work. I knew I could always rely on any colleague in the institute. Here, I would like to acknowledge those who were ready to go out of their way and help me one step further whenever necessary: Walter Ankenbrand, Thomas Maurer and Andreas Umminger of the mechanic workshop; Wolfgang Leber, Dieter Herzberger, Manfred Kilb and Detlef Schädler of the IT department; Christiane Kiefert, Yvonne Wenzel, and Manuel Amlung of the animal facility; Sabine Schultz, Nicole Gruber and Gabriele Muhl of the administration; and Michaela Wicke, department secretary.

The Graduiertenkolleg Neuronale Plastizität supported the initial years of my doctoral training. I would like to specially thank the chair of the program, Herbert Zimmermann, and the coordinator, Gabi Lahner for all their encouragement during my training. I would like to thank Manfred Kössl for accepting to be my supervisor by the University of Frankfurt.

I benefited immensely from the expertise of various brilliant people. I would like to specially thank insights that arose from discussions with Pascal Fries, Eugenio Rodrigues, Gordon Pipa, Wei Wu and my office mate Raul Vicente. Thank you also to Lars Muckli, Matthias Munk, Ruxandra Sireteanu, Bill Phillips, Kerstin Schmidt and Heinz Wässle.

I would like to acknowledge the valuable and fruitful collaboration with Pascal Fries, Martin Vinck, Thilo Womelsdorf, Nan-Hui Chen, Miguel Castelo-Branco, Lucas Pinto and Jerome Baron that was carried out during this work.

Thank you to the colleagues with whom I started my graduate training: Peter Bäuerle, Kai Gansel, Birgit Voigt, Sacha Gotthardt, Frank Borchard and Axel Kohler. I am also grateful for the help and support of several members of the institute: Ovidiu Jurjut, Anna Hassel-Adwan, Danko Nikolic, Lucia Melloni, Ralf Galuske, Peter Uhlhaas, Michael Wibral, Thomas Wunderle, David Eriksson, Martha Havenith, Sara Weigelt, Boris Ebisch, Will Barnes, Caspar Schwiedrzik, Raul Muresan, Arjen Alink, Elen Städtler, Ceyhun Tamer, Zsuzsa Agoston, Evi Scheibinger and Mirko Schmidt.

Thank you to Kerstin Schmidt and Frédéric Roux for providing the two abstract versions in German language.

I would like to thank Jusuf Yaylaci for saving Nico's life after a deadly fight he once had with Kai late in the night. Additionally, I am specially grateful that he was able to reassure my mother on times of despair, when her hope that I would one day finish this work was long gone.

To all my previous mentors and supervisors, I would like to acknowledge their precious contribution to my scientific formation: Mario Fiorani, Ricardo Gattass, Cynthia Kyaw, Sueli Felipe, Valdir Pessoa, Marco Marcondes, Paulo Motta and Ildinete Pereira.

Along these years, I had the privilege of having some of my colleagues transform into very close friends. I would like to thank Frédéric Roux, Ulrike Radden, Ajmal Zemmar, Petra Janson and Martin Glösmann for their companionship and support.

The initial period in a foreign country is never easy. Thank you to Dagmar, Wirtrud and Herbert Gross, to Raphaela Marinho and to Jonathan Butler for making this transition period so joyful. Thank you also for your continuing friendship along these years.

To my loved ones no words will ever be enough. To my parents Ana and Bendix, to my sister Biana, to my aunts Graça, Benilce and Catarina, to my uncle Bernardo, and to my grandmothers, Francisca and Belisa. To my wife, Fernanda.

CURRICULUM VITAE

BRUSS LIMA

July, 2010

Home address:

Ingelheimer Strasse 22
Frankfurt am Main 60529
Germany

Phone: +49 69 93993451
Mobile: +49 178 2848900

Date of Birth: Abril 24, 1974

Place of Birth: Brasilia, DF

Nationality: Brazilian.

Civil condition: Married.

Institutional address:

Max-Planck-Institute for
Brain Research
Frankfurt am Main 60528

+49 69 96769 241 (office)
+49 69 96769 235 (laboratory)
+49 69 96769 327 (FAX)

e-mails:

bruss@mpih-frankfurt.mpg.de

bruss.lima@gmail.com



SCHOLARSHIP

First school;	1981-1982	Colégio Madre Carmen Salles Brasília, Brazil.
	1982-1983	Saint Aloysius First School Oxford, England
Middle school;	1983-1987	Saint Gregory's R C Middle School Oxford, England
	1987-1988	Centro Educacional Horacina C. Preta Brasília, Brazil
High school;	1989-1991	Centro Educacional Leonardo da Vinci Brasília, Brazil
Undergraduation;	1992-1997	Bachelor in Biological Sciences University of Brasília – UnB Brasília, Brazil.

- 3 - **Lima B**, Motta PC. (1998). Biologia dos imaturos das borboletas Ithomiinae (Nymphalidae) em quatro espécies de plantas hospedeiras (Biology of Ithomiinae butterfly immatures (Nymphalidae) in four host plant species). Anais do 4º Congresso de Iniciação Científica da Universidade de Brasília, Brazil.
- 4 - **Lima B**, Motta PC. (2000). Flutuação populacional e biologia dos imaturos de borboletas Ithomiinae em Brasília (Population fluctuations and biology of Ithomiinae butterfly immatures in Brasília). XXIII Congresso Brasileiro de Zoologia. Cuiabá-MT, UFMT/IB, Brazil.
- 5 - **Lima B**, Araujo N, Feres-Filho E, Fiorani M, Gattass R. (2000). Metodologia de implante para registro eletrofisiológico crônico em macacos Cebus acordados (Implant methodology for chronic electrophysiological recording in the awake behaving Capuchin monkey). XV Reunião Anual da Federação de Sociedades de Biologia Experimental-FeSBE. Hotel Gloria. Caxambu-MG, Brazil.
- 6 - **Lima B**, Azzi J, Baron J, Singer W, Neuenschwander S. (2004). C-Plaids: a new stimulus for studying perceptual switches. 1st Neuroscience Symposium: International Institute of Neuroscience of Natal. Natal-RN, Brazil.
- 7 - **Lima B**, Chen N, Singer W, Neuenschwander S. (2005). Plaids stimuli disrupt gamma activity in V1 of the behaving monkey. 35th Annual Meeting – Society for Neuroscience. Washington-DC, USA.
- 8 - **Lima B**, Chen N, Singer W, Neuenschwander S. (2006). Stimulus dependent redistribution of gamma oscillation frequency in monkey V1. 5th Forum of European Neuroscience (FENS). Vienna, Austria.
- 9 - Pinto L, Dias MO, **Lima B**; Neuenschwander S, Baron J. (2006). Response of visual wulst neurons to plaids patterns in the alert burrowing owl. XXI Reunião Anual da Federação de Sociedades de Biologia Experimental-FeSBE. Águas de Lindóia-SP, Brazil.
- 10 - **Lima B**, Chen N, Singer W, Neuenschwander S. (2006). Strength of stimulus-induced gamma oscillations in monkey V1 depend on attention and expectancy. 36th Annual Meeting – Society for Neuroscience. Atlanta-GA, USA.
- 11 - **Lima B**, Chen N, Singer W, Neuenschwander S. (2007). Stimulus-dependent gamma oscillations in monkey V1 and its modulation by expectancy. Seventh Göttingen Meeting of the German Neuroscience Society. Göttingen, Germany.
- 12 - Pinto L, **Lima B**, Neuenschwander S, Baron J. (2007). Directional selectivity in the visual wulst of the awake owl: A comparison between gratings and plaid patterns. 37th Annual Meeting - Society for Neuroscience. San Diego-CA. USA.
- 13 - **Lima B**, Singer W, Neuenschwander S. (2008). Stimulus and task-dependent gamma activity in monkey V1. 6th Forum of European Neuroscience (FENS). Geneva, Switzerland.

14 - Neuenschwander S, **Lima B**, Singer W. (2008). Stimulus and task-related gamma oscillations in monkey V1 induced by local and global contours. 38th Annual Meeting - Society for Neuroscience. Washington-DC. USA.

15 - Womelsdorf T, **Lima B**, Vinck M, Oostenveld R, Bosman C, Singer W, Buffalo EA, Neuenschwander S, Desimone R, Fries P. (2008). Putative excitatory and inhibitory neurons synchronize at different phases of the gamma cycle in visual areas V1 and V4 of awake monkeys. 38th Annual Meeting - Society for Neuroscience. Washington-DC. USA.

16 - Pipa G, Neuenschwander S, **Lima B**, Chen Z, Brown EN. (2008). A comparison of spike time prediction and receptive field mapping with the point process generalized linear models, wiener-volterra kernel and spike-triggered average methods. 38th Annual Meeting - Society for Neuroscience. Washington-DC. USA.

17 - Pipa G, Chen Z, Neuenschwander S, **Lima B**, Brown E. (2009). Efficient spike encoding for mapping visual receptive fields. *Frontiers in Systems Neuroscience*. Conference Abstract: Computational and systems neuroscience. doi: 10.3389/conf.neuro.06.2009.03.086

18 - Womelsdorf T, **Lima B**, Vinck M, Oostenveld R, Singer W, Neuenschwander S, Fries P. (2009). Precise spike synchronization in the gamma band increases information gain in awake monkey V1. *Frontiers in Systems Neuroscience*. Conference Abstract: Computational and systems neuroscience. doi: 10.3389/conf.neuro.06.2009.03.101

19 - Haslinger R, **Lima B**, Pipa G, Brown E, Neuenschwander S. (2009). The effect of global context on the encoding of natural scenes. *Frontiers in Systems Neuroscience*. Conference Abstract: Computational and systems neuroscience. doi: 10.3389/conf.neuro.06.2009.03.115

20 - **Lima B**, Singer W, Neuenschwander S. (2009). Stimulus and task-related gamma oscillations in monkey V1 induced by local and global contours. Eighth Göttingen Meeting of the German Neuroscience Society. Göttingen, Germany.

21 - Neuenschwander S, Pinto L, **Lima B**, Baron J. (2009). Gamma oscillations in the visual Wulst of the owl: a comparative study. Eighth Göttingen Meeting of the German Neuroscience Society. Göttingen, Germany.

COURSES AND WORKSHOPS

- Cooperative dynamics of neural systems. Organizers: Pedro Maldonado and Charles Gray. Pucón, Chile. 2002.

- Structure, function and evolution of the primate visual system. Organizer: Jan Kremers. Tübingen, Germany. 2003.

- Neuroinformatics. Course directors: Emery Brown and Partha Mitra. Marine Biological Laboratory. Woods Hole-MA, EUA. 2005.
- Visualizing large-scale patterns of activity in the brain. Optical and electrical signals. Organizer/moderator: György Buzsáki. Society for Neuroscience. Atlanta-GA, USA. 2006.
- The dynamical brain. Boehringer Ingelheim Fonds International Titisee Conferences. Organizer: Wolf Singer. Titisee, Germany. 2006.

TALKS

- Moving plaids in context: A study in the behaving monkey. Ringberg Castle Department Meeting. Germany. 2005.
- Moving plaids and neuronal oscillations. Salk Institute for Biological Studies. La Jolla-CA, USA. 2006.
- Strength of stimulus-induced gamma oscillations in monkey V1 depend on attention and expectancy. Nathan S. Kline Institute for Psychiatric Research. Orangeburg-NY, USA. 2006.
- Oscillation-based attentional mechanisms in V1. What to expect? Ringberg Castle Department Meeting. Germany. 2007.
- Distributed gamma oscillations induced by expectancy in monkey V1 and V4. Slide Session 338, Visual Cognition: Attention and Search II. 37th Annual Meeting – Society for Neuroscience. San Diego-CA, USA. 2007.
- Oscillation-based attentional mechanisms in V1. What to expect? Institut de Neurosciences Cognitives de la Méditerranée. INCM-CNRS. Marseille, France. 2008.
- Stimulus and task-related modulation of gamma activity in monkey V1. Ringberg Castle Department Meeting. Germany. 2008.
- Oscillation-based attentional mechanisms in V1. What to expect? Department of Neurobiology, Harvard Medical School. Boston, USA. 2008.
- Stimulus and task-related modulation of gamma activity in monkey V1. Bernstein Center for Computational Neuroscience. Berlin, Germany. 2009.
- Gamma responses in V1: when and where to expect. Ringberg Castle Department Meeting. Germany. 2010.

OTHER ACADEMIC ACTIVITIES:

- Member of examination committee.

Student: Joana Amora Ramos

Title of monograph: Context-dependent immediate gene expression in the brain of singing birds.

Partial requirement for the obtention of the bachelor's degree in Biological Sciences

Federal University of Rio de Janeiro - UFRJ, Brazil, 1999.

- Member of organization committee.

Annual scientific meeting of the Max-Planck-Institute for Brain Research (Haussymposium), 2004.

PUBLICATIONS:

1 - **Lima B**, Fiorani M, Gattass R. (2003). Modulation by context of a scene in monkey anterior inferotemporal cortex during a saccadic eye movement task. *An Acad Bras Cienc.* 75: 71-6.

2 - **Lima B**, Fiorani M, Gattass R. (2005). Changes of ongoing activity in Cebus monkey perirhinal cortex correlates with behavioral performance. *Braz J Med Biol Res.* 38: 59-63.

3 - Gattass R, Nascimento-Silva S, Soares JGM, **Lima B**, Jansen AK, Diogo ACM, Farias MF, Marcondes M, Botelho EP, Mariani OS, Azzi J, Fiorani M. (2005). Organization of Cortical Visual Areas in Primates. *Proc R Soc Lond B Biol Sci.* 360: 709-731.

4 - Baron J, Pinto L, Dias MO, **Lima B**, Neuenschwander S (2007). Directional responses of visual wulst neurones to grating and plaid patterns in the awake owl. *Eur. J. Neurosci.* 26: 1950-1968.

5 - Uhlhass PJ, Pipa G, **Lima B**, Melloni L, Neuenschwander S, Nikolic D, Singer W. (2009). Neural synchrony in cortical networks: history, concept and current status. *Front. Integr. Neurosci.* 3: 1-19.

6 - **Lima B**, Singer W, Chen N-H, Neuenschwander S. (2010). Synchronization dynamics in response to plaid stimuli in monkey V1. *Cereb Cortex.* 20: 1556-1573.

7 - Vinck M, **Lima B**, Womelsdorf T, Oostenveld R, Singer W, Neuenschwander S, Fries P. Gamma-phase shifting in awake monkey visual cortex. *J Neurosci.* 30: 1250-1257.

8 - Amarin AKJ, **Lima B**, Gattass R. GABA inactivation of visual area MT modifies direction selectivity of V2 neurons in the Cebus monkey. Under review.

Selbstständigkeitserklärung

Ich erkläre hiermit, dass ich die Doktorarbeit selbständig verfasst und keine anderen als die angegebenen Quellen und Hilfsmittel benutzt habe.

Frankfurt, den 11. Juli. 2010